Chapter 5: Information from Paleoclimate Archives

Coordinating Lead Authors: Valérie Masson-Delmotte (France), Michael Schulz (Germany)

Lead Authors: Ayako Abe-Ouchi (Japan), Juerg Beer (Switzerland), Andrey Ganopolski (Germany), Jesus Fidel González Rouco (Spain), Eystein Jansen (Norway), Kurt Lambeck (Australia), Juerg Luterbacher (Germany), Tim Naish (New Zealand), Timothy Osborn (UK), Bette Otto-Bliesner (USA), Terrence Quinn (USA), Rengaswamy Ramesh (India), Maisa Rojas (Chile), XueMei Shao (China), Axel Timmermann (USA)

Contributing Authors: Patrick de Deckker, Barbara Delmonte, Hubertus Fischer, Claus Froehlich, Alan Haywood, Stefan Mulitza, Olga Solomina, Pavel Tarasov, Yusuke Yokoyama, Dan Zwarz

Review Editors: Fatemeh Rahimzadeh (Iran), Dominique Raynaud (France), Heinz Wanner (Switzerland), De`er Zhang (China)

Date of Draft: 15 April 2011

Notes: TSU Compiled Version

Table of Contents

Executive Summary

[PLACEHOLDER FOR FIRST ORDER DRAFT: Text and Figures will be amended after new CMIP5/PMIP3 simulations are analysed and new publications available. The treatment of uncertainty, following IPCC guidelines, will be systematically implemented in the FOD. Cross-chapter coherency has been planned with Chapters 6 (carbon cycle), 13 (sea level) and 9 (model evaluation) which also use palaeoclimate information.]

Radiative forcings and radiative perturbations from Earth-System feedbacks

- Since AR4, the knowledge about recent natural forcings has progressed. Revised estimates of past solar and volcanic forcings have been published, spanning the current interglacial period and the last 1500 years, respectively. Different representations of solar and volcanic forcings have been used for simulating the climate of the last millennium.
- Records of past black carbon deposition and biomass burning are emerging, in relationship with climate variability and anthropogenic land use change. Large discrepancies are identified in various estimates of pre-industrial anthropogenic land use changes.
- Ice core records of past concentrations and isotopic composition of greenhouse gases have been expanded back to 800 ka, confirming the previous range of glacial-interglacial variations. Less precise pre-Quaternary reconstructions obtained from geological records suggest that CO_2 concentrations above 400 ppmv likely prevailed during the past 65 Ma, until the Pliocene (5.3 to 2.6 Ma).

Earth System responses and feedbacks at global and hemispheric scales

- The available information depicts tight coupling between pre-Quaternary CO_2 levels and global climate including thresholds for Antarctic and Northern Hemisphere ice sheet inceptions. It is likely that CO_2 concentrations were above about 1000 ppmv and global mean surface temperature about 8°C above pe-industrial values about 50 million years ago (the Eocene, the warmest part of the past 65 million years). Global mean temperatures 4 ± 2°C above pre-industrial were encountered during the Pliocene, when CO_2 levels were likely around 400 ppmv.
- While reduced equator-pole temperature gradients are likely for high CO_2 worlds (Eocene to Pliocene), questions remain about the ability of climate models to capture the large polar depicted by terrestrial and marine temperature proxies.New syntheses of Last Glacial Maximum sea surface and ice core temperature reconstructions are compared with climate model simulations in order to constrain climate sensitivity. In climate models, climate sensitivity depends on the climate state (higher in cold climates than in warmer climates) because of cloud feedbacks. climate sensitivity, higher in cold climates.
- New records of glacial-interglacial variability since 800 ka have been used to estimate fast and slow climate sensitivity and assess the strength of the climate-carbon feedbacks. Since AR4, transient glacial-interglacial climate simulations have been performed with coupled climate–ice sheet models, in response to orbital forcing. A correct magnitude of ice ages is only reached when taking into account CO_2 positive feedback.
- At the start of deglaciations and during the beginning of interglacial periods, temperature changes are not synchronous worldwide because of reorganizations in large scale ocean circulation.
- Past interglacials such as the Last Interglacial (130–120 ka) were regionally warmer than today at mid to high latitudes. In response to the known LIG orbital forcing, ocean-atmosphere coupled simulations underestimate Greenland or Eurasian LIG warmth. This may be due to the lack of appropriate land surface and sea ice feedbacks in the models.
- There is new evidence for centennial to millennial climate variability during the current and earlier interglacials, superimposed on long term trends caused by orbital forcing. Climate models explain much of the spatial and temporal complexity of the early to mid Holocene optimum by the interplay of orbital forcing and the regional impacts of ice sheet decay.
- New multi-proxy based statistical reconstructions have been developed to estimate hemispheric and global temperature variations during the last centuries/millennia. Since AR4, larger amplitudes of variations have been documented between the Medieval Climate Anomaly (MCA) and Little Ice Age (LIA). Comparison of the relative warmth of the Medieval and modern periods is still problematic due to considerable uncertainty, both quantified and unquantified. The available evidence provides medium confidence that the last 50 years were, on average, warmer than the Medieval Climate Anomaly for the Northern Hemisphere and perhaps global scales. Evidence for modern warming is more extensive seasonally and geographically than the evidence for Medieval warmth.

- A broad agreement is observed between simulations and reconstructions of NH temperature during the last millennium when forced by natural and athropogenic forcings, but uncertainties in reconstructed temperatures and forcings limit the power of this comparison as a test of climate model performance.

Past changes in sea level and related processes

- Global sea level was very likely by 4–6 m higher during the last interglacial (LIG) than present. A higher sea level anomaly of +6.6–9.4 m cannot be excluded based on one study. While a sea level rise of +4 m during the LIG can be explained by Greenland ice sheet melting and thermosteric effect, any higher sea level would require the response of both polar ice sheets to only moderate levels of warming.
- New evidence does not support a sea level rise by +20 m for the interglacial associated with marine isotope stage 11 (about 400 ka). It is more likely [tbc] that sea level was closer to present [to be quantified].
- Sea level estimates for the warmest interglacials of the Pliocene indicate that global sea level was likely to have been greater than +15 m and very likely to have been greater than +9 m, with a mean value of +22 m above present-day. The complete deglaciation of the marine portions of the West Antarctic Ice Sheet together with, thinning and recession on the margins of the East Antarctic Ice Sheet contributed with +7 m of sea level rise to the global sea level budget during Pliocene interglacials.
- New estimates for rates of deglacial sea level rise support earlier estimates for the abrupt increase called Meltwater Pulse 1a (14–14.5 ka) of about 20 m in less than 500 years with an average annual rise of at least about 40 mm yr^{-1} [to be updated with uncertainty levels when new data published.]

Climate responses and feedbacks at regional scales

- High-amplitude near surface temperature variations on millennial to centennial time scales appear to characterise Holocene ocean temperatures in both hemispheres. Due to time scale uncertainties, the phasing of these significant pre-industrial climate events between the hemispheres remains unclear.
- Marine reconstructions from high-latitude North Atlantic-Arctic ocean areas show century scale temperature anomalies associated with a warm phase centred around 1100 AD and a generally colder phase after 1400 AD that ends in the early 20th century. In the Fram Strait, at the entrance to the Arctic the high modern SSTs appear unprecedented over the past 2000 years.
- During the past few millennia centennial-scale oscillations of the western Pacific warm Pool were synchronous with known changes in Northern Hemisphere climate (e. g., the Little Ice Age and Medieval Climate Anomaly, about 900 to 1350 AD) implying a dynamic link between Northern Hemisphere temperatures and Indo-Pacific Warm Pool hydrology.
- The MCA was not characterized by uniformly warmer temperatures globally, but rather by a range of temperature, hydroclimate and marine changes with distinct regional and seasonal expressions.
- New high resolution records of tropical precipitation document large scale ITCZ shifts at orbital (driven by changes in precession) and millennial scale (very likely linked with AMOC reorganisations) with opposite impacts on Northern Hemisphere and Southern Hemisphere monsoons.
- Solar and volcanic forcings generally played a role throughout the last millennium, particularly in establishing the contrast between MCA and LIA periods and the pacing of cold and warm periods inside this interval. Recent climate model simulations driven with lower levels of past solar forcing variability suggest that internal variability could have had a role in producing many of the observed regional changes.
- Extended periods of megadroughts have been observed during interglacials in North America, South America, Africa and Europe. The length of past megadroughts sometimes exceeds those observed in the instrumental period and can be regarded as a natural part of interglacial climate variability. Extended intervals of drought associated to weak Indian Summer Monsoon in the last 2000 years were synchronous across a large region of Asia including southern Vietnam.
- Reconstructions of ENSO document an active ENSO phase during 1550–1650 and a reduction of eastern equatorial Pacific sea surface temperature variance in the periods 1650–1700, 1760–1780 and 1830–1870 and a gradual increase of variance into the 20th century. Volcanic forcing has been shown to increase the probability of reconstructed El Nino events to occur in the two years following the volcanic eruption.
- The strong positive phases of the North Atlantic Oscillation within the mid-1990s are not unusual in context of the past half millennium. There is also strong evidence that positive NAO phases followed large tropical volcanic eruptions with a lag of a few years.

Evidence and processes of abrupt climate change

- The rate of regional warming in Greenland associated with abrupt Dansgaard-Oeschger events and millennial-scale variability during the last glacial termination ranged from of 8°C to 16 ± 2.5°C within several decades. Abrupt warming was preceded by major reorganizations in atmospheric circulation. Abrupt climate variations at the millennial time scale and associated climate instabilities are a pervasive feature of glacial periods during the last one million years. It still remains under debate whether Dansgaard-Oeschger events can be considered stochastically generated individual events, internal oscillations of the glacial atmosphere-ocean sea-ice system, or whether they require dynamical coupling with ice-sheets, or whether they are astronomically forced.
- The modelled large-scale teleconnection patterns in response to an Atlantic meridional overturning circulation (AMOC) weakening closely resemble those reconstructed for glacial abrupt Dansgaard-Oescher and Heinrich Events, thereby supporting the notion that both types of events are related to large-scale reorganizations of the AMOC.

Paleoclimate perspective on irreversibility in the climate system

- New palaeoclimate information and ice sheet models suggest that the West Antarctic and Greenland ice sheets are highly sensitive to polar warming and CO_2 concentrations. Stability thresholds may be close to the present day climate implying potential future irreversible melting.
- High resolution marine sediment data and coupled ocean-atmosphere climate models consistently depict abrupt changes in ocean currents after a catastrophic freshwater inflow at 8.2 ka (10^{14} m^3 possibly within <0.5 year) and complete recovery within about 200 years.
- Mangrove and forest ecosystems are documented to have recovery time scales of about 50–250 years after destruction caused by hurricanes or pre-industrial anthropogenic land use.
- Based on latitudinal shifts of plant types during the last deglaciation, migration rates of vegetation zones range from 15 to 70 km per century in subtropical Africa, north America and Europe.

5.1 Introduction

Chapters 2–4 have assessed climate variations based on instrumental or satellite records. Prior to the instrumental period, information from documentary sources and natural archives provide quantitative information on past regional to global climate and atmospheric composition variability. Accurate and quantitative reconstructions of key climate variables (including temperature, precipitation, etc.) over a wide range of timescales provide information on both, the responses of the Earth system to external forcings and internal system variability. Palaeoclimatic reconstructions allow the ongoing climate change to be placed in the perspective of natural climate variability.

The Chapter "Palaeoclimate" in AR4 provided an overview of past climate changes, and was organized by timescales (from deep time, 10^6 to 10^7 years, to the last thousand years). Major progress has been accomplished in the acquisition of new and more precise information from palaeoclimate archives since AR4, the synthesis of local information to provide a large-scale documentation of past climate dynamics, and in the modelling of past climate responses to forcings. This chapter focuses on an assessment of the understanding of past climate variations, using both palaeoclimate reconstructions and associated uncertainties as well as a range of Earth-system models and climate models of varying complexities including CMIP5 GCMs.

Section 5.2 assesses new information since AR4 on recent reconstructions of external radiative forcings caused by variations in volcanic and solar activity. It also reports on emerging palaeoclimate information on two aspects of anthropogenic forcing; pre-industrial land-use change and black carbon deposition, both of which affect surface albedo. Section 5.2 also addresses past global radiative perturbations caused by Earth-system feedbacks, with a focus on past changes in atmospheric greenhouse gas and mineral aerosol concentrations.

Section 5.3 is dedicated to Earth-system responses and feedbacks at global and hemispheric scales. It first assesses the palaeoclimate record from past times when atmospheric CO_2 concentrations were comparable or higher than during the industrial era. Such intervals are of special interest because reconstructions of the meridional temperature gradient facilitate the estimates of the magnitude of polar amplification. Section 5.3 also assesses glacial climate sensitivity and associated feedbacks and the Earth-system response to insolation changes due to orbital forcing. An update on the global to hemispheric climate changes during the past 2000 years is given and placed in the perspective of climate variability during the course of the current and past interglacial periods.

Section 5.4 assesses the state of knowledge regarding past magnitudes and rates of sea level change. The focus is on large-amplitude sea level variation during glacial-interglacial transitions and during warm climate intervals. The compiled information is used to help address the stability of ice sheets.

Section 5.5 focuses on the regional aspects of reconstructions and modelling of past climate change, with a focus on temperature, precipitation and drought, modes of climate variability and on the last millennia. This section will include new and upcoming information from reconstructions at the continental scale and uses this information to assess model performance at the regional to continental scale.

Section 5.6 is dedicated to assessing new evidence of abrupt climate change in the past. The goal is to provide insights into the underlying processes associated with abrupt changes in the cryosphere, ocean circulation, in precipitation and droughts, and in variability and occurrence of extremes events.

The final section (Section 5.7) assesses the palaeoclimate perspective on irreversibility in the climate system. It addresses asymmetries in the response of ice sheets, recovery timescales of the Atlantic meridional overturning circulation, and the response of large-scale vegetation patterns to major perturbations.

Throughout this chapter, past climate fluctuations are quantified with respect to two different reference periods: 1) the 1961–1990 climatology for the last 2k; and 2) the pre-industrial period (1850 ± 15 years) for longer time scales. This definition of the pre-industrial period is consistent with that used in the pre-industrial control simulations of the Paleoclimate Modelling Intercomparison Project (PMIP).

5.2 Radiative Forcings and Radiative Perturbations from Earth System Feedbacks

[PLACEHOLDER FOR FIRST ORDER DRAFT]

5.2.1 External Forcings

[PLACEHOLDER FOR FIRST ORDER DRAFT]

5.2.1.1 Orbital Forcing

Orbital forcing is the only well-known forcing for the past and future. Resulting from interactions of the Earth with the Sun, Moon, and planets, the elements of the Earth's orbit–eccentricity, longitude of perihelion (precession) parameter, and the axial tilt parameter (obliquity)–can be calculated accurately for the past 40–50 million years and into the future using the gravitational equations for orbital motion (Berger and Loutre, 1991; Laskar et al., 2004). The additive contributions of the periodic changes in these elements result in perturbations in the annual, seasonal, and latitudinal distribution and magnitude of the solar energy received at the top of the atmosphere (Jansen et al., 2007). Obliquity impacts annual mean insolation and the latitudinal gradient of insolation with opposite effects at low versus high latitudes. Precession results in an interhemispheric out-of-phase signal for seasonal insolation. The durations and intensities of local seasons are also affected (Huybers, 2006; Timm et al., 2008) and have a largely cancelling influence on the integrated seasonal insolation between hemispheres with implications for the orbital pacing of ice age cycles [(Raymo et al., 2006; Huybers et al., 2007)]. Over the last million years, there is no best orbital analogue to our present interglacial. Earlier studies proposed that Marine Isotope Stage 11 (MIS11; about 400 ka), due to the low eccentricity level, as an analog for the present interglacial, but the phase between obliquity and precession is very different from present day (Tzedakis, 2010). MIS19 (about 800 ka) has a more comparable phasing and similar eccentricity, but the magnitude of the obliquity variations is weaker due to long-term amplitude modulation.

Although orbital forcing has usually been considered to explain long-term climatic changes, such as glacial-interglacial cycles, it can also be important for understanding both trends and abrupt changes on millennial time scales (Capron et al., 2010b; Kaufman et al., 2009b). Over the period from 850 CE to present, the principal orbital change is a about 20 day shift in perihelion, leading to an insolation increase of about 4 W m^{-2} in May and a decrease of about 6 W m^{-2} in August at 65°N (Schmidt et al., 2011). These orbital insolation variations are included in the CMIP5 simulations for the last millennium. Although not included in the RCP scenarios, orbitally driven changes in insolation will similarly result in a about 1 W m^{-2} 65°N May insolation increase from 2000 to 2300 CE (about 1.5 W m^{-2} August insolation decrease), with little annual change.

5.2.1.2 Solar Forcing

Over the last two decades, models have been developed to explain the instrumental record of total solar irradiance. Two basically different approaches were chosen. The first approach attributes all TSI changes exclusively to magnetic phenomena (sunspots, faculae, magnetic network) occurring in the photosphere at the solar surface. The second approach includes additional global phenomena (e.g., solar radius) in its estimate. The first approach was able to successfully reproduce all the observed TSI changes in the PMOD composite between 1978 and 2003; hence most efforts went into the refinement of these models (Balmaceda et al., 2007; Crouch et al., 2008). The basic concept of these TSI models is to divide the solar surface into several different magnetic features each of which emits a specific radiative flux. Typical examples of dark features reducing TSI are sunspots (umbra and penumbra). Faculae and the magnetic network are examples of bright features that enhance TSI. Each feature is weighted by the fraction (filling factor) of the total solar surface it covers. TSI is calculated by adding the radiative fluxes of all features plus the contribution from the quiet Sun, the remaining surface free of any magnetic activity. This approach requires detailed information of all the magnetic features and their temporal changes (Wenzler et al., 2005; Krivova and Solanki, 2008).

The extension of the TSI record back into pre-instrumental times poses two main problems. Firstly, the instrumental period that is used to test and to calibrate the models does not show any significant long-term trend. Secondly, detailed information about the various magnetic features is not available and must be deduced from proxies such as sunspots for the past 400 years and cosmogenic radionuclides (^{10}Be and ^{14}C) for the past 10,000 years. TSI can be approximated from sunspot numbers or the open magnetic flux deduced from cosmogenic radionuclides using simple models to relate the magnetic features of the TSI models to the emergence of magnetic flux and its decay during a solar cycle. Since all reconstructions rely ultimately on the same data (sunspots and cosmogenic radionuclides), but differ in the details of the applied models and calibrations, the reconstructions agree rather well in their shape, but differ considerably in their amplitude (Figure 5.1b) (Wang et al., 2005a; Krivova et al., 2007; Krivova et al., 2010; Krivova et al., 2011).

Before 1600 CE, all information about solar activity is derived from ^{10}Be in ice cores and ^{14}C in tree rings. These records reflect not only the open solar magnetic field, but also the geomagnetic dipole field and effects of their respective geochemical cycles. These non-solar components have to be removed before deriving TSI and contribute to the uncertainty of the reconstructions (see grey band in Figure 5.1c). The TSI record is characterized by distinct minima lasting 50–100 years corresponding to the grand solar minima that are superimposed upon the long-term changes. Spectral analysis of the TSI record reveals the existence of well-defined cycles (87, 104, 130, 208, 350, 515, 980 years) with varying amplitudes (Steinhilber et al., 2009; Balmaceda et al., 2007; Lean et al., 2011).

[INSERT FIGURE 5.1 HERE]

Figure 5.1: a) 3 composites of instrumental data from several satellite based radiometers indicated by different colours (Dewitte et al., 2004; Frohlich, 2009; Willson and Mordvinov, 2003). The differences between the composites are due to different combinations of the radiometer data and the application of different corrections (x-axis is YEAR AD -> will be incorporated into the figure). **b)** TSI reconstructions back to 1600 AD. The lack of direct measurements is compensated by proxies of solar activity (e.g., sunspots, ^{10}Be) which are used to estimate the parameters of the models or directly TSI. Depending on the assumptions, the differences between the long-term averages are large and range from no change to 0.4% between the present and the Maunder minimum when the Sun was very quiet. With one exception (SSR) all recent reconstructions show relatively small long-term changes (<0.1%) compared to the [reference needed: Lean et al., xxxx] record (0.24%). The top 5 records have been used by Jungclaus et al. (2010b) to simulate the climate of the past 1000 years. The wavelet analysis of TSI (WLS) shows the 11-year Schwabe cycle which is weak during the Dalton minimum (1790–1830) and absent during the Maunder minimum (1645–1715), and cycles around 80 and 120 years. DB: Delaygue and Bard (2010); MEA: Muscheler et al. (2007); SBF: Steinhilber et al. (2009); WLS: Wang et al. (2005c); VK: Vieira et al. (2011); LBB: Lean et al. (1995); SSR: Shapiro et al. (2011). **c)** TSI reconstruction (low-pass filtered by 100 yeary) covering the past 9300 years (Steinhilber et al., 2009). The grey band represents the 1-sigma uncertainty range. The reconstruction is based on ^{10}Be and calibrated using the relationship between instrumental data of the open magnetic field which modulates the production of ^{10}Be and TSI for the past 4 solar minima. The wavelet analysis shows the existence of several well-defined periodicities with varying amplitudes (87, 104, 130, 150, 208, 350, 515, 970, 2300 years).

5.2.1.3 Volcanic Forcing

Since AR4, the magnitude, latitude, altitude, and timing of stratospheric sulfate injection caused by volcanic eruptions of the past 1500 years has been estimated based on multiple bipolar ice core records of sulfate deposition and atmospheric modeling to take into account deposition rates (Gao et al., 2008; Gao et al., 2006). Another reconstruction of volcanic aerosol optical depth and particle size in four latitudinal bands has been produced at sub-annual resolution based on bipolar ice core records and the comparison between the Pinatubo deposition in Antarctica and satellite data (Crowley and Hyde, 2008; Schmidt et al., 2011; Timmreck et al., 2009). These two reconstructions differ in their source data (ice core records), analysis of the type of eruption (local, hemispheric or global) and methods to estimate optical depths. Both datasets can be used for the boundary conditions of PMIP3-CMIP5 last millennium simulations. Uncertainties on the seasonal timing of the eruptions arise from the ice core sulfate or acidity resolutions and from dating uncertainties, and they increase back in time.

Eruptions that produce stratospheric sulfate aerosols have a specific fingerprint in sulfur isotopic composition caused by mass-independent fractionation during photochemical reactions above the ozone layer (Baroni et al., 2007). This method has been applied to Antarctic ice core data and demonstrates the stratospheric character of several large Antarctic volcanic sulfate deposition events (1809 CE, 1815 CE Tambora, 1452–1453 CE. Kuwae, 1258–1259 CE unknown large event) (Baroni et al., 2008; Cole-Dai et al., 2009). The climate impact of very large eruptions may be strongly limited by increased collision rate and aerosol growth (Timmreck et al., 2009). While a number of ice core volcanic records are available prior to the last 1500 years, they do not yet have sufficient resolution or bipolar dating (Bay et al., 2006) to allow quantitative volcanic forcing reconstructions. Several Antarctic ice core records depict more frequent large eruptions during the past 2000 years, as reviewed by Cole-Dai et al. (2009), while an enhanced volcanic activity has been reported for the early Holocene in the GISP2 Greenland record. Increased subaerial volcanism is documented in deglaciating regions between 12 and 7 ka (thousand years before 1950 CE) and may have contributed to deglacial CO_2 emissions (Huybers and Langmuir, 2009). The links between changes in ice thickness and volcanic activity remain uncertain with implications for future changes (Tuffen, 2010). Antarctic ice flow may be affected by volcanic activity (Corr and Vaughan, 2008; Gow and Meese, 2007).

There is evidence for rare but extremely large volcanic eruptions such as the Toba event (at 73 to 74 ka) (Mason et al., 2004) with uncertainties on its long lasting impacts (Haslam et al., 2010; Louys, 2007; Oppenheimer, 2002; Petraglia et al., 2007; Robock et al., 2009; Williams et al., 2009).

5.2.1.4 Anthropogenic Forcing

For the last millennium, changes in CO_2, CH_4 and N_2O concentrations are included in CMIP5 simulations (Schmidt et al., 2011) using data from multiple cores from Antarctica and Greenland (see Section 5.2.2.1). Millennial simulations previous to the CMIP5 experiments have essentially used the same sources as in Jansen et al. (2007).

Records of past black carbon (BC) and land-use changes are indicative of natural and anthropogenic emissions. Arctic ice core BC records (Banta et al., 2008; McConnell and Edwards, 2008) show good agreement with existing global inventories since the mid 19th century (Junker and Liousse, 2008; Lamarque et al., 2010; McConnell et al., 2007) and reveal North American and European coal combustion influences at the beginning of the 20th century. Late 20th century Asian BC sources have been identified in Himalayan glaciers (Ming et al., 2008; Xu et al., 2009) and may have reached also North America and the Arctic (Hadley et al., 2010; McConnell and Edwards, 2008).

Preindustrial BC from biomass burning is influenced by climatic conditions and modulated by anthropogenic land cover changes (ALCC) (Justino et al., 2010; Pechony and Shindell, 2010; Power et al., 2008). New charcoal and pollen records show increased fire occurrence in the transition to the Holocene in North America (Marlon et al., 2009; Power et al., 2010). A long-term Holocene decline in biomass burning is found in Hudson Bay charcoal sediments likely in response to the decrease in summer insolation (Hely et al., 2010). Charcoal data also show a global biomass burning decrease in the first centuries of the last millennium (Power et al., 2008), in agreement with model simulations where it is mostly driven by precipitation (Pechony and Shindell, 2010). A later increase in the 18th–19th centuries is associated to anthropogenic activities, and a posterior decline is attributed to ALCC and fire management. This is in agreement with isotopic records of CH_4 and CO_2 obtained from Antarctic firn and ice cores that show replacement of biomass burning by agricultural activities (Mischler et al., 2009; Wang et al., 2010).

For the last millennium, the CO_2 forcing associated to theALCC has been found to dominate in model simulations over the physical (albedo) changes (Pongratz et al., 2010; Pongratz et al., 2009) globally and in most regions. This carbon contribution has been hypothesized to account for increased CO_2 after 8 ka. Since AR4, new datasets are available (Gaillard et al., 2010; Kaplan et al., 2009; Olofsson and Hickler, 2008; Pongratz et al., 2008) and further investigations on the preindustrial impact of ALCC on the global carbon cycle have been conducted, with contrasting results for the early Holocene (Kaplan et al., 2011; Ruddiman, 2007; Ruddiman and Ellis, 2009; Stocker et al., 2011); see Chapter 6 for implications for the carbon cycle.

5.2.2 Radiative Perturbations from Earth System Feedbacks

[PLACEHOLDER FOR FIRST ORDER DRAFT]

5.2.2.1 Atmospheric Concentrations of CO_2, CH_4, N_2O from Ice Cores

Air trapped in polar firn and ice cores provide a direct, albeit low-pass filtered (Joos and Spahni, 2008), record of the three most important long-lived GHGs (greenhouse gas concentrations) CO_2, CH_4 and N_2O, complementing direct atmospheric measurements of these gases over the last decades (see AR5 Chapter 2). Since AR4, records of CO_2, CH_4 and N_2O variations during the last millennia have been obtained from new ice cores (Mischler et al., 2009; Siegenthaler et al., 2005) and at higher temporal resolutions (Meure et al., 2006, 2008, Orbital and millennial-scale). Centennial variations of up to 10 ppmv CO_2, 40 ppbv CH_4 and 10 ppbv N_2O occur throughout the pre-industrial period, and the onset of multi-centennial increasing trends (CH_4 and N_2O) start prior to the industrial period. Long-term records previously available back to 650 ka have now been extended to 800 ka using the Antarctic EPICA Dome C ice core (Loulergue et al., 2008; Luthi et al., 2008; Schilt et al., 2010), and hence cover eight glacial/interglacial cycles. The concentrations of the aforementioned GHGs stay within well defined natural limits with maximum interglacial concentrations of about 300 ppmv, 800 ppbv and 300 ppbv for CO_2, CH_4 and N_2O, respectively, and minimum glacial concentrations of about 172 ppmv, 350 ppbv and 200 ppbv. Current atmospheric concentrations or rates of increase are never encountered over the last 800 ky for any of the three GHGs (Joos and Spahni, 2008). The 800 ka Antarctic CO_2 record reveals long term (>200 kyr) trends in addition to glacial interglacial variations (Luthi et al., 2008), which also appear in the records of oxygen isotopic composition of air (Landais et al., 2008). The data depict strong but changing relationships between Antarctic temperature, global sea level and CO_2 (Masson-Delmotte et al., 2010a).

For certain time intervals the N_2O concentrations in ice cores are subject to *in situ* production, which is a function of level of aerosol impurities, as illustrated by a higher scatter in high-resolution records. Using the low impurity Talos Dome ice core from Antarctica, these gaps could be filled for the last glacial cycle and a stacked high-resolution record was compiled for the three major GHG (Schilt et al., 2010). These records show significant centennial variations in CH_4 and N_2O during the last glacial, which are linked to rapid glacial climate changes in the Northern Hemisphere and millennial CO_2 changes connected to their longer-term imprint in the Southern Hemisphere via the bipolar seesaw (Ahn and Brook, 2007; Ahn and Brook, 2008; Capron et al., 2010b; Grachev et al., 2009; Loulergue et al., 2008; Luthi et al., 2008; Schilt et al., 2010). These suborbital GHG variations never exceed the natural glacial/interglacial bounds. Additional information about the sources and processes related to the past GHG concentration changes is provided in AR5, Chapter 6. New records of carbon isotope variations in CO_2 ($\delta^{13}CO_2$) are also providing important constraints. For example, small δ13CO_2 decrease in late Holocene suggests that the 20 ppmv increasing trend in CO_2 is mostly due to carbonate compensation and coral reef formation (Elsig et al., 2009). A significant drop in δ13CO_2 during the last and penultimate termination points to the upwelling of old, carbon enriched deep water contributing to the concurrent CO_2 increase (Lourantou et al., 2010a; Lourantou et al., 2010b). In case of CH_4, the inter-hemispheric gradient as well as carbon and hydrogen isotopes support the role of changes in boreal and tropical wetlands in explaining most of the observed long-term and centennial changes (Bock et al., 2010; Fischer et al., 2008; Petrenko et al., 2009; Sowers, 2006; Sowers, 2010). GHG isotopes in ice cores also clearly support the anthropogenic origin of the current GHG increase (Ferretti et al., 2005; Mischler et al., 2009).

5.2.2.2 Atmospheric CO_2 Concentrations from Geological Proxy Data

The current increase in the atmospheric concentration of the GHG carbon dioxide (CO_2), from 275–285 ppmv in pre-industrial times to about 390 ppmv today, is unprecedented over the last 800 ka of recent Earth history (Section 5.2.2.1). Pre-Quaternary estimates of CO_2 concentration rely on geologic proxies, which have larger uncertainties than those based on ice cores. There are four primary proxies used for pre-Quaternary CO_2 levels (summarised (Jansen et al., 2007; Royer, 2006)): The $\delta^{13}C$ composition of soil-forming minerals (Cerling, 1991; Yapp and Poths, 1992); the $\delta^{13}C$ composition of long-chained alkenones preserved in marine sediments (Honisch et al., 2009; Pagani, 2005; Pagani et al., 2010a; Seki et al., 2010); the $\delta^{11}B$ composition of marine carbonates (foraminifera) as an estimate for ocean pH together with estimates for alkalinity [(Pearson and Palmer, 2000; Foster, 2008; Seki et al., 2010)]; and the empirical relationship between stomatal pores on tree leaves and pCO_2 (Kurschner and Kvacek, 2009; Kurschner et al., 1996; McElwain and Chaloner, 1995). Geologic CO_2 proxies indicate that while there is a wide range in reconstructed CO_2 concentrations for the last 65 Ma (million years before 1950 CE), magnitudes are generally higher than interglacial, pre-industrial values recorded in ice cores. These values ranged between; (i) about 300–600 ppmv from the beginning of the Quaternary (about 2.6 Ma) back to the beginning of the Miocene (about 24 Ma), (ii) about 600–1000 ppmv through the Oligocene back to about 33Ma, and (iii) were generally above 1000 ppmv in the Eocene.

Past Earth-system responses and feedbacks to "higher-than-pre-industrial" CO_2 levels are discussed in Section 5.3. Arguably one of the most important high-CO_2 analogues is the Pliocene (5.3 to 2.6 Ma) when continental and ocean configurations, ecosystems, and ice sheets were broadly similar to today. A number of studies have focussed on the application of CO_2 proxy techniques to the Pliocene epoch, with significant improvements in understanding of the utility of the techniques, and a general convergence towards consistent estimates, albeit still with significant uncertainties compared to ice core estimates (Figure 5.2). Previous estimates of Pliocene CO_2 concentrations ranged between 200–400 ppmv based on: 1) a few low-resolution studies of stomatal leaf density (Kurschner et al., 1996), 2) low-resolution B-isotope measurements (Pearson and Palmer, 2000), and 3) sedimentary bulk organic matter $\delta^{13}C$ determinations (Raymo and Horowitz, 1996). Recent alkenone-based estimates of CO_2 concentrations, based on studies of a diverse suite of marine sediment cores and that, constrain potential biases in phytoplankton ecology, indicate peak Pliocene values between about 365–415 ppmv (Pagani et al., 2010a). A multiproxy analysis of alkenone $\delta^{13}C$ and boron-based CO_2 methods applied to the same ocean sediment core, also provides consistent reconstructions for CO_2 values, that are 50–120 ppmv higher during the Pliocene compared to pre-industrial levels (about 280 ppmv) and comparable to present day-levels (about 390 ppmv) (see Figure 5.3). A 2 Ma long boron-based CO_2 reconstruction from the eastern equatorial Pacific ocean overlaps the ice core record with sufficient resolution to directly compare geologically derived proxy data with ice core CO_2 measurements (Honisch et al., 2009). Although errors (±25 ppmv) are larger for the boron-based estimates, mean values are in close agreement with glacial-interglacial range of CO_2 for the last 800 ka from the ice core records.

[INSERT FIGURE 5.2 HERE]

Figure 5.2: [Radiative perturbations from Earth-system feedbacks since the Pliocene] Radiative perturbations and Earth systems and its response for the last 3.6 Ma. Changes in orbital parameters, a) eccentricity, b) obliquity, d) precession, e) summer insolation at 65°N, and c) integrated summer insolation (calculated for 75°N will replace with 65°N) (Laskar, 2004; Huybers and Raymo, 2007). f) Stacked marine benthic oxygen isotope record, reflecting changes in continental ice volume and ocean temperature ($\delta^{18}O$, ‰; Lisiecki and Raymo, 2005) converted to changes in global mean sea level (m; Naish and Wilson, 2009). Pink shaded curve is based on sea level calibration of δ18O curve using dated coral shorelines (Waelbroeck et al., 2002), green dashed line is the Red Sea sea level record (Siddall et al., 2003; Rohling et al., 2009), (to be added Bintanja et al. 2005 model derived calibration back 5 Ma) and red dots with error bars are weighted mean estimates (using individual standard deviations as weights) for far-field reconstructions of eustatic peaks during mid-Pliocene interglacials (Miller et. al in review, placeholder at present). The dashed horizontal line represents present day sea level. g) Antarctic ice volume simulation (Pollard and DeConto, 2009) expressed as sea level (m) equivalent ice volume and volume (km^3) w.r.t present day (dashed line). h) Stacked tropical SST (dashed line is modern average zonal temperature;°C; Herbert et al., 2010). i) Sortable silt grain size proxy for Pacific abyssal ocean current strength (μm; ODP Site 1123, Hall et al., 2001). j) Wind proxy derived from mass accumulation rates of Chinese loess (g/cm3/ka, brown line; Song et al., 2007) and with EPICA Dome C dust record (ng/g, blue line; Lambert et al., 2008) overlain. k) Atmospheric CO_2 concentration (ppm) measured from EPICA Dome C ice core (black line; Lüthi et al., 2008), and estimates of atmospheric CO2 conent (ppm) from boron $\delta^{11}B$ isotopes in formainifera in marine sediments (grey shaded line, Seki et al., 2010; green shaded line Hönisch et al., 2009), and from organic biomarker alkenone-derived carbon isotope proxies (pink shaded line, Seki et al., 2010; orange, blue and yellow shaded lines Pagani et al., 2010). Note that thickness of shaded line represents the error envelope. Red dashed line = preindustrial atmospheric CO_2 content (1830 AD) and black dashed line = present-day CO_2 (2010).

5.2.2.3 Past Changes in Mineral Dust Aerosol (MDA) Concentrations

MDA subject to long-range transport has a size-dependent atmospheric residence time on the order of day to weeks (see also Chapter 7). Large spatial and temporal fluctuations in atmospheric MDA concentrations make difficult an assessment of the global radiative forcing linked with past MDA changes.

The currently available records of past dust deposition from natural archives provide regional estimates of relative changes in atmospheric MDA concentration, such as the detection of a sharp increase in Sahara dust emissions at the beginning of the 19th century, attributed to human activities linked with agriculture in Sahel [Mulitza et al., 2010]. Global data synthesis is so far only available for the Last Glacial Maximum (LGM) from the DIRTMAP project (Derbyshire, 2003; Maher et al., 2010b).

The dust concentration in Greenland ice cores shows only small preindustrial variations but 1–2 orders of magnitude higher concentrations during glacials and stadial with respect to interglacials and interstadials, due to changes in Asian deserts dust sources, atmospheric dust aerosol lifetime and transportation (Fischer et al., 2007a). A strong coherence is also observed between glacial millennial variability in Greenland dust records and aeolian deposition in European loess, possibly linked with changes in atmospheric dynamics (Antoine et al., 2009).

Ice core records from central Antarctica show a similar picture with dust concentrations being rather constant over the Holocene but enhanced by a factor 50–70 during the last glacial period (Fischer et al., 2007b; Petit and Delmonte, 2009). This enhanced deposition is due to reduced glacial accumulation rates, to the enhancement of glacial dust production in southern South America and to a lesser extent Australia (De Deckker et al., 2010; Vallelonga et al., 2010) and possibly to a change in atmospheric lifetime (Delmonte et al., 2008; Marino et al., 2009). Atmospheric dust load over high southern latitudes was likely enhanced by a factor 10; spatial gradients amongst various Antarctic ice cores indicate regional west-east gradients downwind of dust sources (Fischer et al., 2007a). Glacial-interglacial central Antarctic dust deposition changes are systematically observed during the last 800,000 years, corroborating a tight coupling between Antarctic atmospheric dust flux and climate (Lambert et al., 2008b; Röthlisberger et al., 2008).

For low latitudes, scarse quantitative information is available on MDA fluxes. Calibrated records show a threefold decline of MDA fluxes from western to eastern equatorial Pacific and a similar temporal evolution over the last 500,000 years as found in the Antarctic ice cores (Winckler et al., 2008a). However, glacial-interglacial MDA ratios only vary by a factor of 3–4, much smaller than in Antarctica, pointing to enhanced glacial dust emissions from Asian and northern South American dust sources (Maher et al., 2010b), possibly linked with increased gustiness (McGee et al., 2010).

Dust modelling within an atmospheric model suggests 88% enhanced glacial dust loading associated with a global radiative forcing of 1 W m^{-2} (Mahowald et al., submitted), smaller than some earlier estimates (Kohler et al., 2010).

5.3 Earth System Responses and Feedbacks at Global and Hemispheric Scales

[PLACEHOLDER FOR FIRST ORDER DRAFT]

5.3.1 High CO_2 Worlds and Temperature

Reconstructions of Cenozoic global mean surface temperatures remain challenged by the limited number, and biased geographical distribution, of proxy surface temperature data. Since AR4 further proxy development, and the application of multiple proxy methods at higher temporal resolution, have provided a more detailed description of atmospheric composition and climate. The available data and simulations indicate that climates prior to 3 Ma were generally warmer than today and associated with higher pCO_2 levels (Figure 5.3). Temperature reconstructions based on foraminiferal oxygen isotopes and Mg/Ca ratios, and organic geochemical methods using lipid biomarkers such as alkenones and TEX_{86} show a long-term decrease in surface temperatures from an estimated global average temperature of about 26°C above pre-industrial in the early Eocene (about 50 Ma) to a pre-industrial Holocene average surface value of about 14°C. This temperature decrease is associated with a decline in atmospheric pCO_2 from >1000 ppm in Early Cenozoic (65–33Ma) to pre-industrial levels reached around 2.6 Ma (Pagani et al., 2005; Pearson and Palmer, 2000).

The early Eocene (56–48 Ma) encompasses the warmest climates of the past 65 myrs. Estimates of mean annual sea surface temperatures are depict a world with greatly reduced meridional temperature gradients (Figure 5.3; [Wolfe, 1995, PALEOCLIMATIC; Barron, 1987, Eocene; Huber, 2011, The early Eocene equable climate problem revisited, Clim. Past Discuss.]). Refinements and improvements to the suite of paleotemperature proxies (Huber and Sloan, 2001; Pearson et al., 2007; Pearson et al., 2008; Pearson et al., 2001; Schrag, 1999; Schrag et al., 1995) and the development of new organic geochemical SST proxies such as TEX86 and Mg/Ca [(Schouten et al., 2002, 2003; Pearson et al., 2007; Lear et al., 2008; Sexton et al., 2006; Sluijs et al., 2006, 2007, 2008; Liu et al., 2009). SSTs of 35°C have been reconstructed in the early Eocene tropics (Lear et al., 2008; Liu et al., 2009a; Pearson et al., 2007; Schouten et al., 2002; Schouten et al., 2003; Sexton et al., 2006; Sluijs et al., 2008; Sluijs et al., 2007; Sluijs et al., 2006). Extratropical SSTs have also been reconstructed with values about 10°C warmer than terrestrial temperature proxies of similar altitude (Figure 5.3.; Bijl et al., 2009; Creech et al., 2010; Eldrett et al., 2009; Hollis et al., 2009; Liu et al., 2009a; Sluijs and Brinkhuis, 2009; Sluijs et al., 2006; Zachos et al., 2006). The available data depict a reduced latitudinal temperature gradient, which climate models have had difficulty in reproducing without prescribing unrealistically high CO_2 levels. This has raised questions over both the validity of the proxies, especially in high latitudes, and models which may not fully capture feedbacks important to warmer climates. A recent AOGCM simulation prescribing about 4500 ppm CO_2 (upper range of proxy CO_2 reconstructions; Jansen et al. (2007) demonstrates a close agreement with a terrestrial MAT surface temperature data set, where the model reproduces both the reduced seasonality and polar amplification implied by the data (Figure 5.3; [Huber, 2011, The early Eocene equable climate problem revisited, Clim. Past Discuss.]).

While it has been hypothesised that long term changes in CO_2 concentrations have been attributed to tectonic changes affecting the silicate weathering cycle (e.g., [Ruddiman, 1997]), a number of cooling events occur as more rapid steps paced at orbital-scale, and these punctuate Earth's long term Cenozoic cooling trend. Much like the ice core records of the last 1 Ma, these temperature perturbations appear coupled with changes in CO_2 concentrations. However, unlike the glacial-interglacial CO_2 fluctuations of the last 1 Ma, the amplitude of the perturbation is larger, up to 400 ppm (Pearson et al., 2009).

An abrupt SST (sea surface temperature) cooling of 5°C (Liu et al., 2009a) is associated with widespread glaciation of Antarctica between 34 to 33 Ma (Coxall et al., 2005; Katz et al., 2008), likely occurred as a response to declining CO_2. Modelling studies suggest that cooling and ice sheet formation may have been triggered when atmospheric CO_2 fell below a critical threshold of about 750 ppm (DeConto and Pollard, 2003; DeConto et al., 2008). A high-resolution boron-isotope based reconstruction confirms the decline in CO_2 of about 400 ppm to a central value of about 760 ppm occurred within a few hundred thousand years, and before the main phase of ice growth (Pearson et al., 2009). Coupled ice sheet and climate model simulations suggest that during this time CO_2 levels were above the threshold for Northern Hemisphere ice sheet formation (about 280 ppm) (DeConto et al., 2008).

Proxy-based estimates of CO_2 fell to pre-industrial levels around 24 million years (Pagani et al., 2005) and have remained relatively constant since then, with the exception of Middle Miocene Climatic Optimum (MMCO) (17–14 Ma) and the Pliocene Climatic Optimum (PCO) (5–3 Ma), when CO_2 concentration was aroundabout 400 ppm. In the case of the MMCO, stomatal density proxy data imply a range of 400–600 ppm (Kurschner et al., 2008), and SST reconstructions, while few in number, indicate an average surface temperature between 3 to 5°C above preindustrial levels. Earth´s climate during PCO is better constrained by both proxy data and modelling; CO_2 estimates (discussed Section 5.2.2.2) were about 400 ppm. Both terrestrial and marine paleoclimate proxies show that high latitudes were significantly warmer, but that tropical SSTs and surface air temperatures were little different to present. The result was a substantial decrease in the latitudinal surface temperature gradient (Figure 5.3). In contrast a coupled OAGCM simulation with a CO_2 concentration of 400 ppm produced warming of +3–5°C in the north Atlantic , and 1–3°C in the tropics (Haywood et al., 2005). High-latitude Southern Hemisphere SST proxies are more sparse but indicate near surface warming of 3–5°C (Martinez-Garcia et al., 2010).

The Pliocene intensification of Northern Hemisphere glaciations (culminating at 2.75 Ma) (Kleiven et al., 2002; Lisiecki and Raymo, 2007) also appears to coincide with another global cooling step starting at 3.2 Ma in SST records (e.g., Herbert et al., 2010a; Ravelo, 2010) associated with a about 100 ppm drawdown of CO_2 to preindustrial levels between 3.2–2.8 Ma (Seki et al., 2010), further affirming the link between temperature, CO_2 and ice volume (discussed further in Section 5.4.1).

[PLACEHOLDER FOR FIRST ORDER DRAFT: New SST data from Ross Sea–ANDRILL Project and IODP 318 Wilkes LandPliocene model data comparison (e.g., issues with simulating high-latitude warming, no change in tropics without increased oceanic heat transport ... hurricane hypothesis … Federov and Brierley).]

[PLACEHOLDER FOR FIRST ORDER DRAFT: Section on climate sensitivity implications of MMCO, and particularly PCO, pCO_2 and global av temp reconstructions (e.g., Lunt et al., and Pagani et al., 2010).]

[INSERT FIGURE 5.3 HERE]

Figure 5.3: [PLACEHOLDER FOR FIRST ORDER DRAFT: Meridional temperature distribution for different geological times. Notes on draft of figure: The aim of this figure is to assess changes in meridional temperature gradients based latitudinal temperature profiles and temperature anomalies for LGM, modern (pre-industrial), last interglacial, warm early-mid Pliocene (time interval 3.5–3.0 Ma), and Eocene (4–50Ma) using both, model output (e.g., PMIP, PlioMIP, GSSM etc.) and recontructions. The quality and quantity of the paleotemperature data obviously decreases back in time. In draft Figure 5.3 for LGM, MARGO data (not gridded and zonally biased) and data-constrained model output from Paul and Schäfer-Neth (2003) have been used. Data for the last interglacial is from a compilation by Rohling et al. (in review), and Turney and Jones (2009). Also present day has been plotted from PRISM, AMIP and WOA. Pliocene curve is data-constrained PRISM3 (Dowsett 2007). Brierley et al. (2009), showing expanded Pacific warm pool during Pliocene because of issues with corrections made to proxy data from different times in the Pliocene and different ocean basins has not been used. For the Eocene there is Bijl et al. (2009) data for 40 and 50 Ma and model output from Huber and Cabellero (2010). The latter provides GCM surface temperature for an atmospheric CO_2 concentration of 4480 ppm and compares with a compilation of terrestrial proxy temp data, but ignores the SST data due large discrepancies and perceived issues with and between marine temperature proxies. While there appear to be vast differences in temperatures from the same latitudes and even the same sites using different paleothermoters (e.g., TEX86 vs Mg/Ca; summarised in Huber (2008) and Huber and Cabellero (2010)) SST proxies for the Eocene are undergoing further the development and may yield more reliable estimates within the AR5 time frame. Uncertainties are not yet included in draft; for the final version it foreseen to represent the density of data on each curve as a guide to uncertainty. There are a number of issues to work through with data presentation on this figure including: (1) Standardisation of approach (e.g., land and ocean data or just SSTs, whether to plot zonally averaged proxy data that might be heavily biased by distribution, or data constrained model output, or model data and site specific proxy data independently?). At present the figure represents a range of different approaches. (2) Representing data quality and density. (3) Combining data over a wide temporal range particularly in deeper time slices. (4) Seasonal and spatial biases. (5) Standardised of modern temp gradients for calculating the anomaly. It will take a community effort to bring these datasets together both in the model inter-comparison and proxy communities. The LGM will be covered, but MARGO lacks terrestrial data. Last interglacial data needs more critical assessment (such an effort is underway as part of the European Past4Future Project). The PlioMIP and PRISM communities are well organised. The Paleogene proxy community are aware of the issues and Eocene model inter-comparisons are underway.]

[START BOX 5.1 HERE]

Box 5.1: Polar Amplification

Instrumental temperature records show that the Arctic (Bekryaev et al., 2010) and the Antarctic Peninsula [(Turner et al., 2005; Turner et al., 2009)] are experiencing the strongest warming trends (0.5°C per decade over the past 50 years), almost twice larger than for the hemispheric or global mean temperature [(IPCC, 2007)]. West Antarctic temperature also displays a warming trend of about 0.1°C per decade over the same time period (Steig et al., 2009; [Reference needed: O'Donnell et al., ?]). A number of mechanisms can produce larger magnitudes of polar temperature changes compared to mid or low latitudes. These mechanisms involve the dynamics and variability of atmosphere (Alexeev et al., 2005; Serreze and Francis, 2006) and the ocean-sea ice system (Chylek et al., 2009; Polyakov et al., 2010; Semenov et al., 2010; Spielhagen et al., 2011b), as well as local radiative feedbacks linked with snow (Ghatak et al., 2010), ice albedo, water vapour, clouds (Graversen and Wang, 2009; Screen and Simmonds, 2010), and land surface vegetation changes (Bhatt et al., 2010). Each of these mechanisms has specific fingerprints in the seasonality, latitudinal and vertical structure of temperature changes. Detection/attribution studies conducted for the Arctic and Antarctic (Gillett et al., 2008) concluded that human influence dominated the recent polar warming.

When forced by increasing concentrations of atmospheric greenhouse gases, climate models consistently simulate strong polar amplification [(Polyakov et al. 2002; Holland and Britz, 2003; Bengtsson et al. 2004; Serreze and Francis, 2006; Serreze et al., 2007; IPCC, 2007, Miller et al., 2010; Masson-Delmotte et al., 2005)]. Simulated temperature increases in high latitudes exceed those at low latitudes by factors ranging from two to four [(Holland and Britz, 2003; Miller et al., 2010)]. There are however differences, among different models in their depiction of the time evolution, and magnitude of projected Arctic sea ice (Holland et al., 2010), Antarctic (Bracegirdle et al., 2008) and Arctic surface air temperature changes [(IPCC, 2007)]. The magnitude of polar amplification is also a concern due to its impacts on polar ice sheet stability and sea level (see AR5 Chapter 13) and for the carbon cycle feedbacks for instance linked with permafrost melting (see AR5 Chapter 6).

Past climates allow model-data comparisons for latitudinal temperature changes and polar amplification under different climate states, such as high CO2 worlds, glacial and interglacial climates. However, it should be noted that these past climate states correspond to different boundary conditions and forcings. The presence of glacial ice sheets induces a large radiative perturbation at high northern latitudes. During past interglacials, orbital forcing induces large changes in seasonal and latitudinal distribution of insolation, without significant changes in global mean radiative forcing and temperature. Figure 5.3 provides estimates of latitudinal surface temperature anomalies for different time slices during the last 65 million years (MH, LGM, LIG, Mid Pliocene and early Eocene) with respect to the pre-industrial period. A difficulty in developing these temperature anomaly comparisons is that for most intervals only a limited number of sites are available with quantitative estimates of past temperatures, and the vast majority of these sites reflect most likely summer temperature estimates. Commonly hemispheric anomalies during warmer times are generated using climate models driven by known forcings, or by using data constrained model output approaches [(Dowsett et al, 2005, 2007; Huber and Caballero, 2011; Masson-Delmotte, 2005]; Otto-Bliesner, 2009). For the early Eocene anomalies shown in Figure 5.3, the simulated hemispheric anomalies are broadly consistent with paleoclimate proxy data, but prescribed higher pCO_2 (4500 ppm) concentrations are at the upper boundary of the range implied by Eocene pCO_2 proxy data.

SSTs of 35°C have been reconstructed in the early Eocene tropics [(Pearson et al., 2001b, 2007; Tripati et al., 2003; Tripati and Elderfield, 2004; Zachos et al., 2003)] with a global mean annual surface temperature of 25–28°C [(Huber and Caballero, 2011)]. Significantly warmer extratropical SSTs have also been reconstructed with values about 10°C warmer than terrestrial temperature proxies of similar latitude (Figure 5.3; [Bijl et al., 2009; Sluijs et al., 2006, 2009; Zachos et al., 2006; Hollis et al., 2009; Creech et al., 2010; Liu et al., 2009; Eldrett et al., 2009, Huber and Caballero, 2011]). The available Eocene data-model comparisons depict a reduced latitudinal temperature gradient (also see Section 5.3.1).

Global reconstructions of mid-Pliocene proxy data and general circulation models show an average warming of +4 ± 2°C, with greater warming over land than oceans, and both terrestrial and marine paleoclimate proxies indicate that high latitudes were likely warmer by up to +5°C in the Antarctic and +10°C in the Arctic, but that tropical SSTs and surface air temperatures were little different to present (Figure 5.3; [Budyko et al.,1985; Chandler et al.,1994a; Raymo et al.,1996; Sloan et al.,1996; Dowsett et al.,1999; Haywood and Valdes, 2004, 2006; Jiang et al., 2005; Dowsett et al., 2007; Salzmann et al.,2008]). While only limited data are available for the southern high latitudes, mid-Pliocene SSTs of +4–6°C are reported form organic biomarker temperature proxies applied to drill cores from the Ross Sea and Southern ocean [PLACEHOLDER FOR FIRST ORDER DRAFT: Publications from IODP Leg 318 and ANDRILL].

During the LIG, ice core data [(Masson-Delmotte et al., 2010)] and SSTs [(Rohling et al., in press; Turney and Jones, 2010)] imply polar warming of +2–5°C, with little or no change in 'global' mean annual surface temperature during the LIG. Climate model simulations forced only by changes in orbital configuration underestimate the level of Antarctic and Greenland warming implied by data; this may be linked with missing glaciological feedbacks [(Holden et al., 2010)] (see Section 5.3.4). [PLACEHOLDER FOR FIRST ORDER DRAFT: Publications from the PAST4FUTURE project including model-data comparisons for the LIG].

Coupled-ocean atmosphere model intercomparisons (PMIP1 and 2) simulate warming of about 1°C in Antarctica and Greenland during the Mid-Holocene climatic optimum (MH; c. 6 ka) [Masson-Delmotte et al. (2006)] are generally consistent with ice core based estimates, although they underestimate warming recorded in Greenland ice cores [(Vinther et al., 2009)]. Mean annual changes in global temperature are also negligible during the Mid-Holocene and LGM simulations.

During the LGM, PMIP2 models do simulate the 8–10°C magnitude of central Antarctic cooling (about twice the global mean temperature change) but questions remain regarding the prescribed ice sheet topography (Masson-Delmotte et al., 2010a). The same simulations underestimate the magnitude of Greenland cooling compared to ice borehole data (Dahl-Jensen et al., 1998), possibly because of missing dust and vegetation feedbacks. [PLACEHOLDER FOR FIRST ORDER DRAFT: PMIP3 comparisons using different LGM ice sheet reconstructions].

[PLACEHOLDER FOR FIRST ORDER DRAFT: DO events which have large magnitude of centennial greenland warming with possible discussion of sea ice and other fast feedbacks.]

[END BOX 5.1 HERE]

5.3.2 Glacial Climate Sensitivity and Feedbacks

Glacial climates have been studied to better understand large magnitude changes in climate, validate climate model results, and estimate the climate sensitivity. The best documented glacial episode is the Last Glacial Maximum (LGM), centered at around 21ka. The LGM is known to be relatively stable, the signal of the response is large enough compared to the internal variability and uncertainties in the proxy calibrations and dating, and both the response and the forcing (see Section 5.2) are clearly identified in reconstructions (Braconnot et al., 2007b; Braconnot et al., 2007c). Numerous new reconstructions have been completed since the AR4. Proxies used in glacial climate reconstructions include isotope-based temperature proxies in Antarctic ice cores (Masson-Delmotte et al., 2008) and ocean circulation, temperature, and salinity proxies (Butzin et al., 2005; Tagliabue et al., 2009). The MARGO sea surface temperature reconstruction (Waelbroeck et al., 2009), the most recent synthesis of the LGM SST, employed multiple proxy approaches to revise and refine previous synthesis efforts such as CLIMAP and GLAMAP (Sarnthein et al., 2003a; Sarnthein et al., 2003b) These LGM temperature reconstructions indicate a mean global temperature decrease of 5°C, with a tropical decrease in temperature of about 2°C (Waelbroeck et al., 2009), a decrease in Antarctic temperatures of about 10°C [(Stenni et al, 2010)], and much larger decreases of Greenland temperature of 20–25°C (Kohler et al., 2010; Rohling et al., 2009; Siddall et al., 2010b). The overall pattern of reconstructed tropical SST during the LGM generally is well simulated by atmosphere-ocean coupled GCMs except in regions of tropical upwelling, regions that also have biases in simulations for the present-day (Otto-Bliesner et al., 2009). In addition, questions remain regarding the temperature simulation of Antarctica, which may be the result of overestimation of ice sheet topography, an important boundary condition to the models (Masson-Delmotte et al., 2008). New ice sheet reconstructions based on several different methods [(Lambeck et al., 2010; Peltier et al., 2010; Tarasov et al., 2007)] are introduced for PMIP3 climate model simulations, which are underway and the results of which may help clarify the relation between polar and global temperatures. [PLACEHOLDER FOR FIRST ORDER DRAFT: PMIP3 results.]

Climate sensitivity is estimated or constrained in three fundamental ways ((Edwards et al., 2007), see also Chapter 9). First, climate sensitivity is estimated using both the radiative forcing and climate response to a change of CO_2. In this method, there is an important assumption; i.e., the climate response to a certain amount of radiative forcing is the same even under different climate states (warm or cold climate), even though there is no guarantee that the climate sensitivity is symmetric. Second, multi-model simulations have been constrained by proxy data, including models having structural differences, to show that the ratio of model climate sensitivity (LGM vs $2 \times CO_2$) ranges from 0.6 to 2, which is mainly dependent on the cloud feedback through short wave radiation (Crucifix, 2006) (see Figure 5.4). Dust and vegetation are in many cases not included in these model runs because there is still an uncertainty in their radiative forcing, (Lambert et al., 2008a; Maher et al., 2010a; Mahowald et al., 2006; McGee et al., 2010; Takemura et al., 2009; Winckler et al., 2008b), hence climate sensitivity is more likely overestimated than underestimated. At least, the multi-model constrained by proxy data tend to reject the possibility of large climate sensitivity for future climate. Third, the physics perturbed ensemble method using a single climate model is used (Hargreaves et al., 2007), which shows that cloud feedback even without large ice sheet change brings about the asymmetric temperature response for warm and cold climate with a ratio of about 0.82 (±0.14) (Figure 5.4, [Yoshimori et al., 2011)]. [PLACEHOLDER FOR FIRST ORDER DRAFT: Comparison of short wave and long wave feedback processes of multi-models in PMIP3.]

[PLACEHOLDER FOR FIRST ORDER DRAFT: Changes in LGM AMOC and atmospheric circulation including storm tracks and westerlies.]

[INSERT FIGURE 5.4 HERE]

Figure 5.4: [PLACEHOLDER FOR FIRST ORDER DRAFT: Strengths of feedbacks at LGM from data and multi-model ensembles. This is just an illustration, it will be replaced when additional new experiments by PMIP3/CMIP5 become available.] Relation of feedback parameters between elevated CO_2 and LGM climate simulations: a) scatter plot of climate feedback parameter (i.e., stratosphere-adjusted radiative forcing / equilibrium temperature change) between CO_2 doubling and LGM (or LGMGHG) experiments. Here LGMGHG refers to the experiment with CO_2 concentration being lowered to the LGM level from the pre-industrial reference experiment; b) scatter plot of shortwave cloud feedback parameter (i.e., shortwave component of feedback parameter attributable to the change in clouds); c) individual feedback parameters. In a) and b), red, blue, and green markers indicate coupled atmosphere-ocean GCMs, LGM experiments with atmospheric GCMs coupled to slab ocean models, and LGMGHG experiments with atmospheric GCMs coupled to slab ocean models, respectively. Also plotted are the one-to-one lines. In c), WV, LR, A, CSW, CLW denote water vapor, lapse-rate, surface albedo, shortwave cloud, and longwave cloud feedbacks, respectively. ALL denotes sum of all feedbacks. $R^2 \times CO_2$ indicates $\sqrt{2}$ times CO_2 experiment, and LGMICE refers to the experiment in which ice sheets and orbital configuration at LGM are applied to the reference experiment.

5.3.3 Earth System Response to Orbital Forcing During Glacial-Interglacial Cycles

Antarctic ice cores remain a significant source of information on orbital-scale climate variations over the past 800 ka (Jouzel et al., 2007; Landais et al., 2010; Loulergue et al., 2008; Wolff et al., 2010). New datasets of atmospheric composition from Antarctic ice cores have helped to determine the magnitude and time-evolution of global radiative forcings, providing constraints on past climate sensitivity (Kohler et al., 2010) and carbon cycle-climate feedbacks (Lemoine, 2010). Antarctic ice-core data reveal a strengthening of the interglacial-glacial amplitude around to 400 ka, as well as a change in the relationship between Antarctic temperature and radiative forcing by GHG (Masson-Delmotte et al., 2010a; [Lang, in revision]; Figure 5.5). Orbital-scale variability in GHG concentrations in Antarctica over the last several thousand years correlate well with proxy climate records including reconstructions of global ice-volume (Lisiecki and Raymo, 2007), climatic conditions in central Asia (Prokopenko et al., 2006), biogeochemical conditions in the North Pacific (Jaccard et al., 2010) and other regions, Southern Ocean surface temperatures (Pahnke et al., 2003; [Lang and Wolff, 2011]), deep ocean temperatures (Elderfield et al., 2010), and deep ocean ventilation (Lisiecki et al., 2008). A detailed physical understanding of these teleconnections and their relationship to direct greenhouse gas forcing or the remote effects of Northern Hemispheric ice-sheets is still lacking.

Speleothem records from caves have become a powerful tool to reconstruct long-term changes of hydroclimate. In some East Asia regions, precessional cycles dominate the monsoon signal (Clemens et al., 2010; Wang et al., 2004; Wang et al., 2008), whereas other regions experience stronger variability on about 100 ka glacial-interglacial timescales (Bar-Matthews et al., 2003). Furthermore, it has been shown that winter and summer monsoons in Southeast Asia, experience different phase lags with respect to the precessional cycle (Clemens et al., 2010) raising questions as to the physical forcing mechanisms of monsoon variability on these timescales.

Recent modeling work provides support for the notion that variations in Earth's orbital parameters produce considerable effects on Earth's climate. In particular, in the high latitudes of the Northern Hemisphere, summer temperatures can differ by up to 10°C between climate states corresponding to different orbital configurations. The largest changes in seasonal variations are caused by changes in precession, while changes in obliquity cause synchronous variations in annual temperatures in high latitudes of several degrees [(Broccoli et al., in press)]. GCM experiments support the principal assumption of Milankovitch theory that a reduction in summer insolation produces sufficient cooling to initiate ice sheet growth (Vavrus et al., 2008). EMIC experiments, which incorporate ice sheet models, demonstrate that the rate of growth of the ice sheets during glacial inception is of the right order of magnitude. Together with fast climate feedbacks amplifying the direct effect of the orbital forcing, vegetation [(Calov et al., 2005)] and oceanic feedbacks might also play an important role. It was proposed that the impact of aeolian dust deposition on snow and ice albedos may restrict ice sheet growth in areas with high rates of dust deposition (Krinner et al., 2006).

Obliquity changes, by modulating the annual mean polar insolation in both hemispheres synchronously, play an important role in pacing glacial terminations (Drysdale, 2009; Huybers and Wunsch, 2005; Schulz and Zeebe, 2006). In particular during the early Pleistocene relatively weak glacial cycles occurred on the 41 ka obliquity timescale. But during the late Pleistocene, not every obliquity cycle triggered a glacial termination and the timing was also influenced by precessional forcing [(Cheng, 2009; Huybers, 2011)] in combination with eccentricity (Berger and Loutre, 2004; Lisiecki, 2010). The role of orbital forcing in driving Southern Hemispheric glacial-interglacial variability remains the topic of debate. The excellent correlation between boreal summer insolation (Kawamura et al., 2007), length of the austral summer season (Huybers, 2009; Huybers and Denton, 2008) and austral spring insolation (Stott et al., 2007; Timmermann et al., 2009) has made it difficult to attribute the reconstructed temperature variations in Antarctica to any one of these forcings. One common feature of these suggested mechanisms is that their respective orbital forcings start to increase prior to the reconstructed changes in atmospheric CO_2 and may hence provide a pacemaker for orbital-scale carbon-cycle climate feedbacks in the Southern Hemisphere.

Antarctic temperatures closely follow atmospheric CO_2 concentration during glacial cycles, which reflects the fact that CO_2 explains a large portion of glacial-interglacial temperature variations in Antarctica (Timmermann et al., 2009), although there is also a local response of the annual temperature to obliquity and presessional variations (Huybers and Denton, 2008). At the same time, during most recent terminations, Antarctic temperature changes lead CO_2 changes [(Siegenthaler, 2005)]. This early Antarctic warming compared to CO_2 rise can be explained by the bipolar seesaw response to a weakening of the AMOC during glacial terminations (Ganopolski and Roche, 2009) and by the above mentioned response to orbital forcings.

Experiments performed with climate-ice sheet models forced by orbital variations and CO_2 demonstrate that the models are able to simulate ice volume and other climate characteristics during the last and several previous cycles in agreement with paleoclimate data (Abe-Ouchi et al., 2007; Bonelli et al., 2009; Ganopolski et al., 2010; Figure 5.5). Moreover, in agreement with earlier simulations of glacial cycles [(Pollard, 1988)], it has been shown that 100 kyr cyclicity can be simulated with a constant CO_2 concentration, if the latter is below some critical value. However, the magnitude of 100 kyr cyclicity with constant CO_2 is smaller than observed. Therefore, CO_2 plays an important role in amplification of the glacial cycles, but how this positive feedback operates during different stages of glacial cycles is not yet well understood.

Major bipolar glacial cycles began around 2.7 Ma and temporal dynamics of ice volume variations change considerably from earlier to late Pliocene (Lisiecki and Raymo, 2007). In particular, the dominant periodicity of the glacial cycles changed from 40 ka to 100 ka around 1 Ma (the so-called Mid Pleistocene Transition, MPT). The lack of appreciable precessional variability in marine sediment records prior to the MPT poses a problem for classical Milankovitch theory. Several alternative hypotheses explaining the absence of a precessional component in the 40-kyr world were proposed (Huybers, 2006; Raymo et al., 2006) but remain to be tested with climate-ice sheet models. Recent modelling results [(Ganopolski and Calov, submitted)] indicate that such a transition can be caused both by a gradual lowering of the atmospheric CO_2 concentration (reference) and the removal of the terrestrial sediments from the northern part of North America [(Clark and Pollard, 1998)].

[INSERT FIGURE 5.5 HERE]

Figure 5.5: Orbital, climate, ice sheets, carbon: data and transient model. Variation of climate forcings and climate indicators over the past 800 ka. a) Orbital forcing (maximum summer insolation at 65°N) , b) the atmospheric concentration of CO_2 from Antarctic ice cores, c) Antarctic temperature reconstructed from deuterium, d) Greenland temperature reconstructed from $\delta^{18}O$, e) the stack of benthic $\delta\ ^{18}O$, a proxy for global ice volume and deep ocean temperature, f) the reconstructed sea level, g) the stack of benthic $\delta^{13}C$ in the deep Atlantic, a proxy for the deep ocean ventilation, h) the dust concentration in the Antarctic ice core.

Colour lines represent forcings and proxy data, grey dashed lines depict results of simulation with an Earth system model forced by variations of the orbital parameters and the atmospheric concentrations of the major greenhouse gases. Note the change of the time scale at 125 ka.

5.3.4 Variability Within and Between Interglacials

Quantitative reconstructions and modeling of interglacial climates are of particular interest in a light of the anthropogenic warming and natural climate system development. The temperature and moisture evolution for the current (MIS1/Holocene) interglacial has been established for different regions and selected time-slices (e.g., Bartlein et al., 2010; Jansen et al., 2007; Litt et al., 2009; Tarasov et al., 2009; Wanner, 2008) using multi-decadal- to annual-resolution proxy records. A new synthesis of Greenland ice core data reconstructs a homogeneous Greenland early to mid Holocene warm period with annual mean temperature 2–3°C higher than pre industrial, as well as significant changes in ice sheet topography (Vinther et al., 2009).

Terrestrial data point to a generally warmer-than-present Last Interglacial (LIG) in northern Eurasia and Alaska, particularly during the Arctic summer (Allen and Huntley, 2009; Allen and Sherwood, 2007; Anderson et al., 2006; Rousseau et al., 2007; Tarasov et al., 2005; Velichko et al., 2008). Pollen analyses from nearby marine cores suggest a smaller Greenland Ice Sheet based on the abundance of boreal forest pollen (de Vernal and Hillaire-Marcel, 2008). Segments from Summit and NorthGRIP ice cores show a larger anomaly in stable isotopes than during the early Holocene (Masson-Delmotte et al., 2010a). Pollen, macrofossil and cave speleothem records have been interpreted to indicate stronger NH and weaker SH summer monsoons (Cheng et al., 2009; Rohling et al., 2002; Wang et al., 2004). Debate continues, though, on the attribution of changes indicated by water isotope proxy records to precipitation, temperature, and advective effects (Clemens et al., 2010; Herold and Lohmann, 2009; LeGrande and Schmidt, 2009). Warmer than present day during the early LIG (2–5°C) in Antarctica (Guiot et al., 2009; Sime et al., 2009) [also during the early Holocene (1–2°C) (Verleyen et al., 2011)] may be linked with bipolar seesaw events at the end of NH deglaciation (Holden et al., 2010; Masson-Delmotte et al., 2010a; Stenni et al., 2011). Because of the out of phase behavior at high northern and southern latitudes, these events cannot be interpreted as indicators of global mean temperature.

[PLACEHOLDER FOR FIRST ORDER DRAFT: Discussion of marine records and sea ice to be added.

Climate models forced by orbital forcing capture the sign of the overall temperature and precipitation changes at the LIG but with some notable exceptions (Figure 5.6). The magnitude of the observed Greenland and northern Eurasia warming is not well simulated (Masson-Delmotte et al., 2010a). The underestimation of high northern latitude regional warming may be related to simulations not including natural land surface changes (Schurgers et al., 2007) and/or current models not all consistently capturing fully changes in clouds, sea ice, and large-scale circulation that could amplify the warming (Fischer and Jungclaus, 2010; Groll and Widmann, 2006; Kaspar et al., 2007; Kim et al., 2010). In response to orbital forcing only, they also produce no significant annual mean change in central Antarctica (Masson-Delmotte et al., 2010a) and only simulate a slight warming (1–2°C) when taking into account either Greenland melt and bipolar seesaw or a removal of the WAIS (Holden et al., 2010; Masson-Delmotte et al., 2010a). Discrepancies in simulating the inferred precipitation increases over Southeast China are not fully understood. In addition to debate on the meaning of these proxies, orbital-scale timing of the seasonal and latitudinal gradients of the insolation forcing from the start to end of the LIG needs to be included in simulations of the NH monsoons (Braconnot et al., 2008).

The temporal/spatial resolution, dating quality of the climate archives and availability of the quantitative reconstructions representing the earlier interglacials remain relatively poor. The only continuous and independently-dated centennial-scale temperature reconstruction spanning the last 800 kyr comes from the EPICA Dome C Antarctic ice core. It shows that the mean annual temperature (MAT) remained above the average of the last 1000 years during MIS11.3 (for over about 20 kyr), MIS9.3 (about 10 kyr), MIS7.5 (about 3 kyr), MIS5.5 (about 13 kyr) and MIS1 (about 11.5 kyr). However, MAT remained 0.5–9.5°C below the average between 800–425 kyr (Jouzel et al., 2007; Masson-Delmotte et al., 2010b), consistent with marine records on past sea level and atmospheric concentration in greenhouse gases (Masson-Delmotte et al., 2010a; Tzedakis et al., 2009). The mean intensity of past interglacials may be linked with long term changes in obliquity (Jouzel et al., 2007) and/or with the phase between precession and obliquity through time (Yin and Berger, 2010).

The trends, variability and seasonality of warming are different among the five most recent interglacials. NH terrestrial data suggest an exceptionally long, wet and winter-warm MIS11.3 interglacial (Ashton et al., 2008; Desprat et al., 2005; Kariya et al., 2010; Nakagawa et al., 2008; Nitychoruk et al., 2005; Prokopenko et al., 2010; Wu et al., 2007) and from marine cores possibly a nearly ice free Greenland during MIS11 (de Vernal and Hillaire-Marcel, 2008). The magnitude of the climatic change and climate stability/instability though are still debated (Lozhkin et al., 2007; Reille et al., 2000; Tarasov et al., 2011; Tzedakis, 2007). High resolution records from the Holocene and MIS11 show multi-centennial to millennial variability, with differences depending on the background conditions (Pol, submitted) [similar analysis in preparation for MIS5.5]. Complex trends in regional climate evolution suggested by the climate proxies must be seriously considered.

[INSERT FIGURE 5.6 HERE]
Figure 5.6: [PLACEHOLDER FOR FIRST ORDER DRAFT: New simulations for the LIG, particularly 130–125ka, from PMIP3 and other LIG projects will be included in subsequent versions. A compilation of more proxy estimates will need to be assessed for this figure.] Last Interglacial, comparison of reconstructions with models: Annual (top, left), June-July-August (bottom, left), and December-January-February (bottom, right) surface temperature changes and annual precipitation changes (top, right) for the Last Interglacial from a multi-model and multi-proxy synthesis. The multi-model changes [in this placeholder, CCSM3 T85x1 simulation for 125ka as compared to a preindustrial control simulation] are color contoured and are overlain by proxy estimates of annual changes (circles) [in this placeholder, as compiled in the synthesis of annual surface temperature change by [Turney (2010), Agulhas Current amplification of global temperatures during super-interglacials [tbc]] and from various proxy estimates of precipitation change: [Rohling (2002, African monsoon variability during the previous interglacial maximum);Wang (2004, Wet periods in northeastern Brazil over the past 210 kyr linked to distant climate anomalies); Brewer (2008, The climate in Europe during the Eemian: a multi-method approach using pollen data); Cheng (2009, Ice Age Terminations).].

5.3.5 The last 2000 Years in the Context of the Holocene

Information from proxies about external forcings and temperature changes suggests that externally forced variations over the last 2000 years have probably been quite small. Detecting the response to these external forcings (Hegerl et al., 2007), estimating the climate sensitivity (Hegerl et al., 2006), and evaluating the ability of climate models to realistically simulate the response to these forcings (Goosse et al., 2005) are all restricted when the forced signal is weak relative to the noise of internal variability. Since internal variability is larger at local or subcontinental scales than at global or hemispheric scales, these problems are more tractable when large-scale averages (or perhaps large-scale patterns) of temperature change are considered (Goosse et al., 2005). On the other hand, global and hemispheric means have limited value for distinguishing dynamical changes (Graham et al., 2010) associated with either internal variability or the response to forcings, for which a consideration of regional patterns of past climate is key (see Section 5.5). Focussing on the global/hemispheric scale introduces particular problems, however, such as the need to maximise spatial coverage by combining multiple proxies perhaps with different temporal resolutions or seasonal responses, and the choice of statistical model to link large-scale average temperature to the scattered proxy data (see further review by Frank et al., 2010; Jones et al., 2009b; Mann, 2007).

5.3.5.1 Limitations and Uncertainties (Including Statistical and Methodological Issues)

Reconstructing NH, SH or global-mean temperature variations over the last 2000 years remains a considerable challenge with many limitations (Jones et al., 2009b). Broadly, these can be categorised either as limitations of the individual proxy data or as issues associated with the statistical methods used to optimally make use of the multi-proxy information.

The statistical methods used to develop large-scale average temperature reconstructions from individual proxy series differ in the extent to which spatial co-variance of temperature and proxies, and temperature-proxy correlation, are considered. Simple compositing of individual or regionally-aggregated temperature sensitive proxy records makes no explicit assumption about spatial co-variance, relying on a reasonable geographical spread of information and either an equal weighting for each local or regional series (Hegerl et al., 2007; Ljungqvist, 2010; Mann et al., 2008) or weighting associated with local temperature-proxy correlation (Christiansen, 2011) or NH temperature-proxy correlation (Juckes et al., 2007). Other empirical approaches -- particularly those that reconstruct spatial fields of temperature from which global or hemispheric means can be obtained -- use information about temperature spatial co-variance estimated from the instrumental record (and usually co-variance information between proxy records) to implicitly weight individual proxy series so that they can be combined to represent spatial fields and subsequently (or directly) large-scale averages (Mann et al., 2009a; Mann et al., 2008). This climate field reconstruction approach potentially achieves a more optimal combination of the individual records, and offers a more satisfactory way to incorporate proxy series that are not sensitive to the temperature in their immediate surroundings but which might be indirectly related to temperature elsewhere (Jones et al., 2009b). A further method developed recently (Tingley and Huybers, 2010) specifies *a priori* the structural form of the spatial co-variance and uses instrumental and proxy data to estimate the parameters this form as well as empirical relationships between proxies and local temperatures; the Bayesian approach to determining these parameters offers flexibility in accounting for errors in instrumental temperature and in representing proxies that represent spatial or temporal averages.

The instrumental record is not necessarily long enough, however, to provide an accurate empirical estimate of the temperature co-variance or the NH temperature–proxy correlation needed for some of the methods, potentially leading to inappropriately high weighting of a subset of the proxy records (Juckes et al., 2007). This is especially a concern if spatial co-variance at multi-decadal timescales is estimated because proxy records with lower temporal resolution or that have been temporally filtered are being used (Mann et al., 2009a), though the weights are shown in the latter study. These potential problems have been explored using pseudo-proxy investigations (i.e., attempts to replicate the temperature reconstruction process with synthetic data, usually derived from climate model simulations, with a known outcome), indicating that some reconstructions may be relatively unaffected (Mann et al., 2007). Nevertheless, it seems prudent to continue with both compositing and climate field reconstruction approaches, comparing results for consistency. Palaeoclimate data assimilation is a new approach to this problem developed mostly since AR4 (see review by Widmann et al., 2010). Of the assimilation approaches currently being used for palaeoclimate studies over the last 2000 years, the ensemble member selection (Goosse et al., 2010) is the most amenable for temperature reconstructions; an ensemble of simulations under appropriate external forcing but with small perturbations in initial conditions is generated for each analysis period (e.g., 10 years) and then the ensemble member most consistent with the available individual proxy records is selected for that period and to provide the basis initial conditions for the next period. The selected ensemble members provide spatially complete surface temperatures (and indeed other variables within the atmosphere and oceans) constrained by the proxy records and by the dynamical and physical processes represented in the model equations — thus the temperature co-variance is determined by dynamics rather than empirically estimated from observations. Preliminary assessment indicates close agreement between the average NH temperature reconstructed via assimilation and via compositing or climate field reconstruction methods (Goosse et al., 2010), given similar raw proxy records. Palaeoclimate data assimilation offers a number of further benefits, but there are also various drawbacks (Goosse et al., 2010; Widmann et al., 2010), including the high computational cost that precludes the use of climate models with the most comprehensive representation of the dynamical and physical processes, and the limited utility of the resultant reconstructions for evaluating climate model performance or for detecting the response to external forcings, since model and forcing information has already been used in developing the reconstruction (a similar argument applies to other approaches that use forcing data to constrain the reconstructed temperatures, e.g., Lee et al. (2008), though detection can become part of the reconstruction process).

Pseudo-proxy investigations using millennial-length CGCM simulations have allowed a systematic evaluation of biases and uncertainties associated with a range of statistical reconstruction methods and networks of proxy data with varying error characteristics (Burger et al., 2006; Mann, 2007; Smerdon et al., 2010, and references therein). A key finding (e.g., Lee et al., 2008) is that some published reconstructions are likely to underestimate the overall amplitude of temperature change during the last 2000 years, including those based on forward regression (Briffa et al., 2001) but also some climate field reconstructions (Mann et al., 1998) and other methods to varying degree (Christiansen et al., 2009). The magnitude of this amplitude attenuation in real-world reconstructions is unclear; it is expected to be larger when the correlation between instrumental temperatures and proxies is weaker (a lower signal-to-noise ratio; Lee et al., 2008) and with methods that (perhaps implicitly) assign the error only to the temperature data (Ammann et al., 2010).

Temporal smoothing might ameliorate the affect if it increases the signal-to-noise ratio (Lee et al., 2008), but at the cost of reducing the degrees of freedom available for fitting the statistical model (Christiansen et al., 2010) and possibly also limiting the spatial details that can be resolved in climate field reconstructions. Alternative methods that implicitly (e.g., variance matching — Juckes et al., 2007) or explicitly [e.g., total least squares (TLS) applied to a single composite series (Hegerl et al., 2007) or to a multivariate regression (RegEM with Truncated TLS, Mann et al., 2008)] assign part of the error to the proxy data, or explicitly assign it all to the proxy data (e.g., inverse regression), may result in reduced attenuation of the long-term amplitude of reconstructed temperatures (Lee et al., 2008). Other studies find that this amplitude attenuation may remain, though this is debated (Christiansen et al., 2009; Christiansen et al., 2010; Rutherford et al., 2010). Agreement between reconstructions using data assimilation and some of these statistical approaches (Goosse et al., 2010) suggests that the amplitude of long-term variability may not be biased, though this finding is likely to be sensitive to the local calibration of the proxy series prior to their assimilation. It is clear, however, that amplitude attenuation can be very large if the data are detrended prior to the calibration of the statistical models (Lee et al., 2008; Mann, 2007) and for this reason detrending is not usually performed with published real-world reconstructions. Although it has been argued that the 20th century warming trend contains unique co-variance information between proxies and temperatures (Ammann and Wahl, 2007) it is still more usual statistical practice to detrend data when fitting models, not least because some part of the proxy trend might be due to non-climatic influences (von Storch et al., 2006). It is interesting to note, therefore, a recently proposed reconstruction method involving local inverse calibration of proxies (Christiansen, 2011) that may avoid loss of low-frequency variance even when detrended data are used for calibration (Christiansen, 2011), though further evaluation of its properties is required.

Ongoing research will resolve these methodological issues and more clearly identify the characteristics of reconstructed large-scale temperatures fields/averages. A more fundamental limitation (Jones et al., 2009b) on our ability to draw conclusions about past temperature variability at global/hemispheric scales is the number, geographical distribution, reliability and climatic interpretation/understanding of raw proxy records, both individually and in networks. Increases in a database of high-resolution proxies have been achieved (Mann et al., 2008; Wahl et al., 2010); excluding series obtained from other spatial reconstructions, 198 annually-resolved proxies were available back to 1500 CE (168 in NH, 30 in SH), reducing to 34 back to 900 CE (25 in NH, 9 in SH), supplemented by decadal-resolution proxies (42 back to 1500 CE; 34 back to 900 CE). After screening for likely correlations with local temperature, these reduce further to a total of 105 and 20 back to 1500 CE and 900 CE, respectively. Notable developments include some seasonally-resolved Greenland ice core stable isotope series (Vinther et al., 2010); a multi-millennial chronology of tree-growth from the eastern Alps (Nicolussi et al., 2009); and an expansion of tropical coral records (Wilson et al., 2010).

A simple expansion in numbers is not sufficient; proxies which can in some sense be considered as reliable indicators of past temperature change are required. (McShane and Wyner, 2010) find that climate proxies are no more useful than random series for reconstructing temperature; though this is disputed (e.g., Smerdon et al., 2010), it is nevertheless true that proxies represent at best noisy observations. Proxies that can provide valuable temperature information can be identified empirically though this can be prone to false negative or false positive outcomes when the instrumental record is short or strongly autocorrelated, or the proxies are temporally smoothed [Reference needed]. Empirical results are much more powerful when guided by an *a priori* process-based expectation of proxy sensitivity (e.g., Briffa et al., 2002). Nevertheless, the use of empirical correlations for proxy selection may inflate uncertainty estimates (Bürger, 2007; Osborn and Briffa, 2007), though this has rarely been quantified.

There are other potential sources of error that published uncertainty ranges do no always account for, including model selection (structural uncertainty), parameter estimates and possible violations of uniformitarianism (i.e., non-stationary proxy–climate relationship). The latter concern may apply to many proxy types, though a prominent example is the apparent divergence between some tree-ring chronologies and instrumental temperatures during the last few decades (e.g., Briffa et al., 1998). The divergence phenomenon does not affect all tree-ring records (Wilson et al., 2007b), may have been incorrectly diagnosed in some cases (Esper and Frank, 2009), but is clearly present in some, though the causes remain unclear (D'Arrigo et al., 2008).

5.3.5.2 *New Global or Hemispheric Reconstructions for last 2k or less*

The NH temperature reconstructions assessed in the AR4 provided quite strong evidence for a Medieval Climate Anomaly that was warmer than the average for the past millennium as a whole, followed by a clearly cooler LIA, and then by a modern warming which was also clearly warmer than the average for the whole millennium. Comparison of the relative warmth of the two warmer (Medieval and modern) periods was considered equivocal due to the reconstruction uncertainties (and particularly the sources of error that have not been included in estimated uncertainties — see discussion above), though the central estimates of most MCA temperature reconstructions were lower than the average temperature for 1951–2000 and thus it was considered likely that the latter was the warmer period. Proxy records were too sparse to make an equivalent assessment for the SH, though regional evidence indicated warming from the LIA to the modern period. New reconstructions, and further analysis of the previous reconstructions, methods and proxy data, do not give reason to revise the AR4 conclusions. New reconstruction methods and the inclusion of additional proxy records have overall (Figure 5.7a–[Figure to include the new reconstructions; text below already takes these into account]) have led to an enhancement in the overall amplitude of NH temperature change, providing stronger evidence that the Medieval and modern periods were warm relative to the average for the last 1000 or even 2000 years) and that the Little Ice Age was significantly cooler. Comparison of the relative warmth of the Medieval and modern periods is still problematic due to considerable uncertainty, both quantified and unquantified, though the evidence for Medieval warmth is of course not as strong as that from instrumental data for the modern period which demonstrates warming across all seasons and nearly all regions of the world.

Juckes et al. (2007) tested the sensitivity to proxy data selection and statistical methods, finding that the former could explain many of the differences between previously published NH temperature reconstructions. Compositing records from across some existing studies and scaling their variance to match the observed variance, the Juckes et al. (2007) reconstruction showed modern temperatures significantly above MCA temperatures and a LIA as cool or cooler than most previous studies. Mann et al. (2008) used an expanded database of proxy records and two statistical methods and found enhanced amplitude of millennial NH temperature variations, a warmer MCA than in some previous work though perhaps still cooler than the modern warm period, and that similar findings were obtained without using tree-ring data. For the SH and global-mean temperatures, Mann et al. (2008) found similar results, but with considerably wider uncertainty ranges that are compatible with earlier warmth possibly exceeding modern warmth. Ljungqvist (2010) focussed on the extratropics of the NH, using a composite of 30 temperature sensitive records (16 with annual resolution and 14 lower resolution records, including some with only centennial resolution can be problematic for dating control and for identifying the appropriate scaling to apply to the records). This record shows an earlier warm period (1–300 CE) as well as the MCA and modern warm periods; all three periods in the reconstruction have similar levels of warmth taking the uncertainty into account. (Christiansen and Ljungqvist, 2011) use a similar set of proxy records but with some additions and excluding the lowest resolution series, together with an alternative reconstruction method, and find a much larger amplitude millennial NH temperature change (more than 1 K). [Loehle and McCulloch (2008)] propose a reconstruction of global temperatures using lower resolution proxies; the overall shape of millennial temperature change is compatible with other studies, but the choice of proxies and their resolution inhibits a quantitative comparison of modern and earlier warmth. [this paragraph being considered for placement in a table]

5.3.5.3 *Combining Model-Based Insight with Evidence from the Real World*

[PLACEHOLDER FOR FIRST ORDER DRAFT: Subsection may be revised when the new CMIP5 simulations become available and are analysed; new reconstructions to be include in the figure; potential change in conclusions.]

The number of CGCM simulations of the last millennium has increased significantly since AR4, including some initial condition ensembles [Reference needed], and has been included within the design of CMIP5 (Taylor et al., 2009). These simulations have been driven by natural and anthropogenic forcings, though the particular forcings included and forcing timeseries have varied between studies. The CMIP5 simulations have been driven by weaker solar irradiance variations than many of the non-CMIP5 simulations, following re-evaluation of the evidence for the amplitude of long-term forcing changes (Section 5.2). The considerable uncertainty in past forcings has not been fully explored by CGCM simulations yet. PLACHOLDER FOR FIRST ORDER DRAFT: Consider stating more key elements of the CMIP5 design for the last millennium runs.]

The course of NH temperature change over the last millennium simulated by these climate models is in broad agreement with the available reconstructions (Figure 5.7a–[comparison is not truly fair, since some reconstructions represent a smaller spatial domain than the full NH or seasonal rather than annual mean temperatures, while the annual full NH mean temperature is shown for the models]). This is an interesting test of the models, though it is not a very discriminatory test because of uncertainties in the forcings, reconstructions and internal variability; thus models with very different climate sensitivities might appear to be consistent with the uncertain evidence for past change.

Figure 5.7b-g provides a more powerful test by compositing the temperature response to a number of distinct forcing events, as well as giving insight into the response to different forcings. The models simulate a significant cooling in the NH in response to individual volcanic events (Figure 5.7b-c) that peaks between 0.1 and 0.4 K depending on model a year after the peak forcing, and lasts 3 to 5 years; the reconstructions with annual resolution also show cooling on average, though smaller (0.0 to 0.2 K). Since many reconstructions do not have annual resolution, similar composites are formed showing the response to changes in multi-decadal volcanic forcings (representing clusters of eruptions). The simulated response is again larger than the cooling shown by the reconstructions (though both are significant), though it peaks earlier (<5 years after the peak negative forcing) than the reconstructions and the models and data are in good agreement after this initial peak cooling dissipates. Even at multi-decadal timescales, the solar forcing estimated over the last millennium shows weaker variations than volcanic forcing. Compositing the response to these weaker multi-decadal fluctuations in solar irradiance shows cooling in both simulations and reconstructions of NH temperature of between 0.0 and 0.2 K or 0.0 and 0.1 K, respectively. In both cases cooling shows a double peak (aligned with the forcing change and lagged by 20 years), though the reason is unclear and might arise from variations in other forcings. Across all these composites, the model responses are larger, on average, than the reconstructions. Though too high a climate sensitivity cannot be ruled out, there are a number of other potential explanations: the solar forcing may be too strong; the amplitude of the reconstructions may be too weak (see discussion above) especially for reconstructing temperatures furthest from the calibration period mean; and internal variability and random reconstruction error could dominate these composites based on small samples of events. [to be reconsidered once CMIP5 models and new reconstructions are included.]

The power spectra of reconstructed and simulated NH temperatures are both strongly red even up to century periods, indicating the involvement of climate system components (e.g., deep ocean) with long response times. The simulated and reconstructed spectra ranges overlap each other and encompass the power spectra of instrumental temperature, though on average the models have more variance across most timescales than the reconstructions. This probably arises because regression-based reconstructions do not capture the full variance of the instrumental temperature; a simple adjustment (Collins et al., 2002) to account for this unresolved variance is not possible because its spectral shape is unknown.

Mann et al. (2009b) reconstructed spatial patterns of temperature change over the last 1500 years, suggesting that the MCA period (therein defined as 900–1250 CE) was on average warmer than the LIA period (therein defined as 1400–1700 CE) across most regions except the equatorial Pacific (Figure 5.8). This arises from evidence for more frequent La Nina events and associated North American droughts during the MCA (Cobb et al., 2003; see also Section 5.5.3.1; Graham et al., 2010; Seager et al., 2008). Graham et al. (2010) recently showed that a pattern of change consistent with temperature and hydrological proxy evidence is obtained for the MCA with a climate model if anomalously warm SSTs are induced on the Indian Ocean and western tropical Pacific coeval with a La Niña state, thereby enhancing the zonal gradient. Figure 5.8 shows the MCA-LIA annual temperature differences (hatched areas indicate non significance for a $p < 0.05$ level) in forced simulations from six different models and also in the Mann et al. (2009b) proxy reconstruction. For the specific case of the MPI-ESM, results are shown for four simulations, two arbitrarily selected from ensembles of low (E1) and high (E2) solar variability forcing scenario (Jungclaus et al., 2010a). All simulations tend to produce an almost globally warmer MCA, except for the CNRM (see also Figure 5.7i for NH mean temperature changes). However, the spatial pattern of temperature change is heterogeneous and can vary considerably from model to model and even within simulations of the same model. None of the simulations reproduces the reconstructed pattern depicting a La Niña state or coexisting increased zonal gradient associated with anomalous western Pacific/Indian Ocean warmth. The discrepancy in the simulated and reconstructed temperature changes as well as the inter-model variability suggests that internal variability may play a significant role in the MCA to LIA transition and also that either transient simulations with state-of-the-art models fail to correctly reproduce the mechanisms of response to external forcings, or important problems still dominate in millennium spatial field reconstructions.

[PLACEHOLDER FOR FIRST ORDER DRAFT: Discussion to include published model-data comparisons rather than just what is shown in Figure 5.7; also include the SH (Osborn et al., under review) to be considered. Climate-carbon cycle work (e.g., Frank et al., 2010) is covered in Chapter 6.]

5.3.5.4 Last 2k in Context of Holocene at this Global or Hemispheric Scale

Large-scale temperature changes inferred from palaeo archives or simulated by climate models driven by forcings reconstructed from palaeo archives have demonstrated the complexity of Holocene climate change. The timing and spatial extent of the Holocene thermal maximum was regionally variable, with orbital forcing probably modified by regional effects of ice sheet remnants and dynamical responses in the atmosphere and oceans (Renssen et al., 2009). Wanner (2008) reviews the evidence from data, forcings and models for the subsequent mid-to-late Holocene, finding evidence for long-term summertime cooling in the NH driven primarily by orbital forcing, superimposed with centennial and millennial fluctuations related perhaps to other natural forcings and changes in atmosphere-ocean dynamics.

[INSERT FIGURE 5.7 HERE]

Figure 5.7: [PLACEHOLDER FOR FIRST ORDER DRAFT: Update of AR4, Figure 6.13 (Osborn) or volcanic composite and response. Will be updated with newer reconstructions and CMIP5/PMIP3 simulations. Further consideration also needs to be given to which reconstructions and simulations are included in each panel, according to temporal resolution and representation of internal variability. other considerations: how to make use of reconstruction uncertainties and model ensembles.] Comparison of simulated NH annual temperature change with reconstructions of NH temperature change [some reconstructions are seasonal not annual, and some are for a subset of the NH such as extra-tropical land]. (a) Simulations (filtered) shown by coloured lines; overlap of reconstructed temperatures shown by grey shading. (b-g) Superposed epoch composites based on selecting sequences of temperature from periods with (b, c) individual volcanic forcing events from 1400–present that exceed -1.0 W m^{-2}; (d, e) 50-year smoothed volcanic forcing that exceeds -0.2 W m^{-2}; (f, g) change in band-passed solar forcing over a 50-year period that exceeds -0.2 W m^{-2}, all based on the forcings used by [Ammann et al. (2007)]; for solar forcing it is their "medium" forcing case. Time segments from selected periods are aligned so that the years with the peak negative forcing are aligned. In (b, d) the volcanic forcing for the individual selected events is shown together with the composite mean (thick). In (f) it is the same but for the band-passed solar forcing. (c, e, g) show the NH temperature composite means and 90% range of spread between simulations (dark red line, pink shading) or reconstructions (green), with overlap in shading (not drawn quite correctly yet!) in orange. NH temperatures were also filtered in the same way as the forcings. Only reconstructions with appropriate temporal resolution were used in each case [to be confirmed when newer reconstructions are included]. (h) Power spectral density of reconstructed (green shading shows the full range of results; dark green line: multi-reconstruction mean; individual reconstructions are not shown), simulated (thin red lines: individual models; thick dark red line: multi-model-mean) and instrumental (black line: HadCRUT3) NH temperature [the unexpected peak at $f = 0.3\ a^{-1}$ or around 3 year period seems to be entirely from the COSMOS1 and COSMOS2 runs]. (i) Mean NH temperature difference between MCA (950–1250 CE or 1000–1250 CE for data that begin in 1000 CE) and LIA (1400–1700 CE) from reconstructions (green), multi-reconstruction mean and range (dark green), multi-model mean and range (dark red), and simulations (red). Individual results are sorted into ascending order and labelled. [These MCA and LIA periods were chosen to match Figure 5.8 and Mann et al. (2009); individual ensemble members will be replaced with an ensemble mean and range, so it won't be dominated by the 8 COSMOS runs; also is ECHOG-FOR1 the first "Erik" run with a rather warm start and hence large MCA-LIA difference. If so, this should probably be removed – adjustment to this first "Erik" run was included; also new reconstructions need to be included, and perhaps MBH99 dropped if considered to be superceded by Mann et al. (2008).]

[INSERT FIGURE 5.8 HERE]

Figure 5.8: Temperature anomalies (global or hemispheric maps) for "Medivial Climate Anomaly" and "Little Ice Age". MCA-LIA annual mean temperature difference in forced simulations for the last millennium produced with six different AOGCMs and in [Mann et al. (2009)]. The periods considered for calculating the differences in [Mann et al. (2009)] were taken as reference: MCA (950–1250 CE) and LIA (1400–1700CE). For the simulations starting in 1000CE (CCSM3, ECHO-G, IPSL, CNRM) the period 1000 to 1250 was selected instead to define the MABOUT Hatched areas represent non significant differences at a 0.05 level.

5.4 Past Changes in Sea Level and Related Processes

[PLACEHOLDER FOR FIRST ORDER DRAFT]

5.4.1 Magnitudes of Past Sea Level

The geologic record clearly indicates past changes in Earth's average surface temperature were correlated with substantial changes in ice volume and global sea level (e.g., Alley et al. (2005); Figure 5.9). Direct sea level measurements based upon coastal sedimentary deposits and tropical coral sequences (in tectonically stable settings) show that eustatic sea level was higher than present during the Last Interglacial (LIG) by approximately 4–6m (Muhs et al., 2001; Rostami et al., 2000), despite there being very little difference in atmospheric CO_2 concentrations (Lourantou et al., 2010a). An even higher eustatic peak of +6.6 to +9.4 m is reported for the LIG (Kopp et al., 2009), based on a probabilistic assessment of a global database of proxy sea level measurements. Simulations of Earth's average surface temperature during the LIG generally match proxy reconstructions and are not notably higher than the pre-industrial average of the last 1000 years (see Section 5.3.4 and Figure 5.6). While regional LIG warming is observed especially in the polar regions (Figure 5.3) it is not always synchronous (Masson-Delmotte et al., 2010b). Both North Greenland Ice Core Project (NGRIP) and the Greenland Ice Core Project 2 (GISP) results indicate the Greenland summit region remained ice covered during the LIG (Andersen et al., 2004; Landais et al., 2006; Raynaud and Lorius, 2004; Suwa et al., 2006) [PLACEHOLDER FOR FIRST ORDER DRAFT: NEEM Project results]. The presence of LIG ice on southern Greenland remains equivocal (e.g., Andersen et al., 2004; Koerner and Fisher, 2002; Lhomme et al., 2005), however the absence of pre LIG ice in the Canadian Arctic indicates that they melted completely during the LIG (KOERNER, 1989). Models of Greenland (GIS) and other Arctic ice sheets forced by data , or by temperature and precipitation produced by an AOGCM [references needed] imply a contribution of no more than 2–4m of early LIG sea level rise over several millennia. LIG eustatic sea level of +4 m can be explained by GIS melting and the thermosteric effect, however estimates of +6 to +9 m have implications for the equilibrium response of both polar ice sheets to only moderate levels of warming. Direct evidence from geological data (sediment cores on the continental margin) for retreat of the West Antarctic Ice sheet (WAIS) during the LIG remain equivocal due to difficulties with age assessment (about Naish et al. (2009)), however Pleistocene marine microfossils recovered from sediments beneath WAIS ice streams imply loss of the some of the interior ice sheet within the last 400 ka (Scherer et al., 1998). Significant concentrations of ice berg rafted debris, related to marine ice sheet break-up and transportation by the Antarctic Circumpolar Current are recorded in Southern Ocean sediment cores as far north as Eastern New Zealand during the LIG (Carter et al., 2002; Pollard and DeConto, 2009; [Grobe and Mackensen, 1992). A coupled ice sheet-ice shelf model reconstructs a +2 to +3 m contribution to the magnitude of LIG sea level due to WAIS loss from the Pine Island, Weddell and Siple Coast sectors, where ice is presently, grounded up to 2 km below sea level (Pollard and DeConto, 2009).

Comparison of Holocene sea level with that of the interglacial during MIS 11 (about 400 ka) are of interest because they both displayed long, relatively stable periods of interglacial climate and sea level. Paleo-sea level reconstructions from a range of uplifted coastlines, where shorelines with numeric ages have been preserved, imply a eustatic peak as high as +20 m during MIS 11 (e.g., [Hearty, 2002; Olson and Hearty, 2009]). Although MIS11 interglacial lasted up to 30 kyrs (Augustin et al., 2004; Berger and Loutre, 2002) surface temperatures (Herbert et al., 2010b) and atmospheric CO_2 concentrations (Luthi et al., 2008) display little difference compared with pre-industrial values. An uplift correction based on an extrapolation of LIG uplift rates to MIS 11 shorelines located in the same regional tectonic context, has shown that sea level during MIS 11 was closer to present (Bowen, 2010), and consistent within the range of sea levels estimated from oxygen isotope records corrected for deep-sea temperature (Bintanja et al., 2005; McManus et al., 2003; Rohling et al., 2009; Waelbroeck et al., 2002).

The early and mid-Pliocene (4.5–3.0 Ma) is the last time in Earth's history when mean global surface temperatures where substantially warmer than present day for a sustained period (estimated by GCMs to be about 2°C to 3°C above pre-industrial (Dowsett, 2009), CO_2 concentrations were likely higher than pre-industrial levels (350–415 ppm ; e.g., Pagani et al. (2010b); Seki et al.(2010)) and continents and oceans had reached their present day configuration. With current CO_2 levels approaching 400 ppm and projected to rise higher, Earth's surface temperature is projected to rise an average of about 3°C by the end of the century, the warmest times during the Pliocene provide an accessible example of the equilibrium state of a globally warmer world. A compilation and statistical assessment of far-field paleo-sea level estimates indicates global sea level during the warmest Pliocene interglacials was likely (66%) to have been greater than +15 m and very likely (90%) to have been greater than +9 m, with a mean value of +22 m [(Miller et al., in review, Science)]. This geological proxy database assembles estimates derived from backstripping of shallow-marine continental margin records in Virginia and New Zealand, submergence of well-dated shorelines of a coral atoll (Enewetak, South Pacific), tectonically adjusted heights of uplifted shorelines, and the deconvolution of ice volume from benthic foraminiferal oxygen isotope records. Direct geological evidence from the Northern Hemisphere (summarised in Maslin et al. (2000)) and Antarctic continents (Naish et al., 2008), together with models [(DeConto et al., 2010)], suggest that polar ice volume was similar to the present East Antarctic Ice Sheet (EAIS), with more variable Greenland and West Antarctic ice sheets. During the warmest Pliocene interglacials, SSTs in the Ross Sea and Southern Ocean adjacent to East Antarctic were between +4°C to +6°C relative to present day (based on planktic diatom assemblage, Mg/Ca and organic geochemical paleothermometers place holder). ANDRILL Program drill cores show warm, high productivity conditions and the absence of summer sea-ice in western Ross Sea between 3.6–3.3 Ma (Naish et al., 2009). An ice sheet-ice shelf model, that simulates ice shelf buttressing and is capable of migrating marine based grounding lines, shows complete deglaciation of the marine portions of the WAIS and thinning and recession on the margins of the EAIS contributing +7 m of sea level rise to the global sea level budget during orbital-scale Pliocene interglacials (Pollard and DeConto, 2009). Mass balance changes in this model are primarily sensitive to the influence of ocean temperatures on melt rates at grounding lines, as well as addressing marine ice sheet instabilities. Other ice sheet models that do not account for marine-based ice sheets imply complete deglaciation of Greenland and slightly more contribution from the margins of the EAIS [(Hill et al., 2007)], potentially contributing +15 to +20 m of eustatic sea level rise. The thermosteric contribution to Pliocene sea level is estimated to be +3 m [(Miller et al., in review)].

5.4.2 Rates of Sea Level Change and Meltwater Sources During Glacials and Transitions

Whether eustatic (globally averaged) sea level rise following the onset of deglaciation has been punctuated by periods of acceleration in sea level or by periods of a slow-down in the rate of rise have remained controversial in terms of the magnitudes and timing of the events, as well as in terms of their causes and effects. This is largely because the records of such possible events remain limited in their temporal resolution and spatial coverage, and because spatial variability in these signals can be expected from the combined gravitational (including rotational) and deformational response of the ocean and Earth surfaces to the changing ice sheets (the isostatic response; [Mitrovica et al., (2009)]). Better understanding of such events are, however, important because, if real, they indicate that very rapid changes in the rates of sea level, both rising and falling, have occurred over periods of a few hundred years. This can provide insights into climate impacts of large volumes of cold-dense water added into the ocean [(Aharon et al., 2006; Stanford et al., 2006)] and into the stability of ice sheets at times of rapid sea level rise.

Three possible periods of rapid acceleration in particular have been identified since the LGM. They are, in chronological order, about 19,000 cal years BP [(Yokoyama et al., 2000; DeDeckker and Yokoyama, 2009; Hanebuth et al., 2009)], melt-water pulse (MWP) 1A at about about 14,000–14,500 cal years BP [(Fairbanks, 1989; Deschamps et al. 2008)] and MWP 1B at about 11,300 [(Fairbanks, 1989; Bard et al., 2010)]. The first of these events occurs at a time of Northern Hemisphere insolation increase, of temperature increases in Greenland as recorded in ice cores [(Alley et al., 2002)] and a warming of the southern ocean [(Baker et al., 2009)]. The latter have been associated with major pulses of freshwater added into the oceans from either northern or Southern Hemisphere, or both, sources [(Weaver et al., 2003; Clark et al., (?); Carlson, 2009; Yamane et al., 2011; Mackintosh et al., 2011)]. Recent coral records from Tahiti support earlier estimates for the MWP 1a rise of about 20 m in less than 500 years [to be confirmed against new results when published] with an average annual rise of about 40 mm yr^{-1} or greater and synchronous with the Bolling-Allerod warming [(Deschamps et al., under review 2011)]. But other recent Tahiti core data does not confirm the existence of the MWP 1b [(Bard et al., 2010)] in contrast to a reported rise of about 10 m at Barbados [(Peltier and Fairbanks, 2006)]. It has been suggested [(Mitrovica et al., 2009)] that the spatial variability of the isostatic response may explain the different MWP 1b sea level signals at these two sites in which case it would imply that the sources of the two pulses were distinctly different. [PLACEHOLDER FOR FIRST ORDER DRAFT: Develop this further with new publications in preparation.]

Periods of slow-down in sea level rise during the early Holocene have also been reported. One is for the latter part of the Younger Dryas [(Lambeck et al., 2002; other references)], at a time when the ice margins of the major Northern Hemisphere ice sheets were quasi-stationary. Another is for a about 300 year time interval centred on about 8000 ka [(Bird et al., 2010)] which implies that either a substantial amount of meltwater has been withheld from the oceans at this time or that there was a temporary cessation in melting of either the residual Laurentide ice sheet or of the Antarctic ice sheet.

[PLACEHOLDER FOR FIRST ORDER DRAFT: Meltwater pulses during the pre-LGM period as well as rapid fall events and their relationship with Heinrich events need to be commented on.] There is the question about the magnitude and timing of the freshwater inputs linked with Heinrich events and stadials "The total amount of freshwater released during Heinrich events has not yet been well-constrained and existing estimates range from essentially zero to several tens of meters in global sea level equivalent”. The most debated points for the last several years are that the timing of the HE if it is warm in Greenland or cold [(Alley et al., 1996)], whereas [Chappell (2002) and Arz et al. (2007)] suggested the time of warm temperature in Greenland so the melting was occurred more slowly. This may have been resolved by [Rohling et al. (2008)] using dust flux in the Red Sea core that HE was indeed occurred at cold period in Greenland. Ocean General Circulation Model based experiment explains the mechanism of HE. Again N-S thermal see-saw plays an important role [(Flückinger et al., 2006]. Similar mechanism was also proposed by [Clark (2007), though other mechanisms are also reported such as ice sheet internal processes [(Mac Ayeal, 1993; Papa et al., 2006)], internal oscillations of ice sheet –climate systems [(Calov et al., 2002)] and ice shelf build up and collapse [(Hulbe et al., 2004; Alley et al., 2006)].

5.4.3 Rates of Sea Level Changes During Interglacials

[PLACEHOLDER FOR FIRST ORDER DRAFT]

5.4.3.1 The Start of Interglacials

For historical reasons, the onset of interglacial periods is determined by the beginning of temperature plateau rather than by the end of deglaciations. As a result, at the beginning of the Holocene interglacial (11.7 ka) global sea level was still some 60 meters below modern, substantial North American and Fennoscandian ice sheets were still present, and global sea levels did not stabilize near their present value until nearly 5000 years later. Therefore, the earlier phases of the recent interglacials in fact represent the final stage of glacial terminations with an average global rate of sea level rise by up to 1.5 m per millennium. For the LIG, global sea levels approached their present value at about 130 ka although the planetary warming started earlier such that this interglacial, as defined by the onset of the temperature plateau and by analogy with the Holocene, started at about 135 ka. Since most of the early interglacial sea level rise originated from ice sheets that do not exist any more, these early periods are not directly applicable to the future warming. However, the fact that the ice sheet models forced by variable summer insolation and CO_2 concentration are able to successfully reproduce reconstructed rates of sea level rise during the last deglaciation [(Abe-Ouchi et al., 2007; Carlson et al., 2008; Ganopolski et al., 2010)] lends credibility to the models.

5.4.3.2 Last Interglacial (LIG)

After complete melting of continental Northern Hemisphere ice sheets, remaining sea level variations are primarily explained by contributions from the Greenland and the Antarctic ice sheets. Paleoclimate data suggest that the maximum sea level during the Last Interglacial (130–115 ka) was higher than today by +4 to +6 m [(Stirling et al., 1998; Overpeck et al., 2006)], or even as much as +6 to +8 m [(Kopp et al., 2009)].

[PLACEHOLDER FOR FIRST ORDER DRAFT: A few cautionary comments needed about the validity of the observational evidence.] Ice sheet models forced by reconstructed temperatures or by the output of climate models and constrained by paleoclimate reconstructions indicate that GIS could contribute by up to 4 m to the global sea level during LIG [(Cuffey and Marshall, 2000; Huybrechts, 2002; Tarasov and Peltier, 2002; Otto-Bliesner et al., 2006; Robinson et al, 2010)]. This highstand can be explained by higher summer insolation and higher summer Greenland temperatures during the first half of the LIG as compared to the late Holocene. Palaeoclimate reconstructions and results of climate model simulations indicate that the maximum LIG summer temperatures over and around Greenland were up to 4°C higher than at present [(Otto-Bliesner et al., 2006; Kaspar and Cubasch, 2007)]. As a result, according to model simulations, GIS lost the mass during the first half of LIG with the average rate of 0.5–1 meter in sea level equivalent per millennium till 124–122 ka, when the minimum of the GIS volume was reached [(Robinson et al., 2010)]. [PLACEHOLDER FOR FIRST ORDER DRAFT: Model-data comparison]. If the maximum LIG sea level was much more than 4 m above the present one, this can only be explained by a contribution from the AIS. Since GHGs concentrations and mean annual insolation in the high latitudes were similar to present, while austral summer insolation was lower than at present during LIG, substantial mass loss of the AIS and the reconstructed high Antarctic temperatures during LIG require a different explanation than that for the GIS. A coupled ice sheet-ice shelf model simulation driven by insolation and climate variability demonstrate a possibility of repeated complete disintegration of the WAIS during some interglacials [(Pollard and DeConto, 2009)]. Although in this simulation the complete disintegration of the WAIS did not occur during LIG, nevertheless, this modelling result illustrates potential vulnerability of the WAIS to a relatively small climate fluctuation on the orbital time scale. At the same time, disintegration of WAIS during the penultimate deglaciation can help to explain high Antarctic temperatures during LIG [(Holden et al., 2010)].

Analyses of some palaeoclimate archives [(e.g., Rohling et al., 2008; Hearty et al., 2006)] suggest that during LIG, unlike the present interglacial, sea level experienced fluctuations with magnitude of several meters, even tens of meters at millennium time scale, although others have attributed the larger fluctuations to interpretational errors [(Bowen, ?)] and due to the neglect of glacio-isostatic contributions. [Dutton and Lambeck (?)], for example, have shown that such oscillations are unlikely to have exceeded 1–2 m which is at the limit of the resolution of the available data. In the absence of known climate forcings on this time scale, the larger fluctuations cannot be reproduced by ice sheet models.

5.4.3.3 Holocene

Holocene sea levels are characterized by considerable spatial variability because of tectonic movements of the land surface with respect to which the observations are recorded and because of ongoing deformational and gravitational response of the Earth and ocean to the past glacial cycle. The tectonic contributions tend to be episodic, local, and difficult to evaluate, whereas the isostatic changes are global in scale, vary slowly in time, and for which comprehensive and predictive models exist [(e.g., Milne and Mitrovica, 2008)]. Within the framework of the IPCC report the concern is primarily with the latter part of the Holocene, the time when global ice sheets and sea level stabilized near present-day values. For this interval, in addition to the isostatic and tectonic contributions there is also the contribution from any residual melting or re-growth of ice sheets and mountain glaciers, as well as from thermal changes in the oceans, reflecting possible impacts of climate and the Earth’s response to changes in surface ice-water loads. Thus this contribution will also be spatially variable and a function of time. The time-dependence of sea level is usually expressed by the globally averaged change, or eustatic sea level, which provides a measure of the exchange of the total mass between ice sheets and oceans and of the total change in the heat content of the ocean. For many regions, departures from this global average will be at least as important or considerably larger.

Observational evidence for local change in sea level during the latter part of the Holocene comes from the fossil record of organisms or sediments whose normal living or formation positions can be closely defined within the tidal range but which today are found outside their usual growth or depositional limits. Most important of these indicators are particular coral colonies, micratolls, whose growth limits are well defined by the mean-low water spring tide level [(Hopley et al., 2007)], vermetid reefs that form within a narrow part of the tidal range [(Antoniolli et al., 1999; recent references needed], and certain sedimentological records whose flora and fauna contents specify specific horizons within the tidal range [(Gehrels et al., xxxx)]. Archaeological indicators, where the functional success of a construction requires a close link to sea level as in the fish tanks of Roman time, can also provide precise measures of past sea level. These data sources provide measures of the local sea level change and via tectonic and isostatic modeling, measures of the global changes in ocean volume during this Late Holocene interval.

Coral microatoll data from the tectonically stable Australian east coast have long been seen as sound evidence that for the past about 6 ka there have been no substantial oscillations (< ± 50 cm) in sea level on centennial-to-millennial time scales [(Chappell, 1983)]. In contrast, other studies, also from the same margin but using fixed biological indicators whose relation to mean sea level is less well defined, have reported oscillations of about 1 m during this same interval [(Baker et al., 2001)] but no study has shown that such magnitude oscillations are globally synchronous. More recent results of the height-age distribution of a large number of microatolls from the tectonically stable island of Kiritibati confirm that oscillations in sea level on the centennial-to-millennial time scales are unlikely to have exceeded ± 25 cm [(Woodroffe et al., 2011 submitted)]. [PLACEHOLDER FOR FIRST ORDER DRAFT: Discussion of evidence for oscillations from the salt-march data of van der Plasche and from Wright and Gehrels et al. needs to be introduced; also the new archaeological data in press or in preparation needs to be evaluated.]

The Australian coral data has also demonstrated that the ocean volume has not been constant over the past 6–7 ka but that it has increased by about 3 m sea level-equivalent (or about 1.2 x 10^6 km^3 of grounded ice) in this time interval [reference needed]. More recent analyses from different parts of the world have confirmed this result with most of this increase occurring between about 6 and 3 ka [Milne reference, WCRP Chapter 4].

[PLACEHOLDER FOR FIRST ORDER DRAFT: Sources, rapid change at 7.6 ka, recent fluctuations during MPW AND LIA and description of a figure showing eustatic sea level since 8 ka togenter with tide records and error bars.]

[INSERT FIGURE 5.9 HERE]
Figure 5.9: [PLACEHOLDER FOR FIRST ORDER DRAFT: pCO_2 (or polar Temp.) vs. ice volume (sea level) from data and models (Pliocene to recent)] Relationship between reconstructions of past sea level changes due to ice sheet contributions and estimates of past atmospheric CO_2 concentrations. [This figure (from Alley et al., 2005) to be updated by newly available data and an assessment of uncertainties.]

[INSERT FIGURE 5.10 HERE]
Figure 5.10: [PLACEHOLDER FOR FIRST ORDER DRAFT: Palaeo sea level variations (update of sea level figure in WCRP report). Globally averaged variation in sea level in Late Holocene time. This figure is from the volume edited by Church at al. (Figure 4.14, p.96). It will be supplement it with a couple of side panels showing individual published records, corrected and not corrected for isostatic effects. These figures would like some of the panels in Figure 4.12 or Figure 4.13. These would include results by Woodroffe et al. (submitted to Nature) from corals in the Pacific and new salt marsh records by Gehrels et al. from Tasmania and New Zealand (publications in preparation). There are new results forthcoming from archaeology sites in the Mediterranean.]

[INSERT FIGURE 5.11 HERE]
Figure 5.11: [PLACEHOLDER FOR FIRST ORDER DRAFT: Rates of sea level change during the last interglacial.]

5.5 Climate Responses and Feedbacks at Regional Scales

[PLACEHOLDER FOR FIRST ORDER DRAFT]

5.5.1 Regional Temperature Changes

The PAGES (http://www.pages-igbp.org/) "Regional 2k Network' initiative (http://www.pages-igbp.org/science/last2millennia.html) will provide detailed spatio-temporal quantitative reconstructions combining different proxy archives and dynamical interpretation of the climate of the last 2000 years covering each of the continents and their adjacent ocean regions. The continental syntheses are expected in 2012 and will provide input for this subsection. These results will be presented in Figure 5.12 (comparison of observed continental- and global-scale changes in surface temperature with CMIP models) similar to AR4, Figure TS22.

Since AR4, new syntheses of reconstructed ocean temperature have been produced for various time slices. The MARGO project provided a multi-proxy evaluation of SST for the Last Glacial Maximum (LGM) (Waelbroeck et al., 2009). The study found stronger tropical cooling compared to earlier syntheses (e.g., CLIMAP, 1976, 1981). Most prominent are a 1–3 degree cooling of the W Pacific warm pool and a reduction of the subtropical gyres. At higher latitudes, strong cooling prevailed in the Eastern Boundary currents areaswith some discrepancies between various proxies. Polar fronts moved equatorward to about 45°N in both hemispheres. Seasonally ice free conditions were documented, however, in the NE North Atlantic and in the eastern Nordic Seas, in contrast to the widely used CLIMAP reconstruction (CLIMAP, 1981) which suggested perennial sea ice for these areas.

For the early to mid-Holocene, there is strong evidence that high-latitude areas in the North Atlantic-Arctic Ocean experienced summer SST warmer than their pre-industrial values, due to the orbitally induced stronger summer insolation (Jansen et al., 2007), Figure 6.9, and new data compilations, e.g., Andersson et al. (2010). The highest Holocene temperatures only appear in the stratified uppermost surface ocean layer, below which no Holocene thermal maximum is reconstructed (Andersson et al., 2010; Hald et al., 2007). In the high latitude Southern Ocean, Holocene SST trends also follow the decrease in austral summer insolation (Shevenell et al., 2011). High-amplitude near surface temperature variations on millennial to centennial time scale appear to characterise Holocene ocean temperatures in both hemispheres, particularly after 4 ka (Euler and Ninnemann, 2010; Risebrobakken et al., 2003; Shevenell et al., 2011). Due to time scale uncertainties, the phasing of these significant pre-industrial climate events between the hemispheres remains unclear. [PLACHOLDER FOR FIRST ORDER DRAFT: Compile such information and make throrough assessment.] Century scale temperature anomalies associated with a warm phase centered around 1100 AD and a generally colder phase after 1400 AD, and ending in the first decades of the 20th century are common in many marine proxy records of the High-latitude North Atlantic-Arctic ocean areas (e.g., Sicre et al., 2008). In the Fram Strait, at the entrance to the Arctic the high modern SSTs appear unprecedented over the past 2000 years (Spielhagen et al., 2011a).

Palaeoclimate records indicate an expansion of the western Pacific warm Pool in the Early Holocene (10–7 ka) (Linsley et al., 2010) with 0.5 degrees SSTs higher than modern values. During the past few millennia centennial-scale oscillations of the warm pool SSTs are synchronous with known changes in Northern Hemisphere climate (e.g., the Little Ice Age and Medieval Warm Period) implying a dynamic link between Northern Hemisphere temperatures and Indo-Pacific Warm Pool hydrology (Oppo et al., 2009; Tierney et al., 2010a).

Since AR4, there is a significant increase of available terrestrial temporal high resolution temperature proxy records from different areas of the globe. The majority of proxy records provide estimates for a particular season, making annual estimates and comparisons with other (seasonally different) records problematic (Bradley et al., 2003; Diaz et al., in review). Advances in new regional reconstructions and comparison with model simulations is provided below for various continents in the NH and SH where new evidence is available and with emphasis on the occurrence of changes within the Medieval Climate Anomaly (MCA) and Little Ice Age (LIA). Despite recent efforts (e.g., Conroy et al., 2009; Cook et al., 2006; Jones et al., 2009b; Mann et al., 2008; Neukom et al., 2010; Tierney et al., 2010b) fewer proxy records are available from the Southern Hemisphere (SH) and tropics, particularly at interannual to decadal resolution prior to about 1200 AD. However, new tree ring records from the Andes, northern and southern Patagonia, Tierra del Fuego, New Zealand and Tasmania (Boninsegna et al., 2009; Cook et al., 2006; Villalba et al., 2009), ice cores, lake sediments and documentary evidence from southern South America (Prieto and Herrera, 2009; Vimeux et al., 2009; von Gunten et al., 2009; [Neukom, 2009]) and terrestrial and shallow marine geological records from eastern Antarctica (Verleyen et al., 2011) allow for a better understanding of past temperature variations in parts of the SH.

The MCA (about 900 to 1350 AD) was not characterized by uniformly warmer temperatures globally, but rather by a range of temperature, hydroclimate and marine changes with distinct regional and seasonal expressions (see Section 5.5.2.4; [Jansen et al., 2007]). Since AR4 there is new evidence on the MCA with respect to the amount climate information available, modelling efforts and physical understanding of the underlying mechanism. For instance, 1000–2000 year long cold and warm season temperature reconstructions (based on historical documents and natural archives) generally show warm conditions during the MCA with high level of consistency in different regions within China (Ge et al., 2006; Ge et al., 2010; Ge et al., 2003; Wang et al., 2007a, [2006; Yang et al., 2009; Qian et al., 2008; Zhang et al., 2009; Holmes et al., 2009]). The warming of the last few decades of the 20th century is unprecedented in parts of China within the past 500 years; for the earlier period the large level of uncertainties precludes a quantitative comparison. (e.g., Ge et al., 2010). Millennium long temperature reconstructions and climate model simulations (Liu et al., 2005; Peng et al., 2009; Zhang et al., 2011) consistently show that centennial China temperature variations were controlled by changes in solar radiation and volcanic activity, with the greenhouse gases playing a larger role in the last 150 years. The magnitude of internal variability is though underestimated by the simulations in comparison to some of the reconstructions (Ge et al., 2003; Yang et al., 2002) and is only reconciliable with the [Wang et al. (2007)] record showing lower amplitude of past changes. Further evidence on the MCA and LIA and the current warmth in Asia is also provided by tree ring information from the Western Himalaya (Yadav et al., 2010). They found warm conditions from the 11th to the 15th century, lower temperature afterwards and warming (similar to the MCA) within the 20th century. Extended warmth during similar periods in the MCA and subsequent cooling have also been reported from the southern Tibetan Plateau [(Yang et al., 2003)], and from the northeastern Tibetan Plateau (Zhu et al., 2008), the northern slope of central Tianshan mountains [(Zhang et al., 2009)] as well as from western High Asia (Esper et al., 2007).

Evidence for warmer summer conditions during the MCA in comparison to post medieval times are provided by different studies using tree ring and sedimentary information from Northwest Canada, Canadian Rockies, Alaska and Colorado (MacDonald et al., 2009; Salzer and Kipfmueller, 2005; [Thomas and Briner, 2009; Luckman and Wilson, 2005; Hu et al., 2001; Loso, 2009]), although not in the Gulf of Alaska (Wilson et al., 2007a). Those studies also point to the fact that the entire 20th century or the last decades in most areas were warmer than the MCA, an analysis confirmed by lake and ice core and tree-ring data in the extended Arctic region north of 60ºN (Kaufman et al., 2009b). Kaufman et al. (2009b) also report that the last 2 kyr summer temperature changes in the Arctic have been found to be embedded in a long term trend in response to orbital forcing.

A multiproxy reconstruction of European spring-summer temperatures (Guiot et al., 2010) shows warm medieval conditions, although the last decades were warmer than any other period of the last 1400 years. Scandinavian summer temperatures reconstructed from tree rings (BRIFFA et al., 1992; Gouirand et al., 2008; Grudd, 2008; Grudd et al., 2002; Helama et al., 2009b; Lindholm et al., 2010; [Gunnarson et al., 2010; Kirchhefer, 2001; Linderholm et al., 2009]) also indicate generally warm conditions centered on the 760s, between about 980 and 1100, and again in the 1410–1420s that are comparable to or even higher than conditions during the 1930s and after about 1980 (Buntgen and Schweingruber, 2010).

Tree ring evidence from the Alpine arc (e.g. Buntgen et al., 2006; Buntgen et al., 2005; Corona et al., 2010; Nicolussi et al., 2009; [Buntgen et al., 2009]) point to cooler summer temperatures from the 15th century to about 1820. Warm periods occurred in the 990s and between about 1150–1250. Alpine summer temperatures during the late 20th century appear unprecedented over the past 1500 years (Buntgen et al., 2011; Nicolussi et al., 2009). Shorter temperature reconstructions that reach back into the 12th and 13th centuries are available from the Romanian Carpathians (Popa and Kern, 2009) and the Spanish Pyrenees (Buntgen et al., 2008) that show summer temperature variations that are comparable to those obtained from the Alps.

Modelling results suggest that the warm summer conditions during the early second millennium compared to the climate background state of the 13th–18th century are due to a large extent to the long term cooling induced by changes in land-use in Europe. During the last 200 years, the effect of increasing greenhouse gas concentrations, which was partly levelled off by that of sulphate aerosols, has dominated the climate history over Europe in summer. Volcanic and solar forcing plays a weaker role in this comparison between the last 25 years (that were comparable with the warmth roughly a millennium ago) of the 20th century and the early second millennium. External influence was detectable in European summer temperatures over the period 1500–1900 (Hegerl et al., 2011).

High temporal resolution climate evidence is scarce for cold season temperatures in Europe before 1500 AD. Most of the scattered information on past temperature variations stem from documentary information from western and central Europe (e.g., Brazdil et al., 2005; Brazdil et al., 2010; [Pfister et al., 2008; Brazdil et al., 2005, 2010; Glaser, 2008, Glaser and Riemann, 2009, and references therein]). Evidence for winter is more equivocal than for summer and firm conclusions on the role of external forcing are not possible [(Goosse et al., 2006)] due to large uncertainties in spatial temperature coverage and modeling approximately 1000 years ago. However recently [Hegerl et al. (2011)] found that external forcing contributes significantly to the reconstructed long-term variability of winter and spring temperatures back to AD 1500 and that the winter warming is largely attributable to greenhouse-gas forcing in the last 2 centuries.

In the Southern Hemisphere, Neukom et al. (2010) presented multi-proxy regional austral summer (winter) temperature field reconstruction for Southern South America back to AD 900 (1706). Mean austral summer temperatures between 900 and 1350 are mostly above the 20th century climatology (though associated with large uncertainties). After 1350, there is a sharp transition to colder conditions, which last until approximately 1700. Agreement on the simulation of a warmer MCA period and a cooler LIA is found with two climate models (ECHO-G and CCSM (Luterbacher et al., 2011), although with some differences in the timing of the MCA-LIA transition and in the larger amplitude of simulated warming in the last two centuries. East Antarctic shallow marine geological records do not show clear evidence of an MCA-like phase and only circumstancial local evidence for a cool event comparable to the LIA (Verleyen et al., 2011) in contrast to the Arctic (Kaufman et al., 2009b).

Palaeoclimate reconstructions (see paragraphs above) at regional scale and modelling studies of the MCA provide capability for elucidating key mechanisms governing the climate system including the North Atlantic Oscillation (NAO) and ENSO (Cobb et al., 2003; Conroy et al., 2009; Graham et al., 2010; Graham et al., 2007; Trouet et al., 2009). Changes in the persistency or frequency of climate modes (such as ENSO) may account for some of the thermal features during the MCA (Graham et al., 2010; Graham et al., 2007; Mann et al., 2009a; Mann et al., 2005; Seager et al., 2007; Seager et al., 2008; [Diaz et al., 2011]), with preferred La Niña-like states likely dominating the MABOUT Changes in sea surface temperature (SST) may have led to warm conditions in northern and western Europe through SST-forced changes in large-scale circulation patterns (positive NAO phase) (Graham et al., 2010; Mann et al., 2009a; Trouet et al., 2009; [Diaz et al., 2011]). Sensitivity studies inducing warmer tropical Indian and western Indian and Pacific Oceans with enhancement of the zonal Equator gradient suggest (Graham et al., 2010) a broad range of climate shifts can be induced in agreement with proxy data, including widespread aridity through the Eurasian sub-tropics, shifts in monsoon rainfall patterns across Africa and South Asia and stronger winter westerlies across the North Atlantic and Western Europe, many of those not explained by a cooler tropical Pacific (La Nina type) alone [(Graham et al., 2010)]. One possible mechanism to understand these changes is related to dynamical responses to natural radiative forcing (solar irradiance and explosive tropical volcanism) (e.g., [Mann et al., 2005; Meehl et al., 2009]). Solar activity is generally acknowledged as having played a role throughout the last millennium, particularly in establishing the contrast between MCA and LIA periods (e.g., [Lean, 2010]). This is supported by model simulations of the last millennium (e.g., [IPCC, 2007]), although recent simulations driven with lower levels of past solar forcing variability (Schmidt et al., 2011) suggest that internal variability could have had a role in producing many of the observed regional changes (Jungclaus et al., 2010b).

[INSERT FIGURE 5.12 HERE]

Figure 5.12: [PLACEHOLDER FOR FIRST ORDER DRAFT: Compilation of temperature reconstructions at continental scale (similar to AR4, Figure TS 22) together with CMIP models, model data/comparison.] Regional temperature, reconstructions, comparison with model simulations over the past millennium (1001–1999 CE). Ensemble model mean (black line) plus 20 and 80 percentile (gray envelope). Mean of temperature reconstructions (bold blue line) and estimatetion of error from each reconstruction (light blue line). All lines are smoothed to remove fluctuations under 50 years. Models used: ECHO-G (Gonzalez-Rouco et al., 2006), CCSM (Ammann et al., 2007), CCSM-Bern [reference needed], COSMOS (Jungclaus et al., 2010b), CNRM (Swingedouw et al., 2010). Reconstructions by region: North America [reference needed], South America (Neukom et al., 2010), Arctic (Kaufman et al., 2009a), Europe (Guiot et al., 2010), Africa [reference needed], Antarctica [reference needed], Asia (Yang et al., 2002), Australia [reference needed].

[START BOX 5.2 HERE]

Box 5.2: Glacier Variations During the Holocene

New data on the Holocene glacier and tree line fluctuations published since the AR4 improve our ability to assess the causes of glacier variability. Cosmogenic isotopes technique (^{10}Be) have extensively been deployed to date glacial moraines, especially in the areas formerly underrepresented in the global data sets such as the tropics and the Southern Hemisphere [(Schaefer et al., 2009; Glasser et al., 2009; Licciardi et al., 2009, Jomelli et al., submitted)]. In contrast to the radiocarbon-based glacial chronologies which depend on the availability of organic material, the ^{10}Be-based series allow the dating of glacial landforms themselves. However glacial boulder exposure ages tend to represent the minimum limiting deglaciation ages [(Heyman et al., 2011)]. The ^{14}C and dendrochronological dates of the tree remains located upper the modern tree line and those killed by the advancing glacier also provided widespread information on the former tree line position and glacier advances [(Joerin et al., 2008; Barclay et al., 2009; Menounos et al., 2009)]. Although both glaciers and tree line elevation depend on several climatic and even anthropogenic (in case of tree line) parameters, temperature is one of the most important factor driving their centennial variability [(Oerlemans, 2005; Hormes et al., 2001)]. Both are lagging the climate signal, but the tree line is more inertial, sometimes lagging the temperature rise by several centuries [(Hormes et al., 2001)], while for mountain glaciers the response time is typically a few decades [(Haeberli and Hoelzle, 1995)], therefore some glacier advances and retreats are too short to be registered in the tree line records. The combination of the two independent records in combination with the other proxies, such as lake sediments, greatly decreases the uncertainties in paleoglaciological reconstructions.

Long-term trends

The new data generally confirm the opposite multi-millennial trends in glacier variations in the Southern and Northern Hemispheres (Box 5.2, Figure 1), consistent with the opposite orbital trends of summer insolation in both hemispheres. However there are some exceptions, such as the Central Asian glaciers, which generally decreased through the Holocene [(Seong et al., 2009)]. While earlier studies had suggested large impact on monsoon precipitation to explain this discrepancy, the recently applied mass-balance models reconciled the glacier history with simulated climate changes and attributed the Early Holocene glacier advances in this area to reduced summer temperatures [(Rupper et al., 2009)].

Centennial to multidecadal variability

Despite of improvement of glacial chronologies in several regions (see Box 5.2, Figure 1), the evidence for intra- and inter-hemispheric synchroneity of submillennial glacier fluctuations is still inconclusive [(Wanner et al., 2008; Winkler and Matthews, 2011)]. With more detailed records obtained recently one can distinguish a transition from the time of high tree line and small or absent glaciers and generally colder phase with numerous gradually increasing in magnitude glacier advances around 4.5–3.8 ka in the Northern Hemisphere. The broad similarities of glacier variations in the outer tropics (southern Peru) of and those in Europe during the early Holocene and in the “Little Ice Age” period may reflect migrations of the Atlantic Intertropical Convergence Zone and associated circulation patterns over continental South America [(Liccardi et al., 2009)]. The coherency of high frequency variations in New Zealand with NH glaciers remains controversial [(Schaefer et al., 2009; Winkler and Matthews, 2010)]. The last 2 ka glacial chronologies, which are much better constrained due to the precise tree-ring dating reveal a broad coherency between major glacier advances in the Alps [(Holzhauser et al., 2005)], Alaska [(Wiles et al., 2008)] and Southern Tibet [(Yang et al., 2008)] centered around AD 200, 400, 600, 800–900, 1100, 1300 and in 17 though 19 centuries. This multi-centennial variability was suggested to be linked with multi-centennial variations in solar activity [(Holzhauser et al., 2005; Luckman and Wilson, 2005; Matthews, 2007; Whiles et al., 2008)] and changes in North Atlantic circulation [(Nesje, 2009)], though this coherence is not proved at the global level [(Wanner et al., 2008)] and no comprehensive mechanism for such a correlation is suggested so far.

Modern glacier retreat in the retrospective of Holocene variations

Several glaciers appear to be less extensive today than they have been throughout the Holocene (Canadian Rockies — [Koch et al., 2004]) or at least in the last 6 ka (Quelccaya — [Thompson et al., 2006]; western Scandinavia — [Bakke et al., 2008]). In other regions, however, the strong evidence of higher tree line and smaller glaciers in various periods in the Holocene are found. For instance radiocarbon dates show that ice on Anvers Island, Western Antractica, was at or behind its present position at 700–970 cal yr BP and at least two more times in the last 5600 yr. [(Hall et al., 2010)]. [Joerin et al. (2008)] found out that the equilibrium line altitude (ELA) in the Alps was at least >220 m higher than in the end of 20th century for the periods around 9200 cal yr BP, from 7450 to 6650 cal yr BP and from 6200 to 5650 cal yr BP with glacier advance occurring shortly after 6630 cal yr BP and 5800 to 5650 cal yr BP. This study points out that the range of Holocene ELAs in the Alps may exceed a total amplitude of 320 m [(Joerin et al., 2008)], which is higher that previously thought. Since mean annual temperatures remained almost unchanged during the mid-Holocene [(von Grafenstein et al., 1999)] it is suggested that these changes are related to the enhanced seasonality with higher summer temperatures at that time. The interpretation of these findings in terms of temperatures has to be taken with caution and the mentioned above lag between the glacier status and the climatic signal should be taken into account.

[INSERT BOX 5.2, FIGURE 1 HERE]
Box 5.2, Figure 1: Time–distance diagrams for glaciers (blue) and tree line elevation changes (green) through the Holocene in comparison with the northern timberline dynamics.
1. Northern timberline in Siberia [(Khantemirov, 2011)]
2. Large tidewater glacier systems (Glacier Bay) in southern Alaska [(Barclay et al., 2009)]
3. Baffin Island: a) Laurentide Ice Sheet; b) Northern Baffin Plateau; c) Central Cumberland Peninsula; d) Northern Cumberland Peninsula [(Briner et al., 2009)]
4. Northern Scandinavia [(IPCC, 2007)] [will be updated by Nesje]
5. Southern Scandinavia [(IPCC, 2007)] [will be updated by Nesje]
6. Western Canada [(Clague et al., 2009)]
7. The Alps [(Ivy-Ochs et al., 2009)]
8. Caucasus [(Solomina et al., in preparation)]
9. Altay [(Nazarov, in preparation)]
10. Muztag Ata–Kongur Shan [(Owen, 2009)]. Dashed lines: advances recorded in one valley; solid lines: at least in two valleys
11. Himalaya and Karakoram (Curve by [Roethlisberger and Geyh, 1985]; modified by [Owen, 2009])
12. Peruvian Andes (a) [Licciardi et al., 2009; b) [Glasser et al., 2009])
13. Cordilleras of South America (generalized curve; [Koch and Clague, 2006])
14. New Zealand: Mt. Cook, Mueller, Tasman, and Hooker Glacier [(Schaefer et al., 2009)]

[END BOX 5.2 HERE]

5.5.2 Changes in Precipitation and Droughts

[PLACEHOLDER FOR FIRST ORDER DRAFT]

5.5.2.1 Monsoon Systems

[PLACEHOLDER FOR FIRST ORDER DRAFT: Missing for Figure 5.18, Comparison of monsoon behavior in reconstructions and transient models runs.]

Monsoons provide essential freshwater resources and are the main determinant of agricultural production in densely populated areas where the economy depends on subsistence agriculture. Given their societal relevance, it is of considerable importance to document the historical changes in the Monsoon and to isolate the roles of various natural and anthropogenic factors in the observed changes in Monsoon behavior (e.g., Buckley et al., 2010; Cook et al., 2010a; Fan et al., 2010).

Most of the present-day existing Monsoon systems have been found to respond to orbital forcing of local summer insolation, and to millennial-scale oscillations such as DO and H events. Speleothem records from tropical and subtropical South America indicate the South American Monsoon System (SAMS) has responded to local orbital summer insolation changes at precessional timescales (Cruz et al., 2005; Cruz Jr et al., 2006; Pivel and Toledo, 2010), strengthening during the LGM and the late Holocene, and weakening during the mid-Holocene, in opposition to the NH Monsoons. This antiphase response has been specially well established with Chinese speleothem records of the East Asian Monsoon (Wang et al., 2005b; Wang et al., 2001). The response to insolation forcing has also been found in coupled GCM simulations (Braconnot et al., 2007b; Kutzbach et al., 2008). Abrupt climate changes such H2, H1 and the YR that produce a weakened AMOC, inducing a southward ITCZ shift are recorded as wet conditions in speleothem records in the Northeast Brazil and in the core SAMS region (Cruz et al., 2009), again contrasting with reduced monsoons depicted in the Middle East (Bar-Matthews et al., 2003; Fleitmann et al., 2007) and East Asia (Wang et al., 2005b; Wang et al., 2001).

Orbitally driven variations in summer solar radiation are a dominant control of long-term late Quaternary variations in rainfall in areas influenced by the global monsoonal belt. Between the hemispheres the strength of the summer insolation alternates, primarily at precessional periods, which explains the interhemispheric antiphasing of monsoonal rainfall variations observed in several records (Wang et al., 2006; Wang et al., 2007b). Regionally, the phase relation between orbital insolation and precipitation-related proxies shows complex spatial variations (Cai et al., 2010; Kutzbach et al., 2008). Alternating east-west differences in monsoonal rainfall have been observed for South America (Cruz et al., 2009), Asia (Hong et al., 2005), and South Africa (Chase et al., 2010; Kristen et al., 2010).

Cheng et al. (2009) and Wang et al. (2008) interpret the cave $\delta^{18}O$ in central China as the relative summer to winter East Asian monsoon intensities that vary dominantly and directly in response to the changes in Northern Hemisphere summer solar radiation at orbital scales. Clemens et al. (2010) however report, that marine and terrestrial Indian and Asian monsoon proxies including those studied by Cheng et al. (2009) and Wang et al. (2008) reflect rather the combined influence of summer monsoon forcing with a phase lag of 8 kyrs relative to precession minima and winter temperature forcing that is in phase with precession minima. East Asian Winter Monsoon (EAWM) intensification in cold stadials and early Holocene is suggested by alkenone SST records off the coast of Southern Vietnam in relation with AMOC weakening (Huang et al., 2011). Planktonic foraminifera in the eastern Equatorial Atlantic show West African Monsoon (WAM) precipitation dependence on high latitude climate during the last interglacial and deglaciation while Mg/Ca ratios suggest SST dependence on greenhouse gases and low latitude insolation (Weldeab et al., 2007). δ18O profiles from Arabia and China show that EASM and the Indian Summer Monsoon (ISM) follow insolation during the Holocene with influences of solar activity and North Atlantic climate at centennial to multidecadal time scales (Dong et al., 2010; Fleitmann et al., 2003; Fleitmann et al., 2007; Selvaraj et al., 2011; Wang et al., 2005b). EASM weakens during the LGM in PMIP simulations (Jiang and Lang, 2010), but discrepancies exist for the EAWM, with half of the models suggesting a strengthening. Climate models have been able to simulate the patterns of reduced summer monsoon precipitation associated with the 8.2 ka event (LeGrande and Schmidt, 2008; Wiersma and Renssen, 2006; Wiersma et al., 2011), though details of regional differences and timing will require higher-resolution models and better chronologies (Jin et al., 2007).

The control on past precipitation variability in Asia covering the past thousand years is not exclusively related to temperature, but reflect complex atmospheric circulation and thermodynamic effects with great regional and temporal variations (e.g., Treydte et al., 2006). Based on annually resolved oxygen isotope records from tree-rings (reflects mainly winter precipitation) in the high mountains of northern Pakistan. Treydte et al. (2006) found dry conditions at the beginning of the past millennium and through the eighteenth and early nineteenth centuries. They found the wettest conditions in the 20th century. Stalagmites from central China show periods of stronger summer monsoons during the middle of the first millennium and for parts of the MCA (Tan et al., 2011; Zhang et al., 2008).

Documentary and geologic evidence suggest that extended intervals of drought associated to weak ISM in the last 2 kyr were synchronous across a large region of Asia including southern Vietnam (Berkelhammer et al., 2010; Buckley et al., 2010; Cook et al., 2010a; Davis et al., 2005; Fleitmann et al., 2004; Sinha et al., 2007; Staubwasser and Weiss, 2006; Zhang et al., 2008). Cook et al. (2010a) report about weak monsoons in tropical south and Southeast Asia in the mid-14th and early 15th centuries that are similar in timing to that of severe droughts associated with the demise of the Khmer civilization at Angkor in Cambodia (Buckley et al., 2010), in the late 16th century, at the end of the 17th century. During the LIA, a weaker EASM is also reported (Davis et al., 2005; Tan et al., 2011; Zhang et al., 2008), albeit with certain discrepancies among Tibetan dendroclimatological records (Griessinger et al., 2011) also add Cook et al. (2010a) that show rather moist conditions in the 15th-19th period. Anchukaitis et al. (2010) studied the influence of volcanic radiative forcing on Asian boreal summer drought reconstructions (Buckley et al., 2010; Cook et al., 2010a) since the Medieval period. Superposed epoch analysis reveals significantly wetter conditions over mainland southeast

Asia in the year of an eruption, with drier conditions in central Asia. The proxy/model comparison suggests that GCMs may not yet capture all of the important ocean-atmosphere dynamics responsible for the influence of explosive volcanism on the climate of Asia (Anchukaitis et al., 2010).

Instrumental, tree ring, documentary, stalagmite and sedimentary evidence agree on exceptionally dry conditions over the past decades (Chu et al., 2011; Cook et al., 2010a; Ge et al., 2008; Ge et al., 2011; Griessinger et al., 2011; Tan et al., 2011; Zhang et al., 2008) though often not unprecedented in the context of the past centuries. Fan et al. (2010) analysed the behavior of the Asian Monsoon in Coupled Model Intercomparison Project (CMIP3) multimodel historical simulations and in observational data. The CMIP3 simulations capture the observed trend of weakening of the Asian Monsoon circulation over the past half century, but are unable to reproduce the magnitude of the observed weakening trend. The observed recent decadal weakening trend in this relationship, which has been attributed in some studies to anthropogenic forcing, appears to be well within the variability of the CMIP3 multimodel ensemble.

Geomorphic, isotopic, geochemical and dust records from western Africa covering the last 3 millennia shows intervals of severe droughts lasting decades to centuries characteristic of the WAM and related to natural variations in Atlantic temperatures and circulation (Shanahan et al., 2009). The recent severe droughts in Western Africa are not anomalous in the context of last millennia and largest episodes took place at the turn of the millennium and 200–300 years ago (Mulitza et al., 2010; Shanahan et al., 2009).

[INSERT FIGURE 5.13 HERE]
Figure 5.13: [PLACEHOLDER FOR FIRST ORDER DRAFT: to depict changes in indian monsoon during the current interglacial. This draft figure is based on different marine core parameters.] Related to monsoon variability [timescale to be discussed]; possibly incl. model results.

[INSERT FIGURE 5.14 HERE]
Figure 5.14: [PLACEHOLDER FOR FIRST ORDER DRAFT: showing the link between changes in temp. and corresponding changes in precipitation (as Figure 3 in Solomon et al., 2009).] Option 1: Changes in the global distribution of precipitation per degree of warming for modelled past warm climate (most likely Pliocene) vs preindustrial climate. Figure will be constructed in analogy to Solomon et al. (PNAS 2009; Figure 3 therein) showing changes in % of dry season precipitation per K of local temperature change. Analysis will be based on multi model ensemble. Option 2: Data-model comparison of tropical precipitation changes on orbital timescales in order to asses the relative importance of precessional forcing vs. CO_2 changes (Background climate: Pliocene or late Quaternary). [Selection of option will be based on the availability of reconstructions allowing for-data model comparison.]

5.5.2.2 Shifts in Convergence Zones

Convergence zones are regions of deep convection and extensive rainfall that provide a major heat source for the tropical atmosphere. Changes in these convergence zones affect the strength and position of Hadley circulation (Hack et al., 1989), and trigger large-scale stationary waves that emanate from the tropics, which in turn influence extra-tropical climates (Okumura et al., 2009; Timmermann et al., 2010b). Spatial shifts of these rain bands can result in major disruptions of the regional hydrological cycle. Three convergence zones are of particular importance in terms of climate reconstructions: 1) Inter-Tropical Convergence Zone (ITCZ), an equatorial rain and cloud band that encircles the globe; 2) South Pacific Convergence Zone (SPCZ), which extends from the Solomon Islands southeast to Fiji, Samoa, and Tonga; and 3) South Atlantic Convergence Zone (SACZ), which extends from the Amazon basin southeast into the subtropical Atlantic.

ITCZ reconstructions based on paleoclimate proxies [(Haug et al., 2001; Black et al., 2007; Sachs et al., 2009)] and model results [(Braconnot et al., 2007; Timmermann et al., 2007)] implicate the precessional cycle, which modulates the amplitude of seasonal insolation in both hemispheres in an opposite manner, as a key driver for tropical hydrological changes on millennial to orbital timescales. Some model results also demonstrate the ability of the ITCZ to shift abruptly in response to slowly varying orbital forcing (Timmermann et al., 2007). For example, cooling in the North Atlantic resulting from a weakening of Atlantic Meridional Overturning Circulation (AMOC) and sea-ice changes during Heinrich events, perturbs interhemispheric temperature gradients leading to an intensification of the northeasterly trade winds, enhanced evaporation and further cooling of the eastern tropical Atlantic (Chiang and Bitz, 2005). The positive wind-evaporation-SST feedback is an important element in maintaining the tropical meridional temperature anomalies. Along with the intensified trade winds in the North Atlantic and weakened trade winds in the tropical South Atlantic, the moisture transport and convergence shifts south. These processes are robustly simulated in CGCMs (Stouffer et al., 2006). Proxy evidence suggests that northwestern Africa experiences major hydrological disruptions in response to seasonal to orbital-scale shifts of the Atlantic ITCZ (Tjallingii et al., 2008; Weldeab et al., 2006; Weldeab et al., 2007). Recent reconstructions of tropical Pacific hydrological variability (Leduc et al., 2009) document the linkage between Pacific ITCZ and millennial-scale variability in the North Atlantic.

Regional convergence zones, such as the SACZ and SPCZ, also respond dynamically over different time scales. Paleoclimate SACZ reconstructions [(e.g., Wang et al., 2007)] demonstrate orbital and millennial-scale variations in the hydrologic cycle and link hydrologic changes between the Southern and Northern Hemisphere. Internannual changes in SPCZ position and intensity are driven by El Niño-Southern Oscillation (ENSO) variations, with ENSO warm phases (cool phases) corresponding to northeastward (southwestward) movement of the SPCZ [(Folland et al., 2002)]. A multi-century paleoclimate reconstruction of SPCZ position since 1650 CE displays prominent decadal variability in addition to ENSO-driven interannual variability [(Linsley et al., 2008)]. Modelling evidence further suggests that changes in the tropical Atlantic SST, associated with a weakening of the AMOC, can have an impact also on the position of the Pacific ITCZ (Xie et al., 2008; Zhang and Delworth, 2005) and the SPCZ.

5.5.2.3 Variations in High Latitude Precipitation and Storm Tracks

The mid to high latitudes in Southern Hemisphere (SH) are under the year long influence of the Southern Westerly Winds (SWW) circulation (modern core about 50°S). Because of the strong correlation between SWW and precipitation over the landmasses in the SH (e.g., [Garreaud, 2007]), proxies of precipitation are interpreted as past changes in intensity or latitudinal position of the SWW. Despite many research efforts, the timing and direction of such changes throughout the Holocene are still under debate (e.g., [Do Hume, 2010] and reference therein). [Fletcher and Moreno (2010)] report on nearly synchronous multi-millennial trends in moisture patterns related to zonally symmetric changes in the strength and position of the SWW from terrestrial and marine proxies, over the last 14 kyr, that are opposite to findings by (Lamy et al., 2010) from marine records off Southern Patagonia. These trends coincide with the rise and decline of atmospheric CO_2, supporting the hypothesis of an important role of the SWW in the global carbon cycle through wind-driven upwelling of CO_2-rich waters in the Southern Ocean (Denton et al., 2010; Toggweiler, 2009; Anderson and Carr, 2010).

Knowledge prior the Holocene is sparse and even less conclusive. Limited modelling studies of the SH climate consist of mid-Holocene and Last Glacial Maximum time slices, and these studies produce divergent results (Rojas et al., 2009; [Rojas and Moreno, 2010; Wagner et al., 2007]). Mechanism of circulation and hence precipitation changes are given by tropospheric meridional temperature gradients, forced by insolation changes, similar to the response to GHG concentration for the 21st century [(Groman, 2010)]. For the LGM, these are also dependant on the simulated sea-ice extent [(Rojas et al., 2009)]. In all cases spatial resolution plays a key role in the ability of simulating circulation changes.

Northern Hemisphere (NH) high-latitude storm-tracks follow the westerlies and are heavily influenced by the Northern Annular mode variability both over the Pacific and Atlantic. Holocene precipitation reconstructions exist for Northern Europe based on glacier mass balance reconstructions for winter season precipitation [(e.g., Bakke et al., 2008)] and wetness indicators from lake and bog sediments (e.g., Rosqvist et al., 2007; St Amour et al., 2010). Ice core data provide additional information on snowfall over the Greenland Ice Sheet (Vinther et al., 2006). Since AR4 the quality and analytical framework of Holocene proxy-archives have evolved rapidly. Included in the evolved analytical framework is the effect and better constrained seasonal response of various proxies/archives. In addition stronger emphasis has been placed on non-stationarity of the atmospheric system over time thereby changing the regional impact not only by variations in strength but also in the spatial position of the atmospheric systems relative to the investigated regions. Several proxy-based records document large amplitude multidecadal to century scale regional anomalies in temperature, storm-tracks and precipitation within the Holocene (see review in Wanner, 2008). Accompanying the reduction in summer insolation due to orbital parameters during the Holocene is an enhanced wintertime wetness in Scandinavia with a marked change occurring at about 2 ka (Bakke et al., 2008), followed by more distinct fluctuations at century time scales. It is still unclear what caused the observed variations. There is, however, an apparent link between variability in northern North Atlantic sea ice cover and atmospheric patterns during the most noticeable shifts in precipitation patterns [(Rosqvist et al., 2007; Bakke et al., 2008)].

Modelling experiments are quite inconclusive as to major changes in storm tracks during the Holocene. Of the PMIP2 experiments for 6 ka there is a slight tendency for an increased NAO-like pattern with a northward displaced storm track and wetter wintertime conditions over Northern Europe (Gladstone et al., 2005). In some transient model experiments for the past 1000 years, there are indications of mulitdecadal changes in the phase and strength of the NAO, indicating significant positive NAO following after major volcanic eruptions (Ottera et al., 2010). Model studies of glacial storm tracks indicate reduced storminess and a more confined southern postion of the mid-latitude jet in the Northern Hemisphere during the LGM (Li and Battisti, 2008), consistent with paleoclimatic proxy data.

5.5.2.4 Megadroughts and Floods

Drought and floods are recurring extreme climate events. There is ample historical evidence for their past important physical, economic, social and political consequences (Buckley et al., 2010; Buntgen et al., 2011; Graham et al.; Zhang et al., 2008). Evidence from tree rings, historical documents, stalagmites, lake sediments, peatlands, etc, indicates that severe megadroughts (by modern standards droughts of unusually long duration that typically exceed those observed in the instrumental records; [Woodhouse and Overpeck, 1998; Stahle et al., 2000; Cook et al., 2010]) are a recurrent feature in many regions including North America, east and south Asia, Europe, Africa and India [(Cook, 2007; Herweijer, 2007; Zhang, 2008; Zheng, 2006; Buckley, 2010; Buckley, 2010; Cook, 2010; Helama, 2009; Russell, 2007; Büntgen, 2010; Esper, 2007; Sinha, 2007; Shanahan, 2009; Neukom, 2010; Pfister, 2006; Touchan, 2008; Touchan, 2010; Pauling, 2007; Verschuren, 2000; Christie, 2009; Berkelhammer, 2010; Nicault et al., 2008)].

The occurrence and spatial extent of past megadroughts may be clustered over time following regime changes. There is evidence for more severe droughts during the LIA in South Asia, eastern Northwest China, and Southeast Asia, west Africa and parts of Europe [(Buckley, 2010; Sinha, 2007; Shao, 2010; Zheng, 2006; Zhang, 2008; Sinha, 2007; Sinha, 2007; Helama, 2009; Buntgen, 2011; Pauling, 2007; Cook, 2010 ; Russell, 2007; Shanahan, 2009)] compared to the predating MCA and the last century. In contrast, drought extent in North America, northern and central Europe, and East Africa were significantly greater during 900–1300 than during the LIA and the last century [(Cook, 2007; Cook, 2010; Herweijer, 2007; Helama, 2009; Luoto, 2010; Russell, 2007; Verschuren, 2000; Stager, 2005)]. Proxy information indicate, that intervals of severe drought in western Africa lasting for periods ranging from decades to centuries are characteristic of the monsoon and are linked to natural variations in Atlantic temperatures ([Shanahan et al., 2009]; see also Sections 5.5.2.1 and 5.6.2). Proxy reconstructions and model experiments suggest that variability in the tropical Pacific might partly account for the occurrence of megadroughts in North America with related teleconnections in all continents (Seager et al., 2008). A strengthening of the zonal SST gradient in the tropical Pacific via an enhancement of La Niña state and possibly warming of the Indian Ocean during periods of the MCA may have contributed to arid conditions in North America (Graham et al.; Seager et al., 2008), contrasting with wetter conditions in Asia (Graham et al., 2007). During the MCA, positive NAO conditions (see Section 5.5.5.3) and AMO phases may have favored wetter winter conditions in NW Europe and arid in NW Africa [(Graham, 2007; Esper, 2007; Touchan, 2008; Touchan, 2010)]. El Niño phases seem to have been more prominent during the LIA than the MCA, in coincidence with monsoon weakening (see Section 5.5.2.1) and drought occurrence in Asia (Buckley et al., 2010; Cook et al., 2010a),

Geomorphological, sediment and documentary records provide evidence that floods are also a recurrent feature in many areas in the Pleistocene, Holocene, and the past millennia [(Benito, 2010; Jones, 2010; Williams, 2009; Huang, 2010; Storen, 2010; Greenbaum, 2006; Thorndycraft, 2006; Benito, 2008; Hassan, 2007; Macklin, 2006; Wetter et al., 2011)]. Paleoflood evidence from lake sediments, speleothems and other natural and documentary proxies indicate that in the Mediterranean, periods of region-wide flooding can be indentified in the 2nd, 6–7th, 10th, late 15th and late 18th centuries AD, which all coincide with relatively wet and cold climatic conditions ([Luterbacher et al., 2011], and references therein).

[PLACEHOLDER FOR FIRST ORDER DRAFT: Additional studies on megafloods from other parts of the globe as well as the ability of coupled OA models to simulate the type of megadroughts including intensity, spatial and temporal extent, recurrence, and possible links with external forcings.]

During the LIA, ice cover on large rivers combined with snow melt could also have generated spring floods similar to what is observed today at higher latitudes. Floods could be attributed to increases in regional rainfall intensity and/or duration, timing of melting of glaciers [(Debret et al., 2010)], as well as human activities in the earlier 19th century [(Sierro, 2009; Benito, 2010; Greenbaum, 2006)].

Overall, multiple studies suggest that current drought and flood regimes are not unusual within the context of last 1000 years [(e.g., Cook et al., 2010; Seager et al., 2008; Graham et al., 2010)].

5.5.3 Modes of Climate Variability

The dominant of natural modes of climate variability, such as the El Niño-Southern Oscillation (ENSO), the Indian Ocean Dipole (IOD), the North Atlantic Oscillation (NAO), the Southern Annual Mode (SAM), longer term variability associated with the Atlantic Multidecadal Oscillation (AMO), and others can be considered spatially organized instabilities of the climate background state (see Chapter 14). Longer-term changes in the climate background state, induced by external forcings, may lead to changes in the statistics of these interannual to centennial-scale climate modes, and also to changes in the teleconnections of these modes to other regions.

5.5.3.1 ENSO

Changes in the statistics of ENSO have been studied in response to external forcing, using both CGCMs, as well as historical data and palaeo-proxy reconstructions, using corals, tree rings, ice-cores and sediment cores. Climate models run under LGM boundary conditions document wide ranges of ENSO behaviour and very little consistency (An et al., 2004; Bush, 2007; Otto-Bliesner et al., 2003; Toniazzo, 2006; Zheng et al., 2008) [to be updated with PMIP3/CMIP5 papers]. Existing annually resolved ENSO records for the last glacial period are virtually non-existent (Koutavas and Joanidis, 2009). The response of ENSO to a weakening of the Atlantic Meridional Overturning Circulation, such as during Heinrich event 1 (18.5–14.8 kyr BP) or the Younger Dryas (12.8–11.5 kyr BP) has been studied with CGCMs. A robust response emerges that suggests intensification of the ENSO amplitude and in some cases a reduction of the annual cycle in the Eastern Equatorial Pacific (Merkel et al., 2010; Timmermann et al., 2007). For the mid-Holocene (9–4 kyr BP), when both the obliquity of the Earth's axis was high and the Earth was closer to a boreal summer perihelion position, a number of proxy data indicate with medium to high confidence a reduction of ENSO variability (Koutavas et al., 2006; Tudhope et al., 2001) [to be updated], in qualitative accordance with PMIP3 and other CGCM modeling experiments (Brown et al., 2008a; Brown et al., 2008b; Bush, 2007; Zheng et al., 2008). Interactions with an intensified western Pacific monsoon circulation (Liu et al., 2000), an enhanced zonal equatorial SST gradient associated with an intensified Walker Circulation (Zheng et al., 2008) and reduced level of tropical atmospheric noise (Chiang et al., 2009) have been suggested to explain the reduction of ENSO variance during the mid-Holocene. Reconstructions of ENSO for the Last Millennium, while supporting the notion of a highly variable ENSO system also reveal a high degree of inconsistency among the proxies (Figure 5.15) (McGregor et al., 2010; Wilson et al., 2010). Efforts to extract the joint variability of different ENSO proxies using statistical techniques document an active ENSO phase during 1550–1650 (Wilson et al., 2010) and a reduction of eastern equatorial Pacific sea surface temperature variance in the periods 1650–1700, 1760–1780 and 1830–1870 (Figure 5.15) and a gradual increase of variance into the 20th century (McGregor et al., 2010). Volcanic forcing has been shown to increase the probability of reconstructed El Niño events to occur in the 2 years following the volcanic eruption (Adams et al., 2003; McGregor et al., 2010; Wilson et al., 2010). Simplified intermediate ENSO models are able to reproduce this behaviour (Adams et al., 2003; Emile-Geay et al., 2008), whereas CGCM experiments show a less robust response [(McGregor and Timmermann, 2011, in press)].

5.5.3.2 Indian Ocean Dipole

Coral records have been extensively analyzed (Abram et al., 2008; Abram et al., 2007; Charles et al., 2003; Nakamura et al., 2009; Pfeiffer and Dullo, 2006) to extend the understanding of the evolution of Indian

Ocean SST variability and the Indian Ocean dipole (IOD) (Saji et al., 1999) (Chapter 14), in particular, beyond the instrumental period. Reconstruction of surface-ocean cooling and drought during individual IOD events over the past 6500 years using fossil corals (Abram et al., 2007) suggests that IOD events during the mid Holocene were characterized by a longer durations of strong cooling of the ocean surface, together with droughts that peaked later than those expected by El Niño forcing alone. The physical mechanisms for the long-term modulation of the IOD have not been fully identified yet, although time-slice AOGCM experiments (Brown et al., 2009) demonstrate that the Asian summer monsoon and ENSO may exert counteracting influences on the amplitude of IOD on orbital timescales. Stronger summer IOD variability was simulated during the early Holocene, whereas stronger fall IOD variability occurred under LGM conditions. The IOD index since 1846 shows a gradual increase in the frequency and strength of IOD events during the twentieth century, associated with enhanced seasonal upwelling in the eastern Indian Ocean.

5.5.3.3 North Atlantic Oscillation/Northern Annular Mode

In order to better understand the long-term behavior of the North Atlantic Oscillation (NAO) and the Arctic Oscillation (AO), also known as the Northern Annual Mode, several centuries-long proxy indices have been reconstructed based on long instrumental pressure and ship logbook information, single proxy archives or multi-proxy paleoenvironmental data from Eurasia and North America (Appenzeller et al., 1998; Cook et al., 2002; Cullen et al., 2001; Darrigo et al., 1993; Glueck and Stockton, 2001; Kuttel et al., 2010; Luterbacher et al., 2002; Mann, 2002; Rodrigo et al., 2001; Timm et al., 2004; Trouet et al., 2009). Although the reconstructions differ in many aspects, Figure 5.15 indicates notable coherent decadal- to century-scale variability and the NAO and its interannual variability. Taking reconstruction uncertainties into consideration the strong positive NAO phases within the late 20th century are not unusual in context of the past half millennium. The reasons for the reconstructed multidecadal variations in NAO variance (Figure 5.15d) are hitherto unknown. However a number of unverified hypotheses have been proposed, associating this behavior to Atlantic SST-gradients, AAM, AMO and THC [Grossman1 and Klotzbach, 2009)]. Orbital-scale variability of the AO/NAO was investigated in a series of modeling studies. Under LGM conditions climate models suggest with a high degree of confidence a weakening of the AO and its variability, owing to stronger planetary wave activity (Lu et al., 2010). A significant model-dependent distortion of the simulated LGM NAO pattern may result from the strong topographic ice-sheet forcing (Handorf et al., 2009; Justino and Peltier, 2005; Pausata et al., 2009). The simulated NAO during the mid-Holocene (Gladstone et al., 2005) resembles the pre-industrial NAO, except for an increased tendency for positive NAO phases, which is consistent with reconstructed SST trends during the Holocene (Rimbu et al., 2003).

5.5.3.4 Southern Annular Mode

Understanding of past changes in the Southern Annular Mode (SAM) has been hampered by the limited availability of instrumental station records. Recent trends to a positive SAM mode since the 1980s are most prominent in summer and stand out of reconstructed (Gong and Wang, 1999; Jones et al., 2009a; Marshall, 2003; Visbeck, 2009) and of simulated variability in the last century, with ozone depletion being the dominant contributor, whereas greenhouse gas forcing has been found to play a smaller role in simulated changes. Relatively large summer and autumn reconstructed positive phases at about 1930 and 1960 are likely related to variability from the tropics and not reproduced by historical AOGCM simulations (Fogt et al., 2009). Comparable interannual to multi-decadal variability is found in a 500 yr summer multi-proxy, albeit with no evidence of lower frequency changes (Zhang et al., 2010). Indications of longer term variability are found in a 700 yr reconstruction from Na concentration in Law Dome suggesting an early winter more positive SAM after 1600 AD (Goodwin et al., 2004), also coincident with enhanced westerly winds as interpreted in palynological data in SW Patagonia (Moreno et al., 2009).

5.5.3.5 Multidecadal to Century Scale Variability

Coherent, large-scale sea-surface temperature (SST) variations are observed in the North Atlantic Ocean on multidecadal timescales, most prominent is the basin-wide variation of the Atlantic multidecadal oscillation (AMO), marked by alternation of warm and cold SST anomalies in the North Atlantic with a period of about 60–80 years. Analysis of multiple paleoclimate proxy datasets (Gray et al., 2004) indicates that AMO variability extends, at least, several centuries, if not millennia back in time [(Knudsen et al., 2011)]. Several independent high-resolution time series of marine proxies in the northern North Atlantic also contain multidecadal variability, reminiscent of the AMO during phases of overlap with the instrumental record (Black et al., 2007; Kilbourne et al., 2008; Webb et al., 2008; Sicre et al., 2008). Some of the proxy records, while showing a good correspondence with the instrumental data during the industrial period, diverge amongst each other prior to the industrial period [Reference needed]. It has been suggested, on the basis of climate model simulations and an 8000-year long proxy record from the northern North Atlantic [(Knudsen et al., 2011)], that AMO variations are internally driven and related to multidecadal fluctuations in the Atlantic meridional overturning circulation. However, recent model experiments with AOGCMs forced by solar and volcanic forcing for the past millennium indicate that external solar forcing may play a considerable role in driving the AMO (Ottera et al., 2010). For the 20th century, external forcing associated with greenhouse gas changes, aerosols and solar variability is likely to have played only a secondary role in shaping the observed AMO (Knight, 2009).

[INSERT FIGURE 5.15 HERE]

Figure 5.15: [Compilation of the different modes over time plus associated uncertainties] a) Normalized ensemble mean of 6 ENSO reconstructions, 5 going back to at least 1650 (McGregor et al., 2010) and one going back to 1706 [(Stahle, 1998)]. The dark (light) grey shading is a measure for the coherence within the ensemble of 6 ENSO reconstructions and indicates the ±1 (2) intra-ensemble standard deviation at every point in time. Instrumental annual mean Niño 3 SST data from the HadSST dataset in blue. b) Ensemble mean of relative changes of interannual ENSO variability, as measured by the running standard deviation of the 6 ENSO reconstructions in a 20-year window and as compared to the longterm mean standard deviation. The dark (light) grey shading indicates the ±1 (2) intra-ensemble standard deviation for the ensemble of 6 ENSO running standard deviation time series. c) Normalized ensemble mean of cold season NAO reconstructions, 4 going back to at least 1501 (Cook et al., 2002 ; Glueck and Stockton, 2001; Luterbacher et al., 2002; Rodrigo et al., 2001), 2 going back to 1650 (Appenzeller et al., 1998; Trouet et al., 2009), 2 to 1700 (Darrigo et al., 1993; Timm et al., 2004) and 3 to 1750 (Cullen et al., 2001; Kuttel et al., 2010; Mann, 2002). The dark (light) grey shading indicates the ±1 (2) intra-ensemble standard deviation for the ensemble of NAO reconstructions. d) Ensemble mean of relative changes of interannual NAO variability, as measured by the running standard deviation of the NAO reconstructions in b) in a 20-year window and as compared to the longterm mean standard deviation. The dark (light) grey shading indicates the ±1 (2) intra-ensemble standard deviation for the ensemble NAO running standard deviation time series calculated for the NAO as in b). In blue is the instrumental DJFM NAO index [(Hurrell, 2009)].

5.6 Evidence and Processes of Abrupt Climate Change

Paleoclimate archives are a rich source of information to study climate changes that happened at a rate faster than the rate of background climate variability. Such changes will be called *abrupt* on a time scale of X years, if within a time periods of X years (X>10) the rate of change of a key climate variable exceeds the average rate of change for longer term averaging periods prior and after this change by a considerable amount. A variety of mechanisms have been suggested to explain the emergence of abrupt climate changes. Most of them invoke the existence of nonlinearities, or, more specifically, thresholds in the underlying dynamics of one or more Earth system components. Both internal dynamics as well as external forcing can trigger abrupt changes in the climate state and/or its variability. This section focuses on abrupt climate events that come with an element of surprise, contrasting externally (e.g., orbitally) forced abrupt climate change such as glacial terminations that are predictable to a certain degree (Crucifix and Rougier, 2009).

5.6.1 Abrupt Changes in Cryosphere and Ocean Circulation

[PLACEHOLDER FOR FIRST ORDER DRAFT]

5.6.1.1 DO Events in Greenland and the North Atlantic

Greenland ice core records spanning the last glacial cycle depict 25 abrupt Dansgaard-Oeschger (DO) events (NorthGRIP-community-members, 2004), marked by a cold phase, an abrupt warming, and a more gradual return to cold conditions, as recorded by stable isotopic variations in water. Thermal gas fractionation methods (Severinghaus et al., 1998) suggest that the rate of regional warming in Greenland associated with these events and millennial-scale variability during the last glacial termination (Brinkhuis et al., 2006; Capron et al., 2010b) ranged from of 8°C to 16°C ± 2.5°C within several decades and was preceded by an abrupt shift in dust and deuterium excess, representing major reorganizations in atmospheric circulation (Steffensen et al., 2008). The effects of seasonality, changes in sea ice cover and atmospheric circulation as well as changes in ice-sheet topography may have contributed to the magnitude and abruptness of DO events in Greenland (Li et al., 2010). Corresponding variations in high-resolution SST reconstructions from the eastern subtropical North Atlantic attain values of up to 5°C and exhibit smoother stadial-interstadial transitions than the Greenland record (Martrat et al., 2007). Marine records (Martrat et al., 2007) and Antarctic methane records (Loulergue et al., 2008) further reveal the existence of abrupt glacial climate change events, reminiscent of DO events, extending back through several glacial cycles and as far as 1 Ma [(Kleiven et al., 2011)], thus documenting the pervasive nature of millennial-scale climate instabilities during glacial periods. Recently, terrestrial ecological information from western Europe with sufficient temporal resolution to resolve DO-events have been presented, showing that the temperature anomaly amplitude of the Dansgaard-Oeschger events as recorded on Greenland fade fast with distance such that the summer temperature anomalies in the south-western Alps is only ca 0.5°C–2°C between stadials and interstadials [(Ampel et al.. 2010)]. These results corroborate the results from imposing North-Atlantic sea-ice to explain the Greenland temperature anomalies [(Li et al., 2005)] that show a similar rapid dissipation of the temperature-anomalies with distance.

5.6.1.2 Mechanisms of DO Events and Remote Effects

Climate model simulations show (Otto-Bliesner and Brady, 2010) that the large-scale teleconnection patterns in response to an AMOC weakening closely resemble those reconstructed for DO and HE events, thereby supporting the notion that both types of events are related to large-scale reorganizations of the AMOC. The transition from GIS to GS is accompanied by a weakening of deep ocean ventilation in the North Atlantic (Piotrowski et al., 2008). Periods of weaker overturning circulation are accompanied by a slow build-up of salinity in the subtropical North Atlantic as shown in proxy reconstructions and climate models (Carlson et al., 2008; Yin et al., 2006). This process, in combination with potential subsurface warming in the Nordic Seas (Krebs and Timmermann, 2007; Mignot et al., 2007; Renold et al., 2010) may lead to a rapid resumption of deep convection in the northern North Atlantic and a subsequent recovery of the AMOC and a GIS. It sill remains under debate whether DO events can be considered stochastically generated individual events (Ditlevsen and Ditlevsen, 2009), internal oscillations of the glacial atmosphere-ocean sea-ice system, or whether they require dynamical coupling with ice-sheets [Reference needed], or whether they are astronomically forced (Braun et al., 2005).

Terrestrial and marine paleoclimate data reveal considerable impacts of DO events on climate in regions outside the North Atlantic realm. Precise synchronization between Greenland and high-resolution Antarctic records (Barbante et al., 2006; Capron et al., 2010a; Capron et al., 2010b; Stenni et al., 2011) has further revealed a one-to-one correspondence between DO events and millennial-scale Antarctic climate change. Northern Hemispheric stadial-interstadial transitions typically terminate weak warming trends in Antarctica that accompany stadial phases in the Northern Hemisphere. As a result of large-scale ocean adjustment and damping processes the Southern Hemispheric climate response to DO events has a different temporal dynamics and can be described in terms of the “bipolar seesaw” paradigm (Broecker, 1998; Crowley, 1992; Stocker and Johnsen, 2003). Evidence for DO-related climate variability was reported from the northern North Pacific (Harada et al., 2008; Kiefer et al., 2001; Ono et al., 2005) and the tropical and subtropical North Pacific [(Hendy, 2000; Stott, 2002)]. In particular, abrupt events such as the Bolling Allerod Warming and the Younger Dryas cooling during the last glacial termination have left a detectable and widespread imprint on North Pacific SSTs (Harada et al., 2008; Kiefer and Kienast, 2005; Kienast et al., 2006). Both, atmospheric changes (Okumura et al., 2009; Xie et al., 2008), as well as ocean circulation changes (Saenko et al., 2004; Schmittner et al., 2007) have been suggested to explain these pan-oceanic connections on millennial timescales. Atmospheric circulation changes in response to North Atlantic cooling also exert a strong influence on tropical hydroclimate. DO events and associated temperature variations in the North Atlantic have been shown to affect the position of the ITCZ (Peterson and Haug, 2006), the strength of the Asian summer monsoon (Wang et al., 2008) and the intensity of the west African and Arabian monsoon (Higginson et al., 2004; Itambi et al., 2009; Ivanochko et al., 2005; Mulitza et al., 2008; Tjallingii et al., 2008; Weldeab et al., 2007). A recent compilation of global vegetation data illustrates further that DO events have also influenced vegetation patterns worldwide (Harrison and Goni, 2010). The effect of North Atlantic temperature changes on the prevailing vegetation regimes has also been studied using climate-vegetation models of different complexity (Kohler et al., 2005; Menviel et al., 2008).

[INSERT FIGURE 5.16 HERE]

Figure 5.16: [PLACEHOLDER FOR FIRST ORDER DRAFT: model data to be replaced by ensemble mean of several models having performed the same experiment. Proxy data to be replaced by comprehensive proxy reconstruction data set compiled for the FOD.] [AMOC water hosing under glacial conditions, temperature, wind and precip changes; comparison with proxy data for Heinrich 1 or Younger Dryas.] a) Modelled spatial temperature anomaly in the CCM3 AOGCM showing departure from the modelled Last Glacial maximum state after the LGM control state model was water hosed in the North Atlantic. Left panel shows situation in the 2nd decade after water hosing. Right panel shows situation in the 9th decade after hosing. Symbols on right panel shows location of proxy based temperautre reconstruction for the H1 interval. Blue colour denotes cooling, compared to the LGM, red denotes warming compared to the LGM. b) Same as for a) but showing spatial precipitation anomalies. Red colours on right panel shows drier reconstructed conditions compared to the LGM, blue colours show wetter conditions. c) Modelled maximum overturning strength in the North Atlantic in Sverdrups ($10^6 m^3/s$).

5.6.1.3 Glacial Meltwater Pulses

Some DO stadials correspond to Heinrich events (HE) that represent episodes of massive iceberg discharge into the North Atlantic, primarily from the North American ice sheet (Hemming, 2004). Such northern hemispheric meltwater pulses have occurred during at least the past 600 ka (McManus et al., 1999; Siddall et al., 2010a), but their number and periodicity varied significantly between different glacial cycles. The total amount of freshwater released during HE has not yet been well-constrained and existing estimates range from essentially zero to several tens of meters in global sea level equivalent (Rohling et al., 2008; Siddall et al., 2006; Siddall et al., 2008; Yokoyama et al., 2003). Glacial meltwater pulses, and HE in particular, can be generated by internal instabilities of the Laurentide ice sheet, as originally proposed by [McAyeal (1993)] and later corroborated by more comprehensive ice-sheet models (Calov et al., 2002; Calov et al., 2010; Marshall and Koutnik, 2006). Other triggering mechanisms for HE include the disintegration of shelf ice by strong basal melting during periods of weak AMOC (Alvarez-Solas et al., 2010) or orbital forcing (Calov and Ganopolski, 2005; Timmermann et al., 2010a). Massive inputs of freshwater to the northern North Atlantic during HE (Carlson et al., 2008; Cayre et al., 1999) led to a weakening of the AMOC, and subsequent cooling of the Northern Hemisphere. The resulting global climate response is qualitatively similar to that of DO events (Section 5.6.1.3) and is characterized by the bipolar seesaw pattern in temperature, coupling between North Atlantic and North Pacific and extensive changes in the hydrological cycle, including the ITCZ and the monsoons. Reconstructed large-scale climate patterns agree with simulations conducted with a hierarchy of climate models that were forced with freshwater flux perturbations in the North Atlantic region mimicking the effects of melting icebergs (Dahl et al., 2005; Liu et al., 2009b; Menviel et al., 2008) (Figure 5.16). Reconstructions of deep ocean ventilation during HE show that major sources of deep-water formation may have shifted from the North Atlantic (Robinson and van de Flierdt, 2009) to the North Pacific (Okazaki et al., 2010) and the Southern Ocean (Piotrowski et al., 2008). High-resolution CO_2 measurements from Antarctic ice cores reveal that HE had a discernable impact on the global carbon cycle (Ahn and Brook, 2008). The strong correlation between millennial-scale warming events in Antarctica and CO_2 changes during HE indicates a potential coupling between Southern Hemispheric climate change and the carbon cycle on these time scales.

5.6.1.4 8.2 ka Event and Other Non-DO Events

The 8.2 ka event was previously documented mostly in continental records (Alley and Agustsdottir, 2005) and suspected to be linked with changes in north Atlantic circulation driven by the Lake Agassiz 8.3 ka outburst and associated change in runoff routing (Carlson, 2009). Evidence from the marine sediment record has recently confirmed this scenario (Kleiven et al., 2008). The 9.3 ka cold event attested by Greenland ice cores (Vinther et al., 2009) is now attributed to catastrophic drainage of Lake Superior at 9.3 ka (Yu et al., 2010), while a Mackenzie River flood draining Lake Agassiz into the Arctic appears to coincide with the Younger Dryas (Murton et al., 2010; Hillaire-Marcel et al., 2007; Hillaire-Marcel et al., 2008).

5.6.2 Abrupt Changes in Precipitation and Droughts

Orbitally driven variations in summer solar radiation are a dominant control of long-term late Quaternary variations in rainfall in areas influenced by the global monsoonal belt. The strength of the summer insolation alternates between the hemispheres, primarily at precessional periods, which explains the interhemispheric antiphasing of monsoonal rainfall variations observed in several records (Thompson et al., 2005; Wang et al., 2006; Wang et al., 2007b). Regionally, the phase relation between orbital insolation and precipitation-related proxies shows complex spatial variations (Cai et al., 2010; Kutzbach et al., 2008). Alternating east-west differences in monsoonal rainfall have been observed for South America (Cruz et al., 2009), Asia (Hong et al., 2005), and South Africa (Chase et al., 2010; Kristen et al., 2010).

North Africa experienced a pronounced and abrupt increase in precipitation and vegetation during the African Humid Period (AHP), synchronous with the onset of the Bølling-Allerød warm interval (Niedermeyer et al., 2010; Tierney et al., 2008). Although tropical tree species emerged in the Sahara as gallery forests along rivers and lakes, the vegetation was still dominated by C4 grasses (Collins et al., 2011; Watrin et al., 2009). The combined effects of orbital forcing and vegetation-albedo-precipitation feedback alone are not sufficient to explain the abrupt onset of the AHP, which is most likely the result of the combined effects of changes in summer insolation, ocean circulation atmospheric CO_2 concentrations and ice sheets (Timm et al., 2010).

The abruptness of the decline of the AHP after about 5500 BP is still controversial both with respect to observations (Kropelin et al., 2008) and the underlying mechanism (Liu et al., 2007). Changes in terrestrial ecosystems appear to be asynchronous and gradual across North Africa (Kropelin et al., 2008; Lezine, 2009). Observed abrupt changes in vegetation cover and assemblage can be explained by threshold behavior of certain plant types (Lezine, 2009), but do not necessarily imply abrupt changes in precipitation and the presence of a strong vegetation-albedo-precipitation feedback (Liu et al., 2007).

Extended periods of below average precipitation (megadroughts) have been observed during interglacials in North America (Fawcett et al., 2011), South America (Cordeiro et al., 2011; Haug et al., 2001; Haug et al., 2003), Africa (Moernaut et al., 2010; Shanahan et al., 2009) and Europe (Drysdale et al., 2006; Helama et al., 2009a). Depending on the local hydrological conditions, droughts can last from years to several millennia. The length of past megadroughts exceeds those observed in the instrumental period and can be regarded as a natural part of interglacial climate variability. Several distinct dry periods produced at least a hemispheric-wide signature. Among those are widespread Holocene droughts associated with the 8.2 ka and the 4.2 ka climate events (Booth et al., 2005; Cheng et al., 2010; Drysdale et al., 2006; Gasse, 2000) as well as droughts associated with the Medieval Climate Anomaly (Cook et al., 2010b; Helama et al., 2009a).

Human populations have been affected by past variations in precipitation. The late Holocene desiccation of the eastern Sahara resulted in a gradual southward shift of the main occupation sites (Kuper and Kropelin, 2006). Settlements located in the Nigerian Sahel at Gobero were abandoned during the abrupt 8.2 ka drought (Sereno et al., 2008). The 4.2 ka drought has been associated with the collapses of Akkadien and Indus Civilization (Drysdale et al., 2006). Precipitation-related proxy records from Europe, the Middle East as well as tropical North Africa indicate a drying trend in the first centuries of the first millennium AD (Buntgen et al., 2011; Mulitza et al., 2010; Orland et al., 2009; Shanahan et al., 2009). This aridification trend may have contributed to the decline of the rule of Roman and Byzantine Empires (Buntgen et al., 2011; Orland et al., 2009). Severe multi-year droughts, documented for the 9th and 10th centuries in South America (Haug et al., 2003) and China (Yancheva et al., 2007) and for the middle-12th and late-13th centuries in North America (Benson et al., 2007), affected native human populations. The causes of past megadroughts remain largely unknown, but have been frequently linked to the distribution of sea surface temperature (Cook et al., 2010b; Sachs et al., 2009; Shanahan et al., 2009).

[INSERT FIGURE 5.17 HERE]
Figure 5.17: [PLACEHOLDER FOR FIRST ORDER DRAFT: Figure showing Holocene droughts; to be expanded using different reconstructions and perhaps simulations. Compilation of data for mid-late Holocene droughts (Rengaswamy).]

[INSERT FIGURE 5.18 HERE]
Figure 5.18: Comparisons of monsoon behavior in reconstructions and model simulations. Reconstructed and simulated LGM and deglaciation (21 to 11 kyr BP) changes with reference to preindustrial times. For all

simulations, the green solid lines (shading) represent the ensemble model average (spread). The present model representation is a simplification of the LOVECLIM model simulations in Menviel et al. (2011) involving freshwater forcing transient experiments in the northern North Atlantic and Southern Ocean and using time varying radiative forcing due to solar insolation and greenhouse gases concentration changes, and including the effects of waning glacial ice-sheets on topography and albedo. [LGM simulations and reconstructions and representation of orbital forcings will be considered for FOD. Further available simulations since 18 BP will be also considered.] a) Map showing locations of the paleo-proxy records used to compare model results (see legend for proxy type). b) Simulated changes in maximum of the meridional stream function (Sv) in North Atlantic (top) vs. ^{231}Pa/^{280}th data from cores OCE326-GGC5 (1) (McManus et al., 2004) and SU81-18 (2) (Gherardi et al., 2005) and from ventilation age data from cores RAPID 10-1p, 154P and 17-5P (3) (Thornalley et al., 2011). Simulated maximum overturning strength in North Pacific (middle) and ventilation ages (years) recorded in marine sediment cores from Western North Pacific (4). The ventilation age curve is the smoothed spline interpolation of averaged benthic-planktic foraminifera ages and projection ages in the Western North Pacific (Okazaki et al., 2010). [Representation of precession changes will be considered here (bottom).] Simulated transient precipitation anomalies various monsoon regions in the NH (c) and SH (d) in comparison to regional paleoproxy evidence. NH (c): JJA precipitation anomalies vs. Cariaco basin black reflectance in marine sediment core ODP1002 (6) (Peterson et al., 2000) (lower reflectance has been associated with increased marine productivity due to greater riverine input); jja precipitation anomalies over western Equatorial Africa vs. sea surface salinity reconstruction from the Gulf of Guinea MD03-2707 core (7) (Weldeab et al., 2007); JJA/DJF precipitation anomalies vs. δ^{18}O (permil, black) in stalagmites of the Hulo cave, China (8) (Wang et al., 2001); JJA precipitation anomalies vs. δ^{18}O (permil, black) in marine sediment core 905 from the Arabian Sea (9) (Ivanochko et al., 2005). SH (d): Annual precipitation in Bolivia vs. percentage of fresh diatoms (black) in Lake Titicaca and natural gamma ray profile (grey) from Salar de Uyuni (10) (Baker et al., 2001a; Baker et al., 2001b) (both time axes fror proxy data shifted forward 400 yrs.); DJF precipitation anomalies over Peru vs. δ^{18}O (permil, black) from Huascaran ice core (11) (Thompson et al., 1995); JJA/DJF precipitation anomalies over Brazil vs. δ^{18}O (permil, black) in stalagmites of Botuverá cave (12) (Wang et al., 2007b); JJA/DJF precipitation anomalies over South Africa and δ^{18}O (permil, black) from Makapansgat Valley stalagmites (13) (Holmgren et al., 2003). H1 stands for Heinrich event 1, BWP for Bolling Warm Period, OD for Older Dryas and YD for Younger Dryas. [CONCEPT: The freshwater forcing experiments in H1 and the YD lead to a collapse of the AMOC and enhanced NH cooling relative to LGM and a southward shift of the ITCZ. Dry conditions (weaker monsoon) result in simulated precipitation in Cariaco basin, the Gulf of Guinea (enhanced salinity), reduced JJA/DJF ratio over China and reduced JJA precipitation in the Arabian Sea. In the SH the AMOC shut down leads to a strengthening of the AABW cell strengthens and the poleward heat transport is intensified at 30º S contributing to a warming of the SH, also favoured by greenhouse gases, spring sinsolation, ice retreat around Antarctica and the bipolar seasaw. The cooling of the North Atlantic and the warming in the SH lead to a southward shift of the ITCA and generally wetter conditions in the Southern Hemisphere as supported by the proxy records in Bolivia, Peru, South Africa and Brazil. Discussion about LGM to be included.]

5.6.3 Abrupt Changes of Variability and Occurrence of Extremes

Abrupt changes of climate variability may occur if components of the climate system slowly approach certain types of bifurcation points. In this case transient behaviour is subject to less damping which may result in a temporary enhancement of shorter-term variability and the decorrelation time of fluctuations. This so-called critical slowing-down effect has been invoked to explain features of glacial terminations, and the African Humid Period (Dakos et al., 2008). However, identifying potential nonstationarity in the second moments of past climate records requires long accurately dated proxy timeseries that are not affected by site-specific effects such as time-varying sedimentation rates. Another mechanism that can explain rapid regional changes in variability as well as in the occurrence of extreme events involves the horizontal displacements of climatological fronts. For instance, the abrupt emergence of droughts and megadroughts in the Sahel region, in parts of the US and Asia and the resulting drop in rainfall variance can often be attributed to tropical sea surface temperature forcing and resulting shifts in atmospheric circulation that normally supply moisture to these regions (Giannini et al., 2003).

5.7 Paleoclimate Perspective on Irreversibility in the Climate System

Theoretically, the notion of irreversibility implies that after a perturbation the climate system will never return to its initial state. This requires the existence of multiple equilibrium states in the system. In practice, considering the timescales of perturbations and climate components, irreversibility of climate change can be defined such that the recovery timescale to reach the initial state (through natural processes) is significantly longer than the duration of causal perturbation.

5.7.1 Cryosphere

Modeling studies suggest the existence of multiple equilibrium states for different ice sheets with respect to temperature, CO_2 concentration and orbital forcing phase spaces (Calov and Ganopolski, 2005; DeConto and Pollard, 2003; Ridley et al., 2010). This implies a possibility of irreversible changes in the climate-cryosphere system in the past and future. For example, if rising CO_2 concentration will cause a complete melting of the Greenland ice sheet or disintegration of the West Antarctic ice sheet within centuries/millennia, they may not re-grow even if the external conditions (such as CO_2 concentration) will eventually return to the preindustrial level within tens of thousands of years (Archer et al., 2009).

Abrupt increase in global ice volume (mostly in the Antarctic ice sheet) at the Eocene/Oligocene boundary about 33 million years ago, likely caused by gradual atmospheric CO_2 concentration decline on geological time scale (Pagani et al., 2005), is consistent with the existence of hysteresis behaviour in the East Antarctic Ice sheet simulated by ice sheet models under high CO_2 concentrations (DeConto and Pollard, 2003). More recently,high sea level stand (see Section 5.4) and warmer Antarctic temperature during the LIG (130–120 ka BP) (see Section 5.3), may involve considerable reduction of the West Antarctic ice sheet (Holden et al., 2010), but there is so far no direct observational evidence for WAIS collapse (Naish et al., 2009). The existence of multiple equilibrium states of the WAIS with thresholds close to the present day climate cannot be rule out.

Observational evidence suggest that the Greenland ice sheet was much smaller than today during the late Pliocene when atmospheric CO_2 concentration and global temperature were only moderately higher than present ones (Alley et al., 2010). The Greenland ice sheetwas also likely considerably reduced during long interglacials (MIS11) and the LIG marked by strong Arctic warming cause by its orbital configuration (de Vernal and Hillaire-Marcel, 2008). This would support modelling results which indicate that temperature or CO_2 thresholds for melting and re-growth of the Greenland ice sheet may lay in the close proximity of the present climate state (Gregory and Huybrechts, 2006; Lunt et al., 2008) and that the Greenland ice sheet may have multiple equilibrium states under present day climate state (Ridley et al., 2010). This would imply that the anthropogenic global warming can lead to irreversible melting of the Greenland ice sheet (Charbit et al., 2008) which may not re-grow till the onset of a new ice age (Berger and Loutre, 2002).

[INSERT FIGURE 5.19 HERE]

Figure 5.19: [PLACEHOLDER FOR FIRST ORDER DRAFT: transient and steady state simulations of the response of ice sheets as a function of CO_2 concentration and orbital forcing.] Reconstruction of sea level change for the last 125 ka (red line: [Waelbroeck et al., 2003]) compared with a transient ice sheet model simulation (blue line). The dots on the transient lines are displayed with a 2 ky step, showing an anti-clockwise trajectory. Black triangles display the steady state response of the same model for the last glacial cycle as a function of CO_2 concentration (with fixed present day orbital configuration) and/or orbital forcing (with fixed pre-industrial CO_2), whose effect are converted to summer temperature change relative to present day. The steady states are obtained after 100,000 years for an initial condition, which results in multiple steady states for a certain range. [Only one model is displayed (Abe-Ouchi et al 2007) but a revised version of this figure would incorporate multi-model comparisons.]

5.7.2 Ocean Circulation

The abrupt climate change event at 8.2 ka is an example with which to study the recovery time of the AMOC to freshwater perturbation under near-modern boundary conditions. The Younger Dryas (YD) event (12.8 and 11.5 ka BP) is a glacial example of an abrupt climate change event. The pattern of reconstructed and modelled surface climate anomalies is consistent with a reduction in the strength of the AMOC (see AR4, Section 6.5.2.1 and references therein). Although only indirect evidence for changes in AMOC strength can be inferred from proxy records (Figure 5.20), available proxy records from the North Atlantic support the hypothesis that freshwater input into the North Atlantic reduced the amount of deep and central water-mass formation (Bamberg et al., 2010; Ellison et al., 2006; Kleiven et al., 2008; McManus et al., 2004). The additional freshwater that entered the North Atlantic during the 8.2-ka event is estimated to range between 0.8 and 5 x 10^{14} m^3 (Barber et al., 1999; Clarke et al., 2004; von Grafenstein et al., 1998), with the more recent estimates converging towards the < 2 x 10^{14} m^3. The duration of the meltwater pulse can only be inferred based on paleohydraulic principles and may have been as short as 0.5 years (Clarke et al., 2004). Based on the palaeoceanographic reconstructions, a freshwater perturbation of this size is insufficient to trigger a complete collapse of the AMOC (Ellison et al., 2006; Kleiven et al., 2008). Furthermore, the reconstructions consistently show that the shallow and deep overturning circulation of the North Atlantic recovered completely after the cessation of the meltwater perturbation. The recovery timescale was on the order of 200 years (Bamberg et al., 2010; Ellison et al., 2006). Although one record points to a recovery on a decadal timescale (Kleiven et al., 2008) it is possible, that this record is affected by a threshold effect due to the vertical displacement of water masses. The recovery during the YD appears to be step-wise and not as smooth as indicated in the models. Both, recovery timescale and sensitivity of the AMOC to the freshwater perturbation are consistent with model experiments for the 8200-year event using coarse resolution models (LeGrande and Schmidt, 2008; Li et al., 2009). The recovery timescale of models with a forced freshwater perturbation in the YD is also a few 100 years before the recovery starts, but it takes another several hundred years for a full recovery in the model (Figure 5.20) [PLACEHOLDER FOR FIRST ORDER DRAFT: Currently only based on one model result – more complete assessment to be included in the FOD.] Model experiments with an eddy-permitting model have demonstrated the robustness of these findings (Spence et al., 2008).

Experiments with comprehensive climate models provide evidence that the sensitivity of the AMOC to freshwater perturbation is larger for glacial boundary conditions than for interglacial conditions (Swingedouw et al., 2009) [PLACEHOLDER FOR FIRST ORDER DRAFT: Multi models discussion planned to be included here] and that the recovery time scale of the AMOC is larger for LGM conditions than for the Holocene (Bitz et al., 2007). An assessment of these model results using proxy records is currently not possible.

[INSERT FIGURE 5.20 HERE]
Figure 5.20: [PLACEHOLDER FOR FIRST ORDER DRAFT: to be replaced by newer data] [Phase lag between surface salinity anomaly and ocean circulation from high resolution marine sediment data.] Modelled and reconstructed North Atlantic responses during and after major reductions in the AMOC. a) Blue line: modelled maximum overturning strength in the North Atlantic in Sverdrups ($10^6 m^3/s$) (Otto-Bliesner and Brady, 2010). Red line: Pa/Th record from North Atlantic deep sea sediments through the Younger Dryas event (McManus et al., 2004). b) Near surface temperature and salinity reconstructions from the NE Atlantic [(Dokken et al., in review; Bakke, 2009)]. c) Modelled and reconstructed Greenland temperature during and after major reductions in the AMOC. Blue cureve Modelled T at the Summit of Greenland from the same experiment as in a). Green line: Temperature estimated from the NorthGrip O-isotope record.

5.7.3 Vegetation

Reconstructions of past changes in vegetation can inform about the resilience of plant communities to climate changes, the rates of migration of vegetation zones and the timescale of recovery of vegetation after early-human perturbations.

Tropical rainforest in South America and Africa remained forested throughout the glacial-interglacial cycles of the late Quaternary although glacial plant communities were different from their modern counterparts (Anhuf et al., 2006; Bonnefille, 2010) However, tropical rainforests were affected by the millennial-scale climate perturbations of the last glacial period. While Heinrich stadials are clearly registered in pollen sequences from tropical South America and Africa, Dansgaard-Oeschger events are more muted in South America and absent in Africa (Hessler et al., 2010). Whether this indicates a larger resilience of the African rainforest compared to the Amazon rainforest cannot be stated with certainty due to the lack of a sufficient number of high-resolution records from tropical Africa (Hessler et al., 2010).

Moreover, latitudinal extent of the African tropical rainforest varied on glacial-interglacial timescales. Reconstructions shown a contraction of the tropical rainforest and the associated rainbelt by 5–10° latitude in the Southern Hemisphere and <5° in the Northern Hemisphere (Collins et al., 2011). These findings contradict the results of climate modelling experiments, which suggest a southward migration of the rainbelt (Braconnot et al., 2007a). Based on the latitudinal shifts of plant type during the last deglaciation, migration rates of vegetation zones can be estimated. These range from 15 to 70 km per century in the Sahel and Sahara; these rates are of comparable magnitude as those inferred for postglacial tree expansion in northern America and Europe (Watrin et al., 2009, and references therein).

The recovery timescale of tropical ecosystems to natural and human-induced perturbations has been studied in the Caribbean, where hurricanes have a great potential to damage mangroves. High-resolution pollen data indicate that the time required for full recovery of mangroves after a hurricane ranges from 50-70 years (Gonzalez et al., 2010) to up to 500 years (Urquhart, 2009). The order of magnitude difference in the recovery timescale may reflect differences in the level of damage that cannot be reconstructed. Based on the limited evidence it is likely that a recovery of mangroves after a hurricane will take at least several decades. A similar timescale of vegetation recovery has also been reconstructed for the tropical lowlands in Central America. Here, forest ecosystems recovered within 80–260 years after the demise of the Classic Maya period (Mueller et al., 2010).

[START BOX 5.3 HERE]

Box 5.3: Earth System Feedbacks and Their Role in Paleoclimate Change

The response of the Earth system to perturbations is determined by its internal feedbacks. Depending on whether the climate system components involved in the response tend to amplify or dampen an initial response, positive and negative Earth-system feedbacks are distinguished. The time-evolution of the response is governed by the magnitude and time-scale of the feedback processes; the two being related with each other [(Roe, 2009)]. The combination of feedback processes determines whether a stationary equilibrium response exists, or whether an oscillatory mode of the system is excited. Variability in the Earth system emerges as the response to either external forcings (such as e.g., changes in incoming solar radiation or tectonically driven changes in the atmospheric composition with potential effects for both longwave and shortwave radiation) or through internal feedbacks. Different components of the Earth system have different response time scales (Box 5.3, Figure 1), which implies that the response to a perturbation will be determined by a combination of adjustment processes that act on different timescales. Thus, the equilibrium Earth-system sensitivity to radiative perturbations, which includes the response of the slow components such as ice-sheets and the carbon cycle, may differ significantly from the shorter-term atmosphere-ocean-sea-ice response, often considered in climate sensitivity studies.

Earth system models of intermediate complexity have been successfully employed to estimate the magnitude of slow Earth-system feedbacks [references to be included]. Deriving the efficiency of slow feedbacks directly from paleo-climate data is an alternative approach. It has been found e.g., using paleo-climate reconstructions for the Pliocene period (5.3–2.6 Ma) [(Lunt, 2010)] that the long-term Earth system sensitivity is 30–50% larger than the sensitivity of the fast components alone. How such paleo-estimates translate into values for Earth's future sensitivity to anthropogenic CO_2 emissions still needs to be further explored. In particular, the Earth system sensitivity for cold climates (involving ice-sheet dynamics) is likely to be different from that for warm climates (with ice-sheets playing only a minor role in the latter). This state-dependence results from the nonlinearity of Earth-system feedbacks.

The combined effects of feedbacks operating on different timescales are illustrated here for the last glacial termination [Definition to be included]. Deglacial climate change in both Hemispheres started as early as 19–20 kyr BP (about 1000–2000 years before atmospheric CO_2 concentrations began to rise), with increasing northern hemispheric extratropical summer insolation, increasing southern hemispheric extratropical spring insolation [(Stott, 2007)], and increasing high latitude annual mean insolation in both hemispheres, due to the obliquity cycle. The northern hemispheric ice-sheets responded slowly to the rise in summer insolation with ablation and a negative mass balance, whereas the sea-ice in the Southern Ocean responded quickly to changes in spring and annual mean forcing [(Timmermann, 2009)]. The meltdown of the Laurentide and

Eurasian ice-sheets was further accelerated by positive feedbacks such as the ice-sheet albedo feedback and the ice-elevation feedback. This process was accompanied by the delivery of freshwater to the North Atlantic and Arctic oceans, such as during Heinrich event 1 and the Younger Dryas [(Tarasov, 2005; Murton, 2010; Spielhagen, 2005)] respectively. Reconstructions using ocean-mixing proxies indicate that the reduction in surface ocean density triggered strong decrease in the strength of the Atlantic Meridional Overturning Circulation ([Piotrowski, 2004]). The weakening of this circulation and the associated northward heat transport provided a negative feedback to the glacial termination in the Northern Hemisphere by reducing poleward oceanic heat transport. However, due to the bipolar seesaw response (Section 5.6), the Southern Hemisphere experienced an accelerated warming [(Stenni, 2011)] with potential repercussions for the Antarctic ice-sheet, the atmospheric circulation and the carbon cycle [(Denton, 2010)]. With increasing annual mean and spring insolation sea-ice reduced even further and the positive sea-ice albedo feedback generated a substantial Southern Ocean warming. It has been hypothesized that related changes in winds and ocean circulation [(Anderson, 2010)] and sea-ice [Stephens, 2000)] released CO_2 from the deep ocean to the atmosphere. Potential changes in ocean alkalinity may have exacerbated this effect [(Sigman, 2010)]. Subsequently, the deglacial atmospheric CO_2 rise enhanced the natural greenhouse effect, thereby contributing to the overall global warming during the termination and further melting of the ice-sheets in both hemispheres (see Section 5.X for a detailed discussion of the proposed mechanisms of glacial-interglacial CO_2 variability). Faster atmospheric feedbacks have further contributed to the deglacial temperature evolution and the accompanying decrease of land-ice during this period. This example documents the complexities involved in the Last Glacial Termination and the role of slow and fast feedbacks.

Major uncertainties still remain in the detailed understanding of past and future carbon-cycle climate feedbacks, dust-climate feedbacks [(Claquin, 2003; Ridgwell, 2002; Mahowald, 2006)], cloud feedbacks [(Yoshimori, 2009; Ramstein, 1998; Abbot, 2000; Claussen, 2009)] and water vapour feedback [Reference needed] (see Box 5.3, Figure 1). Quantifying the magnitudes of these feedbacks relative to each other and for different past climate periods requires concerted modelling efforts, using a range of Earth system models in combination with the the analysis of quantitative reconstructions of past climate variations. Since, uncertainties in the estimates of these feedbacks translate into the uncertainty of climate/Earth system sensitivity [(Roe, 2007; Hansen, 1985)], it is essential to further explore and quantify the long-term behaviour of the Earth system.

[INSERT BOX 5.3, FIGURE 1 HERE]

Box 5.3, Figure 1: [PLACEHOLDER FOR FIRST ORDER DRAFT: figure details to be refined after further discussions, determination of level of Scientific Understanding needs to be discussed.] Schematic diagram of Earth-system feedbacks relevant for generating past climate changes, their time scale and the present level of scientific understanding. Red (blue) bars indicate positive (negative) feedbacks. Red to blue shading represents feedbacks whose sign is either uncertain or whose detailed sub-processes can either amplify or damp the response to perturbations.

[END BOX 5.3 HERE]

[START FAQ 5.1 HERE]

FAQ 5.1 How Unusual is the Current Sea Level Rate of Change?

To answer this question we need to define what is meant by sea level change. All past measurements of sea level have been of the position of the mean sea surface relative to the land surface. By ‘mean’ we mean a long-term average, nominally a year or longer, and long enough for the sea level markers to form and be preserved. The measurement is therefore a relative one and we refer to this as relative sea level. Changes in relative sea level at any location could therefore mean changes in the land surface or changes in the water surface with respect to the center of mass of the Earth. Modern measurements of sea level have been made with satellite-borne radar altimeters and the measurement is of the distance of the sea surface from the Earth’s center of mass. The record length for the latter observations is only about a decade whereas records for the relative measurements contained within the geological record go back thousands of years and provide the principal source of information on sea level change. We focus here, therefore, on the latter.

Reasons for relative sea level change are manifold but they fall into three categories; changes in the volume of water contained within the ocean basins; changes in the shape and holding capacity of the ocean basins, i.e., land movements of the basin periphery and basin floor; and a redistribution of water within the basins. Changes in ocean volume, on recent geological time scales, are primarily the result of changes in water (primarily as ice) stored on land and of changes in the density of water (primarily because of ocean temperature changes). Changes in land movements are primarily caused by tectonic upheavals and by the deformation of the planet when stressed by changes in surface loads. On the time scale of glacial cycles the dominant change in surface loads is caused by the cyclic growth and decay of the ice sheets and the concomitant changes in the water distributions within the ocean basins. Thus the changes in land movements and the changes in ocean volumes are closely linked. Changes in the distribution of water within the ocean basins are caused by changes in the basin shape due to land movements and due to changes in the forces acting on the water. These latter include changes in the gravity field that occur when ice sheets are transformed to ocean water, long-period changes in ocean circulation or shifting surface wind patterns (FAQ 5.1, Table 1).

FAQ 5.1, Table 1: Representative time and length scales of some processes contributing to sea level change.

Time scale	Length scale	Process
		Climate
Long term: 10^6 - 10^3 years	Global	Growth and decay of ice sheets
Intermediate: 10^3 - 10^2 years	Regional	Global change in temperature
Short term: 10^2 - 10 years	Local	Decadal-scale climate change, wind circulation.
		Tectonics
Long term: 10^6 - 10^9 years	Global	Plate tectonics and evolution of ocean basins; mid-ocean ridge formation
Intermediate: 10^6 - 10^3(?) years	Regional	Volcanic and sediment loading changes in stress state of lithosphere
Short term: years - seconds	Local	Rapid surface response to long term tectonic forcing

The different processes operate on different length scales with consequence that relative sea level change will be spatially variable as well as vary through time. Sometimes sea level change is defined as eustatic sea level which is the globally averaged change in sea level and will be a function of time only. Thus all information on the spatial variability is lost and regional or local sea level change at any time can be significantly different or off opposite sign to the eustatic change. Emphasis of recent sea level research is therefore on this spatial variability as well as on the globally averaged time function.

For the past few thousand years the phase of major melting of the last ice sheets has been largely completed. But relative sea levels continue to respond to the changes in ice sheets from the last deglaciation because of the Earth’s viscosity. This process is referred to as glacial isostasy. Under the influence of this process, areas that were formerly glaciated, sea levels today are falling at rates of up to 1 m per century (in the Gulf of Bothnia, for example) as the crust, previously depressed under the large ice sheets, gradually rebounds (FAQ 5.1, Figure 1). In areas at some distance from the former ice margins the sea levels relative to the land may rise at rates of 10–30 cm per century [value for Amsterdam and for an east coast US site to be confirmed]. This is due to this isostatic effect where the crust around the large ice sheets subsides slowly in response to flow in the underlying mantle towards the centers of the rebounding areas beneath the former ice sheets. At continental margins far from former ice sheets the sea levels are again expected to fall at rates of up to 40 mm per century [to be confirmed] as the ocean sea floor subsides under the weight of the meltwater added earlier into the ocean basins, dragging the coastline partly down with it.

Superimposed upon the resulting global pattern of recent sea level change will be other geological processes. These are usually more local in scale and include coastal crustal subsidence under the weight of sediments loading the offshore area or subsidence caused by compaction of sediments. Often the latter effects are magnified through human actions such as extraction of groundwater or hydrocarbons from the coastal zone [Bangkok example to be included]. The geological effects also include episodic tectonic events associated with Earthquake activity that can have cumulative uplift or subsidence effects [Huon Peninsula–Huon Gulf examples of large scale uplift and subsidence to be included].

On the scale of the glacial cycles, climate signals other than the waxing and waning of the ice sheets, make only a minor contribution to sea level change, but once the ice sheets have stabilized these signals become relatively more important. Of these changes in thermal expansion of the ocean water column becomes the most important along with changes in mountain glaciers.

[PLACEHOLDER FOR FIRST ORDER DRAFT: Discuss the thermal expansion evidence as well as mountain glaciers.]

[PLACEHOLDER FOR FIRST ORDER DRAFT: Provide a summing up: From glacial rebound analyses the isostatic contributions can be subtracted from observations. If obvious areas of tectonics and subsidence are also avoided, isolation of the climate signal can begin.]

[INSERT FAQ 5.1, FIGURE 1 HERE]
FAQ 5.1, Figure 1: [PLACEHOLDER FOR FIRST ORDER DRAFT: The actual figure will be a variant of this, using results only for the past 3000-4000 years.]

[INSERT FAQ 5.1, FIGURE 2 HERE]
FAQ 5.1, Figure 2: [PLACEHOLDER FOR FIRST ORDER DRAFT: The final figure will be an update on this introducing salt marsh data etc.] Globally averaged sea level rise for the past 6000 years.

[END FAQ 5.1 HERE]

[START FAQ 5.2 HERE]

FAQ 5.2: Is the Sun a Major Driver of Climate Fluctuations/Changes?

The Sun is the main driver of the climate system. In equatorial regions where at noon the Sun is in the zenith the electromagnetic power arriving per square meter at the top of the Earth's atmosphere is largest and corresponds to about 1365 W m^{-2}. This power per square meter for the mean Earth-Sun distance (1 AU) is called Total Solar Irradiance (TSI). The total power received by the Earth is given by its cross section (pR^2) times TSI and amounts to 1.7 10^{17} W, with R being the Earth's radius. The mean global solar power is therefore (pR^2 / $4pR^2$) x TSI = 341.3 W m^{-2}. The solar energy is generated in the core of the Sun by fusion processes turning hydrogen into helium. The standard solar model shows that on times scales of billion of years the fusion process causes a very large steady increase in energy production (FAQ 5.2, Figure 1). However, the insolation change during one million years is only about 0.1 W m^{-2}.

Is the Sun also a major driver of climate fluctuations? A complete answer is not yet possible as it requires a full understanding of the processes in and on the Sun itself which are responsible for the emission of the radiation and its spectral composition. Further also the corresponding response of the climate system is of great relevance which depends on complex feedback processes.

In the following we discuss changes in the orbital parameters which affect the total insolation on multi-millennial time scales and fluctuations in the emission from the Sun.

The orbit of the Earth around the Sun is elliptical which causes annual fluctuations of about 3% in insolation between the smallest distance (perihelion) and the largest distance (aphelion). The eccentricity, the deviation of the Earth's elliptical orbit from a circle, is disturbed by the other planets with cycles of about 100,000 and about 400,000 years. It is generally accepted that the 100,000 years cycle is the main driver of the observed cycles of glacial and interglacial periods during the past million years. Interestingly the mean annual changes in the total solar radiation received between a glacial and an interglacial period is only about 0.2–0.3 W m^{-2} emphasising the non-linearity of the climate response (see Figure [xy]). Orbital forcing is the only forcing which can be calculated accurately for several million years from the past into the future.

The total amount of radiation emitted by the Sun is related to its magnetic activity. Satellite based instrumental records of TSI go back to 1978 and show changes in phase with 11-y activity cycle. The average change of TSI over an 11-year cycle is about 0.1% corresponding to about 1.4 W m^{-2}. Reconstructions of the past centuries to millennia are based on sunspots (back 1600 AD) and cosmogenic radionuclides such as ^{10}Be in ice cores and ^{14}C in tree rings (back to about 10,000 years) which represent proxies of the solar magnetic activity. They are characterized by distinct grand solar minima, periods of 50 to 100 years of very low solar activity such as the Maunder minimum (1645–1715), and cycles with several well-defined periodicities up to 2200 years with varying amplitudes. The estimated average changes between the Maunder minimum and the instrumental period range from 0.1 to 0.4% (see Figure 5.1).

Changes in the spectral solar irradiance (SSI) are also related to the solar magnetic activity and take mainly place at short wave lengths (UV). Satellite based measurements since 1991 show changes larger than 100% depending on the wave length. UV-changes affect the upper atmosphere (where they are absorbed by the ozone layer) with potential dynamical couplings to the troposphere.

The long-term fluctuations in TSI and SSI are not well constrained because the available instrumental data were obtained during a period of high and relatively constant solar activity. This and the limited understanding of the involved processes makes it very difficult to reliably derive the amplitude of long-term changes. The last minimum between cycle 23 and 24 (1908–1909) provided a glimpse of a low-activity Sun. Based on a statistical analysis of the past 10,000 years of solar activity it is likely that the current about 60 year long relatively constant period of high activity comes to an end within the next 1–2 solar cycles (10–20 years) and may provide us some of the missing information of how much lower TSI and SSI have been during a grand minimum such as the Maunder minimum.

Palaeoclimate records covering part or the full Holocene (about 12,000 years) provide growing evidence that solar forcing in combination with orbital and volcanic forcing, land use changes, and internal climate variability played a significant role in preindustrial climate fluctuations on decadal to millennial time scales.

Future variability in TSI will very likely interfere with anthropogenic climate forcing over the next decades, reinforcing the greenhouse gas forcing during solar maxima and attenuating its effect during solar minima.

[INSERT FAQ 5.2, FIGURE 1 HERE]

FAQ 5.2, Figure 1: Long-term variation of the mean global insolation. Upper panel: after the formation of the solar system 4.55 Gyr ago the insolation was some 20% lower than today. It will steadily increase for the next about 5 billion years until the Sun will become a red giant and destroy the Earth. Lower panel: Insolation changes for the past and the future one million years as a result of the planetary effects on the eccentricity of the Earth's orbit around the Sun. 0 corresponds to the present time.

[END FAQ 5.2]

References

Abe-Ouchi, A., T. Segawa, and F. Saito, 2007: Climatic Conditions for modelling the Northern Hemisphere ice sheets throughout the ice age cycle. *Climate of the Past*, 423-438.

Abram, N. J., M. K. Gagan, J. E. Cole, W. S. Hantoro, and M. Mudelsee, 2008: Recent intensification of tropical climate variability in the Indian Ocean. *Nature Geoscience*, **1,** 849-853.

Abram, N. J., M. K. Gagan, Z. Y. Liu, W. S. Hantoro, M. T. McCulloch, and B. W. Suwargadi, 2007: Seasonal characteristics of the Indian Ocean Dipole during the Holocene epoch. *Nature*, **445,** 299-302.

Adams, J. B., M. E. Mann, and C. M. Ammann, 2003: Proxy evidence for an El Nino-like response to volcanic forcing. *Nature*, **426,** 274-278.

Ahn, J., and E. Brook, 2007: Atmospheric CO2 and climate from 65 to 30 ka BP. *Geophysical Research Letters*, -.

Ahn, J., and E. J. Brook, 2008: Atmospheric CO2 and climate on millennial time scales during the last glacial period. *Science*, **322,** 83-85.

Alexeev, V. A., P. L. Langen, and J. R. Bates, 2005: Polar amplification of surface warming on an aquaplanet in "ghost forcing" experiments without sea ice feedbacks. *Climate Dynamics*, **24,** 655-666.

Allen, J. R. M., and B. Huntley, 2009: Last Interglacial palaeovegetation, palaeoenvironments and chronology: a new record from Lago Grande di Monticchio, southern Italy. *Quaternary Science Reviews*, **28,** 1521-1538.

Allen, R. J., and S. C. Sherwood, 2007: Utility of radiosonde wind data in representing climatological variations of tropospheric temperature and baroclinicity in the western tropical Pacific. *Journal of Climate*, **20,** 5229-5243.

Alley, R., and A. Agustsdottir, 2005: The 8k event: cause and consequences of a major Holocene abrupt climate change. *Quaternary Science Reviews*, 1123-1149.

Alley, R., P. Clark, P. Huybrechts, and I. Joughin, 2005: Ice-sheet and sea level changes. *Science*, 456-460.

Alley, R. B., et al., 2010: History of the Greenland Ice Sheet: paleoclimatic insights. *Quaternary Science Reviews*, **29,** 1728-1756.

Alvarez-Solas, J., S. Charbit, C. Ritz, D. Paillard, G. Ramstein, and C. Dumas, 2010: Links between ocean temperature and iceberg discharge during Heinrich events. *Nature Geoscience*, **3,** 122-126.

Ammann, C., and E. Wahl, 2007: The importance of the geophysical context in statistical evaluations of climate reconstruction procedures. *Climatic Change*, **85,** 71-88.

Ammann, C., M. Genton, and B. Li, 2010: Technical Note: Correcting for signal attenuation from noisy proxy data in climate reconstructions. *Climate of the Past*, 273-279.

Ammann, C., F. Joos, D. Schimel, B. Otto-Bliesner, and R. Tomas, 2007: Solar influence on climate during the past millennium: Results from transient simulations with the NCAR Climate System Model. *Proceedings of the National Academy of Sciences*, **104,** 3713.

An, S. I., A. Timmermann, L. Bejarano, F. F. Jin, F. Justino, Z. Liu, and A. W. Tudhope, 2004: Modeling evidence for enhanced El Nino-Southern Oscillation amplitude during the Last Glacial Maximum. *Paleoceanography*, **19**.

Anchukaitis, K., B. Buckley, E. Cook, B. Cook, R. D'Arrigo, and C. Ammann, 2010: Influence of volcanic eruptions on the climate of the Asian monsoon region. *Geophysical Research Letters*, -.

Andersen, K., et al., 2004: High-resolution record of Northern Hemisphere climate extending into the last interglacial period. *Nature*, 147-151.

Anderson, P., et al., 2006: Last Interglacial Arctic warmth confirms polar amplification of climate change. *Quaternary Science Reviews*, **25,** 1383-1400.

Anderson, R. F., and M. E. Carr, 2010: Uncorking the Southern Ocean's Vintage CO2. *Science*, **328,** 1117-1118.

Andersson, C., F. Pausata, E. Jansen, B. Risebrobakken, and R. Telford, 2010: Holocene trends in the foraminifer record from the Norwegian Sea and the North Atlantic Ocean. *Climate of the Past*, 179-193.

Anhuf, D., et al., 2006: Paleo-environmental change in Amazonian and African rainforest during the LGM. *Palaeogeography Palaeoclimatology Palaeoecology*, 510-527.

Antoine, P., et al., 2009: Rapid and cyclic aeolian deposition during the Last Glacial in European loess: a high-resolution record from Nussloch, Germany. *Quaternary Science Reviews*, **28,** 2955-2973.

Appenzeller, C., T. F. Stocker, and M. Anklin, 1998: North Atlantic oscillation dynamics recorded in Greenland ice cores. *Science*, **282,** 446-449.

Archer, D., et al., 2009: Atmospheric Lifetime of Fossil Fuel Carbon Dioxide. *Annual Review of Earth and Planetary Sciences*, 117-134.

Ashton, N., S. G. Lewis, S. A. Parfitt, K. E. H. Penkman, and G. R. Coope, 2008: New evidence for complex climate change in MIS 11 from Hoxne, Suffolk, UK. *Quaternary Science Reviews*, **27,** 652-668.

Augustin, L., et al., 2004: Eight glacial cycles from an Antarctic ice core. *Nature*, 623-628.

Baker, P., C. Rigsby, G. Seltzer, S. Fritz, T. Lowenstein, N. Bacher, and C. Veliz, 2001a: Tropical climate changes at millennial and orbital timescales on the Bolivian Altiplano. *Nature*, **409,** 698-701.

Baker, P., et al., 2001b: The history of South American tropical precipitation for the past 25,000 years. *Science*, **291,** 640-643.

Bakke, J., O. Lie, S. O. Dahl, A. Nesje, and A. E. Bjune, 2008: Strength and spatial patterns of the Holocene wintertime westerlies in the NE Atlantic region. *Global and Planetary Change*, **60,** 28-41.

Balmaceda, L., N. Krivova, and S. Solanki, 2007: Reconstruction of solar irradiance using the group sunspot number. *Advances in Space Research*, 986-989.

Bamberg, A., Y. Rosenthal, A. Paul, D. Heslop, S. Mulitza, C. Rühlemann, and M. Schulz, 2010: Reduced North Atlantic Central Water formation in response to early Holocene ice sheet melting. *Geophysical Research Letters*, **37,** L17705, doi:17710.11029/12010GL043878.
Banta, J., J. McConnell, R. Edwards, and J. Engelbrecht, 2008: Delineation of carbonate dust, aluminous dust, and sea salt deposition in a Greenland glaciochemical array using positive matrix factorization. *Geochemistry Geophysics Geosystems*, **9,** 1-19.
Bar-Matthews, M., A. Ayalon, M. Gilmour, A. Matthews, and C. Hawkesworth, 2003: Sea-land oxygen isotopic relationships from planktonic foraminifera and speleothems in the Eastern Mediterranean region and their implication for paleorainfall during interglacial intervals. *Geochimica Et Cosmochimica Acta***,** 3181-3199.
Barbante, C., et al., 2006: One-to-one coupling of glacial climate variability in Greenland and Antarctiabout *Nature*, **444,** 195-198.
Barber, D. C., et al., 1999: Forcing of the cold event of 8,200 years ago by catastrophic drainage of Laurentide lakes. *Nature*, **400,** 344-348.
Baroni, M., M. Thiemens, R. Delmas, and J. Savarino, 2007: Mass-independent sulfur isotopic compositions in stratospheric volcanic eruptions. *Science***,** 84-87.
Baroni, M., J. Savarino, J. Cole-Dai, V. Rai, and M. Thiemens, 2008: Anomalous sulfur isotope compositions of volcanic sulfate over the last millennium in Antarctic ice cores. *Journal of Geophysical Research-Atmospheres***,** -.
Bartlein, P., et al., 2010: Pollen-based continental climate reconstructions at 6 and 21 ka: a global synthesis. *Climate Dynamics***,** 1-28.
Bay, R., N. Bramall, P. Price, G. Clow, R. Hawley, R. Udisti, and E. Castellano, 2006: Globally synchronous ice core volcanic tracers and abrupt cooling during the last glacial period. *Journal of Geophysical Research-Atmospheres***,** -.
Bekryaev, R. V., I. V. Polyakov, and V. A. Alexeev, 2010: Role of Polar Amplification in Long-Term Surface Air Temperature Variations and Modern Arctic Warming. *Journal of Climate*, **23,** 3888-3906.
Benson, L., K. Petersen, and J. Stein, 2007: Anasazi (pre-Columbian Native-American) migrations during the middle-12th and late-13th centuries - Were they drought induced? *Climatic Change***,** 187-213.
Berger, A., and M. F. Loutre, 1991: Insolation values for the climate of the last 10 million years. *Quaternary Sciences Reviews*, **10,** 297-317.
Berger, A., and M. Loutre, 2002: An exceptionally long interglacial ahead? *Science***,** 1287-1288.
——, 2004: Astronomical theory of climate change. *Journal De Physique Iv***,** 1-35.
Berkelhammer, M., A. Sinha, M. Mudelsee, H. Cheng, R. L. Edwards, and K. Cannariato, 2010: Persistent multidecadal power of the Indian Summer Monsoon. *Earth and Planetary Science Letters*, **290,** 166-172.
Bhatt, U. S., et al., 2010: Circumpolar Arctic tundra vegetation change is linked to sea ice decline. *Earth Interactions*, **14**.
Bijl, P. K., S. Schouten, A. Sluijs, G. J. Reichart, J. C. Zachos, and H. Brinkhuis, 2009: Early Palaeogene temperature evolution of the southwest Pacific Ocean. *Nature*, **461,** 776-779.
Bintanja, R., R. van de Wal, and J. Oerlemans, 2005: Modelled atmospheric temperatures and global sea levels over the past million years. *Nature***,** 125-128.
Bitz, C. M., J. C. H. Chiang, W. Cheng, and J. J. Barsugli, 2007: Rates of thermohaline recovery from freshwater pluses in modern, Last Glacial Maximum, and greenhouse warming climates. *Geophysical Research Letters*, **34,** L07708, 07710.01029/02006GL029237.
Black, D. E., M. A. Abahazi, R. C. Thunell, A. Kaplan, E. J. Tappa, and L. C. Peterson, 2007: An 8-century tropical Atlantic SST record from the Cariaco Basin: Baseline variability, twentieth-century warming, and Atlantic hurricane frequency. *Paleoceanography*, **22,** 10.
Bock, M., J. Schmitt, L. Moller, R. Spahni, T. Blunier, and H. Fischer, 2010: Hydrogen Isotopes Preclude Marine Hydrate CH4 Emissions at the Onset of Dansgaard-Oeschger Events. *Science*, **328,** 1686-1689.
Bonelli, S., S. Charbit, M. Kageyama, M. N. Woillez, G. Ramstein, C. Dumas, and A. Quiquet, 2009: Investigating the evolution of major Northern Hemisphere ice sheets during the last glacial-interglacial cycle. *Climate of the Past*, **5,** 329-345.
Boninsegna, J., et al., 2009: Dendroclimatological reconstructions in South America: A review. *Palaeogeography Palaeoclimatology Palaeoecology***,** 210-228.
Bonnefille, R., 2010: Cenozoic vegetation, climate changes and hominid evolution in tropical Afriabout *Global and Planetary Change***,** 390-411.
Booth, R., S. Jackson, S. Forman, J. Kutzbach, E. Bettis, J. Kreig, and D. Wright, 2005: A severe centennial-scale drought in mid-continental North America 4200 years ago and apparent global linkages. *Holocene***,** 321-328.
Bowen, D., 2010: Sea level similar to 400 000 years ago (MIS 11): analogue for present and future sea level? *Climate of the Past***,** 19-29.
Bracegirdle, T. J., W. M. Connolley, and J. Turner, 2008: Antarctic climate change over the twenty first century. *Journal of Geophysical Research-Atmospheres*, **113**.
Braconnot, P., C. Marzin, L. Grégoire, E. Mosquet, and O. Marti, 2008: Monsoon response to changes in Earth's orbital parameters: comparisons between simulations of the Eemian and of the Holocene. *Clim. Past*, **4,** 281-294.

Braconnot, P., et al., 2007a: Results of PMIP2 coupled simulations of the Mid-Holocene and Last Glacial Maximum - Part 2: feedbacks with emphasis on the location of the ITCZ and mid- and high latitudes heat budget. *Climate of the Past*, **3,** 279-296.
——, 2007b: Results of PMIP2 coupled simulations of the Mid-Holocene and Last Glacial Maximum - Part 2: feedbacks with emphasis on the location of the ITCZ and mid- and high latitudes heat budget. *Climate of the Past***,** 279-296.
——, 2007c: Results of PMIP2 coupled simulations of the Mid-Holocene and Last Glacial Maximum - Part 1: experiments and large-scale features. *Climate of the Past***,** 261-277.
Bradley, R. S., K. R. Briffa, J. E. Cole, M. K. Hughes, and T. J. Osborn, 2003: The Climate of the last Millenium. *??*
Braun, H., et al., 2005: Possible solar origin of the 1,470-year glacial climate cycle demonstrated in a coupled model. *Nature*, **438,** 208-211.
Brazdil, R., C. Pfister, H. Wanner, H. von Storch, and J. Luterbacher, 2005: Historical climatology in Europe - The state of the art. *Climatic change*, **70,** 363-430.
Brazdil, R., P. Dobrovolny, J. Luterbacher, A. Moberg, C. Pfister, D. Wheeler, and E. Zorita, 2010: European climate of the past 500 years: new challenges for historical climatology. *Climatic Change***,** 7-40.
Briffa, K., F. Schweingruber, P. Jones, T. Osborn, S. Shiyatov, and E. Vaganov, 1998: Reduced sensitivity of recent tree-growth to temperature at high northern latitudes. *Nature***,** 678-682.
BRIFFA, K., et al., 1992: FENNOSCANDIAN SUMMERS FROM AD-500 - TEMPERATURE-CHANGES ON SHORT AND LONG TIMESCALES. *Climate Dynamics*, **7,** 111-119.
Briffa, K. R., T. J. Osborn, F. H. Schweingruber, P. D. Jones, S. G. Shiyatov, and E. A. Vaganov, 2002: Tree-ring width and density data around the Northern Hemisphere, Part I: local and regional climate signals. *The Holocene*, **12,** 737-757.
Briffa, K. R., T. J. Osborn, F. H. Schweingruber, I. C. Harris, P. D. Jones, S. G. Shiyatov, and E. A. Vaganov, 2001: Low-frequency temperature variations from a northern tree ring density network. *J.Geophys.Res.*, **106,** 2929-2941.
Brinkhuis, H., et al., 2006: Episodic fresh surface waters in the Eocene Arctic Ocean. *Nature***,** 606-609.
Broecker, W. S., 1998: Paleocean circulation during the last deglaciation A bipolar seasaw ? *Paleoceanography*, **13,** 119-121.
Brown, J., A. H. Lynch, and A. G. Marshall, 2009: Variability of the Indian Ocean Dipole in coupled model paleoclimate simulations. *Journal of Geophysical Research-Atmospheres*, **114**.
Brown, J., A. W. Tudhope, M. Collins, and H. V. McGregor, 2008a: Mid-Holocene ENSO: Issues in quantitative model-proxy data comparisons. *Paleoceanography*, **23**.
Brown, J., M. Collins, A. W. Tudhope, and T. Toniazzo, 2008b: Modelling mid-Holocene tropical climate and ENSO variability: towards constraining predictions of future change with palaeo-data. *Climate Dynamics*, **30,** 19-36.
Buckley, B., et al., 2010: Climate as a contributing factor in the demise of Angkor, Cambodia. *Proceedings of the National Academy of Sciences of the United States of America***,** 6748-6752.
Bürger, G., 2007: Comment on "The Spatial Extent of 20th-century Warmth in the Context of the Past 1200 Years". *Science*, **316,** 1844.
Buntgen, U., and F. Schweingruber, 2010: Environmental change without climate change? *New Phytologist*, **188,** 646-651.
Buntgen, U., D. C. Frank, D. Nievergelt, and J. Esper, 2006: Summer temperature variations in the European Alps, AD 755-2004. *Journal of Climate*, **19,** 5606-5623.
Buntgen, U., D. Frank, H. Grudd, and J. Esper, 2008: Long-term summer temperature variations in the Pyrenees. *Climate Dynamics*, **31,** 615-631.
Buntgen, U., J. Esper, D. Frank, K. Nicolussi, and M. Schmidhalter, 2005: A 1052-year tree-ring proxy for Alpine summer temperatures. *Climate Dynamics***,** 141-153.
Buntgen, U., et al., 2011: 2500 Years of European Climate Variability and Human Susceptibility. *Science*, **331,** 578-582.
Burger, G., I. Fast, and U. Cubasch, 2006: Climate reconstruction by regression - 32 variations on a theme. *Tellus Series a-Dynamic Meteorology and Oceanography***,** 227-235.
Bush, A. B. G., 2007: Extratropical influences on the El Nino-Southern Oscillation through the late Quaternary. *Journal of Climate*, **20,** 788-800.
Butzin, M., M. Prange, and G. Lohmann, 2005: Radiocarbon simulations for the glacial ocean: The effects of wind stress, Southern Ocean sea ice and Heinrich events. *Earth and Planetary Science Letters***,** 45-61.
Cai, Y. J., et al., 2010: The variation of summer monsoon precipitation in central China since the last deglaciation. *Earth and Planetary Science Letters*, **291,** 21-31.
Calov, R., and A. Ganopolski, 2005: Multistability and hysteresis in the climate-cryosphere system under orbital forcing. *Geophysical Research Letters*, **32**.
Calov, R., A. Ganopolski, V. Petoukhov, M. Claussen, and R. Greve, 2002: Large-scale instabilities of the Laurentide ice sheet simulated in a fully coupled climate-system model. *Geophysical Research Letters*, **29,** 4.
Calov, R., et al., 2010: Results from the Ice-Sheet Model Intercomparison Project-Heinrich Event INtercOmparison (ISMIP HEINO). *Journal of Glaciology*, **56,** 371-383.
Capron, E., et al., 2010a: Synchronising EDML and NorthGRIP ice cores using delta O-18 of atmospheric oxygen (delta O-18(atm)) and CH4 measurements over MIS5 (80-123 kyr). *Quaternary Science Reviews*, **29,** 222-234.

——, 2010b: Millennial and sub-millennial scale climatic variations recorded in polar ice cores over the last glacial period. *Climate of the Past*, **6,** 345-365.
Carlson, A., 2009: Geochemical constraints on the Laurentide Ice Sheet contribution to Meltwater Pulse 1A. *Quaternary Science Reviews***,** 1625-1630.
Carlson, A. E., D. W. Oppo, R. E. Came, A. N. LeGrande, L. D. Keigwin, and W. B. Curry, 2008: Subtropical Atlantic salinity variability and Atlantic meridional circulation during the last deglaciation. *Geology*, **36,** 991-994.
Carter, L., H. Neil, and L. Northcote, 2002: Late quaternary ice-rafting events in the SW Pacific Ocean, off eastern New Zealand. *Marine Geology***,** 19-35.
Cayre, O., Y. Lancelot, and E. Vincent, 1999: Paleoceanographic reconstructions from planktonic foraminifera off the Iberian Margin: Temperature, salinity, and Heinrich events. *Paleoceanography*, **14,** 384-396.
CERLING, T., 1991: CARBON-DIOXIDE IN THE ATMOSPHERE - EVIDENCE FROM CENOZOIC AND MESOZOIC PALEOSOLS. *American Journal of Science***,** 377-400.
Charbit, S., D. Paillard, and G. Ramstein, 2008: Amount of CO2 emissions irreversibly leading to the total melting of Greenland. *Geophysical Research Letters***,** -.
Charles, C. D., K. Cobb, M. D. Moore, and R. G. Fairbanks, 2003: Monsoon-tropical ocean interaction in a network of coral records spanning the 20th century. *Marine Geology*, **201,** 207-222.
Chase, B. M., M. E. Meadows, A. S. Carr, and P. J. Reimer, 2010: Evidence for progressive Holocene aridification in southern Africa recorded in Namibian hyrax middens: Implications for African Monsoon dynamics and the "African Humid Period". *Quaternary Research*, **74,** 36-45.
Cheng, H., et al., 2009: Ice Age Terminations. *Science*, **326,** 248-252.
Cheng, J., Z. Y. Liu, F. He, P. W. Guo, Z. X. Chen, and B. Otto-Bliesner, 2010: Model evidence for climatic impact of thermohaline circulation on China at the century scale. *Chinese Science Bulletin*, **55,** 3215-3221.
Chiang, J. C. H., and C. M. Bitz, 2005: Influence of high latitude ice cover on the marine Intertropical Convergence Zone. *Climate Dynamics*, **25,** 477-496.
Chiang, J. C. H., Y. Fang, and P. Chang, 2009: Pacific Climate Change and ENSO Activity in the Mid-Holocene. *Journal of Climate*, **22,** 923-939.
Christiansen, B., 2011: Reconstructing the NH mean temperature: Can underestimation of trends and variability be avoided? *Journal of Climate*, **24,** 674-692.
Christiansen, B., and F. C. Ljungqvist, 2011: Reconstruction of the extra-tropical NH mean temperature over the last millennium with a method that preserves low-frequency variability. *Journal of Climate*, **submitted**.
Christiansen, B., T. Schmith, and P. Thejll, 2009: A Surrogate Ensemble Study of Climate Reconstruction Methods: Stochasticity and Robustness. *Journal of Climate***,** 951-976.
——, 2010: Comments on "A Surrogate Ensemble Study of Climate Reconstruction Methods: Stochasticity and Robustness" Reply. *Journal of Climate*, **23,** 2839-2844.
Chu, G., et al., 2011: Evidence for decreasing South Asian summer monsoon in the past 160 years from varved sediment in Lake Xinluhai, Tibetan Plateau. *Journal of Geophysical Research-Atmospheres*, **116,** D02116.
Chylek, P., C. K. Folland, G. Lesins, M. K. Dubey, and M. Y. Wang, 2009: Arctic air temperature change amplification and the Atlantic Multidecadal Oscillation. *Geophysical Research Letters*, **36**.
Clarke, G., D. Leverington, J. Teller, and A. Dyke, 2004: Paleohydraulics of the last outburst flood from glacial Lake Agassiz and the 8200 BP cold event. *Quaternary Science Reviews***,** 389-407.
Clemens, S. C., W. L. Prell, and Y. B. Sun, 2010: Orbital-scale timing and mechanisms driving Late Pleistocene Indo-Asian summer monsoons: Reinterpreting cave speleothem delta O-18. *Paleoceanography*, **25**.
CLIMAP, 1976: The surface of the ice-age Earth. *Science*, **191,** 1131-1137.
——, 1981: *Seasonal reconstructions of the Earth's surface at the last glacial maximum*. Geol. Soc. Am.
Cobb, K. M., C. D. Charles, H. Cheng, and R. L. Edwards, 2003: El Nino/Southern Oscillation and tropical Pacific climate during the last millennium. *Nature*, **424,** 271-276.
Cole-Dai, J., D. Ferris, A. Lanciki, J. Savarino, M. Baroni, and M. Thiemens, 2009: Cold decade (AD 1810-1819) caused by Tambora (1815) and another (1809) stratospheric volcanic eruption. *Geophysical Research Letters***,** -.
Collins, J. A., et al., 2011: Interhemispheric symmetry of the tropical African rainbelt over the past 23,000 years. *Nature Geoscience*, **4,** 42-45.
Collins, M., T. Osborn, S. Tett, K. Briffa, and F. Schweingruber, 2002: A comparison of the variability of a climate model with paleotemperature estimates from a network of tree-ring densities. *Journal of Climate***,** 1497-1515.
Conroy, J., A. Restrepo, J. Overpeck, M. Steinitz-Kannan, J. Cole, M. Bush, and P. Colinvaux, 2009: Unprecedented recent warming of surface temperatures in the eastern tropical Pacific Ocean. *Nature Geoscience*, **2,** 46-50.
Cook, E., B. Buckley, J. G. Palmer, P. Fenwick, M. Peterson, G. Boswijk, and A. Fowler, 2006: Millennia-long tree-ring records from Tasmania and New Zealand: a basis for modelling climate variability and forcing, past, present and future. *Journal of Quaternary Science*, **21,** 689-699.
Cook, E. R., R. D. D'Arrigo, and M. E. Mann, 2002: A well-verified, multiproxy reconstruction of the winter North Atlantic Oscillation index since AD 1400. *Journal of Climate*, **15,** 1754-1764.
Cook, E. R., K. J. Anchukaitis, B. M. Buckley, R. D. D'Arrigo, G. C. Jacoby, and W. E. Wright, 2010a: Asian Monsoon Failure and Megadrought During the Last Millennium. *Science*, **328,** 486-489.

Cook, E. R., R. Seager, R. R. Heim, R. S. Vose, C. Herweijer, and C. Woodhouse, 2010b: Megadroughts in North America: placing IPCC projections of hydroclimatic change in a long-term palaeoclimate context. *Journal of Quaternary Science*, **25,** 48-61.
Cordeiro, R., et al., 2011: Biogeochemical indicators of environmental changes from 50 Ka to 10 Ka in a humid region of the Brazilian Amazon. *Palaeogeography Palaeoclimatology Palaeoecology*, 426-436.
Corona, C., J. Guiot, J. Edouard, F. Chalie, U. Buntgen, P. Nola, and C. Urbinati, 2010: Millennium-long summer temperature variations in the European Alps as reconstructed from tree rings. *Climate of the Past*, **6,** 379-400.
Corr, H., and D. Vaughan, 2008: A recent volcanic eruption beneath the West Antarctic ice sheet. *Nature Geoscience*, 122-125.
Coxall, H., P. Wilson, H. Palike, C. Lear, and J. Backman, 2005: Rapid stepwise onset of Antarctic glaciation and deeper calcite compensation in the Pacific Ocean. *Nature*, 53-57.
Creech, J., J. Baker, C. Hollis, H. Morgans, and E. Smith, 2010: Eocene sea temperatures for the mid-latitude southwest Pacific from Mg/Ca ratios in planktonic and benthic foraminifera. *Earth and Planetary Science Letters*, 483-495.
Crouch, A., P. Charbonneau, G. Beaubien, and D. Paquin-Ricard, 2008: A model for the total solar irradiance based on active region decay. *Astrophysical Journal*, 723-741.
Crowley, T., and W. Hyde, 2008: Transient nature of late Pleistocene climate variability. *Nature*, 226-230.
Crowley, T. J., 1992: North Alantic Deep Water Cools The Southern Hemisphere. *Paleoceanography*, **7,** 489-497.
Crucifix, M., 2006: Does the Last Glacial Maximum constrain climate sensitivity? *Geophysical Research Letters*, -.
Crucifix, M., and J. Rougier, 2009: On the use of simple dynamical systems for climate predictions. *European Physical Journal-Special Topics*, **174,** 11-31.
Cruz, F., et al., 2005: Insolation-driven changes in atmospheric circulation over the past 116,000 years in subtropical Brazil. *Nature*, **434,** 63-66.
Cruz, F. W., et al., 2009: Orbitally driven east-west antiphasing of South American precipitation. *Nature Geoscience*, **2,** 210-214.
Cruz Jr, F., S. Burns, I. Karmann, W. Sharp, M. Vuille, and J. Ferrari, 2006: A stalagmite record of changes in atmospheric circulation and soil processes in the Brazilian subtropics during the Late Pleistocene. *Quaternary Science Reviews*, **25,** 2749-2761.
Cullen, H. M., R. D. D'Arrigo, E. R. Cook, and M. E. Mann, 2001: Multiproxy reconstructions of the North Atlantic Oscillation. *Paleoceanography*, **16,** 27-39.
D'Arrigo, R., R. Wilson, B. Liepert, and P. Cherubini, 2008: On the 'divergence problem' in northern forests: a review of the tree-ring evidence and possible causes. *Global and Planetary Change*, **60,** 289-305.
Dahl-Jensen, D., K. Mosegaard, N. Gundestrup, G. D. Clow, S. J. Johnsen, A. W. Hansen, and N. Balling, 1998: Past temperatures directly from the Greenland ice sheet. *Science*, **282,** 268-271.
Dahl, K., A. Broccoli, and R. Stouffer, 2005: Assessing the role of North Atlantic freshwater forcing in millennial scale climate variability: a tropical Atlantic perspective. *Climate Dynamics*, **24,** 325-346.
Dakos, V., M. Scheffer, E. H. van Nes, V. Brovkin, V. Petoukhov, and H. Held, 2008: Slowing down as an early warning signal for abrupt climate change. *Proceedings of the National Academy of Sciences of the United States of America*, **105,** 14308-14312.
Darrigo, R. D., E. R. Cook, G. C. Jacoby, and K. R. Briffa, 1993: NAO AND SEA-SURFACE TEMPERATURE SIGNATURES IN TREE-RING RECORDS FROM THE NORTH-ATLANTIC SECTOR. *Quaternary Science Reviews*, **12,** 431-440.
Davis, M., L. Thompson, T. Yao, and N. Wang, 2005: Forcing of the Asian monsoon on the Tibetan Plateau: Evidence from high-resolution ice core and tropical coral records. *Journal of Geophysical Research-Atmospheres*, **110,** D04101.
De Deckker, P., M. Norman, I. D. Goodwin, A. Wain, and F. X. Gingele, 2010: Lead isotopic evidence for an Australian source of aeolian dust to Antarctica at times over the last 170,000 years. *Palaeogeography Palaeoclimatology Palaeoecology*, **285,** 205-223.
de Vernal, A., and C. Hillaire-Marcel, 2008: Natural variability of Greenland climate, vegetation, and ice volume during the past million years. *Science*, **320,** 1622-1625.
DeConto, R., and D. Pollard, 2003: Rapid Cenozoic glaciation of Antarctica induced by declining atmospheric CO2. *Nature*, 245-249.
DeConto, R. M., D. Pollard, P. A. Wilson, H. Palike, C. H. Lear, and M. Pagani, 2008: Thresholds for Cenozoic bipolar glaciation. *Nature*, **455,** 652-U652.
Delaygue, G., and E. Bard, 2010: An Antarctic view of Beryllium-10 and solar activity for the past millennium. *Climate Dynamics*.
Delmonte, B., P. S. Andersson, M. Hansson, H. Schoberg, J. R. Petit, I. Basile-Doelsch, and V. Maggi, 2008: Aeolian dust in East Antarctica (EPICA-Dome C and Vostok): Provenance during glacial ages over the last 800 kyr. *Geophysical Research Letters*, **35**.
Denton, G. H., R. F. Anderson, J. R. Toggweiler, R. L. Edwards, J. M. Schaefer, and A. E. Putnam, 2010: The Last Glacial Termination. *Science*, **328,** 1652-1656.
Derbyshire, E., 2003: Loess, and the Dust Indicators and Records of Terrestrial and Marine Palaeoenvironments (DIRTMAP) database. *Quaternary Science Reviews*, **22,** 1813-1819.

Desprat, S., et al., 2005: Is vegetation responsible for glacial insolation inception during periods of muted changes? *Quaternary Science Reviews*, **24,** 1361-1374.
Dewitte, S., D. Crommelynck, S. Mekaoui, and A. Joukoff, 2004: Measurement and uncertainty of the long-term total solar irradiance trend. *Solar Physics*, **224,** 209-216.
Diaz, H. F., R. M. Trigo, M. K. Hughes, M. E. Mann, E. Xoplaki, and D. Barriopedro, in review: Spatial and temporal characteristics of Climate in medieval times revisited. *Bulletin of the American Meteorological Society*.
Ditlevsen, P. D., and O. D. Ditlevsen, 2009: On the Stochastic Nature of the Rapid Climate Shifts during the Last Ice Age. *Journal of Climate*, **22,** 446-457.
Dong, J., et al., 2010: A high-resolution stalagmite record of the Holocene East Asian monsoon from Mt Shennongjia, central China. *Holocene*, **20,** 257-264.
Dowsett, H., 2009: The PRISM paleoclimate reconstruction and Pliocene sea-surface temperature. *Deep-time perspectives on climate change: Marrying the signal from computer models and biological proxies*, M. Williams, A. Haywood, J. Gregory, and D. Schmidt, Eds., The Mineralogical Society, 459-458.
Drysdale, R., 2009: Evidence for obliquity forcing of glacial Termination II (vol 325, pg 1527, 2009). *Science***,** 798-798.
Drysdale, R., et al., 2006: Late Holocene drought responsible for the collapse of Old World civilizations is recorded in an Italian cave flowstone. *Geology*, **34,** 101-104.
Edwards, T., M. Crucifix, and S. Harrison, 2007: Using the past to constrain the future: how the palaeorecord can improve estimates of global warming. *Progress in Physical Geography***,** 481-500.
Elderfield, H., et al., 2010: A record of bottom water temperature and seawater delta O-18 for the Southern Ocean over the past 440 kyr based on Mg/Ca of benthic foraminiferal Uvigerina spp. *Quaternary Science Reviews***,** 160-169.
Eldrett, J., D. Greenwood, I. Harding, and M. Huber, 2009: Increased seasonality through the Eocene to Oligocene transition in northern high latitudes. *Nature***,** 969-U991.
Ellison, C. R. W., M. R. Chapman, and I. R. Hall, 2006: Surface and deep ocean interactions during the cold climate event 8200 years ago. *Science*, **312,** 1929-1932.
Elsig, J., et al., 2009: Stable isotope constraints on Holocene carbon cycle changes from an Antarctic ice core. *Nature*, **461,** 507-510.
Emile-Geay, J., R. Seager, M. A. Cane, E. R. Cook, and G. H. Haug, 2008: Volcanoes and ENSO over the past millennium. *Journal of Climate*, **21,** 3134-3148.
Esper, J., and D. Frank, 2009: Divergence pitfalls in tree-ring research. *Climatic Change*, **94,** 261-266.
Esper, J., D. Frank, R. Wilson, U. Buntgen, and K. Treydte, 2007: Uniform growth trends among central Asian low- and high-elevation juniper tree sites. *Trees-Structure and Function*, **21,** 141-150.
Euler, C., and U. Ninnemann, 2010: Climate and Antarctic Intermediate Water coupling during the late Holocene. *Geology***,** 647-650.
Fan, F., M. Mann, S. Lee, and J. Evans, 2010: Observed and Modeled Changes in the South Asian Summer Monsoon over the Historical Period. *Journal of Climate*, **23,** 5193-5205.
Fawcett, P. J., et al., 2011: Extended megadroughts in the southwestern United States during Pleistocene interglacials. *Nature*, **470,** 518-521.
Ferretti, D., et al., 2005: Unexpected changes to the global methane budget over the past 2000 years. *Science*, **309,** 1714-1717.
Fischer, H., M. L. Siggaard-Andersen, U. Ruth, R. Rothlisberger, and E. Wolff, 2007a: Glacial/interglacial changes in mineral dust and sea-salt records in polar ice cores: Sources, transport, and deposition. *Reviews of Geophysics*, **45**.
Fischer, H., et al., 2008: Changing boreal methane sources and constant biomass burning during the last termination. *Nature*, **452,** 864-867.
——, 2007b: Reconstruction of millenial changes in dust emission, transport and regional sea-ice coverage using the deep EPICA ice cores from the Atlantic and Indian Ocean sector of Antarctiabout *Earth and Planetary Science Letters*, **260,** 340-354.
Fischer, N., and J. H. Jungclaus, 2010: Effects of orbital forcing on atmosphere and ocean heat transports in Holocene and Eemian climate simulations with a comprehensive Earth system model. *Climate of the Past*, **6,** 155-168.
Fleitmann, D., S. Burns, U. Neff, M. Mudelsee, A. Mangini, and A. Matter, 2004: Palaeoclimatic interpretation of high-resolution oxygen isotope profiles derived from annually laminated speleothems from Southern Oman. *Quaternary Science Reviews*, **23,** 935-945.
Fleitmann, D., S. Burns, M. Mudelsee, U. Neff, J. Kramers, A. Mangini, and A. Matter, 2003: Holocene forcing of the Indian monsoon recorded in a stalagmite from Southern Oman. *Science***,** 1737-1739.
Fleitmann, D., et al., 2007: Holocene ITCZ and Indian monsoon dynamics recorded in stalagmites from Oman and Yemen (Socotra). *Quaternary Science Reviews*, **26,** 170-188.
Fogt, R., J. Perlwitz, A. Monaghan, D. Bromwich, J. Jones, and G. Marshall, 2009: Historical SAM Variability. Part II: Twentieth-century Variability and Trends from Reconstructions, Observations, and the IPCC AR4 Models. *Journal of Climate*, **22,** 5346-5365.
Frank, D., J. Esper, E. Zorita, and R. Wilson, 2010: A noodle, hockey stick, and spaghetti plate: a perspective on high-resolution paleoclimatology. *Wiley Interdisciplinary Reviews: Climate Change*, **1**.
Frohlich, C., 2009: Evidence of a long-term trend in total solar irradiance. *Astronomy & Astrophysics*, **501,** L27-U508.

Gaillard, M., et al., 2010: Holocene land-cover reconstructions for studies on land cover-climate feedbacks. *Climate of the Past*, 483-499.
Ganopolski, A., and D. M. Roche, 2009: On the nature of lead-lag relationships during glacial-interglacial climate transitions. *Quaternary Science Reviews*, **28**, 3361-3378.
Ganopolski, A., R. Calov, and M. Claussen, 2010: Simulation of the last glacial cycle with a coupled climate ice-sheet model of intermediate complexity. *Climate of the Past*, **6**, 229-244.
Gao, C., A. Robock, and C. Ammann, 2008: Volcanic forcing of climate over the past 1500 years: An improved ice core-based index for climate models. *Journal of Geophysical Research-Atmospheres*, -.
Gao, C., et al., 2006: The 1452 or 1453 AD Kuwae eruption signal derived from multiple ice core records: Greatest volcanic sulfate event of the past 700 years. *Journal of Geophysical Research-Atmospheres*, -.
Gasse, F., 2000: Hydrological changes in the African tropics since the Last Glacial Maximum. *Quaternary Science Reviews*, 189-211.
Ge, Q., S. Wang, and J. Zheng, 2006: Reconstruction of temperature series in China for the last 5000 years. *Progress in Natural Science*, 838-845.
Ge, Q., X. Guo, J. Zheng, and Z. Hao, 2008: Meiyu in the middle and lower reaches of the Yangtze River since 1736. *Chinese Science Bulletin*, **53**, 107-114.
Ge, Q., Z. Hao, Y. Tian, F. He, and J. Zheng, 2011: The rainy season in the Northwestern part of the East Asian Summer Monsoon in the 18th and 19th centuries. *Quaternary International*, **229**, 16-23.
Ge, Q., J. Zheng, Z. Hao, X. Shao, W. Wang, and J. Luterbacher, 2010: Temperature variation through 2000 years in China: An uncertainty analysis of reconstruction and regional difference. *Geophysical Research Letters*, -.
Ge, Q., J. Zheng, X. Fang, Z. Man, X. Zhang, P. Zhang, and W. Wang, 2003: Winter half-year temperature reconstruction for the middle and lower reaches of the Yellow River and Yangtze River, China, during the past 2000 years. *Holocene*, 933-940.
Ghatak, D., A. Frei, G. Gong, J. Stroeve, and D. Robinson, 2010: On the emergence of an Arctic amplification signal in terrestrial Arctic snow extent. *Journal of Geophysical Research-Atmospheres*, **115**.
Gherardi, J., L. Labeyrie, J. McManus, R. Francois, L. Skinner, and E. Cortijo, 2005: Evidence from the Northeastern Atlantic basin for variability in the rate of the meridional overturning circulation through the last deglaciation. *Earth and Planetary Science Letters*, 710-723.
Giannini, A., R. Saravanan, and P. Chang, 2003: Oceanic forcing of Sahel rainfall on interannual to interdecadal time scales. *Science*, **302**, 1027-1030.
Gillett, N., et al., 2008: Attribution of polar warming to human influence. *Nature Geoscience*, **1**, 750-754.
Gladstone, R. M., et al., 2005: Mid-Holocene NAO: A PMIP2 model intercomparison. *Geophysical Research Letters*, **32**.
Glueck, M. F., and C. W. Stockton, 2001: Reconstruction of the North Atlantic Oscillation, 1429-1983. *International Journal of Climatology*, **21**, 1453-1465.
Gong, D., and S. Wang, 1999: Definition of Antarctic Oscillation Index. *Geophysical Research Letters*, **26**, 459-462.
Gonzalez-Rouco, J., H. Beltrami, E. Zorita, and H. von Storch, 2006: Simulation and inversion of borehole temperature profiles in surrogate climates: Spatial distribution and surface coupling. *Geophysical Research Letters*, -.
Gonzalez, C., L. Urrego, J. Martinez, J. Polania, and Y. Yokoyama, 2010: Mangrove dynamics in the southwestern Caribbean since the 'Little Ice Age':A history of human and natural disturbances. *Holocene*, 849-861.
Goodwin, I., T. van Ommen, M. Curran, and P. Mayewski, 2004: Mid latitude winter climate variability in the South Indian and southwest Pacific regions since 1300 AD. *Climate Dynamics*, **22**, 783-794.
Goosse, H., H. Renssen, A. Timmermann, and R. Bradley, 2005: Internal and forced climate variability during the last millennium: a model-data comparison using ensemble simulations. *Quaternary Science Reviews*, 1345-1360.
Goosse, H., E. Crespin, A. de Montety, M. E. Mann, H. Renssen, and A. Timmermann, 2010: Reconstructing surface temperature changes over the past 600 years using climate model simulations with data assimilation. *Journal of Geophysical Research-Atmospheres*, **115**.
Gouirand, I., H. Linderholm, A. Moberg, and B. Wohlfarth, 2008: On the spatiotemporal characteristics of Fennoscandian tree-ring based summer temperature reconstructions. *Theoretical and Applied Climatology*, **91**, 1-25.
Gow, A., and D. Meese, 2007: The distribution and timing of tephra deposition at Siple Dome, Antarctica: possible climatic and rheologic implications. *Journal of Glaciology*, 585-596.
Grachev, A., E. Brook, J. Severinghaus, and N. Pisias, 2009: Relative timing and variability of atmospheric methane and GISP2 oxygen isotopes between 68 and 86 ka. *Global Biogeochemical Cycles*, -.
Graham, N., C. Ammann, D. Fleitmann, K. Cobb, and J. Luterbacher, 2010: Support for global climate reorganization during the “Medieval Climate Anomaly”. *Climate Dynamics*.
Graham, N., et al., 2007: Tropical Pacific - mid-latitude teleconnections in medieval times. *Climatic Change*, 241-285.
Graversen, R. G., and M. H. Wang, 2009: Polar amplification in a coupled climate model with locked albedo. *Climate Dynamics*, **33**, 629-643.
Gray, S. T., L. J. Graumlich, J. L. Betancourt, and G. T. Pederson, 2004: A tree-ring based reconstruction of the Atlantic Multidecadal Oscillation since 1567 AD. *Geophysical Research Letters*, **31**.
Gregory, J., and P. Huybrechts, 2006: Ice-sheet contributions to future sea level change. *Philosophical Transactions of the Royal Society a-Mathematical Physical and Engineering Sciences*, 1709-1731.

Griessinger, J., A. Bräuning, G. Helle, A. Thomas, and G. Schleser, 2011: Late Holocene Asian summer monsoon variability reflected by d18O in tree-rings from Tibetan junipers. *Geophys. Res. Lett.*, **38,** L03701.
Groll, N., and M. Widmann, 2006: Sensitivity of temperature teleconnections to orbital changes in AO-GCM simulations. *Geophysical Research Letters*, **33,** 4.
Grudd, H., 2008: Tornetrask tree-ring width and density AD 500-2004: a test of climatic sensitivity and a new 1500-year reconstruction of north Fennoscandian summers. *Climate Dynamics*, **31,** 843-857.
Grudd, H., K. Briffa, W. Karlen, T. Bartholin, P. Jones, and B. Kromer, 2002: A 7400-year tree-ring chronology in northern Swedish Lapland: natural climatic variability expressed on annual to millennial timescales. *Holocene*, **12,** 657-665.
Guiot, J., C. Corona, and ESCARSEL, 2010: Growing Season Temperatures in Europe and Climate Forcings Over the Past 1400 Years. *Plos One*, **5,** e9972.
Guiot, J., et al., 2009: Europe heat waves much more probalble now than ever in 1400 years. *Submitted to PNAS*.
Hack, J. J., W. H. Schubert, D. E. Stevens, and H. C. Kuo, 1989: RESPONSE OF THE HADLEY CIRCULATION TO CONVECTIVE FORCING IN THE ITCZ. *Journal of the Atmospheric Sciences*, **46,** 2957-2973.
Hadley, O., C. Corrigan, T. Kirchstetter, S. Cliff, and V. Ramanathan, 2010: Measured black carbon deposition on the Sierra Nevada snow pack and implication for snow pack retreat. *Atmospheric Chemistry and Physics***,** 7505-7513.
Hald, M., et al., 2007: Variations in temperature and extent of Atlantic Water in the northern North Atlantic during the Holocene. *Quaternary Science Reviews***,** 3423-3440.
Handorf, D., K. Dethloff, A. G. Marshall, and A. Lynch, 2009: Climate Regime Variability for Past and Present Time Slices Simulated by the Fast Ocean Atmosphere Model. *Journal of Climate*, **22,** 58-70.
Harada, N., M. Sato, and T. Sakamoto, 2008: Freshwater impacts recorded in tetraunsaturated alkenones and alkenone sea surface temperatures from the Okhotsk Sea across millennial-scale cycles. *Paleoceanography*, **23**.
Hargreaves, J. C., A. Abe-Ouchi, and J. D. Annan, 2007: Linking glacial and future climates through an ensemble of GCM simulations. *Clim. Past*, **3,** 77-87.
Harrison, S. P., and M. F. S. Goni, 2010: Global patterns of vegetation response to millennial-scale variability and rapid climate change during the last glacial period. *Quaternary Science Reviews*, **29,** 2957-2980.
Haslam, M., et al., 2010: The 74 ka Toba super-eruption and southern Indian hominins: archaeology, lithic technology and environments at Jwalapuram Locality 3. *Journal of Archaeological Science***,** 3370-3384.
Haug, G. H., K. A. Hughen, D. M. Sigman, L. C. Peterson, and U. Rohl, 2001: Southward migration of the intertropical convergence zone through the Holocene. *Science*, **293,** 1304-1308.
Haug, G. H., D. Gunther, L. C. Peterson, D. M. Sigman, K. A. Hughen, and B. Aeschlimann, 2003: Climate and the collapse of Maya civilization. *Science*, **299,** 1731-1735.
Haywood, A., P. Dekens, A. Ravelo, and M. Williams, 2005: Warmer tropics during the mid-Pliocene? Evidence from alkenone paleothermometry and a fully coupled ocean-atmosphere GCM. *Geochemistry Geophysics Geosystems***,** -.
Hegerl, G., J. Luterbacher, F. Gonzalez-Rouco, S. Tett, T. Crowley, and E. Xoplaki, 2011: Influence of human and natural forcing on European seasonal temperatures. *Nature Geoscience***,** 99-103.
Hegerl, G. C., T. J. Crowley, W. T. Hyde, and D. J. Frame, 2006: Climate sensitivity constrained by temperature reconstructions over the past seven centuries. *Nature*, **440,** 1029-1032.
Hegerl, G. C., T. J. Crowley, M. Allen, W. T. Hyde, H. N. Pollack, J. Smerdon, and E. Zorita, 2007: Detection of human influence on a new, validated 1500-year temperature reconstruction. *Journal of Climate*, **20,** 650-666.
Helama, S., J. Merilainen, and H. Tuomenvirta, 2009a: Multicentennial megadrought in northern Europe coincided with a global El Nino-Southern Oscillation drought pattern during the Medieval Climate Anomaly. *Geology*, **37,** 175-178.
Helama, S., et al., 2009b: Summer temperature variations in Lapland during the Medieval Warm Period and the Little Ice Age relative to natural instability of thermohaline circulation on multi-decadal and multi-centennial scales. *J. Quaternary Science*, **24,** 450-456.
Hely, C., M. Girardin, A. Ali, C. Carcaillet, S. Brewer, and Y. Bergeron, 2010: Eastern boreal North American wildfire risk of the past 7000 years: A model-data comparison. *Geophysical Research Letters***,** -.
Hemming, S. R., 2004: Heinrich events: Massive late pleistocene detritus layers of the North Atlantic and their global climate imprint. *Reviews of Geophysics*, **42**.
Herbert, T., L. Peterson, K. Lawrence, and Z. Liu, 2010a: Tropical Ocean Temperatures Over the Past 3.5 Million Years. *Science***,** 1530-1534.
Herbert, T. D., L. C. Peterson, K. T. Lawrence, and Z. H. Liu, 2010b: Tropical Ocean Temperatures Over the Past 3.5 Million Years. *Science*, **328,** 1530-1534.
Herold, M., and G. Lohmann, 2009: Eemian tropical and subtropical African moisture transport: an isotope modelling study. *Climate Dynamics*, **33,** 1075-1088.
Hessler, I., et al., 2010: Millennial-scale changes in vegetation records from tropical Africa and South America during the last glacial. *Quaternary Science Reviews*, **29,** 2882-2899.
Higginson, M. J., M. A. Altabet, D. W. Murray, R. W. Murray, and T. D. Herbert, 2004: Geochemical evidence for abrupt changes in relative strength of the Arabian monsoons during a stadial/interstadial climate transition. *Geochimica Et Cosmochimica Acta*, **68,** 3807-3826.

Hillaire-Marcel, C., A. de Vernal, and D. J. W. Piper, 2007: Lake Agassiz final drainage event in the northwest North Atlantic. *Geophysical Research Letters*, **34**.

Hillaire-Marcel, C., J. F. Helie, J. McKay, and A. de Vernal, 2008: Elusive isotopic properties of deglacial meltwater spikes into the North Atlantic: example of the final drainage of Lake Agassiz. *Canadian Journal of Earth Sciences*, **45,** 1235-1242.

Holden, P. B., N. R. Edwards, E. W. Wolff, N. J. Lang, J. S. Singarayer, P. J. Valdes, and T. F. Stocker, 2010: Interhemispheric coupling and warm Antarctic interglacials. *Clim. Past. Discuss.*, **5,** 2555-2575.

Holland, M. M., M. C. Serreze, and J. Stroeve, 2010: The sea ice mass budget of the Arctic and its future change as simulated by coupled climate models. *Climate Dynamics*, **34,** 185-200.

Hollis, C., et al., 2009: Tropical sea temperatures in the high-latitude South Pacific during the Eocene. *Geology***,** 99-102.

Holmgren, K., et al., 2003: Persistent millenial-scale climate variability over the past 25,000 years in Southern Afriabout *Quaternary Science Reviews*, **2003,** 2311-2326.

Hong, Y., et al., 2005: Inverse phase oscillations between the East Asian and Indian Ocean summer monsoons during the last 12,000 years and paleo-El Nino. *Earth and Planetary Science Letters***,** 337-346.

Honisch, B., N. G. Hemming, D. Archer, M. Siddall, and J. F. McManus, 2009: Atmospheric Carbon Dioxide Concentration Across the Mid-Pleistocene Transition. *Science*, **324,** 1551-1554.

Huang, E., J. Tian, and S. Steinke, 2011: Millennial-scale dynamics of the winter cold tongue in the southern South China Sea over the past 26 ka and the East Asian winter monsoon. *Quaternary Research*, **75,** 196-204.

Huber, M., and L. Sloan, 2001: Heat transport, deep waters, and thermal gradients: Coupled simulation of an Eocene Greenhouse Climate. *Geophysical Research Letters***,** 3481-3484.

Huybers, P., 2006: Early Pleistocene glacial cycles and the integrated summer insolation forcing. *Science*, **313,** 508-511.

——, 2009: Antarctica's orbital beat. *Science*, **325,** 1085-1086.

Huybers, P., and C. Wunsch, 2005: Obliquity pacing of the late Pleistocene glacial terminations. *Nature*, **434,** 491-494.

Huybers, P., and G. Denton, 2008: Antarctic temperature at orbital timescales controlled by local summer duration. *Nature Geoscience*, **1,** 787-792.

Huybers, P., and C. Langmuir, 2009: Feedback between deglaciation, volcanism, and atmospheric CO2. *Earth and Planetary Science Letters***,** 479-491.

Itambi, A. C., T. von Dobeneck, S. Mulitza, T. Bickert, and D. Heslop, 2009: Millennial-scale northwest African droughts related to Heinrich events and Dansgaard-Oeschger cycles: Evidence in marine sediments from offshore Senegal. *Paleoceanography*, **24**.

Ivanochko, T. S., R. S. Ganeshram, G. J. A. Brummer, G. Ganssen, S. J. A. Jung, S. G. Moreton, and D. Kroon, 2005: Variations in tropical convection as an amplifier of global climate change at the millennial scale. *Earth and Planetary Science Letters*, **235,** 302-314.

Jaccard, S., E. Galbraith, D. Sigman, and G. Haug, 2010: A pervasive link between Antarctic ice core and subarctic Pacific sediment records over the past 800 kyrs. *Quaternary Science Reviews***,** 206-212.

Jansen, E., et al., 2007: Palaeoclimate. *Climate Change 2007: The Physical Science Basis. Contribution of Working Group I to the Fourth Assessment Report of the Intergovernmental Panel on Climate Change*, Cambridge University Press.

Jiang, D., and X. Lang, 2010: Last Glacial Maximum East Asian Monsoon: Results of PMIP Simulations. *Journal of Climate*, **23,** 5030-5038.

Jin, Z., J. Yu, H. Chen, Y. Wu, S. Wang, and S. Chen, 2007: The influence and chronological uncertainties of the 8.2 ka cooling event on continental climate records in China. *Holocene***,** 1041-1050.

Jones, J., R. Fogt, M. Widmann, G. Marshall, P. Jones, and M. Visbeck, 2009a: Historical SAM Variability. Part I: century-Length Seasonal Reconstructions. *Journal of Climate*, **22,** 5319-5345.

Jones, P. D., et al., 2009b: High-resolution palaeoclimatology of the last millennium: a review of current status and future prospects. *Holocene*, **19,** 3-49.

Joos, F., and R. Spahni, 2008: Rates of change in natural and anthropogenic radiative forcing over the past 20,000 years. *Proceedings of the National Academy of Sciences of the United States of America***,** 1425-1430.

Jouzel, J., et al., 2007: Orbital and millennial Antarctic climate variability over the past 800,000 years. *Science*, **317,** 793-796.

Juckes, M., et al., 2007: Millennial temperature reconstruction intercomparison and evaluation. *Climate of the Past***,** 591-609.

Jungclaus, J., et al., 2010a: Climate and carbon-cycle variability over the last millennium. *Climate of the Past*, **6,** 723-737.

Jungclaus, J. H., et al., 2010b: Climate and carbon-cycle variability over the last millennium. *Climate of the Past*, **6,** 723-737.

Junker, C., and C. Liousse, 2008: A global emission inventory of carbonaceous aerosol from historic records of fossil fuel and biofuel consumption for the period 1860-1997. *Atmospheric Chemistry and Physics*, **8,** 1195-1207.

Justino, F., and W. R. Peltier, 2005: The glacial North Atlantic Oscillation. *Geophysical Research Letters*, **32,** 4.

Justino, F., W. Peltier, and H. Barbosa, 2010: Atmospheric susceptibility to wildfire occurrence during the Last Glacial Maximum and mid-Holocene. *Palaeogeography Palaeoclimatology Palaeoecology*, **295,** 76-88.

Kaplan, J., K. Krumhardt, and N. Zimmermann, 2009: The prehistoric and preindustrial deforestation of Europe. *Quaternary Science Reviews*, **28,** 3016-3034.

Kaplan, J., K. Krumhardt, E. Ellis, W. Ruddiman, C. Lemmen, and K. Goldewijk, 2011: Holocene carbon emissions as a result of anthropogenic land cover change. *The Holocene*, -.
Kariya, C., M. Hyodo, K. Tanigawa, and H. Sato, 2010: Sea level variation during MIS 11 constrained by stepwise Osaka Bay extensions and its relation with climatic evolution. *Quaternary Science Reviews*, **29**, 1863-1879.
Kaspar, F., T. Spangehl, and U. Cubasch, 2007: Northern hemisphere winter storm tracks of the Eemian interglacial and the last glacial inception. *Climate of the Past*, **3**, 181-192.
Katz, M., K. Miller, J. Wright, B. Wade, J. Browning, B. Cramer, and Y. Rosenthal, 2008: Stepwise transition from the Eocene greenhouse to the Oligocene icehouse. *Nature Geoscience*, 329-334.
Kaufman, D., et al., 2009a: Recent Warming Reverses Long-Term Arctic Cooling. *Science*, **325,** 1236-1239.
Kaufman, D. S., et al., 2009b: Recent Warming Reverses Long-Term Arctic Cooling. *Science*, **325,** 1236-1239.
Kawamura, K., et al., 2007: Northern Hemisphere forcing of climatic cycles in Antarctica over the past 360,000 years. *Nature*, **448,** 912-915.
Kiefer, T., and M. Kienast, 2005: Patterns of deglacial warming in the Pacific Ocean: a review with emphasis on the time interval of Heinrich event 1. *Quaternary Science Reviews*, **24,** 1063-1081.
Kiefer, T., M. Sarnthein, H. Erlenkeuser, P. M. Grootes, and A. P. Roberts, 2001: North Pacific response to millennial-scale changes in ocean circulation over the last 60 kyr. *Paleoceanography*, **16,** 179-189.
Kienast, M., S. S. Kienast, S. E. Calvert, T. I. Eglinton, G. Mollenhauer, R. Francois, and A. C. Mix, 2006: Eastern Pacific cooling and Atlantic overturning circulation during the last deglaciation. *Nature*, **443,** 846-849.
Kilbourne, K., T. Quinn, R. Webb, T. Guilderson, J. Nyberg, and A. Winter, 2008: Paleoclimate proxy perspective on Caribbean climate since the year 1751: Evidence of cooler temperatures and multidecadal variability. *Paleoceanography*, -.
Kim, S. J., et al., 2010: Climate response over Asia/Arctic to change in orbital parameters for the last interglacial maximum. *Geosciences Journal*, **14,** 173-190.
Kleiven, H. F., E. Jansen, T. Fronval, and T. M. Smith, 2002: Intensification of Northern Hemisphere glaciations in the circum Atlantic region (3.5-2.4 Ma) - ice-rafted detritus evidence. *Palaeogeography Palaeoclimatology Palaeoecology*, **184,** 213-223.
Kleiven, H. F., C. Kissel, C. Laj, U. S. Ninnemann, T. O. Richter, and E. Cortijo, 2008: Reduced North Atlantic Deep Water coeval with the glacial Lake Agassiz freshwater outburst. *Science*, **319,** 60-64.
Knight, J. R., 2009: The Atlantic Multidecadal Oscillation Inferred from the Forced Climate Response in Coupled General Circulation Models. *Journal of Climate*, **22,** 1610-1625.
KOERNER, R., 1989: ICE CORE EVIDENCE FOR EXTENSIVE MELTING OF THE GREENLAND ICE-SHEET IN THE LAST INTERGLACIAL. *Science*, 964-968.
Koerner, R., and D. Fisher, 2002: Ice-core evidence for widespread Arctic glacier retreat in the Last Interglacial and the early Holocene. *Annals of Glaciology, Vol 35*, 19-24.
Kohler, P., F. Joos, S. Gerber, and R. Knutti, 2005: Simulated changes in vegetation distribution, land carbon storage, and atmospheric CO2 in response to a collapse of the North Atlantic thermohaline circulation. *Climate Dynamics*, **25,** 689-708.
Kohler, P., R. Bintanja, H. Fischer, F. Joos, R. Knutti, G. Lohmann, and V. Masson-Delmotte, 2010: What caused Earth's temperature variations during the last 800,000 years? Data-based evidence on radiative forcing and constraints on climate sensitivity. *Quaternary Science Reviews*, **29,** 129-145.
Kopp, R. E., F. J. Simons, J. X. Mitrovica, A. C. Maloof, and M. Oppenheimer, 2009: Probabilistic assessment of sea level during the last interglacial stage. *Nature*, **462,** 863-U851.
Koutavas, A., and S. Joanidis, 2009: El Nino during the last glacial maximum. *Geochimica Et Cosmochimica Acta*, **73,** A690-A690.
Koutavas, A., P. B. Demenocal, G. C. Olive, and J. Lynch-Stieglitz, 2006: Mid-Holocene El Nino-Southern Oscillation (ENSO) attenuation revealed by individual foraminifera in eastern tropical Pacific sediments. *Geology*, **34,** 993-996.
Krebs, U., and A. Timmermann, 2007: Fast advective recovery of the Atlantic meridional overturning circulation after a Heinrich event. *Paleoceanography*, **22**.
Krinner, G., O. Boucher, and Y. Balkanski, 2006: Ice-free glacial northern Asia due to dust deposition on snow. *Climate Dynamics*, 613-625.
Kristen, I., et al., 2010: Biomarker and stable carbon isotope analyses of sedimentary organic matter from Lake Tswaing: evidence for deglacial wetness and early Holocene drought from South Afriabout *Journal of Paleolimnology*, **44,** 143-160.
Krivova, N., and S. Solanki, 2008: Models of solar irradiance variations: Current status. *Journal of Astrophysics and Astronomy*, 151-158.
Krivova, N., L. Balmaceda, and S. Solanki, 2007: Reconstruction of solar total irradiance since 1700 from the surface magnetic flux. *Astronomy & Astrophysics*, 335-346.
Krivova, N., L. Vieira, and S. Solanki, 2010: Reconstruction of solar spectral irradiance since the Maunder minimum. *Journal of Geophysical Research-Space Physics*, -.
Krivova, N., S. Solanki, and Y. Unruh, 2011: Towards a long-term record of solar total and spectral irradiance. *Journal of Atmospheric and Solar-Terrestrial Physics*, 223-234.

Kropelin, S., et al., 2008: Climate-driven ecosystem succession in the Sahara: The past 6000 years. *Science*, **320,** 765-768.
Kuper, R., and S. Kropelin, 2006: Climate-controlled Holocene occupation in the Sahara: Motor of Africa's evolution. *Science*, **313,** 803-807.
Kurschner, W., and Z. Kvacek, 2009: Oligocene-Miocen CO2 fluctuations, climatic and palaeofloristic trends inferred from fossil plant assemblages in central Europe. *Bulletin of Geosciences***,** 189-202.
Kurschner, W., Z. Kvacek, and D. Dilcher, 2008: The impact of Miocene atmospheric carbon dioxide fluctuations on climate and the evolution of terrestrial ecosystems. *Proceedings of the National Academy of Sciences of the United States of America***,** 449-453.
Kurschner, W., J. vanderBurgh, H. Visscher, and D. Dilcher, 1996: Oak leaves as biosensors of late Neogene and early Pleistocene paleoatmospheric CO2 concentrations. *Marine Micropaleontology***,** 299-312.
Kuttel, M., et al., 2010: The importance of ship log data: reconstructing North Atlantic, European and Mediterranean sea level pressure fields back to 1750. *Climate Dynamics*, **34,** 1115-1128.
Kutzbach, J. E., X. D. Liu, Z. Y. Liu, and G. S. Chen, 2008: Simulation of the evolutionary response of global summer monsoons to orbital forcing over the past 280,000 years. *Climate Dynamics*, **30,** 567-579.
Lamarque, J., et al., 2010: Historical (1850-2000) gridded anthropogenic and biomass burning emissions of reactive gases and aerosols: methodology and application. *Atmospheric Chemistry and Physics***,** 7017-7039.
Lambert, F., et al., 2008a: Dust-climate couplings over the past 800,000 years from the EPICA Dome C ice core. *Nature*, **452,** 616-619.
——, 2008b: Dust-climate couplings over the past 800,000 years from the EPICA Dome C ice core. *Nature*, **452,** 616-619.
Lamy, F., R. Kilian, H. W. Arz, J. P. Francois, J. Kaiser, M. Prange, and T. Steinke, 2010: Holocene changes in the position and intensity of the southern westerly wind belt. *Nature Geoscience*, **3,** 695-699.
Landais, A., E. Barkan, and B. Luz, 2008: The record of $d^{18}O$ and ^{17}O-excess in ice from Vostok, Antarctica, during the last 150 000 years. *Geophys. Res. Lett.*, **19,** L02709.
Landais, A., et al., 2006: The glacial inception as recorded in the NorthGRIP Greenland ice core: timing, structure and associated abrupt temperature changes. *Climate Dynamics***,** 273-284.
——, 2010: What drives the millennial and orbital variations of delta O-18(atm)? *Quaternary Science Reviews*, **29,** 235-246.
Laskar, J., P. Robutel, F. Joutel, M. Gastineau, A. C. M. Correia, and B. Levrard, 2004: A long-term numerical solution for the insolation quantities of the Earth. *Astron. Astrophys.*, **428,** 261-285.
Lean, J., T. Woods, F. Eparvier, R. Meier, D. Strickland, J. Correira, and J. Evans, 2011: Solar extreme ultraviolet irradiance: Present, past, and future. *Journal of Geophysical Research-Space Physics***,** -.
Lean, J. L., O. R. White, and A. Skumanich, 1995: On the Solar Ultraviolet Spectral Irradiance During the Maunder Minimum. *Global Biogeochemical Cycles*, **9,** 171-182.
Lear, C., T. Bailey, P. Pearson, H. Coxall, and Y. Rosenthal, 2008: Cooling and ice growth across the Eocene-Oligocene transition. *Geology***,** 251-254.
Leduc, G., L. Vidal, K. Tachikawa, and E. Bard, 2009: ITCZ rather than ENSO signature for abrupt climate changes across the tropical Pacific? *Quaternary Research*, **72,** 123-131.
Lee, T., F. Zwiers, and M. Tsao, 2008: Evaluation of proxy-based millennial reconstruction methods. *Climate Dynamics*, **31**.
LeGrande, A., and G. Schmidt, 2008: Ensemble, water isotope-enabled, coupled general circulation modeling insights into the 8.2 ka event. *Paleoceanography***,** -.
LeGrande, A. N., and G. A. Schmidt, 2009: Sources of Holocene variability of oxygen isotopes in paleoclimate archives. *Climate of the Past*, **5,** 441-455.
Lemoine, D. M., 2010: Paleoclimatic warming increased carbon dioxide concentrations. *Journal of Geophysical Research-Atmospheres*, **115**.
Lezine, A. M., 2009: Timing of vegetation changes at the end of the Holocene Humid Period in desert areas at the northern edge of the Atlantic and Indian monsoon systems. *Comptes Rendus Geoscience*, **341,** 750-759.
Lhomme, N., G. Clarke, and S. Marshall, 2005: Tracer transport in the Greenland Ice Sheet: constraints on ice cores and glacial history. *Quaternary Science Reviews***,** 173-194.
Li, C., and D. S. Battisti, 2008: Reduced Atlantic storminess during last glacial maximum: Evidence from a coupled climate model. *Journal of Climate*, **21,** 3561-3579.
Li, C., D. S. Battisti, and C. M. Bitz, 2010: Can North Atlantic Sea Ice Anomalies Account for Dansgaard-Oeschger Climate Signals? *Journal of Climate*, **23,** 5457-5475.
Li, Y.-X., H. Renssen, A. P. Wiersma, and T. E. Törnqvist, 2009: Investigating the impact of Lake Agassiz drainage routes on the 8.2 ka cold event with a climate model. *Climate of the Past*, **5,** 471-480.
Lindholm, M., R. Jalkanen, H. Salminen, T. Aalto, and M. Ogurtsov, 2010: The height-increment record of summer temperature extended over the last Millennium in Fennoscandia. *The Holocene*, **xx,** xx-xx.
Linsley, B. K., Y. Rosenthal, and D. W. Oppo, 2010: Holocene evolution of the Indonesian throughflow and the western Pacific warm pool. *Nature Geoscience*, **3,** 578-583.
Lisiecki, L., 2010: Links between eccentricity forcing and the 100,000-year glacial cycle. *Nature Geoscience***,** 349-352.

Lisiecki, L., and M. Raymo, 2007: Plio-Pleistocene climate evolution: trends and transitions in glacial cycle dynamics. *Quaternary Science Reviews***,** 56-69.
Lisiecki, L. E., M. E. Raymo, and W. B. Curry, 2008: Atlantic overturning responses to Late Pleistocene climate forcings. *Nature*, **456,** 85-88.
Litt, T., C. Scholzel, N. Kuhl, and A. Brauer, 2009: Vegetation and climate history in the Westeifel Volcanic Field (Germany) during the past 11 000 years based on annually laminated lacustrine maar sediments. *Boreas*, **38,** 679-690.
Liu, J., H. Storch, C. Xing, E. Zorita, J. Zheng, and W. Sumin, 2005: Simulated and reconstructed winter temperature in the eastern China during the last millennium. *Chinese Science Bulletin***,** 2872-2877.
Liu, Z., et al., 2009a: Global Cooling During the Eocene-Oligocene Climate Transition. *Science***,** 1187-1190.
——, 2007: Simulating the transient evolution and abrupt change of Northern Africa atmosphere-ocean-terrestrial ecosystem in the Holocene. *Quaternary Science Reviews*, **26,** 1818-1837.
——, 2009b: Transient Simulation of Last Deglaciation with a New Mechanism for Bolling-Allerod Warming. *Science*, **325,** 310-314.
Liu, Z. Y., J. Kutzbach, and L. X. Wu, 2000: Modeling climate shift of El Nino variability in the Holocene. *Geophysical Research Letters*, **27,** 2265-2268.
Ljungqvist, F. C., 2010: A new reconstruction of temperature variability in the extra-tropical Northern Hemisphere during the last two millennia. *Geografiska Annaler: Series A, Physical Geography*, **92**.
Loulergue, L., et al., 2008: Orbital and millennial-scale features of atmospheric CH4 over the past 800,000 years. *Nature*, **453,** 383-386.
Lourantou, A., J. Chappellaz, J. M. Barnola, V. Masson-Delmotte, and D. Raynaud, 2010a: Changes in atmospheric CO_2 and its carbon isotopic composition during the penultimate deglaciation. *Quarternary Science Reviews*, **29,** 1983-1992.
Lourantou, A., et al., 2010b: Constraint of the CO2 rise by new atmospheric carbon isotopic measurements during the last deglaciation. *Global Biogeochemical Cycles*, **24**.
Louys, J., 2007: Limited effect of the Quaternary's largest super-eruption (Toba) on land mammals from Southeast Asia. *Quaternary Science Reviews***,** 3108-3117.
Lozhkin, A. V., P. M. Anderson, T. V. Matrosova, P. S. Minyuk, J. Brigham-Grette, and M. Melles, 2007: Continuous Record of Environmental Changes in Chukotka during the Last 350 Thousand Years. *Russian Journal of Pacific Geology*, **1,** 550-555.
Lu, J. M., S. J. Kim, A. Abe-Ouchi, Y. Q. Yu, and R. Ohgaito, 2010: Arctic Oscillation during the Mid-Holocene and Last Glacial Maximum from PMIP2 Coupled Model Simulations. *Journal of Climate*, **23,** 3792-3813.
Lunt, D. J., G. L. Foster, A. M. Haywood, and E. J. Stone, 2008: Late Pliocene Greenland glaciation controlled by a decline in atmospheric CO2 levels. *Nature*, **454,** 1102-U1141.
Luterbacher, J., R. Neukom, J. González-Rouco, L. Fernández-Donado, C. Raible, and E. Zorita, 2011: Reconstructed and simulated Medieval Climate Anbomaly in southern South Ameriabout *PAGES Newsletters*, **xx,** xx-xx.
Luterbacher, J., et al., 2002: Reconstruction of sea level pressure fields over the Eastern North Atlantic and Europe back to 1500. *Climate Dynamics*, **18,** 545-561.
Luthi, D., et al., 2008: High-resolution carbon dioxide concentration record 650,000-800,000 years before present. *Nature***,** 379-382.
MacDonald, G., D. Porinchu, N. Rolland, K. Kremenetsky, and D. Kaufman, 2009: Paleolimnological evidence of the response of the central Canadian treeline zone to radiative forcing and hemispheric patterns of temperature change over the past 2000 years. *Journal of Paleolimnology*, **41,** 129-141.
Maher, B., J. Prospero, D. Mackie, D. Gaiero, P. Hesse, and Y. Balkanski, 2010a: Global connections between aeolian dust, climate and ocean biogeochemistry at the present day and at the last glacial maximum. *Earth-Science Reviews***,** 61-97.
Maher, B. A., J. M. Prospero, D. Mackie, D. Gaiero, P. P. Hesse, and Y. Balkanski, 2010b: Global connections between aeolian dust, climate and ocean biogeochemistry at the present day and at the last glacial maximum. *Earth-Sci. Rev.*, **99,** 61-97.
Mahowald, N., M. Yoshioka, W. D. Collins, A. J. Conley, D. W. Fillmore, and D. B. Coleman, submitted: Climate response and radiative forcing from mineral aerosols during the last glacial maximum, pre-industrial, current and doubled-carbon dioxide climates. *Geophys. Res. Lett.*
Mahowald, N. M., M. Yoshioka, W. D. Collins, A. J. Conley, D. W. Fillmore, and D. B. Coleman, 2006: Climate response and radiative forcing from mineral aerosols during the last glacial maximum, pre-industrial, current and doubled-carbon dioxide climates. *Geophysical Research Letters*, **33**.
Mann, M., et al., 2009a: Global Signatures and Dynamical Origins of the Little Ice Age and Medieval Climate Anomaly. *Science***,** 1256-1260.
Mann, M. E., 2002: Large-scale climate variability and connections with the Middle East in past centuries. *Climatic Change*, **55,** 287-314.
——, 2007: Climate over the past two millennia. *Annual Review of Earth and Planetary Sciences*, **35,** 111-136.
Mann, M. E., R. S. Bradley, and M. K. Hughes, 1998: Global-scale temperature patterns and climate forcing over the past six centuries. *Nature*, **392**.

Mann, M. E., S. Rutherford, E. Wahl, and C. Ammann, 2005: Testing the fidelity of methods used in proxy-based reconstructions of past climate. *J. Climate*, **18,** 4097-4107.
——, 2007: Robustness of proxy-based climate field reconstruction methods. *Journal of Geophysical Research*, **112,** D12109.
Mann, M. E., Z. H. Zhang, M. K. Hughes, R. S. Bradley, S. K. Miller, S. Rutherford, and F. B. Ni, 2008: Proxy-based reconstructions of hemispheric and global surface temperature variations over the past two millennia. *Proceedings of the National Academy of Sciences of the United States of America*, **105,** 13252-13257.
Mann, M. E., et al., 2009b: Global Signatures and Dynamical Origins of the Little Ice Age and Medieval Climate Anomaly. *Science*, **326,** 1256-1260.
Marino, F., et al., 2009: Coherent composition of glacial dust on opposite sides of the Earth Antarctic Plateau inferred from the deep EPICA ice cores. *Geophys. Res. Lett.*, **36**.
Marlon, J. R., et al., 2009: Wildfire responses to abrupt climate change in North Ameriabout *Proceedings of the National Academy of Sciences of the United States of America*, **106,** 2519-2524.
Marshall, G. J., 2003: Trends in the southern annular mode from observations and reanalyses. *J. Climate*, **16,** 4134-4143.
Marshall, S. J., and M. R. Koutnik, 2006: Ice sheet action versus reaction: distinguishing between Heinrich events and Dansgaard-Oeschger cycles in the North Atlantic. *Paleoceanography*, **21**.
Martinez-Garcia, A., A. Rosell-Mele, E. L. McClymont, R. Gersonde, and G. H. Haug, 2010: Subpolar Link to the Emergence of the Modern Equatorial Pacific Cold Tongue. *Science*, **328,** 1550-1553.
Martrat, B., J. O. Grimalt, N. J. Shackleton, L. de Abreu, M. A. Hutterli, and T. F. Stocker, 2007: Four climate cycles of recurring deep and surface water destabilizations on the Iberian margin. *Science*, **317,** 502-507.
Maslin, M., et al., 2000: Palaeoreconstruction of the Amazon River freshwater and sediment discharge using sediments recovered at Site 942 on the Amazon Fan. *Journal of Quaternary Science***,** 419-434.
Mason, B., D. Pyle, and C. Oppenheimer, 2004: The size and frequency of the largest explosive eruptions on Earth. *Bulletin of Volcanology***,** 735-748.
Masson-Delmotte, V., et al., 2010a: EPICA Dome C record of glacial and interglacial intensities. *Quaternary Science Reviews*, **29,** 113-128.
——, 2010b: Abrupt change of Antarctic moisture origin at the end of Termination II. *Proceedings of the National Academy of Sciences of the United States of America*, **107,** 12091-12094.
——, 2008: A review of Antarctic surface snow isotopic composition: Observations, atmospheric circulation, and isotopic modeling. *Journal of Climate*, **21,** 3359-3387.
McConnell, J., and R. Edwards, 2008: Coal burning leaves toxic heavy metal legacy in the Arctic. *Proceedings of the National Academy of Sciences of the United States of America*, **105,** 12140-12144.
McConnell, J., et al., 2007: 20th-century industrial black carbon emissions altered arctic climate forcing. *Science*, **317,** 1381-1384.
MCELWAIN, J., and W. CHALONER, 1995: STOMATAL DENSITY AND INDEX OF FOSSIL PLANTS TRACK ATMOSPHERIC CARBON-DIOXIDE IN THE PALEOZOIC. *Annals of Botany***,** 389-395.
McGee, D., W. S. Broecker, and G. Winckler, 2010: Gustiness: The driver of glacial dustiness? *Quaternary Science Reviews*, **29,** 2340-2350.
McGregor, S., A. Timmermann, and O. Timm, 2010: A unified proxy for ENSO and PDO variability since 1650. *Climate of the Past*, **6,** 1-17.
McManus, J., D. Oppo, J. Cullen, and S. Healey, 2003: Marine Isotope Stage 11 (MIS 11): analog for Holocene and future climate. *Earth's Climate and Orbital Eccentricity: The Marine Isotope Stage 11*, A. Droxler, R. Z. Poore, and L. H. Burkle, Eds., American Geophysical Union, 69-85.
McManus, J. F., D. W. Oppo, and J. L. Cullen, 1999: A 0.5-million-year record of millennial-scale climate variability in the North Atlantic. *Science*, **283,** 971-975.
McManus, J. F., R. Francois, J.-M. Gherardi, L. D. Kelgwin, and S. Brown-Leger, 2004: Collapse and rapid resumption of Atlantic meridional circulation linked to deglacial climate changes. *Nature*, **428,** 834-837.
McShane, B. B., and A. J. Wyner, 2010: A statistical analysis of multiple temperature proxies: are reconstructions of surface temperatures over the last 1000 years reliable? *Annals of Applied Statistics*.
Menviel, L., A. Timmermann, A. Mouchet, and O. Timm, 2008: Meridional reorganizations of marine and terrestrial productivity during Heinrich events. *Paleoceanography*, **23**.
Menviel, L., A. Timmermann, O. Elison Timm, and A. Mouchet, 2011: Deconstruting the Last Glacial Termination: the role of millennial and orbital-scale forcings. *Quaternary Science Reviews***,** Accepted.
Merkel, U., M. Prange, and M. Schulz, 2010: ENSO variability and teleconnections during glacial climates. *Quaternary Science Reviews*, **29,** 86-100.
Meure, C., et al., 2006: Law Dome CO2, CH4 and N2O ice core records extended to 2000 years BP. *Geophysical Research Letters*, **10,** L14810.
Mignot, J., A. Ganopolski, and A. Levermann, 2007: Atlantic subsurface temperatures: Response to a shutdown of the overturning circulation and consequences for its recovery. *Journal of Climate***,** 4884-4898.
Ming, J., H. Cachier, C. Xiao, D. Qin, S. Kang, S. Hou, and J. Xu, 2008: Black carbon record based on a shallow Himalayan ice core and its climatic implications. *Atmospheric Chemistry and Physics*, **8,** 1343-1352.

Mischler, J. A., et al., 2009: Carbon and hydrogen isotopic composition of methane over the last 1000 years. *Global Biogeochemical Cycles*, **23**.
Moernaut, J., D. Verschuren, F. Charlet, I. Kristen, M. Fagot, and M. De Batist, 2010: The seismic-stratigraphic record of lake-level fluctuations in Lake Challa: Hydrological stability and change in equatorial East Africa over the last 140 kyr. *Earth and Planetary Science Letters*, **290,** 214-223.
Moreno, P., J. Francois, R. Villa-Martínez, and C. Moy, 2009: Millennial-scale variability in Southern Hemisphere westerly wind activity over the last 5000 years in SW Patagonia. *Quaternary Science Reviews*, **28,** 25-38.
Mueller, A., et al., 2010: Recovery of the forest ecosystem in the tropical lowlands of northern Guatemala after disintegration of Classic Maya polities. *Geology***,** 523-526.
Muhs, D., T. Ager, and J. Beget, 2001: Vegetation and paleoclimate of the last interglacial period, central Alaska. *Quaternary Science Reviews***,** 41-61.
Mulitza, S., et al., 2008: Sahel megadroughts triggered by glacial slowdowns of Atlantic meridional overturning. *Paleoceanography*, **23**.
——, 2010: Increase in African dust flux at the onset of commercial agriculture in the Sahel region. *Nature***,** 226-228.
Murton, J. B., M. D. Bateman, S. R. Dallimore, J. T. Teller, and Z. R. Yang, 2010: Identification of Younger Dryas outburst flood path from Lake Agassiz to the Arctic Ocean. *Nature*, **464,** 740-743.
Muscheler, R., F. Joos, J. Beer, S. A. Muller, M. Vonmoos, and I. Snowball, 2007: Solar activity during the last 1000 yr inferred from radionuclide records. *Quaternary Science Reviews*, **26,** 82-97.
Naish, T., G. Wilson, G. Dunbar, and P. Barrett, 2008: Constraining the amplitude of Late Oligocene bathymetric changes in western Ross Sea during orbitally-induced oscillations in the East Antarctic Ice Sheet: (2) Implications for global sea level changes. *Palaeogeography Palaeoclimatology Palaeoecology***,** 66-76.
Naish, T., et al., 2009: Obliquity-paced Pliocene West Antarctic ice sheet oscillations. *Nature*, **458,** 322-U384.
Nakagawa, T., et al., 2008: Regulation of the monsoon climate by two different orbital rhythms and forcing mechanisms. *Geology*, **36,** 491-494.
Nakamura, N., H. Kayanne, H. Iijima, T. R. McClanahan, S. K. Behera, and T. Yamagata, 2009: Mode shift in the Indian Ocean climate under global warming stress. *Geophysical Research Letters*, **36**.
Neukom, R., et al., 2010: Multiproxy summer and winter surface air temperature field reconstructions for southern South America covering the past centuries. *Climate Dynamics***,** 1-17.
Nicolussi, K., M. Kaufmann, T. Melvin, J. van der Plicht, P. Schiessling, and A. Thurner, 2009: A 9111 year long conifer tree-ring chronology for the European Alps: a base for environmental and climatic investigations. *Holocene***,** 909-920.
Niedermeyer, E. M., E. Schefuss, A. L. Sessions, S. Mulitza, G. Mollenhauer, M. Schulz, and G. Wefer, 2010: Orbital- and millennial-scale changes in the hydrologic cycle and vegetation in the western African Sahel: insights from individual plant wax delta D and delta C-13. *Quaternary Science Reviews*, **29,** 2996-3005.
Nitychoruk, J., K. Binka, J. Hoefs, H. Ruppert, and J. Schneider, 2005: Climate reconstruction for the Holsteinian Interglacial in eastern Poland and its comparison with isotopic data from Marine Isotope Stage 11. *Quaternary Science Reviews*, **24,** 631-644.
NorthGRIP-community-members, 2004: High resolution climate record of the northern hemisphere reaching into last interglacial period. *Nature*, **431,** 147-151.
O'Donnell, R., N. Lewis, S. McIntyre, and J. Condon: Improved methods for PCA-based reconstructions: case study using the Steig et al. 2009 Antarctic temperature reconstruction. *Journal of Climate*, **0,** null.
Okazaki, Y., et al., 2010: Deepwater Formation in the North Pacific During the Last Glacial Termination. *Science*, **329,** 200-204.
Okumura, Y. M., C. Deser, A. Hu, A. Timmermann, and S. P. Xie, 2009: North Pacific Climate Response to Freshwater Forcing in the Subarctic North Atlantic: Oceanic and Atmospheric Pathways. *Journal of Climate*, **22,** 1424-1445.
Olofsson, J., and T. Hickler, 2008: Effects of human land-use on the global carbon cycle during the last 6,000 years. *Vegetation History and Archaeobotany*, **17,** 605-615.
Ono, A., K. Takahashi, K. Katsuki, Y. Okazaki, and T. Sakamoto, 2005: The Dansgaard-Oeschger cycles discovered in the up stream source region of the North Pacific Intermediate Water formation. *Geophysical Research Letters*, **32**.
Oppenheimer, C., 2002: Limited global change due to the largest known Quaternary eruption, Toba approximate to 74 kyr BP? *Quaternary Science Reviews***,** 1593-1609.
Oppo, D. W., Y. Rosenthal, and B. K. Linsley, 2009: 2,000-year-long temperature and hydrology reconstructions from the Indo-Pacific warm pool. *Nature*, **460,** 1113-1116.
Orland, I. J., M. Bar-Matthews, N. T. Kita, A. Ayalon, A. Matthews, and J. W. Valley, 2009: Climate deterioration in the Eastern Mediterranean as revealed by ion microprobe analysis of a speleothem that grew from 2.2 to 0.9 ka in Soreq Cave, Israel. *Quaternary Research*, **71,** 27-35.
Osborn, T., and K. Briffa, 2007: Response to comment on "The spatial extent of 20th-century warmth in the context of the past 1200 years". *Science***,** -.
Ottera, O. H., M. Bentsen, H. Drange, and L. L. Suo, 2010: External forcing as a metronome for Atlantic multidecadal variability. *Nature Geoscience*, **3,** 688-694.
Otto-Bliesner, B. e. a., 2009: A comparison of PMIP2 model simulations and the MARGO proxy reconstruction for tropical sea surface temperatures at the last glacial maximum. *Climate Dynamics*, **32,** 799-815.

Otto-Bliesner, B. L., and E. C. Brady, 2010: The sensitivity of the climate response to the magnitude and location of freshwater forcing: last glacial maximum experiments. *Quaternary Science Reviews*, **29,** 56-73.
Otto-Bliesner, B. L., E. C. Brady, S. I. Shin, Z. Y. Liu, and C. Shields, 2003: Modeling El Nino and its tropical teleconnections during the last glacial-interglacial cycle. *Geophysical Research Letters*, **30**.
Otto-Bliesner, B. L., et al., 2009: A comparison of PMIP2 model simulations and the MARGO proxy reconstruction for tropical sea surface temperatures at last glacial maximum. *Climate Dynamics*, **32,** 799-815.
Pagani, M., 2005: Controls on paleo-alkenone delta C-13. *Geochimica Et Cosmochimica Acta***,** A545-A545.
Pagani, M., Z. Liu, J. LaRiviere, and A. C. Ravelo, 2010a: High Earth-system climate sensitivity determined from Pliocene carbon dioxide concentrations. *Nature Geoscience*, **3,** 27-30.
Pagani, M., Z. Liu, J. LaRiviere, and A. Ravelo, 2010b: High Earth-system climate sensitivity determined from Pliocene carbon dioxide concentrations. *Nature Geoscience***,** 27-30.
Pagani, M., J. Zachos, K. Freeman, B. Tipple, and S. Bohaty, 2005: Marked decline in atmospheric carbon dioxide concentrations during the Paleogene. *Science***,** 600-603.
Pahnke, K., R. Zahn, H. Elderfield, and M. Schulz, 2003: 340,000-year centennial-scale marine record of Southern Hemisphere climatic oscillation. *Science*, **301,** 948-952.
Pausata, F. S. R., C. Li, J. J. Wettstein, K. H. Nisancioglu, and D. S. Battisti, 2009: Changes in atmospheric variability in a glacial climate and the impacts on proxy data: a model intercomparison. *Climate of the Past*, **5,** 489-502.
Pearson, P., and M. Palmer, 2000: Atmospheric carbon dioxide concentrations over the past 60 million years. *Nature***,** 695-699.
Pearson, P., B. van Dongen, C. Nicholas, R. Pancost, S. Schouten, J. Singano, and B. Wade, 2007: Stable warm tropical climate through the Eocene Epoch. *Geology***,** 211-214.
Pearson, P., I. McMillan, B. Wade, T. Dunkley Jones, H. Coxall, P. Bown, and C. Lear, 2008: Extinction and environmental change across the Eocene-Oligocene boundary in Tanzania. *Geology***,** 179-182.
Pearson, P., et al., 2001: Warm tropical sea surface temperatures in the Late Cretaceous and Eocene epochs. *Nature***,** 481-487.
Pearson, P. N., G. L. Foster, and B. S. Wade, 2009: Atmospheric carbon dioxide through the Eocene-Oligocene climate transition. *Nature*, **461,** 1110-U1204.
Pechony, O., and D. Shindell, 2010: Driving forces of global wildfires over the past millennium and the forthcoming century. *Proceedings of the National Academy of Sciences of the United States of America***,** 19167-19170.
Peng, Y., Y. Xu, and L. Jin, 2009: Climate changes over eastern China during the last millennium in simulations and reconstructions. *Quaternary International*, **208,** 11-18.
Peterson, L. C., and G. H. Haug, 2006: Variability in the mean latitude of the Atlantic Intertropical Convergence Zone as recorded by riverine input of sediments to the Cariaco Basin (Venezuela). *Palaeogeography Palaeoclimatology Palaeoecology*, **234,** 97-113.
Peterson, L. C., G. H. Haug, K. A. Hughen, and U. Rohl, 2000: Rapid changes in the hydrologic cycle of the tropical Atlantic during the last glacial. *Science*, **290,** 1947-1951.
Petit, J. R., and B. Delmonte, 2009: A model for large glacial–interglacial climate-induced changes in dust and sea salt concentrations in deep ice cores (central Antarctica): palaeoclimatic implications and prospects for refining ice core chronologies. *Tellus*, **61B,** 768-790.
Petraglia, M., et al., 2007: Middle paleolithic assemblages from the Indian subcontinent before and after the Toba super-eruption. *Science***,** 114-116.
Petrenko, V. V., et al., 2009: (CH4)-C-14 Measurements in Greenland Ice: Investigating Last Glacial Termination CH4 Sources. *Science*, **324,** 506-508.
Pfeiffer, M., and W. C. Dullo, 2006: Monsoon-induced cooling of the western equatorial Indian Ocean as recorded in coral oxygen isotope records from the Seychelles covering the period of 1840-1994 AD. *Quaternary Science Reviews*, **25,** 993-1009.
Piotrowski, A. M., S. L. Goldstein, S. R. Hemming, R. G. Fairbanks, and D. R. Zylberberg, 2008: Oscillating glacial northern and southern deep water formation from combined neodymium and carbon isotopes. *Earth and Planetary Science Letters*, **272,** 394-405.
Pivel, M., and F. Toledo, 2010: FORAMINIFERAL RECORD OF CHANGES IN SUMMER MONSOON PRECIPITATION AT THE SOUTHEASTERN BRAZILIAN CONTINENTAL MARGIN SINCE THE LAST GLACIAL MAXIMUM. *REVISTA BRASILEIRA DE PALEONTOLOGIA*, **13,** 79-88.
Pollard, D., and R. M. DeConto, 2009: Modelling West Antarctic ice sheet growth and collapse through the past five million years. *Nature*, **458,** 329-332.
Polyakov, I. V., et al., 2010: Arctic Ocean Warming Contributes to Reduced Polar Ice Cap. *Journal of Physical Oceanography*, **40,** 2743-2756.
Pongratz, J., C. Reick, T. Raddatz, and M. Claussen, 2008: A reconstruction of global agricultural areas and land cover for the last millennium. *Global Biogeochemical Cycles*, **22,** GB3018.
——, 2010: Biogeophysical versus biogeochemical climate response to historical anthropogenic land cover change. *Geophysical Research Letters*, **37,** L08072.
Pongratz, J., T. Raddatz, C. Reick, M. Esch, and M. Claussen, 2009: Radiative forcing from anthropogenic land cover change since AD 800. *Geophysical Research Letters*, **36,** L02709.

Popa, I., and Z. Kern, 2009: Long-term summer temperature reconstruction inferred from tree-ring records from the Eastern Carpathians. *Climate Dynamics*, **32,** 1107-1117.
Power, M., J. Marlon, P. Bartlein, and S. Harrison, 2010: Fire history and the Global Charcoal Database: A new tool for hypothesis testing and data exploration. *Palaeogeography Palaeoclimatology Palaeoecology***,** 52-59.
Power, M., et al., 2008: Changes in fire regimes since the Last Glacial Maximum: an assessment based on a global synthesis and analysis of charcoal data. *Climate Dynamics*, **30,** 887-907.
Prieto, M., and R. Herrera, 2009: Documentary sources from South America: Potential for climate reconstruction. *Palaeogeography Palaeoclimatology Palaeoecology***,** 196-209.
Prokopenko, A., L. Hinnov, D. Williams, and M. Kuzmin, 2006: Orbital forcing of continental climate during the Pleistocene: a complete astronomically tuned climatic record from Lake Baikal, SE Siberia. *Quaternary Science Reviews***,** 3431-3457.
Prokopenko, A. A., E. V. Bezrukova, G. K. Khursevich, E. P. Solotchina, M. I. Kuzmin, and P. E. Tarasov, 2010: Climate in continental interior Asia during the longest interglacial of the past 500 000 years: the new MIS 11 records from Lake Baikal, SE Siberia. *Climate of the Past*, **6,** 31-48.
Ravelo, A., 2010: PALAEOCLIMATE Warmth and glaciation. *Nature Geoscience***,** 672-674.
Raymo, M., L. Lisiecki, and K. Nisancioglu, 2006: Plio-pleistocene ice volume, Antarctic climate, and the global delta O-18 record. *Science***,** 492-495.
Raymo, M. E., and M. Horowitz, 1996: Organic carbon paleo-pCO_2 and marine-ice core correlations and chronology. *Geophys. Res. Lett.*, **23,** 367-370.
Raynaud, D., and C. Lorius, 2004: Atmospheric properties of past climatic changes are recorded in the polar ice. *Comptes Rendus Geoscience***,** 647-656.
Reille, M., J. L. De Beaulieu, H. Svobodova, V. Andrieu-Ponel, and C. Goeury, 2000: Pollen analytical biostratigraphy of the last five climatic cycles from a long continental sequence from the Velay region (Massif Central, France). *Journal of Quaternary Science*, **15,** 665-685.
Renold, M., C. C. Raible, M. Yoshimori, and T. F. Stocker, 2010: Simulated resumption of the North Atlantic meridional overturning circulation - Slow basin-wide advection and abrupt local convection. *Quaternary Science Reviews*, **29,** 101-112.
Renssen, H., H. Seppa, O. Heiri, D. M. Roche, H. Goosse, and T. Fichefet, 2009: The spatial and temporal complexity of the Holocene thermal maximum. *Nature Geoscience*, **2,** 410-413.
Ridley, J., J. Gregory, P. Huybrechts, and J. Lowe, 2010: Thresholds for irreversible decline of the Greenland ice sheet. *Climate Dynamics***,** 1065-1073.
Rimbu, N., G. Lohmann, J. Kim, H. Arz, and R. Schneider, 2003: Arctic/North Atlantic Oscillation signature in Holocene sea surface temperature trends as obtained from alkenone data. *Geophysical Research Letters***,** -.
Risebrobakken, B., E. Jansen, C. Andersson, E. Mjelde, and K. Hevroy, 2003: A high-resolution study of Holocene paleoclimatic and paleoceanographic changes in the Nordic Seas. *Paleoceanography***,** -.
Robinson, L. F., and T. van de Flierdt, 2009: Southern Ocean evidence for reduced export of North Atlantic Deep Water during Heinrich event 1. *Geology*, **37,** 195-198.
Robock, A., C. Ammann, L. Oman, D. Shindell, S. Levis, and G. Stenchikov, 2009: Did the Toba volcanic eruption of similar to 74 ka BP produce widespread glaciation? *Journal of Geophysical Research-Atmospheres***,** -.
Rodrigo, F. S., D. Pozo-Vazquez, M. J. Esteban-Parra, and Y. Castro-Diez, 2001: A reconstruction of the winter North Atlantic Oscillation index back to AD 1501 using, documentary data in southern Spain. *Journal of Geophysical Research-Atmospheres*, **106,** 14805-14818.
Rohling, E. J., K. Grant, M. Bolshaw, A. P. Roberts, M. Siddall, C. Hemleben, and M. Kucera, 2009: Antarctic temperature and global sea level closely coupled over the past five glacial cycles. *Nature Geoscience*, **2,** 500-504.
Rohling, E. J., et al., 2008: New constraints on the timing of sea level fluctuations during early to middle marine isotope stage 3. *Paleoceanography*, **23**.
——, 2002: African monsoon variability during the previous interglacial maximum. *Earth and Planetary Science Letters*, **202,** 61-75.
Rojas, M., et al., 2009: The Southern Westerlies during the last glacial maximum in PMIP2 simulations. *Climate Dynamics***,** 525-548.
Rosqvist, G. C., M. J. Leng, and C. Jonsson, 2007: North Atlantic region atmospheric circulation dynamics inferred from a late-Holocene lacustrine carbonate isotope record, northern Swedish Lapland. *Holocene*, **17,** 867-873.
Rostami, K., W. Peltier, and A. Mangini, 2000: Quaternary marine terraces, sea level changes and uplift history of Patagonia, Argentina: comparisons with predictions of the ICE-4G (VM2) model of the global process of glacial isostatic adjustment. *Quaternary Science Reviews***,** 1495-1525.
Röthlisberger, R., et al., 2008: The southern hemisphere at glacial terminations: insights from the Dome C ice core. *Climate of the Past*, **4,** 345-356.
Rousseau, D.-D., C. Hatte, D. Duzer, P. Schevin, G. Kukla, and J. Guiot, 2007: Estimates of temperature and precipitation variations during the Eemian Interglacial: New data from the Grande Pile Record (GP XXI). *Climate of past interglacials*, f. i. d. f. B. r. b. <button aria-disabled="false" aria-labelledby="dijit_form_Button_2_label" class="dijitReset dijitStretch dijitButtonContents" dojoattachpoint="titleNode, et al., Eds., Elsevier.

Royer, D., 2006: CO2-forced climate thresholds during the Phanerozoic. *Geochimica Et Cosmochimica Acta*, 5665-5675.

Ruddiman, W., 2007: The early anthropogenic hypothesis: Challenges and responses. *Reviews of Geophysics*, -.

Ruddiman, W., and E. Ellis, 2009: Effect of per-capita land use changes on Holocene forest clearance and CO2 emissions. *Quaternary Science Reviews*, 3011-3015.

Rutherford, S. D., M. E. Mann, C. M. Ammann, and E. R. Wahl, 2010: Comments on "A Surrogate Ensemble Study of Climate Reconstruction Methods: Stochasticity and Robustness". *Journal of Climate*, **23,** 2832-2838.

Sachs, J. P., D. Sachse, R. H. Smittenberg, Z. H. Zhang, D. S. Battisti, and S. Golubic, 2009: Southward movement of the Pacific intertropical convergence zone AD 1400-1850. *Nature Geoscience*, **2,** 519-525.

Saenko, O. A., A. Schmittner, and A. J. Weaver, 2004: The Atlantic-Pacific seesaw. *Journal of Climate*, **17,** 2033-2038.

Saji, N. H., B. N. Goswami, P. N. Vinayachandran, and T. Yamagata, 1999: A dipole mode in the tropical Indian Ocean. *Nature*, **401,** 360-363.

Salzer, M., and K. Kipfmueller, 2005: Reconstructed temperature and precipitation on a millennial timescale from tree-rings in the Southern Colorado Plateau, USA. *Climatic Change*, **70,** 465-487.

Sarnthein, M., U. Pflaumann, and M. Weinelt, 2003a: Past extent of sea ice in the northern North Atlantic inferred from foraminiferal paleotemperature estimates. *Paleoceanography*, -.

Sarnthein, M., S. Van Kreveld, H. Erlenkeuser, P. Grootes, M. Kucera, U. Pflaumann, and M. Schulz, 2003b: Centennial-to-millennial-scale periodicities of Holocene climate and sediment injections off the western Barents shelf, 75 degrees N. *Boreas*, 447-461.

Scherer, D., M. Gude, M. Gempeler, and E. Parlow, 1998: Atmospheric and hydrological boundary conditions for slushflow initiation due to snowmelt. *Annals of Glaciology, Vol 26, 1998*, 377-380.

Schilt, A., M. Baumgartner, T. Blunier, J. Schwander, R. Spahni, H. Fischer, and T. Stocker, 2010: Glacial-interglacial and millennial-scale variations in the atmospheric nitrous oxide concentration during the last 800,000 years. *Quaternary Science Reviews*, 182-192.

Schmidt, G. A., et al., 2011: Climate forcing reconstructions for use in PMIP simulations of the last millennium (v1.0). *Geosci. Model Dev.*, **4,** 33-45.

Schmittner, A., E. D. Galbraith, S. W. Hostetler, T. F. Pedersen, and R. Zhang, 2007: Large fluctuations of dissolved oxygen in the Indian and Pacific oceans during Dansgaard-Oeschger oscillations caused by variations of North Atlantic Deep Water subduction. *Paleoceanography*, **22**.

Schouten, S., E. Hopmans, E. Schefuss, and J. Damste, 2002: Distributional variations in marine crenarchaeotal membrane lipids: a new tool for reconstructing ancient sea water temperatures? *Earth and Planetary Science Letters*, 265-274.

Schouten, S., E. Hopmans, A. Forster, Y. van Breugel, M. Kuypers, and J. Damste, 2003: Extremely high sea-surface temperatures at low latitudes during the middle Cretaceous as revealed by archaeal membrane lipids. *Geology*, 1069-1072.

Schrag, D., 1999: Effects of diagenesis on the isotopic record of late paleogene tropical sea surface temperatures. *Chemical Geology*, 215-224.

SCHRAG, D., D. DEPAOLO, and F. RICHTER, 1995: RECONSTRUCTING PAST SEA-SURFACE TEMPERATURES - CORRECTING FOR DIAGENESIS OF BULK MARINE CARBONATE. *Geochimica Et Cosmochimica Acta*, 2265-2278.

Schulz, K., and R. Zeebe, 2006: Pleistocene glacial terminations triggered by synchronous changes in Southern and Northern Hemisphere insolation: The insolation canon hypothesis. *Earth and Planetary Science Letters*, 326-336.

Schurgers, G., U. Mikolajewicz, M. Groger, E. Maier-Reimer, M. Vizcaino, and A. Winguth, 2007: The effect of land surface changes on Eemian climate. *Climate Dynamics*, **29,** 357-373.

Screen, J. A., and I. Simmonds, 2010: The central role of diminishing sea ice in recent Arctic temperature amplification. *Nature*, **464,** 1334-1337.

Seager, R., N. Graham, C. Herweijer, A. Gordon, Y. Kushnir, and E. Cook, 2007: Blueprints for Medieval hydroclimate. *Quat. Sci. Rev.*, **26,** 2322-2336.

Seager, R., R. Burgman, Y. Kushnir, A. Clement, E. Cook, N. Naik, and J. Miller, 2008: Tropical Pacific Forcing of North American Medieval Megadroughts: Testing the Concept with an Atmosphere Model Forced by Coral-Reconstructed SSTs. *Journal of Climate*, **21,** 6175-6190.

Seki, O., G. Foster, D. Schmidt, A. Mackensen, K. Kawamura, and R. Pancost, 2010: Alkenone and boron-based Pliocene pCO(2) records. *Earth and Planetary Science Letters*, 201-211.

Selvaraj, K., C. Chen, J. Lou, and B. Kotlia, 2011: Holocene weak summer East Asian monsoon intervals in Taiwan and plausible mechanisms. *Quaternary International*, **229,** 57-66.

Semenov, V. A., M. Latif, D. Dommenget, N. S. Keenlyside, A. Strehz, T. Martin, and W. Park, 2010: The Impact of North Atlantic-Arctic Multidecadal Variability on Northern Hemisphere Surface Air Temperature. *Journal of Climate*, **23,** 5668-5677.

Sereno, P. C., et al., 2008: Lakeside Cemeteries in the Sahara: 5000 Years of Holocene Population and Environmental Change. *Plos One*, **3**.

Severinghaus, J. P., T. Sowers, E. J. Brook, R. B. Alley, and M. L. Bender, 1998: Timing of abrupt climate change at the end of the Younger Dryas interval from thermally fractionated gases in polar ice. *Nature*, **391,** 141-146.

Sexton, P., P. Wilson, and P. Pearson, 2006: Microstructural and geochemical perspectives on planktic foraminiferal preservation: "Glassy" versus "Frosty". *Geochemistry Geophysics Geosystems*, -.
Shanahan, T. M., et al., 2009: Atlantic Forcing of Persistent Drought in West Afriabout *Science*, **324,** 377-380.
Shapiro, A., W. Schmutz, E. Rozanov, M. Schoell, M. Haberreiter, A. Shapiro, and S. Nyeki, 2011: New reconstruction technique reveals large historical variability in solar radiative forcing. *Astronomy & Astrophysics*, **in press**.
Shevenell, A., A. Ingalls, E. Domack, and C. Kelly, 2011: Holocene Southern Ocean surface temperature variability west of the Antarctic Peninsula. *Nature***,** 250-254.
Sicre, M. A., et al., 2008: A 4500-year reconstruction of sea surface temperature variability at decadal time-scales off North Iceland. *Quaternary Science Reviews*, **27,** 2041-2047.
Siddall, M., E. Bard, E. J. Rohling, and C. Hemleben, 2006: Sea level reversal during termination II. *Geology*, **34,** 817-820.
Siddall, M., E. J. Rohling, W. G. Thompson, and C. Waelbroeck, 2008: MARINE ISOTOPE STAGE 3 SEA LEVEL FLUCTUATIONS: DATA SYNTHESIS AND NEW OUTLOOK. *Reviews of Geophysics*, **46**.
Siddall, M., E. J. Rohling, T. Blunier, and R. Spahni, 2010a: Patterns of millennial variability over the last 500 ka. *Climate of the Past*, **6,** 295-303.
Siddall, M., M. R. Kaplan, J. M. Schaefer, A. Putnam, M. A. Kelly, and B. Goehring, 2010b: Changing influence of Antarctic and Greenlandic temperature records on sea level over the last glacial cycle. *Quaternary Science Reviews*, **29,** 410-423.
Siegenthaler, U., et al., 2005: Supporting evidence from the EPICA Dronning Maud Land ice core for atmospheric CO2 changes during the past millennium. *Tellus Series B-Chemical and Physical Meteorology***,** 51-57.
Sime, L. C., E. W. Wolff, K. I. C. Oliver, and J. C. Tindall, 2009: Evidence for warmer interglacials in East Antarctic ice cores. *Nature*, **462,** 342-U105.
Sinha, A., et al., 2007: A 900-year (600 to 1500 A. D.) record of the Indian summer monsoon precipitation from the core monsoon zone of India. *Geophysical Research Letters*, **34,** -.
Sluijs, A., and H. Brinkhuis, 2009: A dynamic climate and ecosystem state during the Paleocene-Eocene Thermal Maximum: inferences from dinoflagellate cyst assemblages on the New Jersey Shelf. *Biogeosciences***,** 1755-1781.
Sluijs, A., U. Rohl, S. Schouten, H. Brumsack, F. Sangiorgi, J. Damste, and H. Brinkhuis, 2008: Arctic late Paleocene-early Eocene paleoenvironments with special emphasis on the Paleocene-Eocene thermal maximum (Lomonosov Ridge, Integrated Ocean Drilling Program Expedition 302). *Paleoceanography***,** -.
Sluijs, A., et al., 2007: Environmental precursors to rapid light carbon injection at the Palaeocene/Eocene boundary. *Nature***,** 1218-U1215.
——, 2006: Subtropical arctic ocean temperatures during the Palaeocene/Eocene thermal maximum. *Nature*, 610-613.
Smerdon, J. E., A. Kaplan, D. Chang, and M. N. Evans, 2010: A Pseudoproxy Evaluation of the CCA and RegEM Methods for Reconstructing Climate Fields of the Last Millennium. *Journal of Climate*, **23**.
Sowers, T., 2006: Late Quaternary atmospheric CH4 isotope record suggests marine clathrates are stable. *Science*, **311,** 838-840.
——, 2010: Atmospheric methane isotope records covering the Holocene period. *Quaternary Science Reviews***,** 213-221.
Spence, J., M. Eby, and A. Weaver, 2008: The sensitivity of the Atlantic meridional overturning circulation to freshwater forcing at eddy-permitting resolutions. *Journal of Climate***,** 2697-2710.
Spielhagen, R., et al., 2011a: Enhanced Modern Heat Transfer to the Arctic by Warm Atlantic Water. *Science***,** 450-453.
Spielhagen, R. F., et al., 2011b: Enhanced Modern Heat Transfer to the Arctic by Warm Atlantic Water. *Science*, **331,** 450-453.
St Amour, N. A., D. Hammarlund, T. W. D. Edwards, and B. B. Wolfe, 2010: New insights into Holocene atmospheric circulation dynamics in central Scandinavia inferred from oxygen-isotope records of lake-sediment cellulose. *Boreas*, **39,** 770-782.
Staubwasser, M., and H. Weiss, 2006: Holocene climate and cultural evolution in late prehistoric-early historic West Asia - Introduction. *Quaternary Research*, **66,** 372-387.
Steffensen, J. P., et al., 2008: High-resolution Greenland Ice Core data show abrupt climate change happens in few years. *Science*, **321,** 680-684.
Steig, E. J., D. P. Schneider, S. D. Rutherford, M. E. Mann, J. C. Comiso, and D. T. Shindell, 2009: Warming of the Antarctic ice-sheet surface since the 1957 International Geophysical Year. *Nature*, **457,** 459-U454.
Steinhilber, F., J. Beer, and C. Frohlich, 2009: Total solar irradiance during the Holocene. *Geophysical Research Letters***,** -.
Stenni, B., et al., 2011: Expression of the bipolar see-saw in Antarctic climate records during the last deglaciation. *Nature Geoscience*, **4,** 46-49.
Stocker, B., K. Strassmann, and F. Joos, 2011: Sensitivity of Holocene atmospheric CO2 and the modern carbon budget to early human land use: analyses with a process-based model. *Biogeosciences***,** 69-88.
Stocker, T., and S. Johnsen, 2003: A minimum thermodynamic model for the bipolar seesaw. *Paleoceanography*, **18,** 1087.
Stott, L., A. Timmermann, and R. Thunell, 2007: Southern hemisphere and deep-sea warming led deglacial atmospheric CO2 rise and tropical warming. *Science*, **318,** 435-438.
Stouffer, R. J., et al., 2006: Investigating the causes of the response of the thermohaline circulation to past and future climate changes. *Journal of Climate*, **19,** 1365-1387.

Suwa, M., J. von Fischer, M. Bender, A. Landais, and E. Brook, 2006: Chronology reconstruction for the disturbed bottom section of the GISP2 and the GRIP ice cores: Implications for Termination II in Greenland. *Journal of Geophysical Research-Atmospheres*, -.
Swingedouw, D., J. Mignot, P. Braconnot, E. Mosquet, M. Kageyama, and R. Alkama, 2009: Impact of Freshwater Release in the North Atlantic under Different Climate Conditions in an OAGCM. *Journal of Climate*, **22,** 6377-6403.
Swingedouw, D., L. Terray, C. Cassou, A. Voldoire, D. Salas-Mélia, and J. Servonnat, 2010: Natural forcing of climate during the last millennium: fingerprint of solar variability. *Climate Dynamics*, 1-16.
Tagliabue, A., et al., 2009: Quantifying the roles of ocean circulation and biogeochemistry in governing ocean carbon-13 and atmospheric carbon dioxide at the last glacial maximum. *Climate of the Past*, 695-706.
Takemura, T., M. Egashira, K. Matsuzawa, H. Ichijo, R. O'ishi, and A. Abe-Ouchi, 2009: A simulation of the global distribution and radiative forcing of soil dust aerosols at the Last Glacial Maximum. *Atmospheric Chemistry and Physics*, 3061-3073.
Tan, L., Y. Cai, R. Edwards, H. Cheng, C. Shen, and H. Zhang, 2011: Centennial- to decadal-scale monsoon precipitation variability in the semi-humid region, northern China during the last 1860 years: Records from stalagmites in Huangye Cave. *The Holocene*, **21,** 287-296.
Tarasov, P., W. Granoszewski, E. Bezrukova, S. Brewer, M. Nita, A. Abzaeva, and H. Oberhansli, 2005: Quantitative reconstruction of the last interglacial vegetation and climate based on the pollen record from Lake Baikal, Russia. *Climate Dynamics*, **25,** 625-637.
Tarasov, P. E., E. V. Bezrukova, and S. K. Krivonogov, 2009: Late Glacial and Holocene changes in vegetation cover and climate in southern Siberia derived from a 15 kyr long pollen record from Lake Kotokel. *Climate of the Past*, **5,** 285-295.
Tarasov, P. E., et al., 2011: Progress in reconstruction of Quaternary climate dynamics in the Northwest Pacific: New modern-analogue reference dataset and its application to the 430-kyr pollen record fro Lake Biwa. *Earth-Science Reviews*.
Thompson, L. G., M. E. Davis, E. Mosley-Thompson, P. N. Lin, K. A. Henderson, and T. A. Mashiotta, 2005: Tropical ice core records: evidence for asynchronous glaciation on Milankovitch timescales. *Journal of Quaternary Science*, **20,** 723-733.
Thompson, L. G., et al., 1995: Last glacial stage and Holocene tropica ice core records from Huascaran, Peru. *Science*, **269,** 46-50.
Thornalley, D. J. R., S. Barker, W. S. Broecker, H. Elderfield, and I. N. McCave, 2011: The Deglacial Evolution of North Atlantic Deep Convection. *Science*, **331,** 202-205.
Tierney, J., D. Oppo, Y. Rosenthal, J. Russell, and B. Linsley, 2010a: Coordinated hydrological regimes in the Indo-Pacific region during the past two millennia. *Paleoceanography*, -.
Tierney, J., M. Mayes, N. Meyer, C. Johnson, P. Swarzenski, A. Cohen, and J. Russell, 2010b: Late-twentieth-century warming in Lake Tanganyika unprecedented since AD 500. *Nature Geoscience*, **3,** 422-425.
Tierney, J. E., J. M. Russell, Y. S. Huang, J. S. S. Damste, E. C. Hopmans, and A. S. Cohen, 2008: Northern hemisphere controls on tropical southeast African climate during the past 60,000 years. *Science*, **322,** 252-255.
Timm, O., E. Ruprecht, and S. Kleppek, 2004: Scale-dependent reconstruction of the NAO index. *Journal of Climate*, **17,** 2157-2169.
Timm, O., P. Kohler, A. Timmermann, and L. Menviel, 2010: Mechanisms for the Onset of the African Humid Period and Sahara Greening 14.5-11 ka BP. *Journal of Climate*, **23,** 2612-2633.
Timm, O., A. Timmermann, A. Abe-Ouchi, F. Saito, and T. Segawa, 2008: On the definition of seasons in paleoclimate simulations with orbital forcing. *Paleoceanography*, **23**.
Timmermann, A., O. Timm, L. Stott, and L. Menviel, 2009: The Roles of CO2 and Orbital Forcing in Driving Southern Hemispheric Temperature Variations during the Last 21 000 Yr. *Journal of Climate*, **22,** 1626-1640.
Timmermann, A., J. Knies, O. E. Timm, A. Abe-Ouchi, and T. Friedrich, 2010a: Promotion of glacial ice sheet buildup 60-115 kyr B.P. by precessionally paced Northern Hemispheric meltwater pulses. *Paleoceanography*, **25**.
Timmermann, A., et al., 2010b: Towards a quantitative understanding of millennial-scale Antarctic warming events. *Quaternary Science Reviews*, **29,** 74-85.
——, 2007: The influence of a weakening of the Atlantic meridional overturning circulation on ENSO. *Journal of Climate*, **20,** 4899-4919.
Timmreck, C., S. Lorenz, T. Crowley, S. Kinne, T. Raddatz, M. Thomas, and J. Jungclaus, 2009: Limited temperature response to the very large AD 1258 volcanic eruption. *Geophysical Research Letters*, -.
Tingley, M. P., and P. Huybers, 2010: A Bayesian Algorithm for Reconstructing Climate Anomalies in Space and Time. Part I: Development and Applications to Paleoclimate Reconstruction Problems. *Journal of Climate*, **23,** 2759-2781.
Tjallingii, R., et al., 2008: Coherent high- and low-latitude control of the northwest African hydrological balance. *Nature Geoscience*, **1,** 670-675.
Toggweiler, J., 2009: Shifting Westerlies. *Science*, 1434-1435.
Toniazzo, T., 2006: Properties of El Nino-Southern Oscillation in different equilibrium climates with HadCM3. *Journal of Climate*, **19,** 4854-4876.

Treydte, K., G. H. Schleser, G. Helle, D. C. Frank, M. Winiger, G. H. Haug, and J. Esper, 2006: The twentieth century was the wettest period in northern Pakistan over the past millenium. *Nature*, **440,** 1179-1182.
Trouet, V., J. Esper, N. E. Graham, A. Baker, J. D. Scourse, and D. C. Frank, 2009: Persistent Positive North Atlantic Oscillation Mode Dominated the Medieval Climate Anomaly. *Science*, **324,** 78-80.
Tudhope, A., et al., 2001: Variability in the El Nino - Southern oscillation through a glacial-interglacial cycle. *Science*, 1511-1517.
Tuffen, H., 2010: How will melting of ice affect volcanic hazards in the twenty-first century? *Philosophical Transactions of the Royal Society a-Mathematical Physical and Engineering Sciences*, 2535-2558.
Tzedakis, P., 2007: Pollen records, Last Interglacial of Europe. *Encyclopedia of Quaternary Sciences*, S. A. Elias, Ed., Elsevier.
Tzedakis, P. C., 2010: The MIS 11-MIS 1 analogy, southern European vegetation, atmospheric methane and the 'early anthropogenic hypothesis'. *Climate of the Past*, **6,** 131-144.
Tzedakis, P. C., D. Raynaud, J. F. McManus, A. Berger, V. Brovkin, and T. Kiefer, 2009: Interglacial diversity. *Nature Geoscience*, **2,** 751-755.
Urquhart, G., 2009: Paleoecological record of hurricane disturbance and forest regeneration in Nicaragua. *Quaternary International*, 88-97.
Vallelonga, P., et al., 2010: Lead isotopic compositions in the EPICA Dome C ice core and Southern Hemisphere Potential Source Areas. *Quaternary Science Reviews*, **29,** 247-255.
Vavrus, S., W. Ruddiman, and J. Kutzbach, 2008: Climate model tests of the anthropogenic influence on greenhouse-induced climate change: the role of early human agriculture, industrialization, and vegetation feedbacks. *Quaternary Science Reviews*, 1410-1425.
Velichko, A. A., O. K. Borisova, and E. M. Zelikson, 2008: Paradoxes of the Last Interglacial climate: reconstruction of the northern Eurasia climate based on palaeofloristic data. *Boreas*, **37,** 1-19.
Verleyen, E., et al., 2011: Post-glacial regional climate variability along the East Antarctic coastal margin-Evidence from shallow marine and coastal terrestrial records. *Earth-Science Reviews*, **104,** 199-212.
Vieira, L. E., S. K. Solanki , A. V. Krivov, and I. G. Usoskin 2011: Evolution of the solar irradiance during the Holocene. *Astronomy & Astrophysics*, **submitted**.
Villalba, R., M. Grosjean, and T. Kiefer, 2009: Long-term multi-proxy climate reconstructions and dynamics in South America (LOTRED-SA): State of the art and perspectives Preface. *Palaeogeography Palaeoclimatology Palaeoecology*, 175-179.
Vimeux, F., P. Ginot, M. Schwikowski, M. Vuille, G. Hoffmann, L. Thompson, and U. Schotterer, 2009: Climate variability during the last 1000 years inferred from Andean ice cores: A review of methodology and recent results. *Palaeogeography Palaeoclimatology Palaeoecology*, 229-241.
Vinther, B., P. Jones, K. Briffa, H. Clausen, K. Andersen, D. Dahl-Jensen, and S. Johnsen, 2010: Climatic signals in multiple highly resolved stable isotope records from Greenland. *Quaternary Science Reviews*, 522-538.
Vinther, B., et al., 2006: A synchronized dating of three Greenland ice cores throughout the Holocene. *Journal of Geophysical Research-Atmospheres*, -.
Vinther, B. M., et al., 2009: Holocene thinning of the Greenland ice sheet. *Nature*, **461,** 385-388.
Visbeck, M., 2009: A Station-Based Southern Annular Mode Index from 1884 to 2005. *Journal of Climate*, **22,** 940-950.
von Grafenstein, U., E. Erlenkeuser, J. Müller, J. Jouzel, and S. Johnsen, 1998: The cold event 8,200 years ago documented in oxygen isotope records of precipitation in Europe and Greenland. *Climate Dynamics*, **14,** 73-81.
von Gunten, L., M. Grosjean, B. Rein, R. Urrutia, and P. Appleby, 2009: A quantitative high-resolution summer temperature reconstruction based on sedimentary pigments from Laguna Aculeo, central Chile, back to AD 850. *Holocene*, 873-881.
von Storch, H., E. Zorita, J. M. Jones, F. Gonzalez-Rouco, and S. F. B. Tett, 2006: Response to comment on "Reconstructing past climate from noisy data". *Science*, **312**.
Waelbroeck, C., et al., 2002: Sea level and deep water temperature changes derived from benthic foraminifera isotopic records. *Quaternary Science Reviews*, 295-305.
——, 2009: Constraints on the magnitude and patterns of ocean cooling at the Last Glacial Maximum. *Nature Geoscience*, **2,** 127-132.
Wahl, E., et al., 2010: An archive of high-resolution temperature reconstructions over the past 2+millennia. *Geochemistry Geophysics Geosystems*, -.
Wang, S., X. Wen, Y. Luo, W. Dong, Z. Zhao, and B. Yang, 2007a: Reconstruction of temperature series of China for the alst 1000 years. *Chinese Science Bulletin*, **52,** 3272-3280.
Wang, X. F., A. S. Auler, R. L. Edwards, H. Cheng, E. Ito, and M. Solheid, 2006: Interhemispheric anti-phasing of rainfall during the last glacial period. *Quaternary Science Reviews*, **25,** 3391-3403.
Wang, X. F., et al., 2004: Wet periods in northeastern Brazil over the past 210 kyr linked to distant climate anomalies. *Nature*, **432,** 740-743.
——, 2007b: Millennial-scale precipitation changes in southern Brazil over the past 90,000 years. *Geophysical Research Letters*, **34**.
Wang, Y., J. Lean, and N. Sheeley, 2005a: Modeling the sun's magnetic field and irradiance since 1713. *Astrophysical Journal*, 522-538.

Wang, Y., et al., 2005b: The Holocene Asian monsoon: Links to solar changes and North Atlantic climate. *Science*, **308,** 854-857.
Wang, Y. J., H. Cheng, R. L. Edwards, Z. S. An, J. Y. Wu, C. C. Shen, and J. A. Dorale, 2001: A high-resolution absolute-dated Late Pleistocene monsoon record from Hulu Cave, China. *Science*, **294,** 2345-2348.
Wang, Y. J., et al., 2008: Millennial- and orbital-scale changes in the East Asian monsoon over the past 224,000 years. *Nature*, **451,** 1090-1093.
Wang, Y. M., J. L. Lean, and N. R. Sheeley, 2005c: Modeling the sun's magnetic field and irradiance since 1713. *Astrophysical Journal*, **625,** 522-538.
Wang, Z., J. Chappellaz, K. Park, and J. Mak, 2010: Large Variations in Southern Hemisphere Biomass Burning During the Last 650 Years. *Science*, **330,** 1663-1666.
Wanner, H., Beer, J., Bu¨ tikofer, J., Crowley, T.J., Cubasch, U., Flu¨ ckiger, J., Goosse, H., Grosjean, M., Joos, F., Kaplan, J.O., Ku¨ ttel, M., Mu¨ ller, S.A., Prentice, I.C., Solomina, O., Stocker, T.F., Tarasov, P., Wagner, M., Widmann, M., 2008: Mid- to Late Holocene climate change: an overview. *Quaternary Science Reviews*, **27,** 1791–1828.
Watrin, J., A. M. Lezine, and C. Hely, 2009: Plant migration and plant communities at the time of the "green Sahara". *Comptes Rendus Geoscience*, **341,** 656-670.
Weldeab, S., R. R. Schneider, and M. Kolling, 2006: Deglacial sea surface temperature and salinity increase in the western tropical Atlantic in synchrony with high latitude climate instabilities. *Earth and Planetary Science Letters*, **241,** 699-706.
Weldeab, S., D. W. Lea, R. R. Schneider, and N. Andersen, 2007: 155,000 years of West African monsoon and ocean thermal evolution. *Science*, **316,** 1303-1307.
Wenzler, T., S. Solanki, and N. Krivova, 2005: Can surface magnetic fields reproduce solar irradiance variations in cycles 22 and 23? *Astronomy & Astrophysics*, 1057-1061.
Widmann, M., H. Goosse, G. van der Schrier, R. Schnur, and J. Barkmeijer, 2010: Using data assimilation to study extratropical Northern Hemisphere climate over the last millennium. *Climate of the Past*, **6,** 627-644.
Wiersma, A., and H. Renssen, 2006: Model-data comparison for the 8.2 ka BP event: confirmation of a forcing mechanism by catastrophic drainage of Laurentide Lakes. *Quaternary Science Reviews*, 63-88.
Wiersma, A., D. Roche, and H. Renssen, 2011: Fingerprinting the 8.2 ka event climate response in a coupled climate model. *Journal of Quaternary Science*, 118-127.
Williams, M., S. Ambrose, S. van der Kaars, C. Ruehlemann, U. Chattopadhyaya, J. Pal, and P. Chauhan, 2009: Environmental impact of the 73 ka Toba super-eruption in South Asia. *Palaeogeography Palaeoclimatology Palaeoecology*, 295-314.
Willson, R. C., and A. V. Mordvinov, 2003: Secular total solar irradiance trend during solar cycles 21-23. *Geophysical Research Letters*, **30**.
Wilson, R., G. Wiles, R. D'Arrigo, and C. Zweck, 2007a: Cycles and shifts: 1,300 years of multi-decadal temperature variability in the Gulf of Alaska. *Climate Dynamics*, 425-440.
Wilson, R., E. Cook, R. D'Arrigo, N. Riedwyl, M. N. Evans, A. Tudhope, and R. Allan, 2010: Reconstructing ENSO: the influence of method, proxy data, climate forcing and teleconnections. *Journal of Quaternary Science*, **25,** 62-78.
Wilson, R., et al., 2007b: A matter of divergence: Tracking recent warming at hemispheric scales using tree ring data. *Journal of Geophysical Research*, **112,** 17103.
Winckler, G., R. F. Anderson, M. Q. Fleisher, D. Mcgee, and N. Mahowald, 2008a: Covariant glacial-interglacial dust fluxes in the equatorial Pacific and Antarctiabout *Science*.
Winckler, G., R. F. Anderson, M. Q. Fleisher, D. McGee, and N. Mahowald, 2008b: Covariant glacial-interglacial dust fluxes in the equatorial Pacific and Antarctiabout *Science*, **320,** 93-96.
Wolff, E. W., J. Chappellaz, T. Blunier, S. O. Rasmussen, and A. Svensson, 2010: Millennial-scale variability during the last glacial: The ice core record. *Quaternary Science Reviews*, **29,** 2828-2838.
Wu, N. Q., X. Y. Chen, D. D. Rousseau, F. J. Li, Y. P. Pei, and B. Wu, 2007: Climatic conditions recorded by terrestrial mollusc assemblages in the Chinese Loess Plateau during marine oxygen isotope Stages 12-10. *Quaternary Science Reviews*, **26,** 1884-1896.
Xie, S. P., Y. Okumura, T. Miyama, and A. Timmermann, 2008: Influences of Atlantic climate change on the tropical Pacific via the Central American Isthmus. *Journal of Climate*, **21,** 3914-3928.
Xu, B., et al., 2009: Deposition of anthropogenic aerosols in a southeastern Tibetan glacier. *Journal of Geophysical Research-Atmospheres*, -.
Yadav, R., A. Bräuning, and J. Singh, 2010: Tree ring inferred summer temperature variations over the last millennium in western Himalaya, India. *Climate Dynamics*.
Yancheva, G., et al., 2007: Influence of the intertropical convergence zone on the East Asian monsoon. *Nature*, **445,** 74-77.
Yang, B., A. Braeuning, K. Johnson, and Y. Shi, 2002: General characteristics of temperature variation in China during the last two millennia. *Geophysical Research Letters*, **29,** 1324.
YAPP, C., and H. POTHS, 1992: ANCIENT ATMOSPHERIC CO2 PRESSURES INFERRED FROM NATURAL GOETHITES. *Nature*, 342-344.

Yin, J. J., M. E. Schlesinger, N. G. Andronova, S. Malyshev, and B. Li, 2006: Is a shutdown of the thermohaline circulation irreversible? *Journal of Geophysical Research-Atmospheres*, **111**.
Yin, Q. Z., and A. Berger, 2010: Insolation and CO2 contribution to the interglacial climate before and after the Mid-Brunhes Event. *Nature Geoscience*, **3,** 243-246.
Yokoyama, Y., T. M. Esat, M. T. McCulloch, G. E. Mortimer, J. Chappell, and K. Lambeck, 2003: Large sea level excursions during the Marine Isotope Stages 4 and 3 obtained from Huon Peninsula uplifted coral terraces. *Geochimica Et Cosmochimica Acta*, **67,** A568-A568.
Yu, S. Y., et al., 2010: Freshwater Outburst from Lake Superior as a Trigger for the Cold Event 9300 Years Ago. *Science*, **328,** 1262-1266.
Zachos, J., et al., 2006: Extreme warming of mid-latitude coastal ocean during the Paleocene-Eocene Thermal Maximum: Inferences from TEX86 and isotope data. *Geology***,** 737-740.
Zhang, D., R. Blender, X. Zhu, and K. Fraedrich, 2011: Temperature variability in China in an ensemble simulation for the last 1,200 years. *Theoretical and Applied Climatology***,** 387-399.
Zhang, P. Z., et al., 2008: A Test of Climate, Sun, and Culture Relationships from an 1810-Year Chinese Cave Record. *Science*, **322,** 940-942.
Zhang, R., and T. Delworth, 2005: Simulated tropical response to a substantial weakening of the Atlantic thermohaline circulation. *Journal of Climate***,** 1853-1860.
Zhang, Z. Y., D. Y. Gong, X. Z. He, Y. N. Lei, and S. H. Feng, 2010: Statistical reconstruction of the Antarctic Oscillation index based on multiple proxies. *Atmos. Oce. Sci. Lett.*, **3,** 283-287.
Zheng, W., P. Braconnot, E. Guilyardi, U. Merkel, and Y. Yu, 2008: ENSO at 6ka and 21ka from ocean-atmosphere coupled model simulations. *Climate Dynamics*, **30,** 745-762.
Zhu, H., F. Zheng, X. Shao, X. Liu, X. Yan, and E. Liang, 2008: Millennial temperature reconstruction based on tree-ring widths of Qilian juniper from Wulan, Qinghai province, China. *Chin. Sci. Bull.*, **53,** 3914-3920.

Chapter 5: Information from Paleoclimate Archives

Coordinating Lead Authors: Valérie Masson-Delmotte (France), Michael Schulz (Germany)

Lead Authors: Ayako Abe-Ouchi (Japan), Juerg Beer (Switzerland), Andrey Ganopolski (Germany), Jesus Fidel González Rouco (Spain), Eystein Jansen (Norway), Kurt Lambeck (Australia), Juerg Luterbacher (Germany), Tim Naish (New Zealand), Timothy Osborn (UK), Bette Otto-Bliesner (USA), Terrence Quinn (USA), Rengaswamy Ramesh (India), Maisa Rojas (Chile), XueMei Shao (China), Axel Timmermann (USA)

Contributing Authors: Patrick de Deckker, Barbara Delmonte, Hubertus Fischer, Claus Froehlich, Alan Haywood, Stefan Mulitza, Olga Solomina, Pavel Tarasov, Yusuke Yokoyama, Dan Zwarz

Review Editors: Fatemeh Rahimzadeh (Iran), Dominique Raynaud (France), Heinz Wanner (Switzerland), De`er Zhang (China)

Date of Draft: 15 April 2011

Notes: TSU Compiled Version

Figures

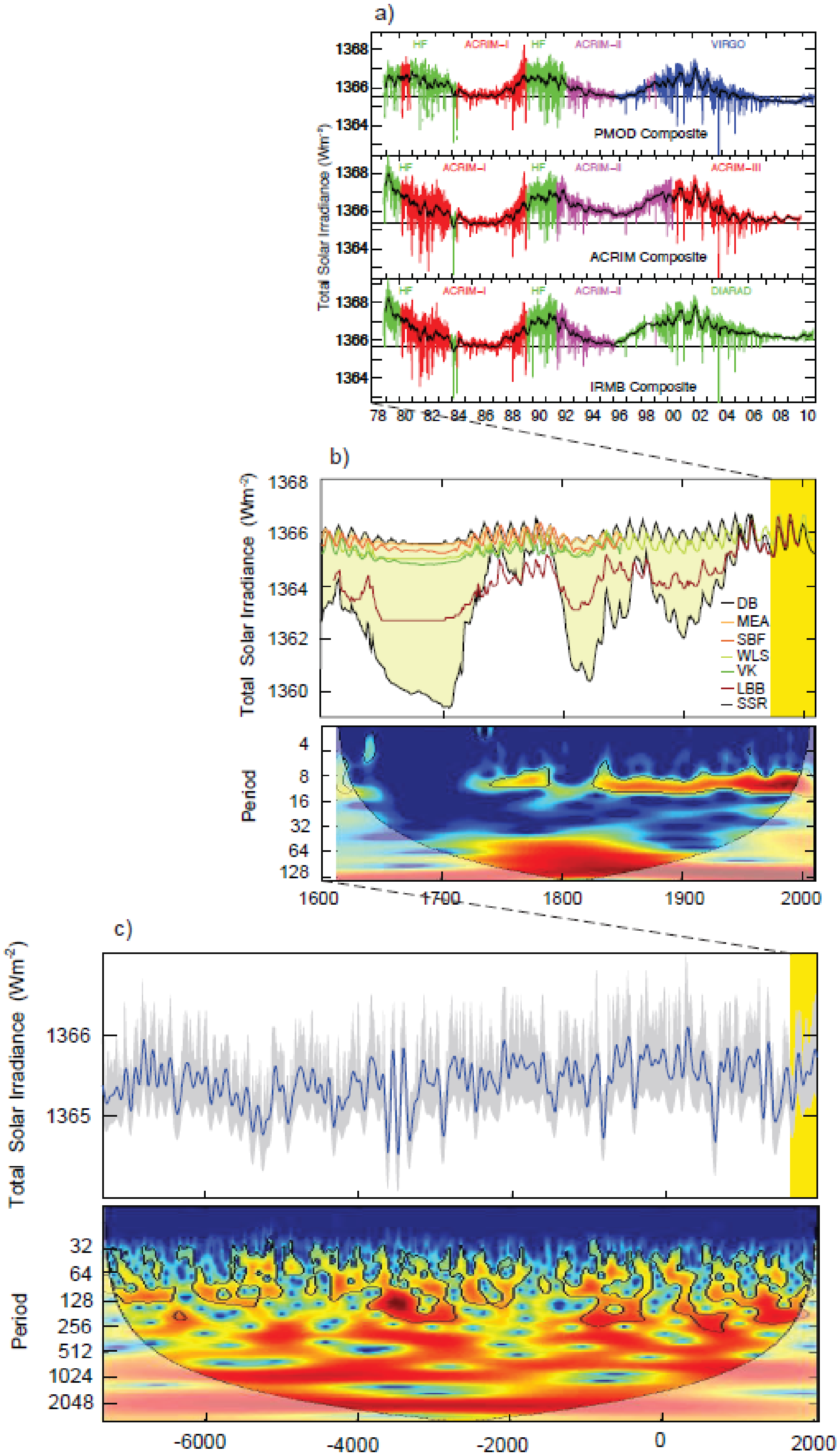

Figure 5.1: a) 3 composites of instrumental data from several satellite based radiometers indicated by different colours (Dewitte et al., 2004; Frohlich, 2009; Willson and Mordvinov, 2003). The differences between the composites are due to different combinations of the radiometer data and the application of

different corrections (x-axis is YEAR AD -> will be incorporated into the figure). **b)** TSI reconstructions back to 1600 AD. The lack of direct measurements is compensated by proxies of solar activity (e.g., sunspots, ^{10}Be) which are used to estimate the parameters of the models or directly TSI. Depending on the assumptions, the differences between the long-term averages are large and range from no change to 0.4% between the present and the Maunder minimum when the Sun was very quiet. With one exception (SSR) all recent reconstructions show relatively small long-term changes (<0.1%) compared to the [reference needed: Lean et al., xxxx] record (0.24%). The top 5 records have been used by Jungclaus et al. (2010b) to simulate the climate of the past 1000 years. The wavelet analysis of TSI (WLS) shows the 11-year Schwabe cycle which is weak during the Dalton minimum (1790–1830) and absent during the Maunder minimum (1645–1715), and cycles around 80 and 120 years. DB: Delaygue and Bard (2010); MEA: Muscheler et al. (2007); SBF: Steinhilber et al. (2009); WLS: Wang et al. (2005c); VK: Vieira et al. (2011); LBB: Lean et al. (1995); SSR: Shapiro et al. (2011). **c)** TSI reconstruction (low-pass filtered by 100 yeary) covering the past 9300 years (Steinhilber et al., 2009). The grey band represents the 1-sigma uncertainty range. The reconstruction is based on ^{10}Be and calibrated using the relationship between instrumental data of the open magnetic field which modulates the production of ^{10}Be and TSI for the past 4 solar minima. The wavelet analysis shows the existence of several well-defined periodicities with varying amplitudes (87, 104, 130, 150, 208, 350, 515, 970, 2300 years).

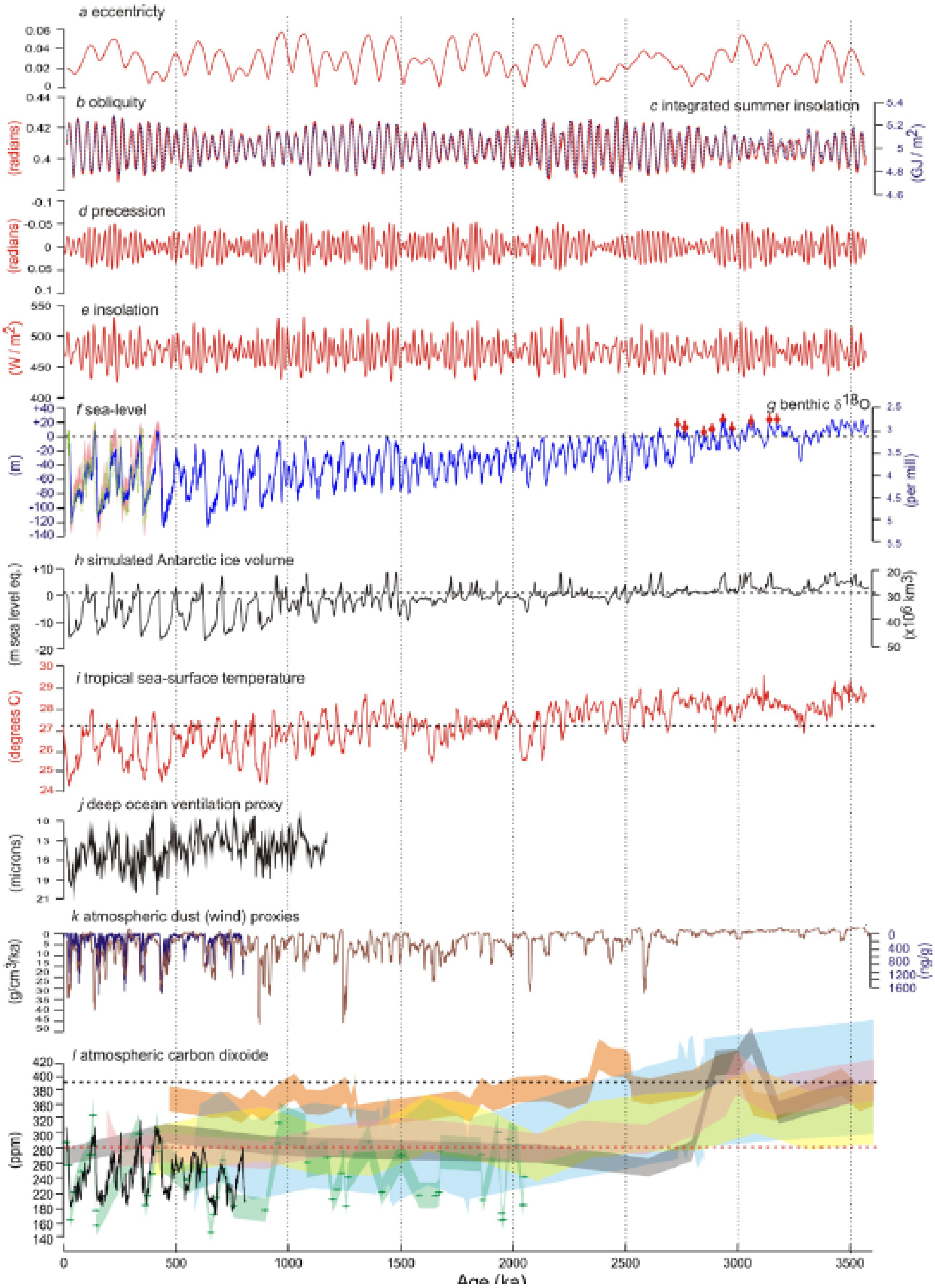

Figure 5.2: [Radiative perturbations from Earth-system feedbacks since the Pliocene] Radiative perturbations and Earth systems and its response for the last 3.6 Ma. Changes in orbital parameters, a) eccentricity, b) obliquity, d) precession, e) summer insolation at 65°N, and c) integrated summer insolation (calculated for 75°N will replace with 65°N) (Laskar, 2004; Huybers and Raymo, 2007). f) Stacked marine benthic oxygen isotope record, reflecting changes in continental ice volume and ocean temperature ($\delta^{18}O$, ‰; Lisiecki and Raymo, 2005) converted to changes in global mean sea level (m; Naish and Wilson, 2009). Pink shaded curve is based on sea level calibration of δ18O curve using dated coral shorelines (Waelbroeck et al., 2002), green dashed line is the Red Sea sea level record (Siddall et al., 2003; Rohling et al., 2009), (to be added Bintanja et al. 2005 model derived calibration back 5 Ma) and red dots with error bars are weighted mean estimates (using individual standard deviations as weights) for far-field reconstructions of eustatic peaks during mid-Pliocene interglacials (Miller et. al in review, placeholder at present). The dashed

horizontal line represents present day sea level. g) Antarctic ice volume simulation (Pollard and DeConto, 2009) expressed as sea level (m) equivalent ice volume and volume (km^3) w.r.t present day (dashed line). h) Stacked tropical SST (dashed line is modern average zonal temperature;°C; Herbert et al., 2010). i) Sortable silt grain size proxy for Pacific abyssal ocean current strength (μm; ODP Site 1123, Hall et al., 2001). j) Wind proxy derived from mass accumulation rates of Chinese loess (g/cm3/ka, brown line; Song et al., 2007) and with EPICA Dome C dust record (ng/g, blue line; Lambert et al., 2008) overlain. k) Atmospheric CO_2 concentration (ppm) measured from EPICA Dome C ice core (black line; Lüthi et al., 2008), and estimates of atmospheric CO_2 conent (ppm) from boron $\delta^{11}B$ isotopes in formainifera in marine sediments (grey shaded line, Seki et al., 2010; green shaded line Hönisch et al., 2009), and from organic biomarker alkenone-derived carbon isotope proxies (pink shaded line, Seki et al., 2010; orange, blue and yellow shaded lines Pagani et al., 2010). Note that thickness of shaded line represents the error envelope. Red dashed line = preindustrial atmospheric CO_2 content (1830 AD) and black dashed line = present-day CO_2 (2010).

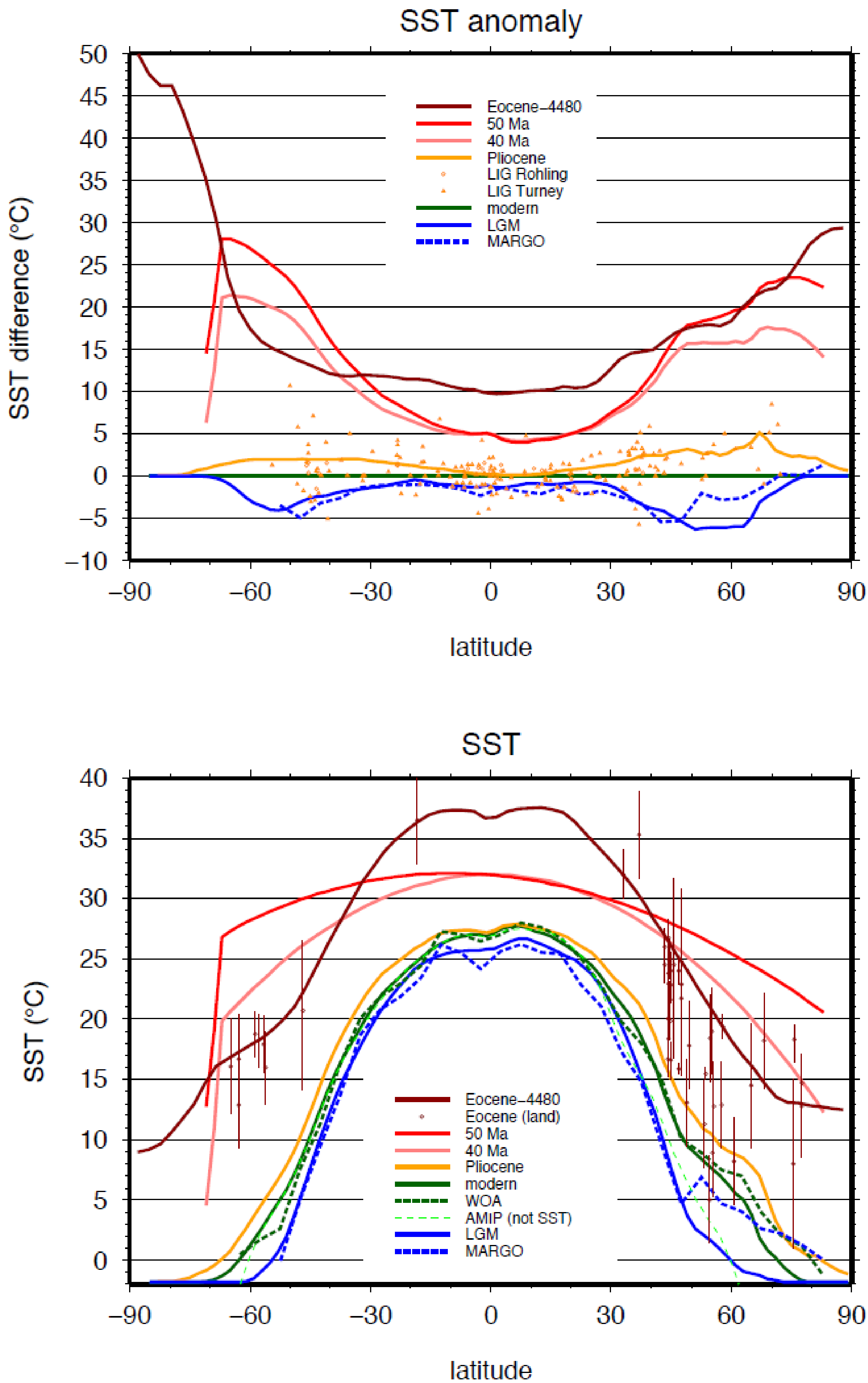

Figure 5.3: [PLACEHOLDER FOR FIRST ORDER DRAFT: Meridional temperature distribution for different geological times. Notes on draft of figure: The aim of this figure is to assess changes in meridional temperature gradients based latitudinal temperature profiles and temperature anomalies for LGM, modern (pre-industrial), last interglacial, warm early-mid Pliocene (time interval 3.5–3.0 Ma), and Eocene (4–50Ma)

using both, model output (e.g., PMIP, PlioMIP, GSSM etc.) and recontructions. The quality and quantity of the paleotemperature data obviously decreases back in time. In draft Figure 5.3 for LGM, MARGO data (not gridded and zonally biased) and data-constrained model output from Paul and Schäfer-Neth (2003) have been used. Data for the last interglacial is from a compilation by Rohling et al. (in review), and Turney and Jones (2009). Also present day has been plotted from PRISM, AMIP and WOA. Pliocene curve is data-constrained PRISM3 (Dowsett 2007). Brierley et al. (2009), showing expanded Pacific warm pool during Pliocene because of issues with corrections made to proxy data from different times in the Pliocene and different ocean basins has not been used. For the Eocene there is Bijl et al. (2009) data for 40 and 50 Ma and model output from Huber and Cabellero (2010). The latter provides GCM surface temperature for an atmospheric CO_2 concentration of 4480 ppm and compares with a compilation of terrestrial proxy temp data, but ignores the SST data due large discrepancies and perceived issues with and between marine temperature proxies. While there appear to be vast differences in temperatures from the same latitudes and even the same sites using different paleothermoters (e.g., TEX86 vs Mg/Ca; summarised in Huber (2008) and Huber and Cabellero (2010)) SST proxies for the Eocene are undergoing further the development and may yield more reliable estimates within the AR5 time frame. Uncertainties are not yet included in draft; for the final version it foreseen to represent the density of data on each curve as a guide to uncertainty. There are a number of issues to work through with data presentation on this figure including: (1) Standardisation of approach (e.g., land and ocean data or just SSTs, whether to plot zonally averaged proxy data that might be heavily biased by distribution, or data constrained model output, or model data and site specific proxy data independently?). At present the figure represents a range of different approaches. (2) Representing data quality and density. (3) Combining data over a wide temporal range particularly in deeper time slices. (4) Seasonal and spatial biases. (5) Standardised of modern temp gradients for calculating the anomaly. It will take a community effort to bring these datasets together both in the model inter-comparison and proxy communities. The LGM will be covered, but MARGO lacks terrestrial data. Last interglacial data needs more critical assessment (such an effort is underway as part of the European Past4Future Project). The PlioMIP and PRISM communities are well organised. The Paleogene proxy community are aware of the issues and Eocene model inter-comparisons are underway.]

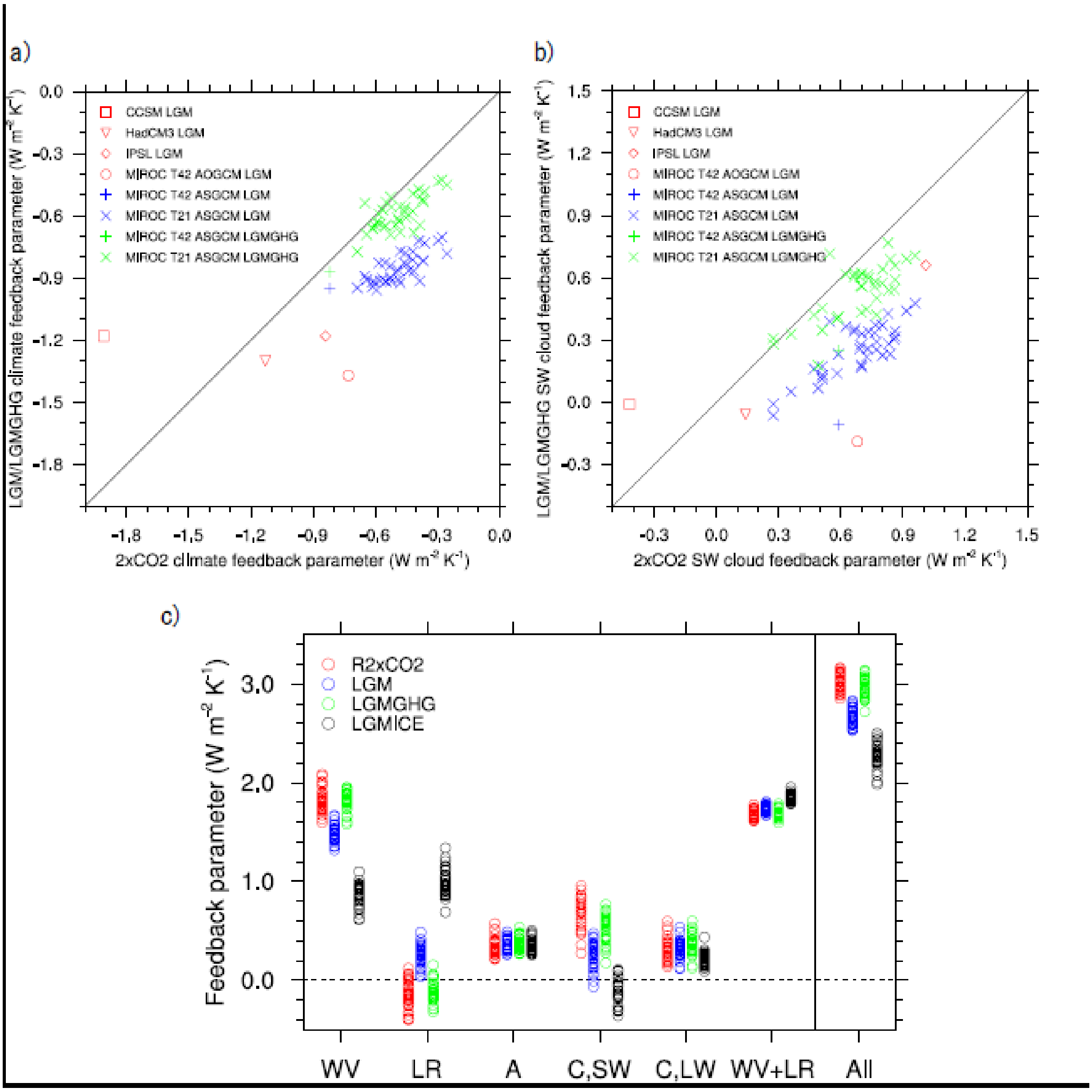

Figure 5.4: [PLACEHOLDER FOR FIRST ORDER DRAFT: Strengths of feedbacks at LGM from data and multi-model ensembles. This is just an illustration, it will be replaced when additional new experiments by PMIP3/CMIP5 become available.] Relation of feedback parameters between elevated CO_2 and LGM climate simulations: a) scatter plot of climate feedback parameter (i.e., stratosphere-adjusted radiative forcing / equilibrium temperature change) between CO_2 doubling and LGM (or LGMGHG) experiments. Here LGMGHG refers to the experiment with CO_2 concentration being lowered to the LGM level from the pre-industrial reference experiment; b) scatter plot of shortwave cloud feedback parameter (i.e., shortwave component of feedback parameter attributable to the change in clouds); c) individual feedback parameters. In a) and b), red, blue, and green markers indicate coupled atmosphere-ocean GCMs, LGM experiments with atmospheric GCMs coupled to slab ocean models, and LGMGHG experiments with atmospheric GCMs coupled to slab ocean models, respectively. Also plotted are the one-to-one lines. In c), WV, LR, A, CSW, CLW denote water vapor, lapse-rate, surface albedo, shortwave cloud, and longwave cloud feedbacks, respectively. ALL denotes sum of all feedbacks. R2xCO2 indicates $\sqrt{2}$ times CO_2 experiment, and LGMICE refers to the experiment in which ice sheets and orbital configuration at LGM are applied to the reference experiment.

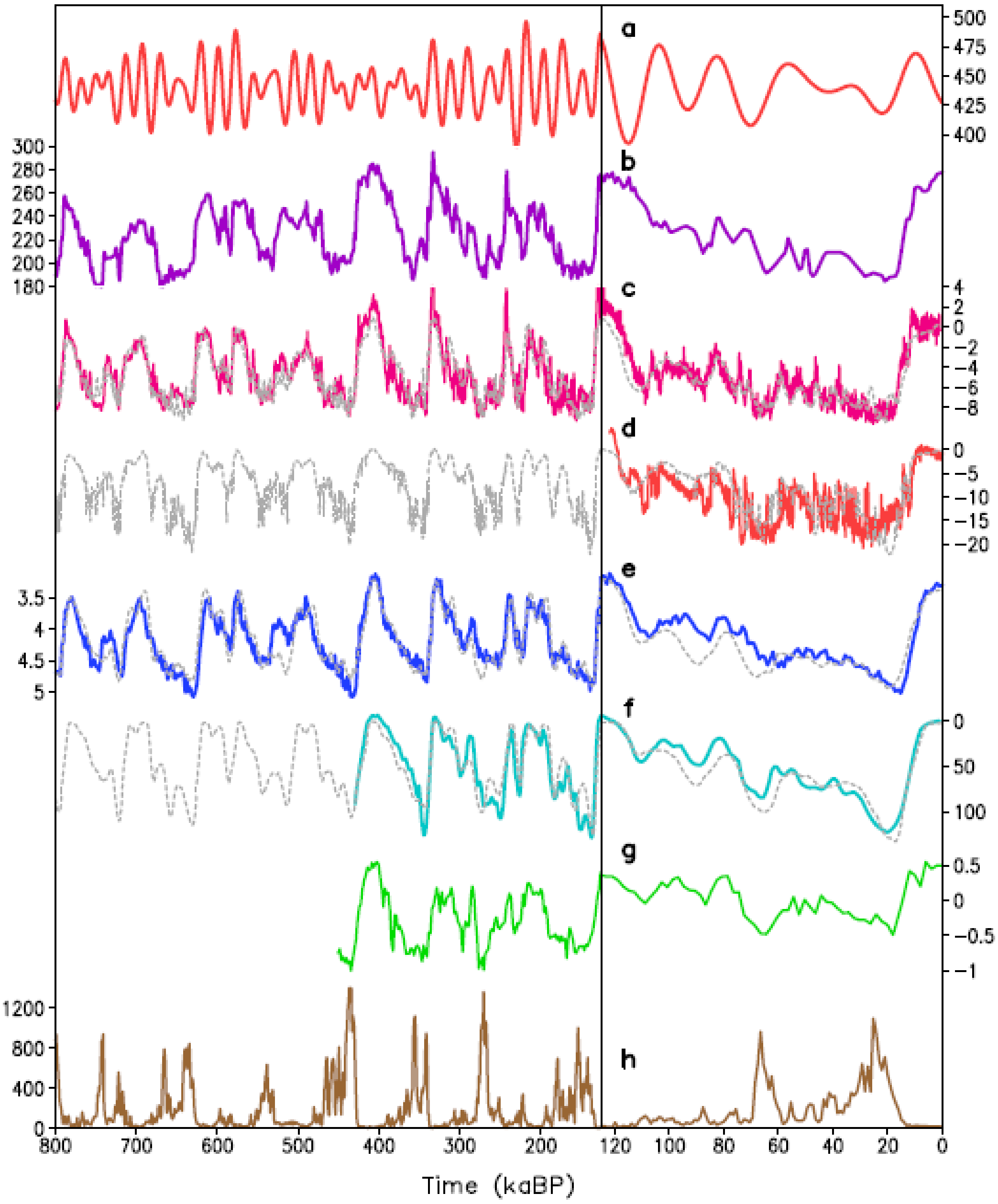

Figure 5.5: Orbital, climate, ice sheets, carbon: data and transient model. Variation of climate forcings and climate indicators over the past 800 ka. a) Orbital forcing (maximum summer insolation at 65°N) , b) the atmospheric concentration of CO_2 from Antarctic ice cores, c) Antarctic temperature reconstructed from deuterium, d) Greenland temperature reconstructed from $\delta^{18}O$, e) the stack of benthic $\delta^{18}O$, a proxy for global ice volume and deep ocean temperature, f) the reconstructed sea level, g) the stack of benthic $\delta^{13}C$ in the deep Atlantic, a proxy for the deep ocean ventilation, h) the dust concentration in the Antarctic ice core. Colour lines represent forcings and proxy data, grey dashed lines depict results of simulation with an Earth system model forced by variations of the orbital parameters and the atmospheric concentrations of the major greenhouse gases. Note the change of the time scale at 125 ka.

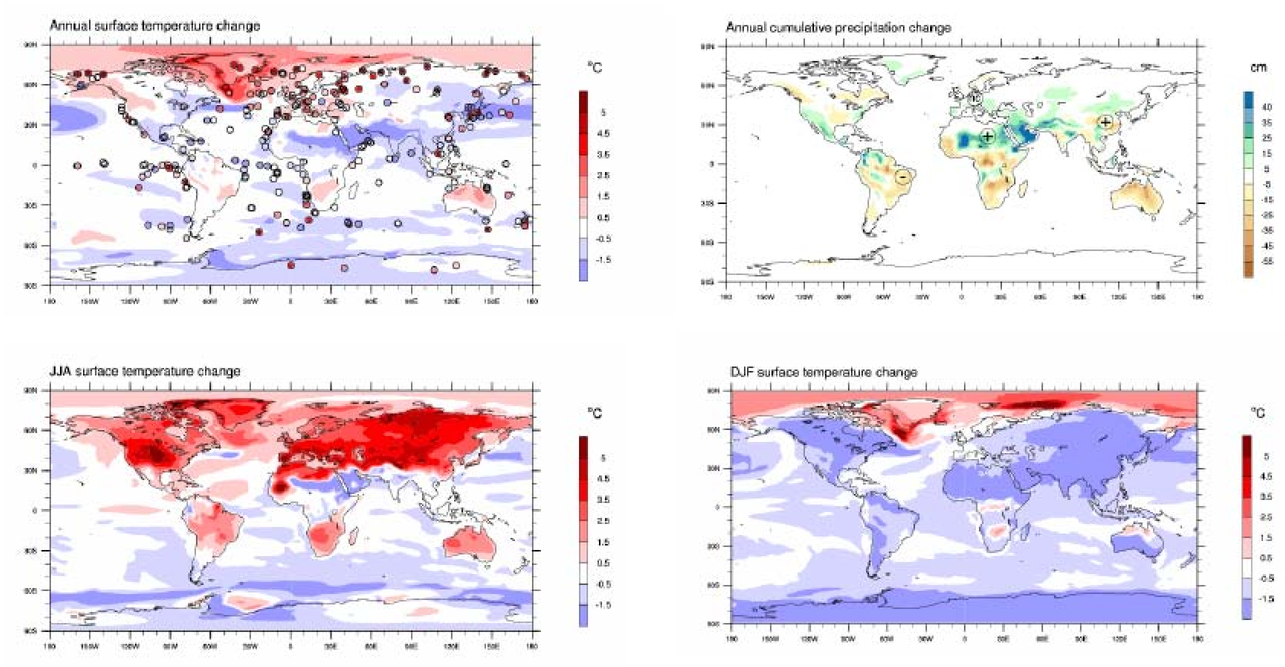

Figure 5.6: [PLACEHOLDER FOR FIRST ORDER DRAFT: New simulations for the LIG, particularly 130–125ka, from PMIP3 and other LIG projects will be included in subsequent versions. A compilation of more proxy estimates will need to be assessed for this figure.] Last Interglacial, comparison of reconstructions with models: Annual (top, left), June-July-August (bottom, left), and December-January-February (bottom, right) surface temperature changes and annual precipitation changes (top, right) for the Last Interglacial from a multi-model and multi-proxy synthesis. The multi-model changes [in this placeholder, CCSM3 T85x1 simulation for 125ka as compared to a preindustrial control simulation] are color contoured and are overlain by proxy estimates of annual changes (circles) [in this placeholder, as compiled in the synthesis of annual surface temperature change by [Turney (2010, Agulhas Current amplification of global temperatures during super-interglacials [tbc]] and from various proxy estimates of precipitation change: [Rohling (2002, African monsoon variability during the previous interglacial maximum);Wang (2004, Wet periods in northeastern Brazil over the past 210 kyr linked to distant climate anomalies); Brewer (2008, The climate in Europe during the Eemian: a multi-method approach using pollen data); Cheng (2009, Ice Age Terminations).].

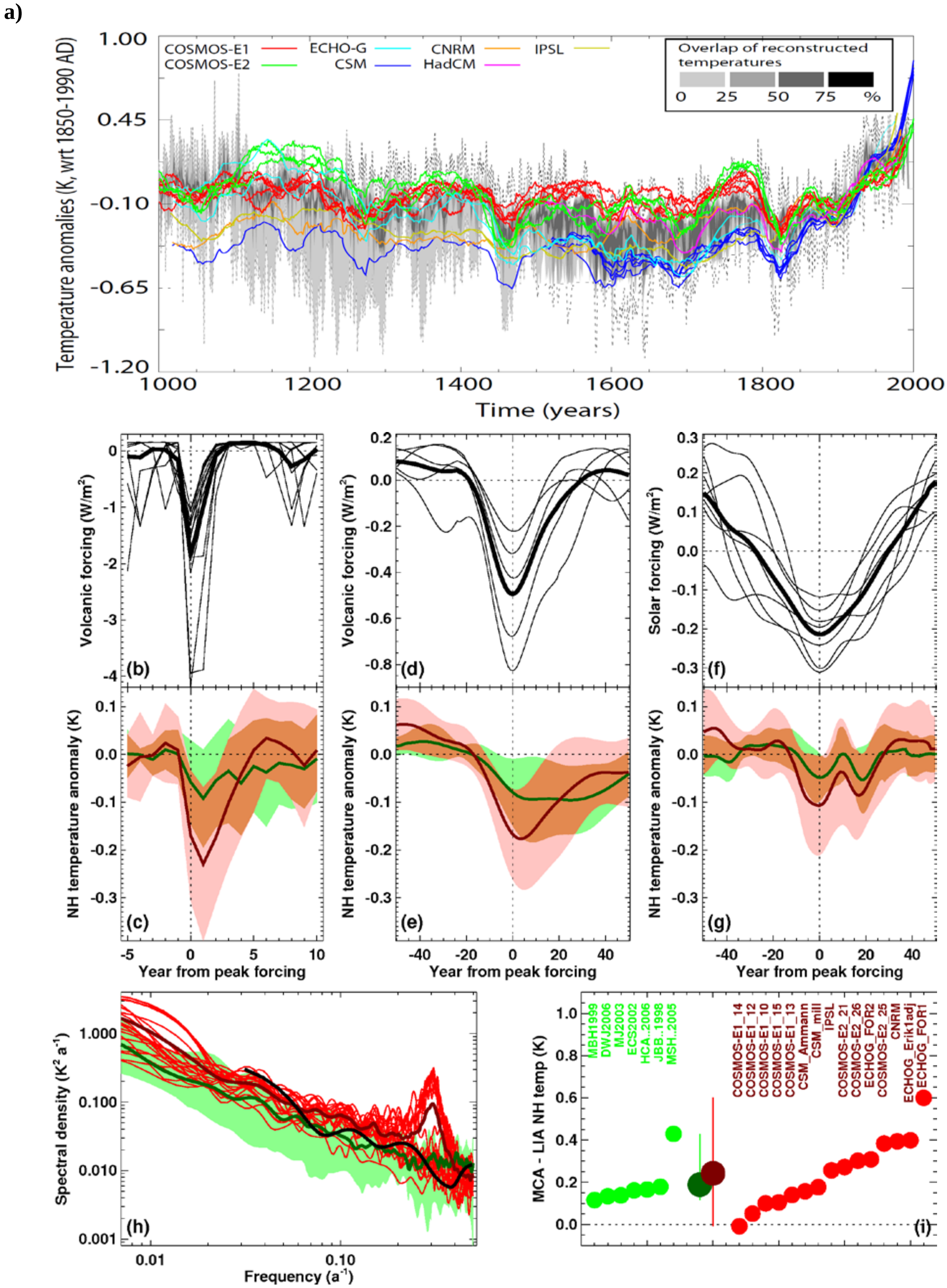

Figure 5.7: [PLACEHOLDER FOR FIRST ORDER DRAFT: Update of AR4, Figure 6.13 (Osborn) or volcanic composite and response. Will be updated with newer reconstructions and CMIP5/PMIP3 simulations. Further consideration also needs to be given to which reconstructions and simulations are included in each panel, according to temporal resolution and representation of internal variability. other considerations: how to make use of reconstruction uncertainties and model ensembles.] Comparison of

simulated NH annual temperature change with reconstructions of NH temperature change [some reconstructions are seasonal not annual, and some are for a subset of the NH such as extra-tropical land]. (a) Simulations (filtered) shown by coloured lines; overlap of reconstructed temperatures shown by grey shading. (b-g) Superposed epoch composites based on selecting sequences of temperature from periods with (b, c) individual volcanic forcing events from 1400–present that exceed -1.0 W m^{-2}; (d, e) 50-year smoothed volcanic forcing that exceeds -0.2 W m^{-2}; (f, g) change in band-passed solar forcing over a 50-year period that exceeds -0.2 W m^{-2}, all based on the forcings used by [Ammann et al. (2007)]; for solar forcing it is their "medium" forcing case. Time segments from selected periods are aligned so that the years with the peak negative forcing are aligned. In (b, d) the volcanic forcing for the individual selected events is shown together with the composite mean (thick). In (f) it is the same but for the band-passed solar forcing. (c, e, g) show the NH temperature composite means and 90% range of spread between simulations (dark red line, pink shading) or reconstructions (green), with overlap in shading (not drawn quite correctly yet!) in orange. NH temperatures were also filtered in the same way as the forcings. Only reconstructions with appropriate temporal resolution were used in each case [to be confirmed when newer reconstructions are included]. (h) Power spectral density of reconstructed (green shading shows the full range of results; dark green line: multi-reconstruction mean; individual reconstructions are not shown), simulated (thin red lines: individual models; thick dark red line: multi-model-mean) and instrumental (black line: HadCRUT3) NH temperature [the unexpected peak at f = 0.3 a^{-1} or around 3 year period seems to be entirely from the COSMOS1 and COSMOS2 runs]. (i) Mean NH temperature difference between MCA (950–1250 CE or 1000–1250 CE for data that begin in 1000 CE) and LIA (1400–1700 CE) from reconstructions (green), multi-reconstruction mean and range (dark green), multi-model mean and range (dark red), and simulations (red). Individual results are sorted into ascending order and labelled. [These MCA and LIA periods were chosen to match Figure 5.8 and Mann et al. (2009); individual ensemble members will be replaced with an ensemble mean and range, so it won't be dominated by the 8 COSMOS runs; also is ECHOG-FOR1 the first "Erik" run with a rather warm start and hence large MCA-LIA difference. If so, this should probably be removed – adjustment to this first "Erik" run was included; also new reconstructions need to be included, and perhaps MBH99 dropped if considered to be superceded by Mann et al. (2008).]

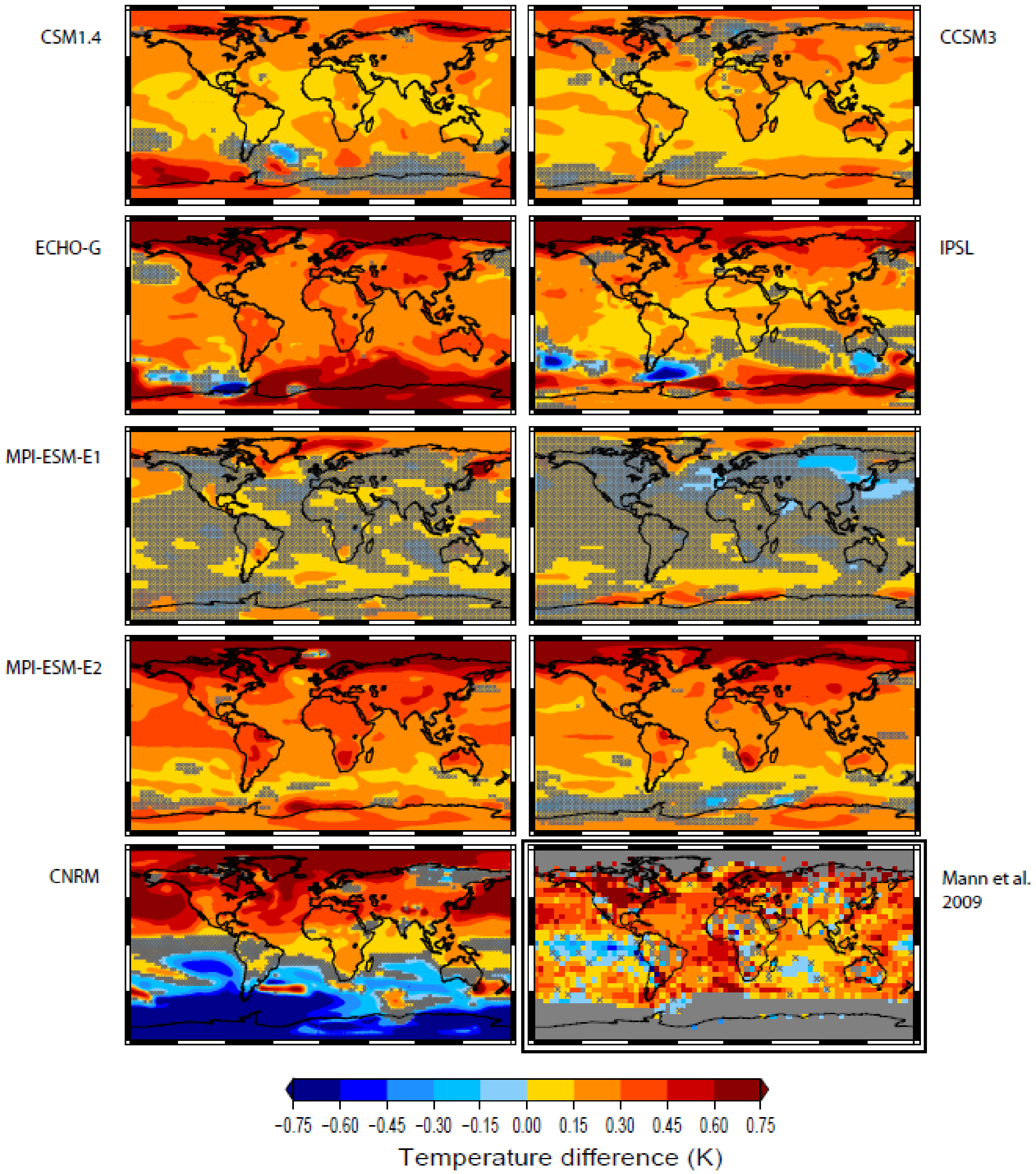

Figure 5.8: Temperature anomalies (global or hemispheric maps) for "Medivial Climate Anomaly" and "Little Ice Age". MCA-LIA annual mean temperature difference in forced simulations for the last millennium produced with six different AOGCMs and in [Mann et al. (2009)]. The periods considered for calculating the differences in [Mann et al. (2009)] were taken as reference: MCA (950–1250 CE) and LIA (1400–1700CE). For the simulations starting in 1000CE (CCSM3, ECHO-G, IPSL, CNRM) the period 1000 to 1250 was selected instead to define the MABOUT Hatched areas represent non significant differences at a 0.05 level.

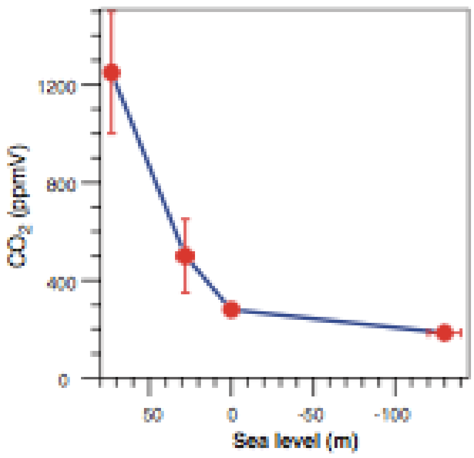

Figure 5.9: [PLACEHOLDER FOR FIRST ORDER DRAFT: pCO_2 (or polar Temp.) vs. ice volume (sea level) from data and models (Pliocene to recent)] Relationship between reconstructions of past sea level changes due to ice sheet contributions and estimates of past atmospheric CO_2 concentrations. [This figure (from Alley et al., 2005) to be updated by newly available data and an assessment of uncertainties.]

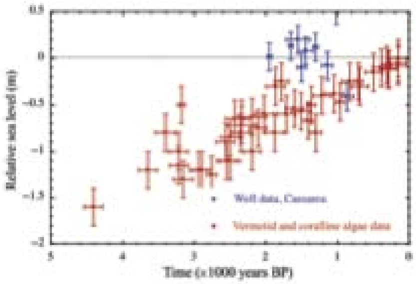

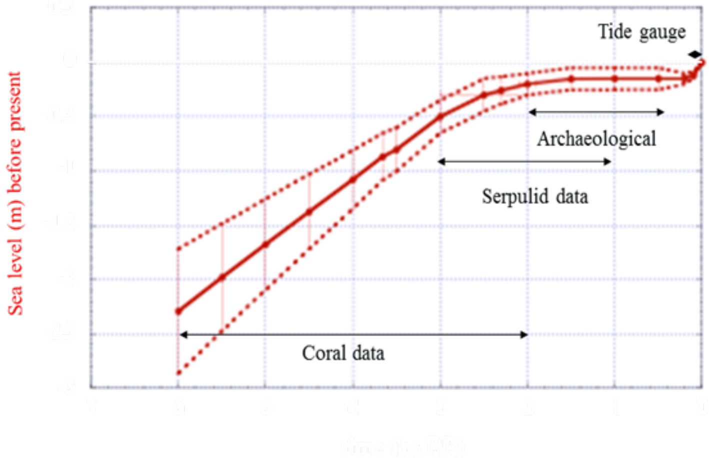

Horizontal scale is 1000 years/division. Vertical scale is im/division.

Figure 5.10: [PLACEHOLDER FOR FIRST ORDER DRAFT: Palaeo sea level variations (update of sea level figure in WCRP report). Globally averaged variation in sea level in Late Holocene time. This figure is from the volume edited by Church at al. (Figure 4.14, p.96). It will be supplement it with a couple of side panels showing individual published records, corrected and not corrected for isostatic effects. These figures would like some of the panels in Figure 4.12 or Figure 4.13. These would include results by Woodroffe et al. (submitted to Nature) from corals in the Pacific and new salt marsh records by Gehrels et al. from Tasmania and New Zealand (publications in preparation). There are new results forthcoming from archaeology sites in the Mediterranean.]

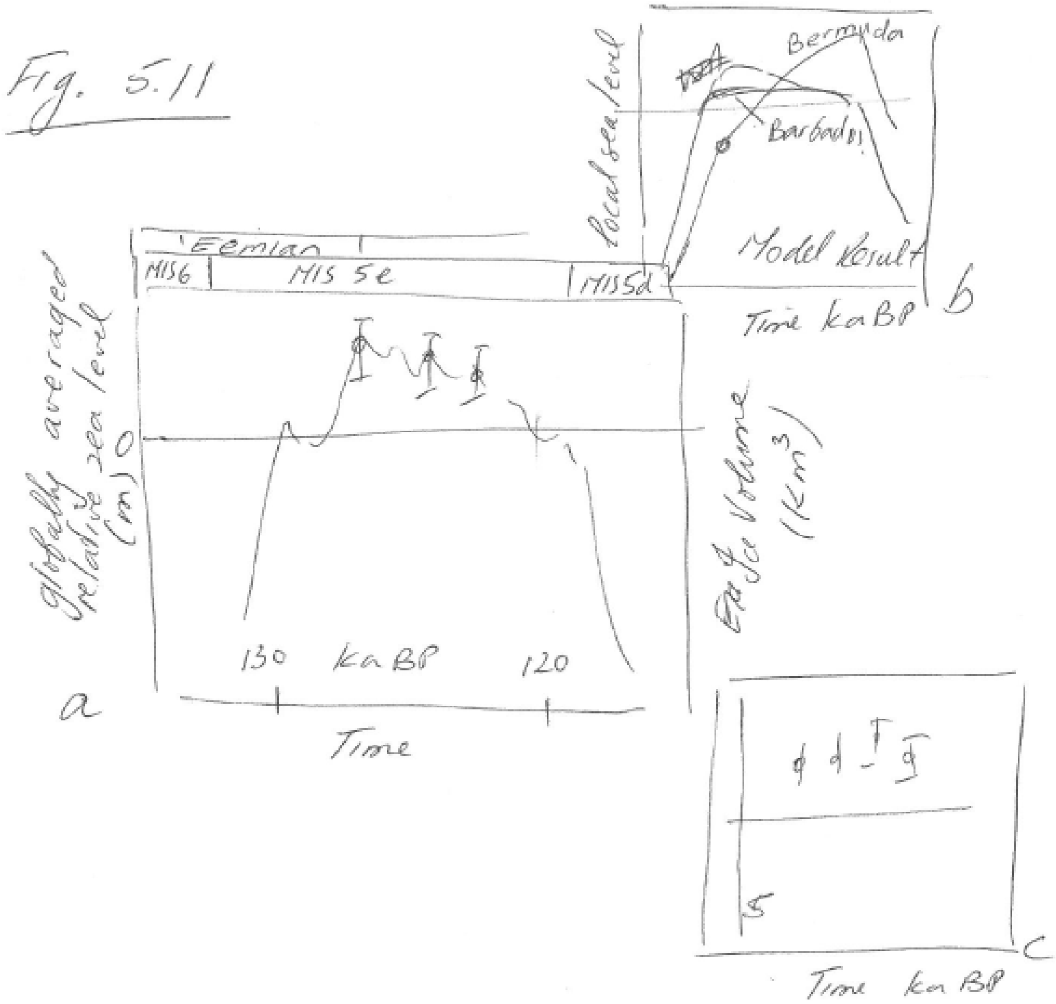

(a) in the main figure - from Dutton et al. Presented @ Palaeooceanography meeting San Diego. 2010. (In prep.), plus the result of Kopp. Text will explain the difference;
(b) Model results for different locations within the Caribean (Bermuda/Bahamas/Barbados/Yukatan).
(c) Individual site observational data Western Australia (Stirling/Dutton)

Figure 5.11: [PLACEHOLDER FOR FIRST ORDER DRAFT: Rates of sea level change during the last interglacial.]

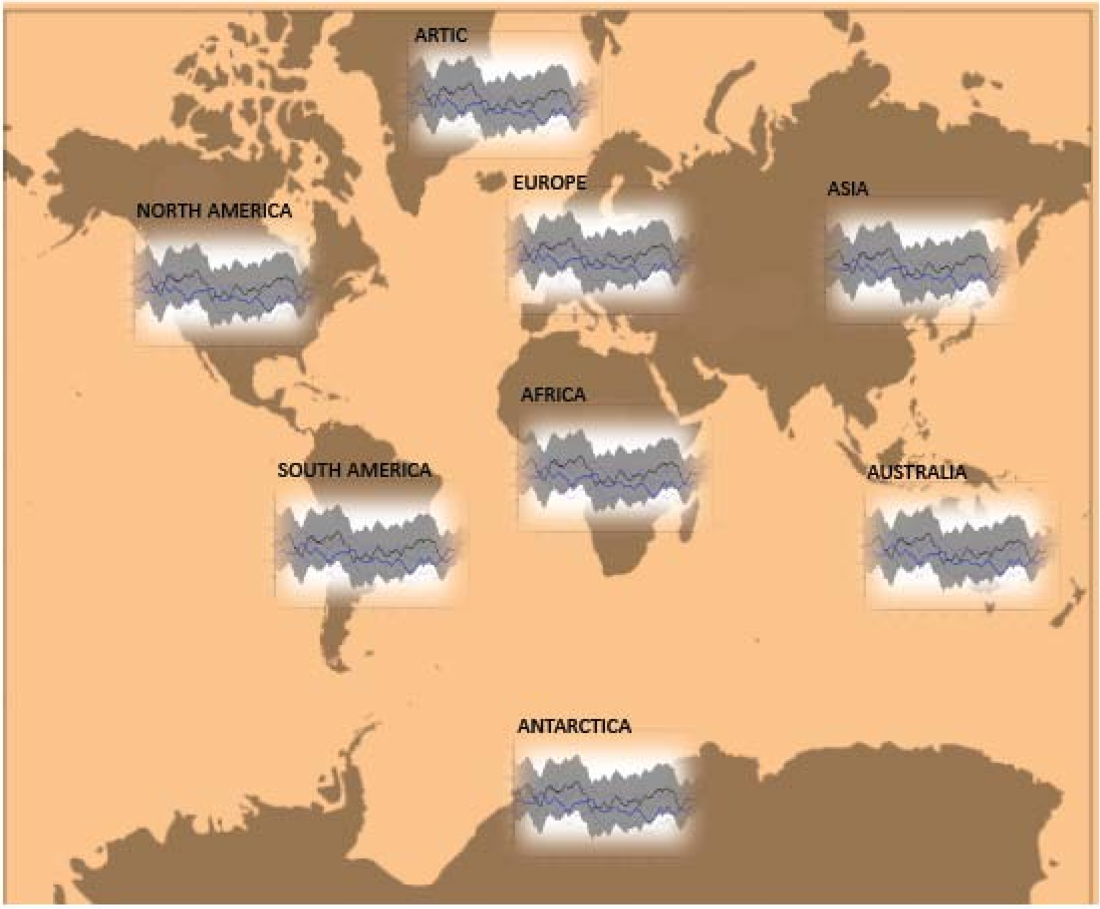

Figure 5.12: [PLACEHOLDER FOR FIRST ORDER DRAFT: Compilation of temperature reconstructions at continental scale (similar to AR4, Figure TS 22) together with CMIP models, model data/comparison.] Regional temperature, reconstructions, comparison with model simulations over the past millennium (1001–1999 CE). Ensemble model mean (black line) plus 20 and 80 percentile (gray envelope). Mean of temperature reconstructions (bold blue line) and estimatetion of error from each reconstruction (light blue line). All lines are smoothed to remove fluctuations under 50 years. Models used: ECHO-G (Gonzalez-Rouco et al., 2006), CCSM (Ammann et al., 2007), CCSM-Bern [reference needed], COSMOS (Jungclaus et al., 2010b), CNRM (Swingedouw et al., 2010). Reconstructions by region: North America [reference needed], South America (Neukom et al., 2010), Arctic (Kaufman et al., 2009a), Europe (Guiot et al., 2010), Africa [reference needed], Antarctica [reference needed], Asia (Yang et al., 2002), Australia [reference needed].

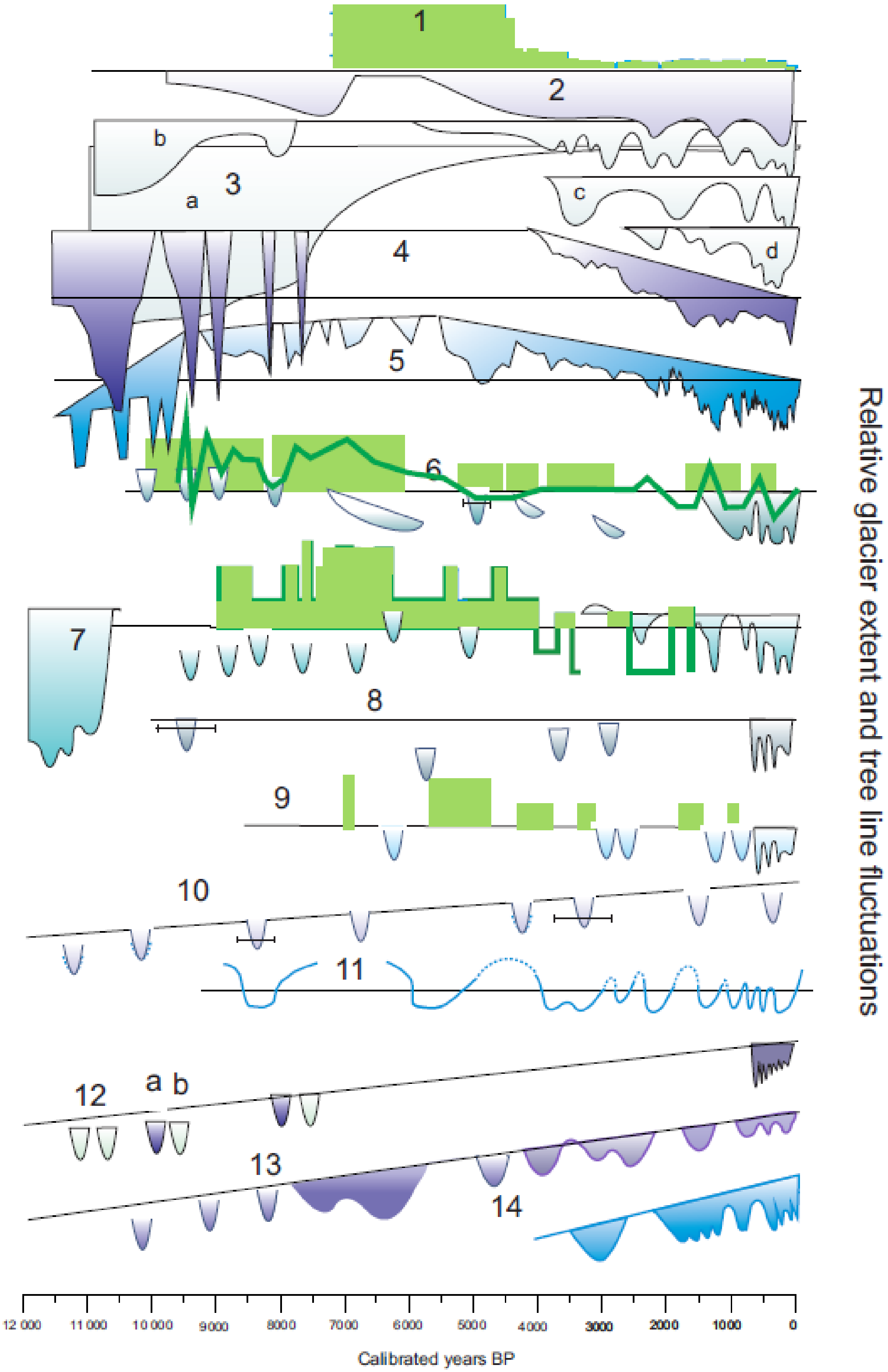

Box 5.2, Figure 1: Time–distance diagrams for glaciers (blue) and tree line elevation changes (green) through the Holocene in comparison with the northern timberline dynamics.
1. Northern timberline in Siberia [(Khantemirov, 2011)]
2. Large tidewater glacier systems (Glacier Bay) in southern Alaska [(Barclay et al., 2009)]
3. Baffin Island: a) Laurentide Ice Sheet; b) Northern Baffin Plateau; c) Central Cumberland Peninsula; d) Northern Cumberland Peninsula [(Briner et al., 2009)]

4. Northern Scandinavia [(IPCC, 2007)] [will be updated by Nesje]
5. Southern Scandinavia [(IPCC, 2007)] [will be updated by Nesje]
6. Western Canada [(Clague et al., 2009)]
7. The Alps [(Ivy-Ochs et al., 2009)]
8. Caucasus [(Solomina et al., in preparation)]
9. Altay [(Nazarov, in preparation)]
10. Muztag Ata–Kongur Shan [(Owen, 2009)]. Dashed lines: advances recorded in one valley; solid lines: at least in two valleys
11. Himalaya and Karakoram (Curve by [Roethlisberger and Geyh, 1985]; modified by [Owen, 2009])
12. Peruvian Andes (a) [Licciardi et al., 2009; b) [Glasser et al., 2009])
13. Cordilleras of South America (generalized curve; [Koch and Clague, 2006])
14**.** New Zealand: Mt. Cook, Mueller, Tasman, and Hooker Glacier [(Schaefer et al., 2009)]

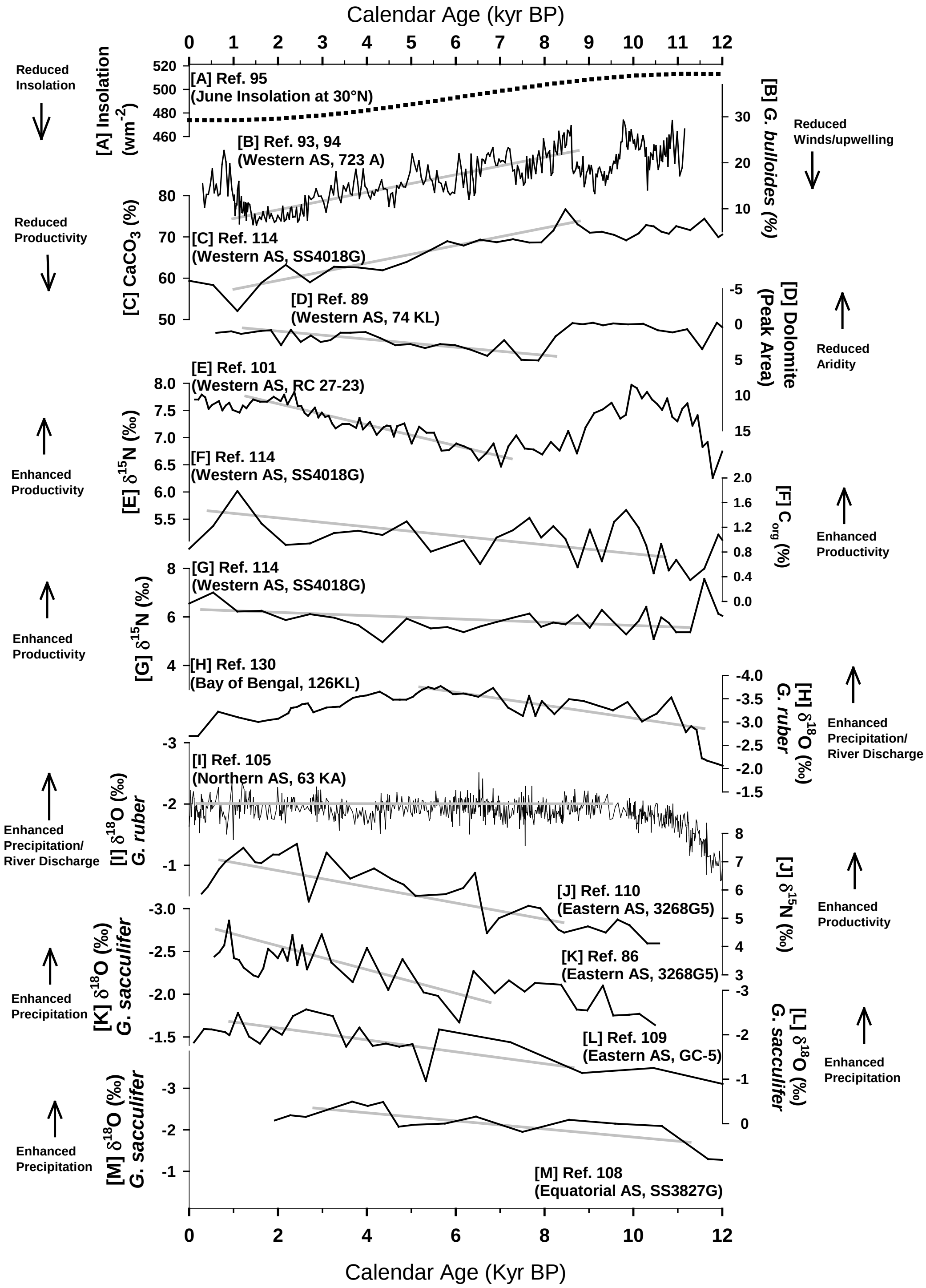

Figure 5.13: [PLACEHOLDER FOR FIRST ORDER DRAFT: to depict changes in indian monsoon during the current interglacial. This draft figure is based on different marine core parameters.] Related to monsoon variability [timescale to be discussed]; possibly incl. model results.

Figure 5.14: [PLACEHOLDER FOR FIRST ORDER DRAFT: showing the link between changes in temp. and corresponding changes in precipitation (as Figure 3 in Solomon et al., 2009).] Option 1: Changes in the global distribution of precipitation per degree of warming for modelled past warm climate (most likely Pliocene) vs preindustrial climate. Figure will be constructed in analogy to Solomon et al. (PNAS 2009; Figure 3 therein) showing changes in % of dry season precipitation per K of local temperature change. Analysis will be based on multi model ensemble. Option 2: Data-model comparison of tropical precipitation changes on orbital timescales in order to asses the relative importance of precessional forcing vs. CO_2 changes (Background climate: Pliocene or late Quaternary). [Selection of option will be based on the availability of reconstructions allowing for-data model comparison.]

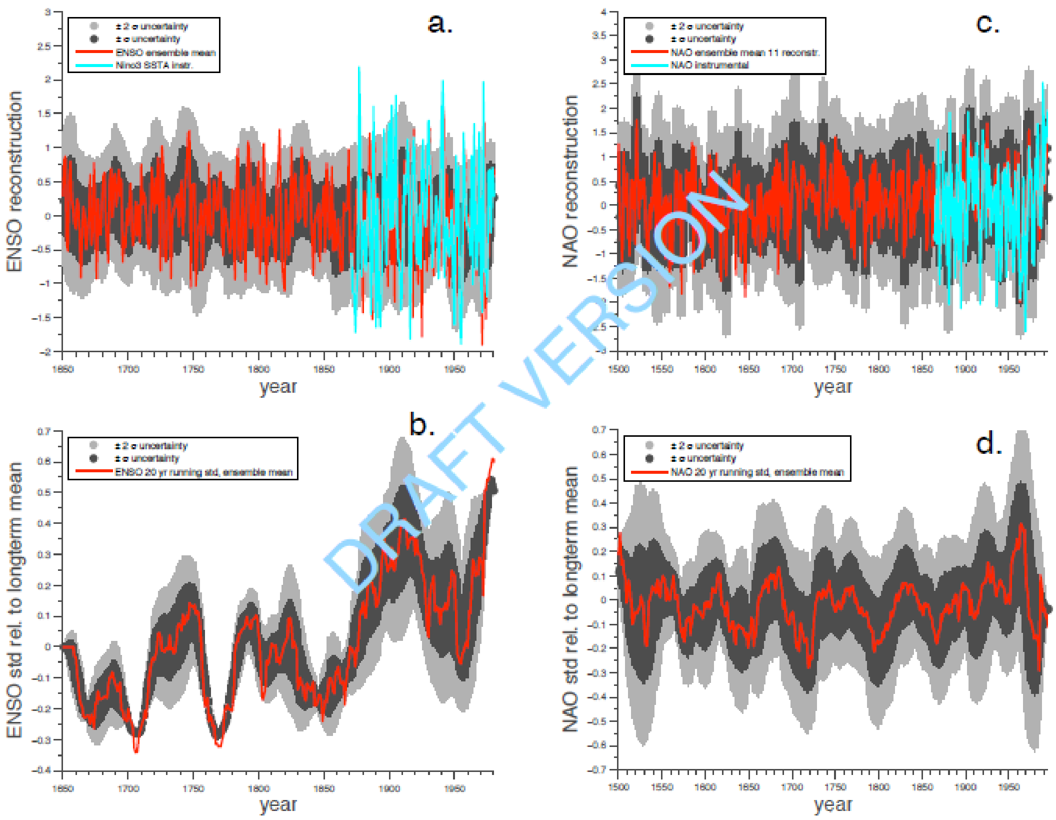

Figure 5.15: [Compilation of the different modes over time plus associated uncertainties] a) Normalized ensemble mean of 6 ENSO reconstructions, 5 going back to at least 1650 (McGregor et al., 2010) and one going back to 1706 [(Stahle, 1998)]. The dark (light) grey shading is a measure for the coherence within the ensemble of 6 ENSO reconstructions and indicates the ±1 (2) intra-ensemble standard deviation at every point in time. Instrumental annual mean Niño 3 SST data from the HadSST dataset in blue. b) Ensemble mean of relative changes of interannual ENSO variability, as measured by the running standard deviation of the 6 ENSO reconstructions in a 20-year window and as compared to the longterm mean standard deviation. The dark (light) grey shading indicates the ±1 (2) intra-ensemble standard deviation for the ensemble of 6 ENSO running standard deviation time series. c) Normalized ensemble mean of cold season NAO reconstructions, 4 going back to at least 1501 (Cook et al., 2002 ; Glueck and Stockton, 2001; Luterbacher et al., 2002; Rodrigo et al., 2001), 2 going back to 1650 (Appenzeller et al., 1998; Trouet et al., 2009), 2 to 1700 (Darrigo et al., 1993; Timm et al., 2004) and 3 to 1750 (Cullen et al., 2001; Kuttel et al., 2010; Mann, 2002). The dark (light) grey shading indicates the ±1 (2) intra-ensemble standard deviation for the ensemble of NAO reconstructions. d) Ensemble mean of relative changes of interannual NAO variability, as measured by the running standard deviation of the NAO reconstructions in b) in a 20-year window and as compared to the longterm mean standard deviation. The dark (light) grey shading indicates the ±1 (2) intra-ensemble standard deviation for the ensemble NAO running standard deviation time series calculated for the NAO as in b). In blue is the instrumental DJFM NAO index [(Hurrell, 2009)].

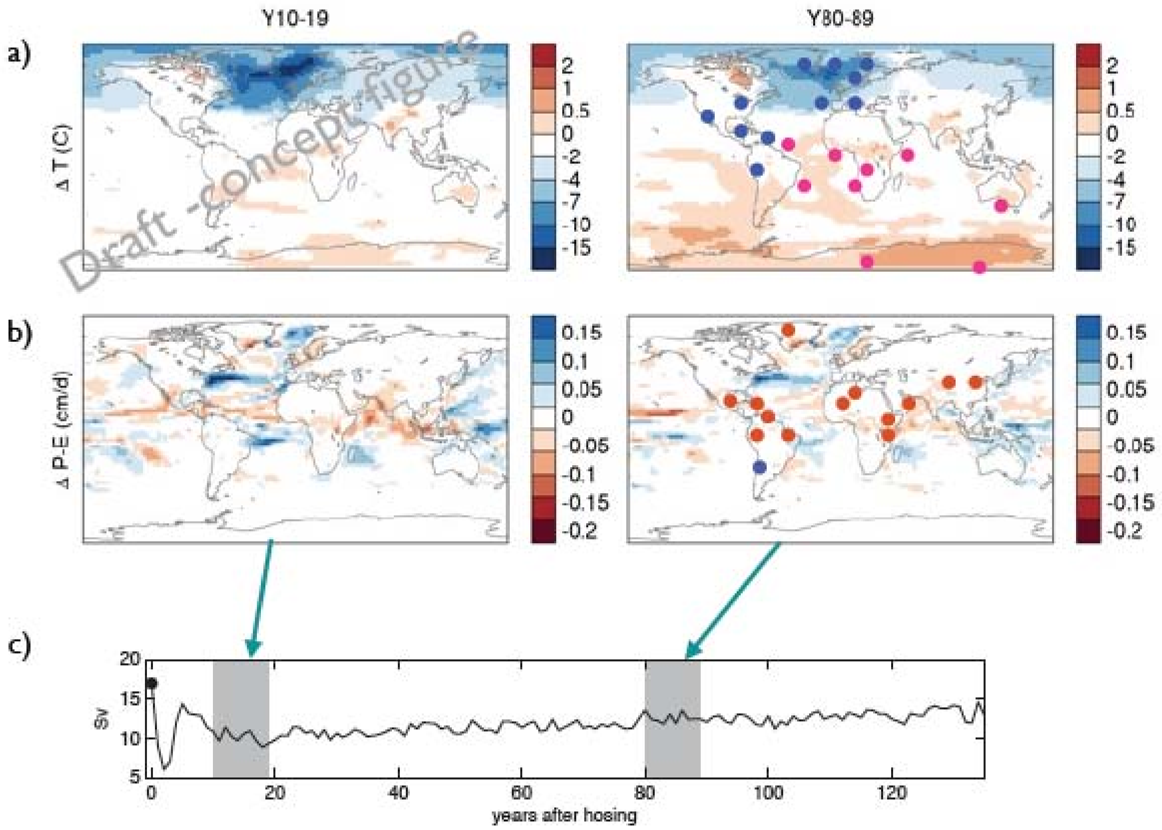

Figure 5.16: [PLACEHOLDER FOR FIRST ORDER DRAFT: model data to be replaced by ensemble mean of several models having performed the same experiment. Proxy data to be replaced by comprehensive proxy reconstruction data set compiled for the FOD.] [AMOC water hosing under glacial conditions, temperature, wind and precip changes; comparison with proxy data for Heinrich 1 or Younger Dryas.] a) Modelled spatial temperature anomaly in the CCM3 AOGCM showing departure from the modelled Last Glacial maximum state after the LGM control state model was water hosed in the North Atlantic. Left panel shows situation in the 2nd decade after water hosing. Right panel shows situation in the 9th decade after hosing. Symbols on right panel shows location of proxy based temperautre reconstruction for the H1 interval. Blue colour denotes cooling, compared to the LGM, red denotes warming compared to the LGM. b) Same as for a) but showing spatial precipitation anomalies. Red colours on right panel shows drier reconstructed conditions compared to the LGM, blue colours show wetter conditions. c) Modelled maximum overturning strength in the North Atlantic in Sverdrups ($10^6 m^3/s$).

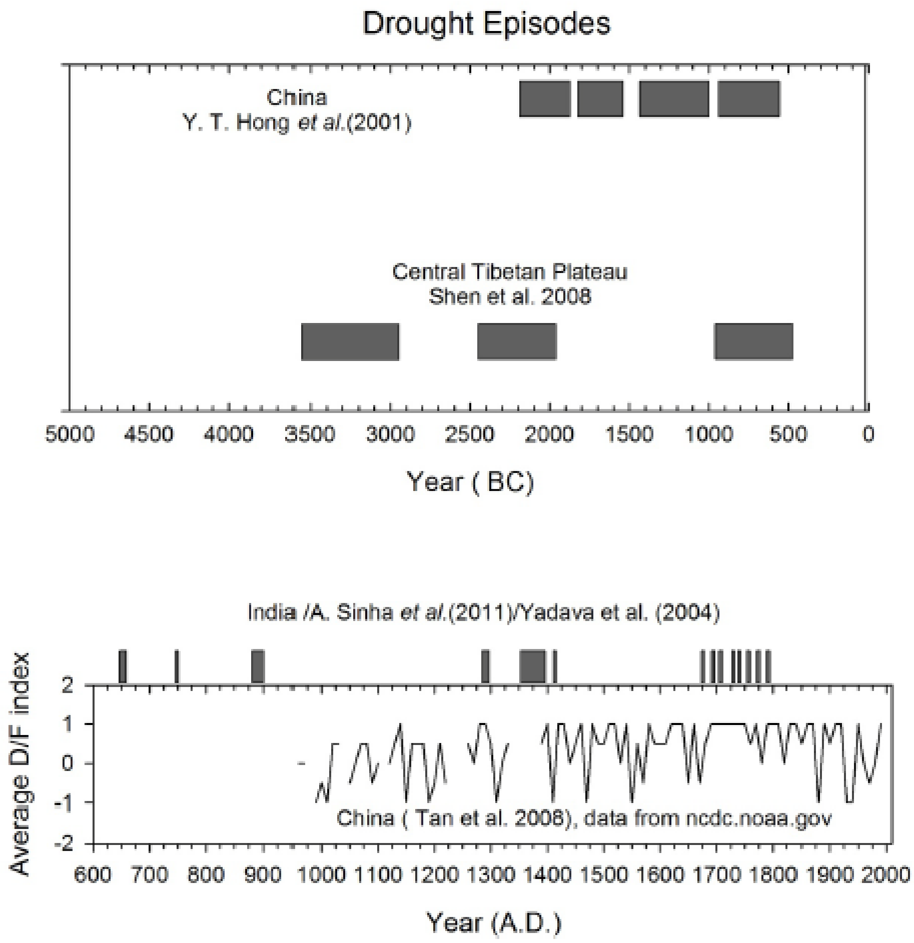

Figure caption: The upper panel shows drought episodes in Tibet reconstructed from Lake pollen profile (Shen et al., 2008) and in China from peat cellulose (Y.T. Hong et al, 2001). After the Christian era the drought conditions are available from Chinese historical records (Tan *et al*., 2008) and from India using stalagmites (A. Sinha *et al*., 2011; Yadava *et al*. 2004).

Figure 5.17: [PLACEHOLDER FOR FIRST ORDER DRAFT: for a figure showing Holocene droughts; to be expanded using different reconstructions and perhaps simulations. Compilation of data for mid-late Holocene droughts (Rengaswamy).]

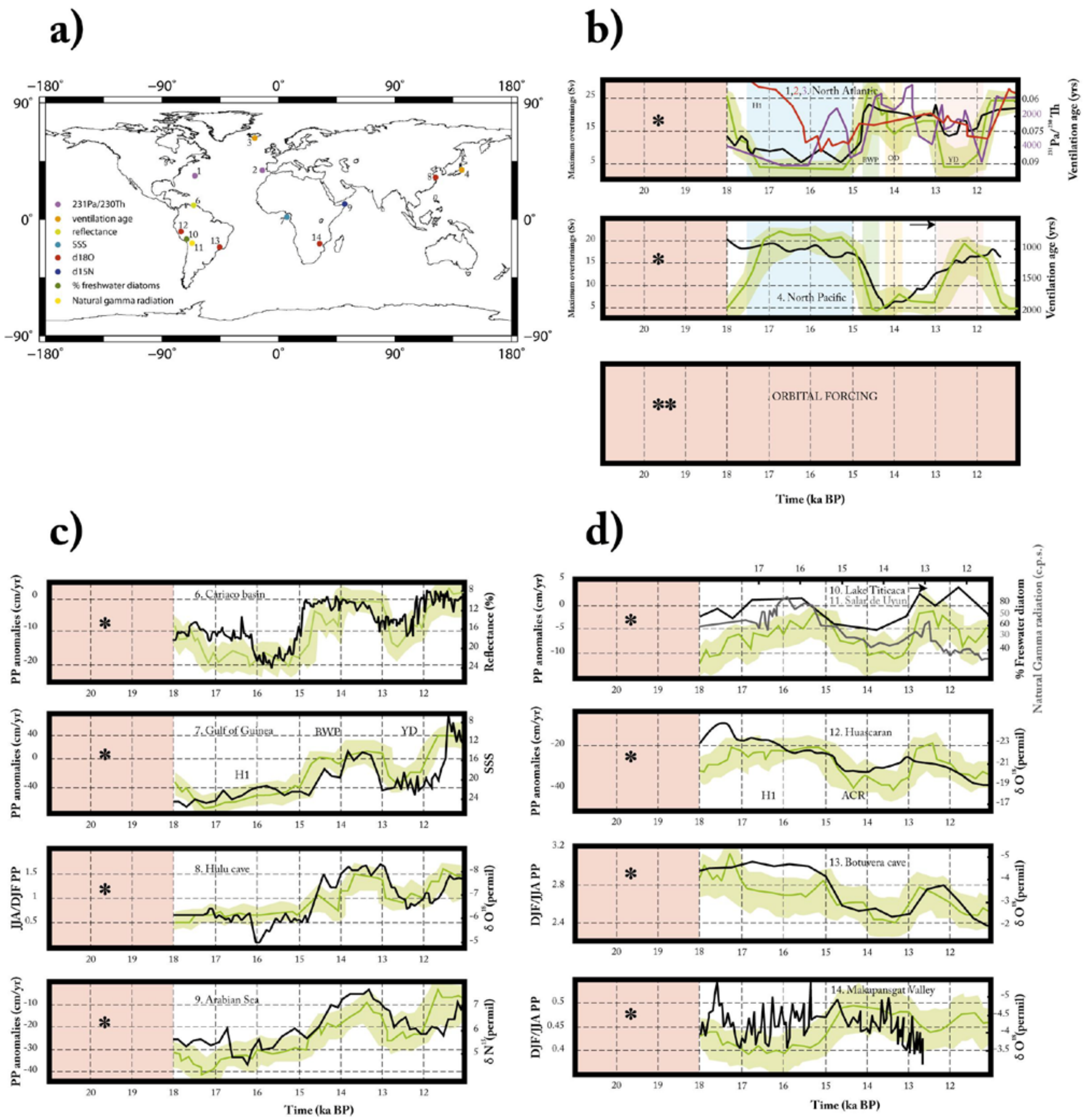

Figure 5.18: Comparisons of monsoon behavior in reconstructions and model simulations. Reconstructed and simulated LGM and deglaciation (21 to 11 kyr BP) changes with reference to preindustrial times. For all simulations, the green solid lines (shading) represent the ensemble model average (spread). The present model representation is a simplification of the LOVECLIM model simulations in Menviel et al. (2011) involving freshwater forcing transient experiments in the northern North Atlantic and Southern Ocean and using time varying radiative forcing due to solar insolation and greenhouse gases concentration changes, and including the effects of waning glacial ice-sheets on topography and albedo. [LGM simulations and reconstructions and representation of orbital forcings will be considered for FOD. Further available simulations since 18 BP will be also considered.] a) Map showing locations of the paleo-proxy records used to compare model results (see legend for proxy type). b) Simulated changes in maximum of the meridional stream function (Sv) in North Atlantic (top) vs. ^{231}Pa/^{280}th data from cores OCE326-GGC5 (1) (McManus et al., 2004) and SU81-18 (2) (Gherardi et al., 2005) and from ventilation age data from cores RAPID 10-1p, 154P and 17-5P (3) (Thornalley et al., 2011). Simulated maximum overturning strength in North Pacific (middle) and ventilation ages (years) recorded in marine sediment cores from Western North Pacific (4). The ventilation age curve is the smoothed spline interpolation of averaged benthic-planktic foraminifera ages and projection ages in the Western North Pacific (Okazaki et al., 2010). [Representation of precession changes

will be considered here (bottom).] Simulated transient precipitation anomalies various monsoon regions in the NH (c) and SH (d) in comparison to regional paleoproxy evidence. NH (c): JJA precipitation anomalies vs. Cariaco basin black reflectance in marine sediment core ODP1002 (6) (Peterson et al., 2000) (lower reflectance has been associated with increased marine productivity due to greater riverine input); jja precipitation anomalies over western Equatorial Africa vs. sea surface salinity reconstruction from the Gulf of Guinea MD03-2707 core (7) (Weldeab et al., 2007); JJA/DJF precipitation anomalies vs. $\delta^{18}O$ (permil, black) in stalagmites of the Hulo cave, China (8) (Wang et al., 2001); JJA precipitation anomalies vs. $\delta^{18}O$ (permil, black) in marine sediment core 905 from the Arabian Sea (9) (Ivanochko et al., 2005). SH (d): Annual precipitation in Bolivia vs. percentage of fresh diatoms (black) in Lake Titicaca and natural gamma ray profile (grey) from Salar de Uyuni (10) (Baker et al., 2001a; Baker et al., 2001b) (both time axes fror proxy data shifted forward 400 yrs.); DJF precipitation anomalies over Peru vs. $\delta^{18}O$ (permil, black) from Huascaran ice core (11) (Thompson et al., 1995); JJA/DJF precipitation anomalies over Brazil vs. $\delta^{18}O$ (permil, black) in stalagmites of Botuverá cave (12) (Wang et al., 2007b); JJA/DJF precipitation anomalies over South Africa and $\delta^{18}O$ (permil, black) from Makapansgat Valley stalagmites (13) (Holmgren et al., 2003). H1 stands for Heinrich event 1, BWP for Bolling Warm Period, OD for Older Dryas and YD for Younger Dryas. [CONCEPT: The freshwater forcing experiments in H1 and the YD lead to a collapse of the AMOC and enhanced NH cooling relative to LGM and a southward shift of the ITCZ. Dry conditions (weaker monsoon) result in simulated precipitation in Cariaco basin, the Gulf of Guinea (enhanced salinity), reduced JJA/DJF ratio over China and reduced JJA precipitation in the Arabian Sea. In the SH the AMOC shut down leads to a strengthening of the AABW cell strengthens and the poleward heat transport is intensified at 30º S contributing to a warming of the SH, also favoured by greenhouse gases, spring sinsolation, ice retreat around Antarctica and the bipolar seasaw. The cooling of the North Atlantic and the warming in the SH lead to a southward shift of the ITCA and generally wetter conditions in the Southern Hemisphere as supported by the proxy records in Bolivia, Peru, South Africa and Brazil. Discussion about LGM to be included.]

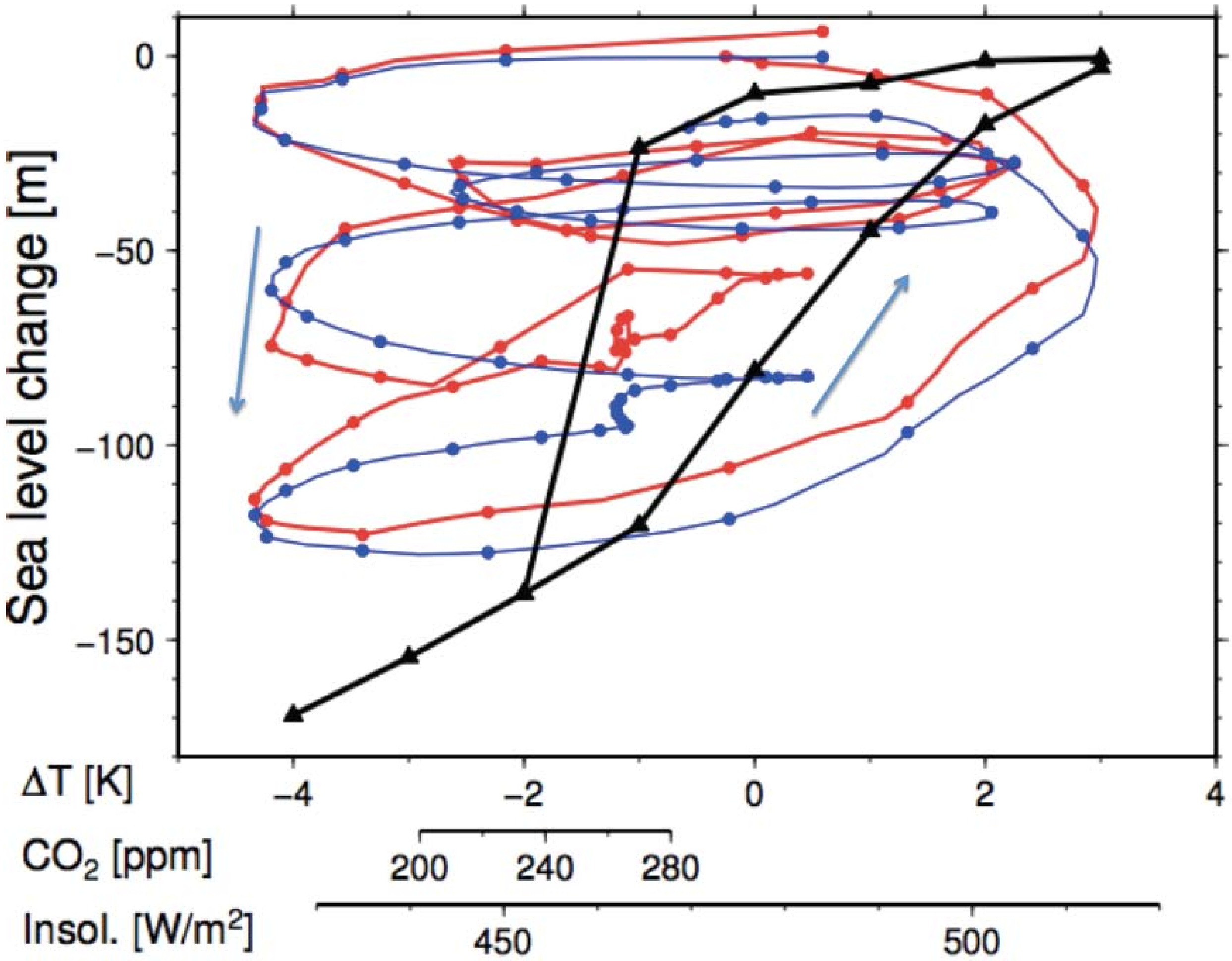

Figure 5.19: [PLACEHOLDER FOR FIRST ORDER DRAFT: transient and steady state simulations of the response of ice sheets as a function of CO_2 concentration and orbital forcing.] Reconstruction of sea level change for the last 125 ka (red line: [Waelbroeck et al., 2003]) compared with a transient ice sheet model simulation (blue line). The dots on the transient lines are displayed with a 2 ky step, showing an anti-clockwise trajectory. Black triangles display the steady state response of the same model for the last glacial cycle as a function of CO_2 concentration (with fixed present day orbital configuration) and/or orbital forcing (with fixed pre-industrial CO_2), whose effect are converted to summer temperature change relative to present day. The steady states are obtained after 100,000 years for an initial condition, which results in multiple steady states for a certain range. [Only one model is displayed (Abe-Ouchi et al 2007) but a revised version of this figure would incorporate multi-model comparisons.]

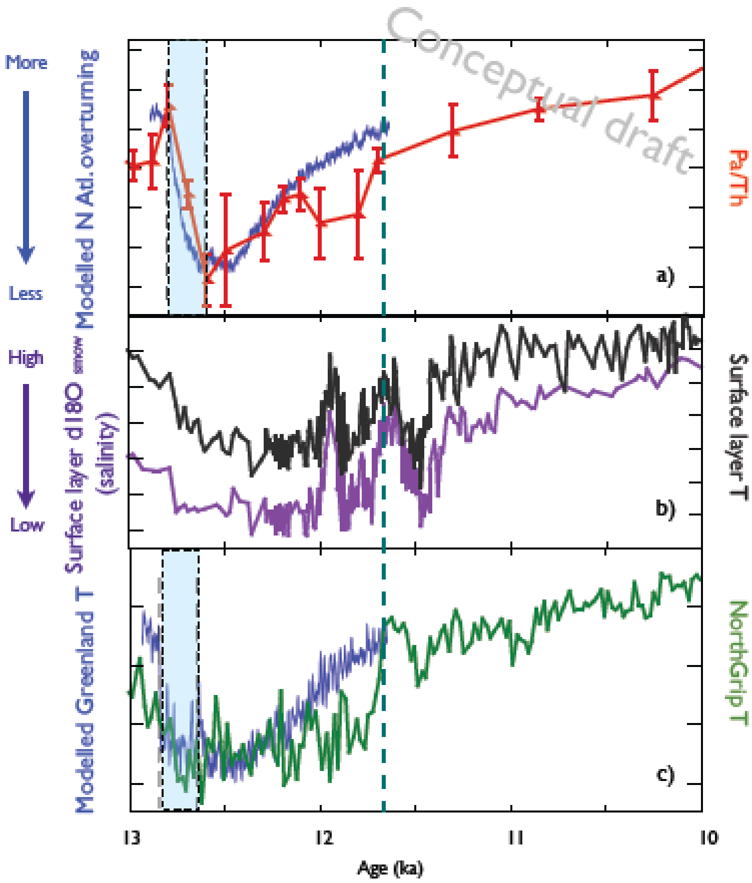

Figure 5.20: [PLACEHOLDER FOR FIRST ORDER DRAFT: to be replaced by newer data] [Phase lag between surface salinity anomaly and ocean circulation from high resolution marine sediment data.] Modelled and reconstructed North Atlantic responses during and after major reductions in the AMOC. a) Blue line: modelled maximum overturning strength in the North Atlantic in Sverdrups ($10^6 m^3/s$) (Otto-Bliesner and Brady, 2010). Red line: Pa/Th record from North Atlantic deep sea sediments through the Younger Dryas event (McManus et al., 2004). b) Near surface temperature and salinity reconstructions from the NE Atlantic [(Dokken et al., in review; Bakke, 2009)]. c) Modelled and reconstructed Greenland temperature during and after major reductions in the AMOC. Blue cureve Modelled T at the Summit of Greenland from the same experiment as in a). Green line: Temperature estimated from the NorthGrip O-isotope record.

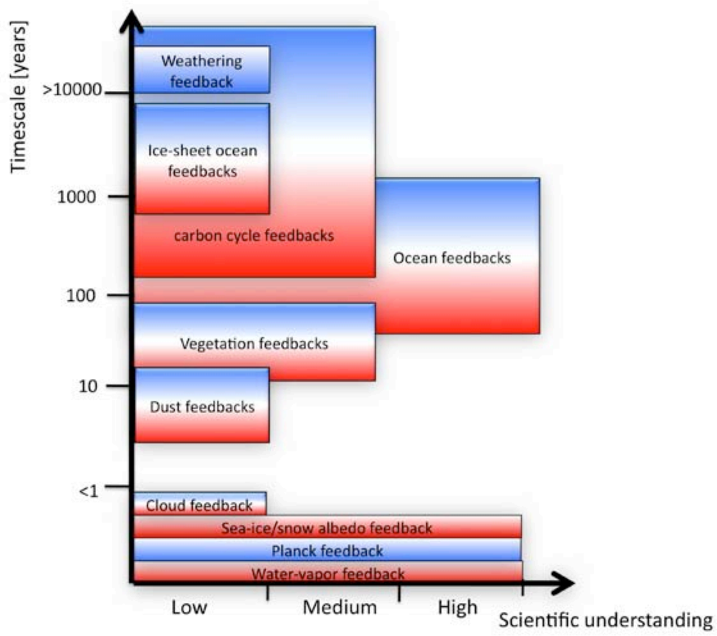

Box 5.3, Figure 1: [PLACEHOLDER FOR FIRST ORDER DRAFT: figure details to be refined after further discussions, determination of level of Scientific Understanding needs to be discussed.] Schematic diagram of Earth-system feedbacks relevant for generating past climate changes, their time scale and the present level of scientific understanding. Red (blue) bars indicate positive (negative) feedbacks. Red to blue shading represents feedbacks whose sign is either uncertain or whose detailed sub-processes can either amplify or damp the response to perturbations.

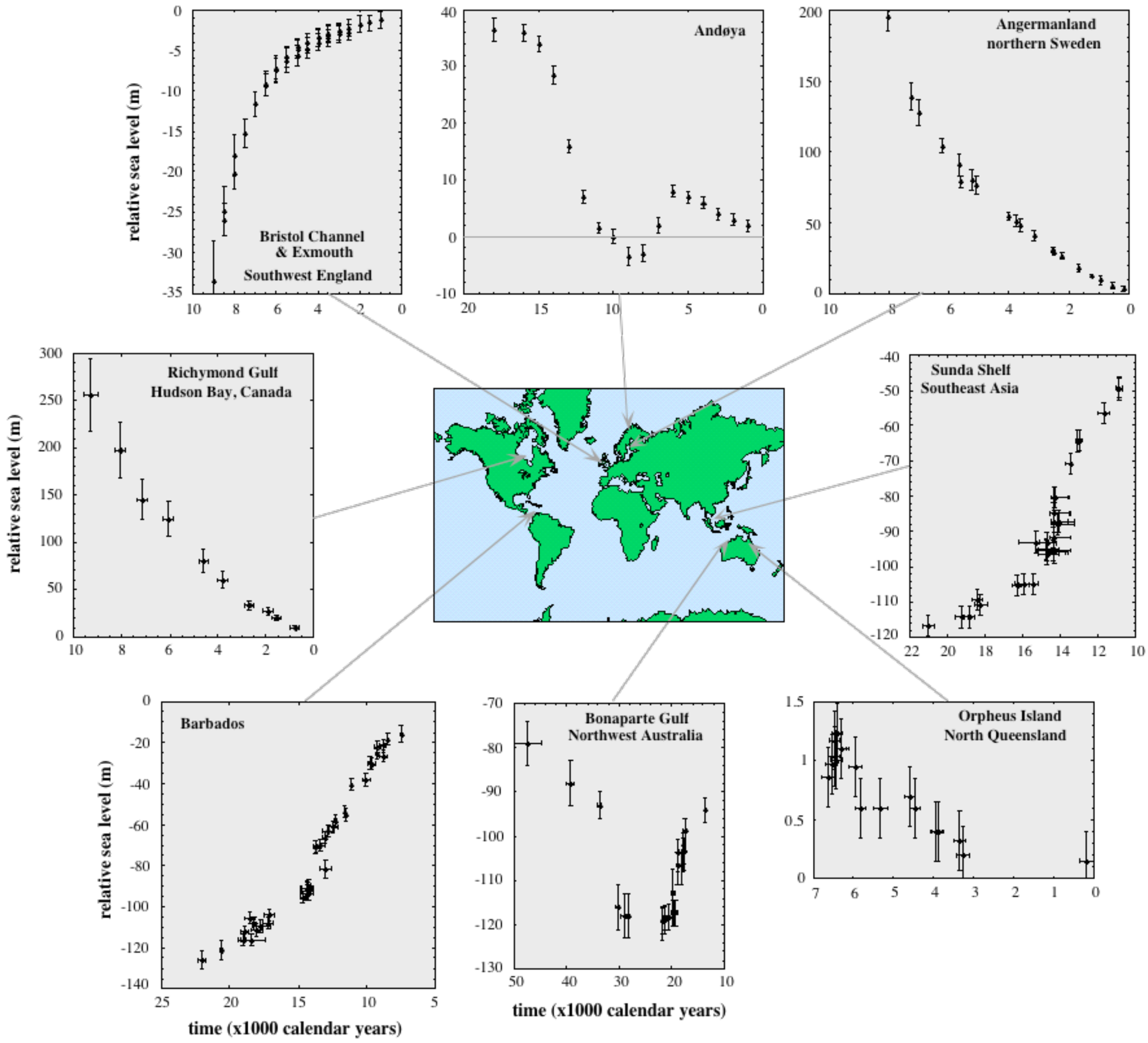

FAQ 5.1, Figure 1: [PLACEHOLDER FOR FIRST ORDER DRAFT: The actual figure will be a variant of this, using results only for the past 3000–4000 years.]

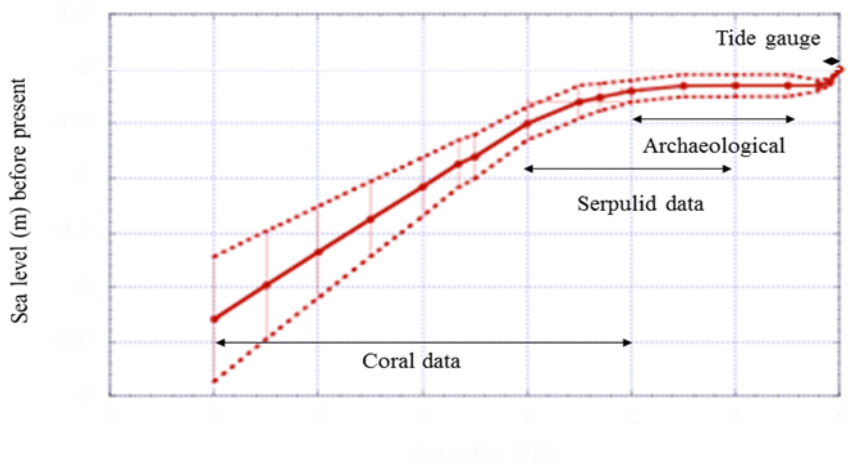

FAQ 5.1, Figure 2: [PLACEHOLDER FOR FIRST ORDER DRAFT: The final figure will be an update on this introducing salt marsh data etc.] Globally averaged sea level rise for the past 6000 years.

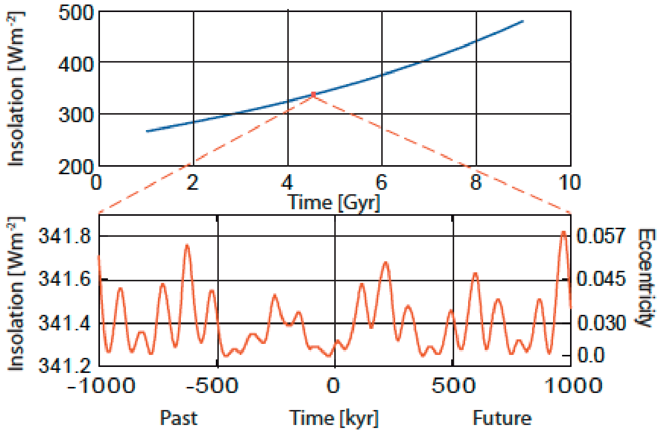

FAQ 5.2, Figure 1: Long-term variation of the mean global insolation. Upper panel: after the formation of the solar system 4.55 Gyr ago the insolation was some 20% lower than today. It will steadily increase for the next about 5 billion years until the Sun will become a red giant and destroy the Earth. Lower panel: Insolation changes for the past and the future one million years as a result of the planetary effects on the eccentricity of the Earth's orbit around the Sun. 0 corresponds to the present time.